INTEGRATION, TESTING, AND VALIDATION OF A SMALL HYBRID-ELECTRIC REMOTELY-PILOTED AIRCRAFT

THESIS

Joseph K. Ausserer, Second Lieutenant, USAF

AFIT/GAE/ENY/12-M02

DEPARTMENT OF THE AIR FORCE
AIR UNIVERSITY

AIR FORCE INSTITUTE OF TECHNOLOGY

Wright-Patterson Air Force Base, Ohio

AFIT/GAE/ENY/12-M02

INTEGRATION, TESTING, AND VALIDATION OF A SMALL HYBRID-ELECTRIC REMOTELY-PILOTED AIRCRAFT

THESIS

Presented to the Faculty

Department of Aeronautical and Astronautical Engineering

Graduate School of Engineering and Management

Air Force Institute of Technology

Air University

Air Education and Training Command

In Partial Fulfillment of the Requirements for the

Degree of Master of Science in Aeronautical Engineering

Joseph K. Ausserer

Second Lieutenant, USAF

March 2012

APPROVED FOR PUBLIC RELEASE; DISTRIBUTION IS UNLIMITED

AFIT/GAE/ENY/12-M02

INTEGRATION, TESTING, AND VALIDATION OF A SMALL HYBRID-ELECTRIC REMOTELY-PILOTED AIRCRAFT

Joseph K. Ausserer, BS
Second Lieutenant, USAF

Approved:

________________________________	__________
Frederick G. Harmon, Lt Col, USAF (Chairman)	Date
________________________________	__________
David R. Jacques, Ph.D., (Member)	Date
________________________________	__________
Marc D. Polanka, Ph.D (Member)	Date

Abstract

Parallel hybrid-electric technology offers a wide variety of new mission capabilities including low-observable loiter operations and increased fuel efficiency for small remotely-piloted aircraft. This research focused on the integration, validation, and testing of a hybrid-electric propulsion system consisting of commercially available components to fabricate a small remotely-piloted aircraft capable of extended low-observable operation. Three novel aspects contributed to the success of the design: optimization of the propulsive components to the integrated system, torque control of the components for additive power, and a one-way bearing/ pulley mechanism (patent pending) mechanically linking the hybrid system components. To the knowledge of the author at the time of publication, this project represents the first functional parallel hybrid-electric propulsion system for a remotely-piloted aircraft. The integration phase entailed the selection, testing, and assembly of components chosen based on prior design simulations. The propulsion system was retrofitted onto a glider airframe with a 12 ft wingspan and a maximum takeoff weight of 35 lbs, also based on the initial design simulations. During the validation and testing phases, results from bench, ground, and flight testing were compared to the design simulations. The designed propulsion system was well matched to the power estimates of the design simulations. Bench and ground tests demonstrated that hybrid mode, electric only mode, combustion only mode, and regeneration mode are fully functional. Comparison of bench test results to an engine only variant of the airframe indicate the HE system is capable of flying the aircraft.

Acknowledgements

There is no "I" in "team", nor is there an "I" in "Condor". The integration and testing of the hybrid system would not have been possible without the dedication and hard work of the Condor team as well as a number of associated individuals. Specifically, I would like thank Lt Col Fred Harmon, my thesis advisor, for his help and guidance on the project. Similarly, I must also thank Dr. David Jacques who filled in as my day-to-day advisor while Lt Col Harmon was deployed. I would also like to thank my fellow students, Capt Jacob English, Capt Michael Molesworth, and Lt Chris Giacomo for their help during integration, planning, and testing. Without their assistance, the hybrid system would still be on the bench looking for an aircraft. A thank you also goes out to Chris Harkless at the AFIT Model Shop, Rick Patton at CESI, and Justin Delmar at AFRL/RZ for their support with component fabrication, aircraft assembly, and the electrical motor and controller, respectively. Finally, I would like to thank my wife for her support and encouragement and her perpetual belief in that the project would succeed.

Table of Contents

List of Figures

List of Tables

List of Abbreviations

AC	Alternating Current
AFRL	Air Force Research Laboratory
COTS	Commercial off the Shelf
DC	Direct Current
EM	Electric Motor
GWOT	Global War on Terror
HALE	High Altitude Long Endurance
HE	Hybrid-Electric
IC	Internal Combustion
ICE	Internal Combustion Engine
IED	Improvised Explosive Device
ISR	Intelligence Surveillance Reconnaissance
Li-Ion	Lithium-ion
Li-Po	Lithium-ion Polymer
Ni-Cd	Nickel-Cadmium
NiMH	Nickel-Metal-Hydride
R/C	Remote Controlled
RPA	Remotely-piloted Aircraft
UAV	Unmanned Aerial Vehicle
USAF	United States Air Force
USN	United States Navy

Nomenclature

Symbol	Description (Units)
b	wing span (m)
B	magnetic field strength (T)
c	wing chord (m)
c_{SFC}	power specific fuel consumption (k/s/W)
C_D	drag coefficient
$C_{D,o}$	zero lift drag coefficient
C_L	lift coefficient
$C_{L,max}$	maximum lift coefficient
C_T	thrust coefficient
C_P	power coefficient
C_Q	Torque coefficient
D	propeller diameter (m), drag (N)
e	Oswald efficiency factor
E	Energy in batteries (W-hr)
F/A	fuel to air ratio (kg fuel/kg air)
g	acceleration of gravity (m/s^2)
I	current (A)
$\bar{I}$	average current draw (A)
I_{clutch}	coil current (A)
I_o	no load current (A)
J	advance ratio
K	squared term constant in drag polar
k_t	motor torque constant (N-m/A)
k_v	motor voltage constant (rpm/V)
l	length (m)
L/D	lift to drag ratio
m_f	fuel mass (kg)
$\dot{m}_f$	fuel mass flow rate (kg/s)
MEP	mean effective pressure (Pa)
n_R	revolutions per stroke
$n_{R,min}$	load factor for minimum radius turn
N	rotational speed (revolution/s)
P	power (W)
P_A	power available (W)
$P_{electric}$	power delivered to motor (W)
P_{prop}	propeller power (W)
P_R	power required (W)
P_{shaft}	shaft power (W)

P_{SL}	power at standard sea level (W)
r	distance to magnetic field (m)
R	aircraft range (m)
R_m	internal resistance (Ω)
R_{min}	radius for minimum radius turn (m)
R/C	rate of climb (m/s)
S	wing area (m^2)
SFC	specific fuel consumption (kg/s)
t_{end}	endurance time (s)
T	thrust (N)
$T_{A,max}$	maximum available thrust
T/W	thrust to weight ratio
u	angle between coil element and magnetic field (rad)
Q	torque (N-m)
Q_{HV}	heating value of fuel (J/kg)
Q_m	motor torque (N-m)
V	voltage (V)
$\bar{V}$	average voltage (V)
V_{cruise}	cruise velocity (m/s)
V_d	cylinder displacement volume (m^3)
$V_{endurance}$	endurance velocity (m/s)
V_{max}	maximum velocity (m/s)
$V_{R,min}$	velocity for minimum radius turn (m/s)
V_{stall}	stall velocity (m/s)
V_∞	aircraft flight velocity (m/s)
W	aircraft weight (N)
W_0	aircraft weight without fuel (N)
W_1	fully fuelled aircraft weight (N)
η_f	power conversion efficiency
η_m	motor efficiency
η_{prop}	propeller efficiency
η_v	volumetric efficiency
μ_o	magnetic dipole moment (J/T)
ρ_{SL}	standard sea level density (kg/m^3)
ρ_∞	free stream air density (kg/m^3)
τ	torque (N-m)
ω_{prop}	propeller speed (rpm)
ω_m	motor speed (rpm)

INTEGRATION, TESTING, AND VALIDATION OF A SMALL HYBRID-ELECTRIC REMOTELY-PILOTED AIRCRAFT

I. Introduction

1. Background

On December 17, 1903, Orville and Wilbur Wright demonstrated the first man-made vehicle capable of powered flight [**1**]. During World War I, the powered aircraft made its global debut on the battlefield in both a fighter and bomber capacity, and by World War II multiple countries were projecting airpower off of the decks of ships to attack enemy forces despite the absence of land based runways. At the start of the Cold War in the 1950's, the U.S. Army recognized the value of an unmanned aircraft for surveillance and the first flight test of the SD-1 drone opened the doorway to unmanned aviation for the United States military [**2**].

Similar to the explosive innovation of the manned aircraft industry in the first half of the 20th century, the unmanned aircraft industry has seen exponential growth, especially in military applications, over the last 60 years. In Vietnam, unmanned aircraft fulfilled surveillance and surface-to-air missile detection roles, and during the first Gulf War both the United States Air Force (USAF) and United States Navy (USN) used unmanned aircraft to deliver ordinance to battlefield targets. The Global War on Terror (GWOT) has only served to increase the demand for unmanned platforms. The USAF's most heavily used remotely-piloted aircraft (RPA), the MQ-1 Predator, entered active duty in July 1994 and accumulated over 900,000 flying hours by March 2011; 300,000 of those hours were in the preceding 2 years [**3**] and most of those hours supported the GWOT.

The explosion in unmanned aircraft is not limited to just the USAF and USN. An ever increasing number of governmental and private sector entities both at home and abroad are adding unmanned aircraft to their operational capabilities. According to the Teal Group's 2010 market study, annual expenditures on unmanned systems are expected to more than double from

$4.9 billion in 2010 to over $11 billion by 2020 with 42% of that investment from foreign entities [**4**]. In the civilian sector, unmanned aircraft primarily fulfill a monitoring role watching everything from urban roadway traffic and wildlife to forest fires. The Japanese Government utilized a small Fuji made RPA to survey the crippled Fukushima nuclear power plant following the March 2011 earthquake and tsunami. The Department of Homeland Security flies unmanned systems to observe the United States border. In April 2011, the Predator's replacement, the MQ-9 Reaper, passed 20,000 flight hours in Afghanistan, not by U.S. forces, but by the Royal Air Force.

Despite the payload and munitions capability of aircraft like the Predator and Reaper, the largest demand in both the civilian and military sectors remains for persistent surveillance, reconnaissance, and monitoring. It is the number one priority for all levels of military commanders in a survey published in the Unmanned Systems Roadmap (2007-2032) from the Office of the Secretary of Defense [**5**], and the 2006 Quadrennial Defense review listed persistent surveillance as a key mission need. The very nature of unmanned aircraft offers the capability to unrelentingly pursue a target in a way the stamina of a human pilot simply cannot match. Unmanned systems can enter sites unsafe for pilots due to enemy fire, biological contaminants, or radiation levels. "The attributes of persistence, efficiency, flexibility of missions and attack capability have repeatedly proven to be force multipliers across the spectrum of global joint military operations" [**6**]. Therefore, it is crucial to the future of national defense to develop, harness, and exploit the capability of these RPA.

2. Motivation

Intelligence, surveillance, and reconnaissance (ISR) are the common denominator in the drive for most new unmanned aerial systems; active attack systems such as the MQ-9 Reaper are in the minority. And, as alluded to earlier, not all surveillance situations are created equally. The largest physical danger to coalition troops during the GWOT has not been enemy combatants but rather improvised explosive devices (IED). Insurgent and terrorist groups in both Afghanistan and Iraq understand how to build IEDs out of non-metallic and common place materials making them difficult to detect and even more difficult to recognize at a safe distance. The IED threat is so significant that in 2006, Department of Defense Directive 2000.19E created a Joint Improvised Explosive Device Defeat Organization, tasked with supporting Combatant Commanders in developing tools for counter-IED operations.

Small RPAs offer a sizable portion of the current solution to the IED problem. A small RPA can monitor IED hotspots at a much closer range and for an extended period unmatchable by a manned reconnaissance aircraft, such as the U2. Furthermore, a small RPA has no aircrew and is relatively inexpensive, mitigating personnel, political, and financial risks. Such a RPA should be small and silent making it difficult to detect from the ground and allowing it to loiter in the target are for as long as possible. After all, if the insurgent planting the IED is aware of the monitoring system, or coverage is chronological spotty, he or she could simply plant the IED elsewhere, plant it at a different time, or simply disappear. The need for a small RPA capable of undetectable observation has not gone unrecognized; both the 2003 Defense Science Board and the Air Force Scientific Advisory Board included a small, low-observable, unmanned platform in their lists of recommended capabilities [**7**].

Although sufficient in its own right, counter-IED operations are not the only missions that could benefit from a small, hard to detect, RPA. There are any number of other surveillance operations in both the government and civilian sectors that such an aircraft could enable or enhance. In Africa's Great Rift Valley, governments struggle to prevent poaching and other illegal activity on parkland. They have limited funding and manpower, the terrain is rugged and foot patrols are dangerous; in the last decade, twenty rangers have been killed in Virunga National Park alone [**8**]. International borders, like those between the United States and Mexico and between in the United States and Canada, often go unmonitored for long stretches, leaving them wide open to drug smuggling and other illegal activity. Near silent, persistent surveillance delivered by a small and relatively inexpensive aerial platform would significantly aid in both counter poaching and anti-smuggling operations. A low-observable aircraft could fulfill peacetime and other diplomatically sensitive missions without the risk to flight crews and foreign relations accompanying manned systems, especially if the aircraft is downed on the wrong side of a border. Therefore, while the main thrust of this research is to create a small low detectable RPA to meet the needs of the war fighter, the applicability is not limited to solely wartime counter IED operations.

3. Problem Statement

To meet the operational concept described above, the small RPA must be low-observable and possess reasonable endurance so the operators are removed from the target observation zone. Currently, internal combustion (IC) powered RPA systems provide the war fighter with sufficient observational endurance. However, the platforms have notable acoustic and thermal signatures making them either detectable at low altitudes or requiring them to maintain an altitude not conducive to effective sensor performance. Electric platforms possess low acoustic and thermal signatures, but suffer from limited range due to the poor specific energy available from even leading battery technology [**9**]. Therefore, electric and combustion propulsion systems meet complementary mission needs; neither is a singular solution.

The Unmanned Aerial Systems Roadmap (2005-2030) encourages propulsive efficiency through exploiting alternative power sources, specifically for endurance and unwarned ISR. A hybrid IC and electric system fuses the propulsive types, allowing each to overcome the other type's shortcomings. The electric system would provide low-observable loiter at the target area, compensating for the acoustic and thermal signatures of the IC engine, which is disengaged for that portion of the operation. The IC system would in turn provide extended range to the vehicle and recharge the batteries, overcoming the batteries' low specific energy with the relatively high energy density of hydrocarbon fuel. A hybrid-electric (HE) propulsion system could provide a RPA with improved fuel efficiency and decreased acoustic signature, much like similar systems have done in the automotive industry. The Unmanned Aerial Systems Roadmap 2007-2032 suggests that hybrid systems may be the answer to meet power requirements for long endurance ISR missions. A HE system leverages the advantages of combustion and electric power to meet the demands for low-observable ISR.

4. Research Objectives

The objectives of this research effort naturally divide into two tiers: integration and validation. The over arching goal of the integration phase is to assemble commercially available components to create a HE propulsion system for a small RPA. The components were chosen to match previous optimization studies for an HE-RPA completed by Lt Col Frederick Harmon (AFIT professor) and Capt Ryan Hiserote (AFIT graduate student) [**10**,**11**]. Based on the project motivation, there are several envisioned mission segments for the HE system. These segments are summarized graphically in Figure 1, modified from the conceptual work of Hiserote [**12**].

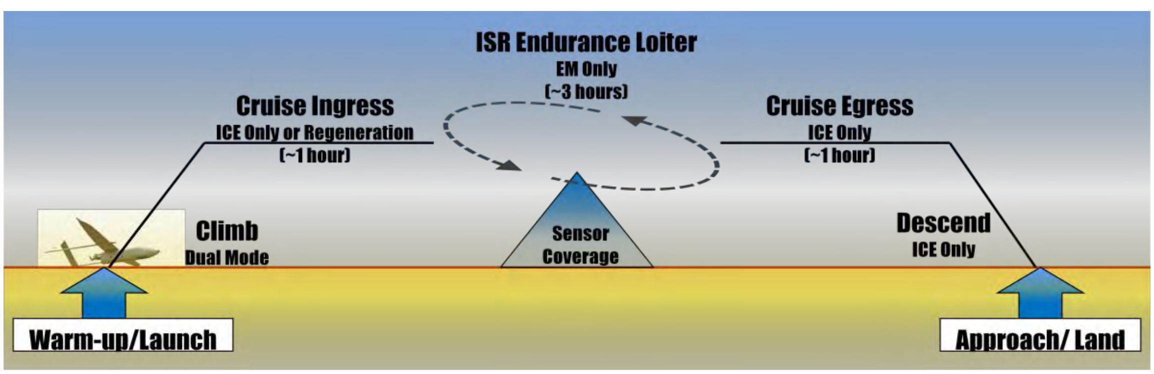

Figure 1: Proposed mission profile for a small HE-RPA

As depicted in Figure 1, the propulsion system must have at least four operational modes: EM-only to facilitate near silent loiter, ICE-only for use during ingress and egress, a regeneration mode to recharge the batteries, and a Dual Mode where both components provide power for demanding maneuvers such as takeoff and climb. Additionally, there should be some way to restart the ICE during flight so that it can be turned off during loiter operations. If mid air restart is unavailable or infeasible, it may be possible to find an engine that is sufficiently silent at idle for low-observable operation.

The validation tier involves testing the propulsion system on the bench, in the airframe on the ground, and finally in the airframe in flight and comparing the tests to single point static simulations from the design codes in [**12**] and [**13**] used to design the airframe and match the propulsion system components. Thus the ultimate goal of the project is to demonstrate a functional HE system for a small RPA and to validate the underlying design code.

5. Research Scope

There were two goals of this research. The first goal is to integrate and demonstrate a hybrid-electric system for a small remotely-piloted aircraft capable of performing as many of the objectives described in the concept of operation in Section 4 as possible. The second goal was to take sufficient data from the hybrid system to make single point comparisons to the design code. If possible the project would have culminated in a flight test of the hybrid system on the airframe. However, schedule limitations precluded a flight test and thus the effort ended in bench and ground demonstrations and comparison of the bench and ground data to the design codes.

The scope of this research effort must be contextualized within the overall project. The Hybrid-Electric Unmanned Aerial Vehicle Project began with the work of Harmon on control strategies applicable to controlling the propulsive components of a HE system [**14**]. Then Hiserote developed a code optimizing the airframe design for a small Unmanned Aerial Vehicle (UAV) with a HE propulsion system performing the mission profile from Figure 1. Following Hiserote, other students tested ICEs [**15**], programmed custom controllers [**16**,**17**], and developed a code to match propellers, EMs, and ICEs [**13**].

This research effort builds on those works to instantiate and test a physical HE system for a small RPA. It does not involve the development of the airframe itself, which was the work of CLMax Engineering; rather, it exchanges the stock propulsion system for an HE system. This project also does not include a full flight characterization of the aircraft nor does it involve the rigorous acoustic measurements necessary to assess whether the developed system delivers a sufficiently small acoustic signature to be considered low-observable.

There are a number of other parallel efforts critical to the success of this project, but not within the scope of this paper. The sum of these efforts, including this paper, is the Condor Project which the reader should view as the physical implementation of the theoretical HE-UAV project started by Harmon. The controls for the aircraft (not the propulsion system) were implemented by Lt Christopher Giacomo (AFIT graduate student) [**18**]. Test planning and testing of the airframe without the hybrid system were carried out by Capt Jacob English and Capt Michael Molesworth (AFIT graduate students) [**19**]. Thus, the creation of the HE system is part of a larger effort to demonstrate the operational concept.

6. Research Methodology

The integration tier of the project was split into two phases. During the first phase, the entire system was assembled onto a dynamometer to examine internal combustion engine (ICE), electric motor (EM), and hybrid operation. Several iterations of the avionics system, mounting brackets, and even some of the components were required to eliminate incompatibilities and bugs from the system. During the second phase, the propulsion system was migrated from the dynamometer to the airframe. The airframe was secured to a test stand in the laboratory to verify system function using the propeller as a load before proceeding to ground testing. During both the ground and flight tests the aircraft performed an abbreviated version of the mission profile in Figure 1 to verify functionality of the system.

7. Thesis Overview

Chapter II provides background on the Condor project followed by an examination of each component in the HE system, focusing on the modeling equations and relevant work performed by other groups. Chapter II concludes with a summary of flight test techniques applicable to the HE-RPA. Chapter III examines the integration and initial bench testing of the HE system. Chapter IV compares the results of ground and flight testing to the simulations used to match the components and design the aircraft. Lastly, Chapter V summarizes the conclusions from the project and offers suggestions for future work.

II. Literature Review

1. Chapter Overview

This chapter covers the background applicable to the development and flight testing of the HE-RPA developed at AFIT, based originally on Harmon's work at the University of California - Davis [**14**]. The chapter begins by examining the history of the hybrid-electric concept and the conceptual design of the AFIT aircraft. Then it focuses in detail on each of the components of the propulsion system, specifically the modeling equations and the relevant work done by other groups on similar components and systems. It concludes by examining flight test techniques for small RPAs and their propulsion systems.

2. Background on the Hybrid-Electric RPA Concept

The term 'hybrid' often refers to automobiles, where it primarily describes gasoline-electric vehicles designed to increase fuel efficiency and reduce emissions. On vehicles such as the Honda *Insight*, Toyota *Prius*, and Chevrolet *Volt*, this is implemented by utilizing electricity stored in batteries to supplement or replace the fossil fuel power produced by the internal combustion (IC) engine during the vehicle's operation [**20**]. While the electricity in these examples is provided by batteries, other hybrid-electric systems use generators, solar cells, or even hydrogen fuel cells. Conceptually, a hybrid-electric aircraft is no different. This section discusses the history behind the hybrid-electric concept and the AFIT aircraft.

2.1. The Hybrid-Electric RPA Concept

Before continuing, it seems prudent to define the hybrid RPA and the HE-RPA concepts. Hybrid RPA is the more general description and simply indicates a RPA that uses two (or more) forms of power to drive the propulsion system. In essentially all instances, the primary form of power is an internal combustion (IC) engine that is supplemented by some form of electric energy such as batteries, fuel cells, or solar panels. Throughout this paper, HE-RPA will refer specifically to the battery and fossil fuel combination. Usually, the secondary energy source has a lower specific energy (energy/mass) than fossil fuel and thus, offers some additional capability in exchange for the increase in weight or decrease in range. Currently, the extra weight of the hybrid system makes improved fuel economy, the objective on an automobile, difficult to achieve on a small aircraft system [**11**]. However, the hybrid concept does offer a number of new and unique objectives.

2.2. Motivations and Objectives for a Hybrid-Electric RPA

In lieu of increased fuel economy, the hybrid-electric concept creates a variety of new capabilities for an RPA which Glassock outlines in [**21**]. The most notable are: decreased acoustic signature, the capability to remotely start the IC engine, sprint capability, and propulsion system redundancy. The decreased acoustic signature, obtained during electric only flight, would allow for near-silent low altitude surveillance, a capability useful to both civilian and military agencies. Additionally, a second onboard propulsion source would allow remote restart of the IC engine and provide a partial backup in case of engine failure. Use of the two power systems in tandem would provide 'boost' power, which Glassock's research at Queensland University suggests could provide a small RPA with a 35% increase in power for a 5% increase in weight [**22**].

The decreased acoustic signature is also mentioned in both the 2005 and the 2007 Unmanned Aerial Systems Roadmaps published by the Office of the Secretary of Defense [**5**,**7**]. These reports suggest that a small size RPA (less than 50 lbs) that uses fossil fuel for ingress and egress and electric power to achieve near silent low altitude surveillance would fill a significant gap in current RPA capabilities [**5**,**7**]. Therefore, it is no surprise that the decreased acoustic signature was the main motivation behind Harmon's and subsequently Hiserote's work in the development and conceptual design for the AFIT aircraft [**11**]. The foundations of such a conceptual design are the aircraft power sources and the propulsion configurations, which are the subjects of the two next sections.

2.3. Power Sources

There are numerous options for the power sources on hybrid aircraft including generators, solar panels, fuel cells, and batteries. Generators are the most straightforward and the easiest form of hybridization. In a generator system, a fossil fuel is burnt to power a generator which delivers electric energy to a motor which in turn drives the propeller; typically this system is used in a series configuration, as discussed in the next section. Diesel locomotives have used a series generator system for decades, although the electric motors drive the train wheels instead of a propeller. Meanwhile, aerospace company AeroVironment's high altitude long endurance (HALE) Global Observer is fueled on liquid hydrogen which drives an electric generator to turn its eight propellers [**23**,**9**]. The airframe first flew in August 2010 and the first hydrogen powered flight was in January 2011. Engine and automobile manufacturer Rolls Royce has also researched matching its turbine engines to electric generators for a variety of UAV applications [**24**].

Photovoltaic solar panels create an electrical potential when exposed to solar radiation, effectively converting sunlight to electrical energy that can be stored in batteries or used directly. Solar panels are primarily used on glider like HALE vehicles since the large wings provide ample space for panels and the vehicles' high altitude flight conditions provide ample sunlight and minimal atmospheric attenuation of solar energy. The NASA *Pathfinder* and *Helios* aircraft are prime examples of such technology, and interestingly, were actually developed by AeroVironment [**25**,**26**]. Propelled by 14 engines powered by solar energy stored in lithium ion batteries, the *Helios Prototype* cruised for 40 minutes at 96,863 feet on 14 April 2001, setting a world record for sustained flight by winged aircraft [**25**].

Hydrogen fuel cells are another possible hybrid power source, although many current efforts utilize straight fuel cell power in favor of a hybrid system. Fuel cells are thermodynamically efficient, but they require pressurized hydrogen which also has a very low specific energy compared to fossil fuels. However, numerous examples of fuel cells on aircraft exist, especially since modifying existing electric aircraft to carry fuel cells in place of batteries is relatively straightforward. In one of the most successful cases, AeroVironment exchanged the batteries on its *Puma AE* aircraft for fuel cells and tripled the endurance from 3 to 9 hours [**27**]. The *Puma* only has a range of 15 km, but its electric system is able to provide quiet ISR [**28**]. Meanwhile, aircraft manufacturer Boeing flew a manned aircraft powered by a fuel cell and lithium-ion battery system in April 2008. The modified Diamond Aircraft *Dimona* glider flew for 20 minutes at over 60 mph [**29**]. There is also at least one group working specifically on a small RPA similar to the one under development at AFIT. A group at Colorado State University and Georgia Institute of Technology performed hardware testing on an IC engine and fuel cell hybrid propulsion system [**30**]. While their laboratory results demonstrate aircraft endurance and range comparable to a straight fossil fuel burning IC engine, they have not yet flight tested their hybrid system.

Finally, batteries have been used on small RPAs (especially hobbyist aircraft) for years as the sole source of power. Due to the low specific energy of batteries, such RPAs typically suffer from poor endurance and range compared to their IC engine driven counterparts. Nonetheless, there are several recent attempts to create battery based hybrids of various sizes. In 2009, German aircraft builder Flight Design demonstrated a light, manned, sport aircraft where a 40 hp electric motor provided approximately 5 minutes of boost power to an 115 hp IC engine [**31**]. Since the electric motor could provide additional power during takeoff, the IC engine size was reduced, in turn reducing the overall aircraft weight. In June of 2011, Siemens AG, Diamond Aircraft, and EADS flew the world's first manned series hybrid-electric [**32**]. The aircraft's propeller is driven by a 70 kW electric motor run on batteries and a 30 kW combustion engine generator [**32**]. The series configuration allows for more fuel efficient flight since the engine always runs at its ideal speed. It also allows for quiet takeoff in electric only operation [**32**].

In the RPA world, Bye Aerospace's unmanned HALE *Silent Sentinel* combines a turbofan engine with lithium-ion batteries recharged by solar panels [**9**]. Additionally, Glassock's work at Queensland University focuses on a battery hybrid of a similar size to the AFIT aircraft, but is ultimately more focused on boost speed than silent endurance capability [**21**]. The performance gains reported by Glassock are qualitatively similar to those noted by Flight Design: using the electric motor for boost power on takeoff reduced the required IC engine size, leading to improved aircraft performance, but not providing for significant electric only operation during loiter. Following the selection of the power sources, the drive train configuration is the second key decision preceding aircraft conceptual design.

2.4. Possible Configurations

Hybrid systems are categorized into one of three configurations: series, parallel, and split power. A schematic of a series configuration is shown below in Figure 2 [**33**]. In a series configuration, the IC engine is disconnected from the drive shaft and acts as a generator providing electric power to the motor which runs the drive train. The advantage of a series configuration is that the generator may operate at its peak efficiency and store surplus energy in batteries or fly wheels during periods of low demand for use during periods of high demand. The series configuration also has two disadvantages. First, the electric motor must be capable of providing full power for the vehicle which carries a large weight penalty. Second, there are large losses associated with the numerous power conversions of the series system. This makes the series configuration impractically heavy for an aircraft and it is instead typically found on heavy ground vehicles such a diesel trains.

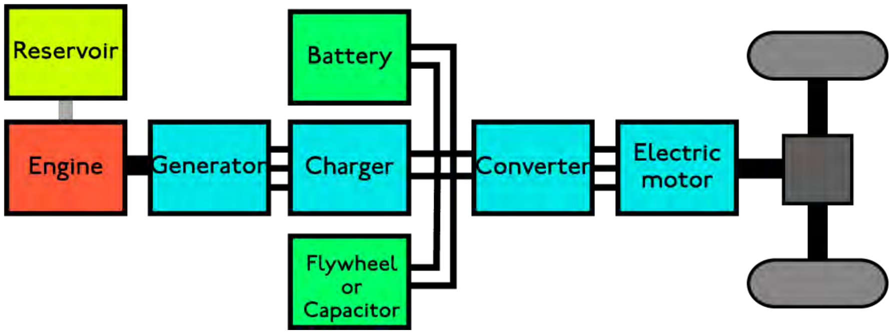

Figure 2: Series hybrid system configuration [**33**]

In a parallel configuration, the electric motor and the IC engine are both connected to the driveshaft by a mechanical clutch as shown in Figure 3 [**34**]. The electric motor operates in tandem with the IC engine in a capacity ranging from power assist to dual mode. Power assist uses the motor during acceleration to level out engine power requirements. The motor then acts as a generator during regenerative braking. Dual mode is the other end of the operational spectrum where 30% or more of the vehicle's power is provided by the electric motor. The Honda *Insight*, arguably the first mass produced hybrid automobile, uses Honda's *Integrated Motor Assist Technology*, which is essentially a power assist configuration [**35**]; the newer Chevrolet Volt is a dual mode configuration [**20**]. Since both engine and motor provide power to the drive train, the size of each component is reduced as neither needs to provide the maximum power required by the vehicle [**12**]. While a dual mode implementation increases the system complexity, the weight savings provide a significant advantage for implementation on aircraft.

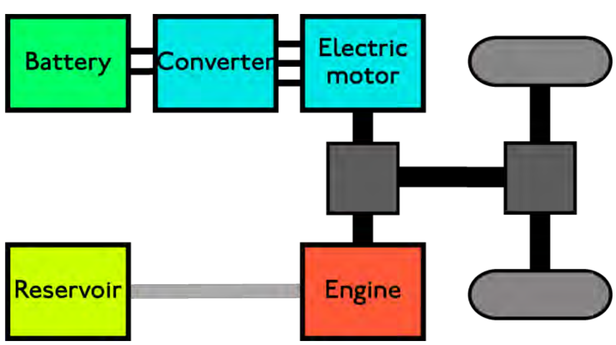

Figure 3: Parallel hybrid system configuration [**34**]

Finally, the split power configuration uses planetary gears to keep the electric motor in-line with the IC engine as shown in Figure 4 [**36**]. This configuration still benefits from the weight savings of a parallel system; the primary difference is the use of a planetary gear instead of a clutch. For example, the Toyota *Prius*, which entered the US market in 2001 and topped 1,000,000 sales in 2009, uses a split power configuration [**37**]. In the air, Aurora Flight Sciences is currently working on a diesel engine that places a motor/generator between the turbine and compressor, simplifying the design and operation of small diesel engines [**38**]. A team at the University of Colorado Boulder is also working on an HE-RPA utilizing planetary gearing [**39**]. Thus far, they have tested the planetary gearing system using two electric motors, but they have not yet tested an IC engine and electric motor configuration.

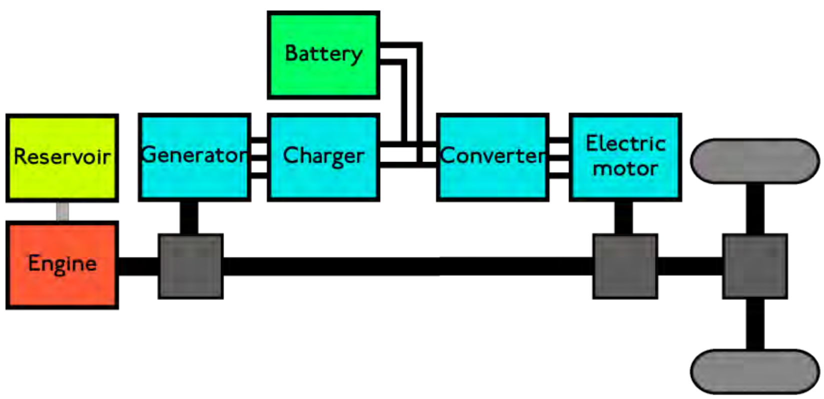

Figure 4: Split power hybrid configuration [**36**]

All of the configurations use control strategies to control when the various power sources operate. A high level overview of such strategies is presented in the next section to provide the remaining context for the AFIT aircraft conceptual design.

2.5. Hybrid Operational Modes

The operational modes for a hybrid-electric system are built upon three different strategies employed to control the batteries in the system: electric only, charge depleting, and charge sustaining. In electric only operation, the electric motor provides the sole power for the system, drawing its power from the batteries. In charge sustaining operation, the electric motor may provide power to the system, but the batteries are then recharged by the IC engine during a period of low demand. For example, the motor could intermittently provide boost power during climb and cruise. When the batteries reach some critical level, say 20%, the IC engine would engage and the motor would be used as a generator to recharge the batteries [**14**,**20**]. This strategy is used commonly in hybrid automobiles, such as the *Volt*, to extend the limited electric range of the vehicle. It is a challenging strategy to implement; care must be taken to manage the charge and discharge cycles of the batteries to prevent premature degradation or failure. In the charge depletion strategy, the electric motor pulls power from the batteries until they are depleted. This strategy is common in plug in vehicles such as electric scooters.

By combining these strategies, a variety of flight modes for an HE-RPA were developed by Harmon and implemented on a Microchip *PIC32 Microcontroller* by Greiser [**14**,**17**]. While there were a number of modes implemented to include aircraft startup and landing, the critical modes for aircraft operation are takeoff/climb, cruise, cruise with regeneration, and endurance. In takeoff and climb mode, the propulsion system draws power from the IC engine up to its ideal operating line and then engages the electric motor to provide additional power, which is referred to as a torque split strategy. During cruise with regeneration, the IC engine is operated at its most efficient point beyond the power required for cruise; the excess power is fed to the motor, now acting as a generator, to recharge the batteries. In cruise without regeneration, the IC engine provides only the power required to fly the aircraft. Lastly, endurance mode entails electric only operation of the aircraft.

2.6. AFIT Aircraft Design

To the best of the author's knowledge at the time of writing, the AFIT HE aircraft is the first demonstration of a functional parallel hybrid-electric propulsion system on an RPA, although there are some other similar project mentioned throughout the literature review. The AFIT aircraft was conceptually designed as a parallel dual-mode hybrid using batteries to supply the electric motor. The aircraft design is the culmination of work by a number of different parties, the first of which was Harmon. During his dissertation work at University of California–Davis, Harmon developed a neural network controller for a small hybrid-electric aircraft of approximately 30 pounds [**14**]. While the project focused mainly on the controller, Harmon also performed an initial conceptual design of the aircraft, shown in Table 1. The conceptual design was based on a two point static optimization. The aircraft was designed to minimize the power required during electric-only endurance [**10**]. This effectively minimizes the battery weight, electric motor weight, and maximizes the time available for near silent loiter. Then the ICE was selected to meet the cruise power requirement for ingress and egress. The mission profile used by Harmon stipulated one hour of ingress, one hour of near silent loiter, and an hour of egress [**10**].

Table 1: Conceptual design parameters for HE-RPA [**12**,**10**]

Design Parameter	**Harmon**	**Hiserote**	**Performance Parameter**	**Harmon**	**Hiserote**
Aspect Ratio	14.6	14.42	Maximum speed	~33 m/s	30.9 m/s
Wing Loading	90 N/m^2	90 N/m^2	Endurance time	1 hour	3 hour
Wing Area (S)	1.48 m^2	1.48 m^2	Cruise Speed	25.7 m/s	20.5 m/s
Wing Span (b)	4.65 m	4.62 m	**Aerodynamic Parameter**	**Harmon**	**Hiserote**
Wing Chord (c)	0.32 m	0.321 m	$C_{L,max}$	1.25	1.25
Aircraft Weight	13.6 kg	13.6 kg	$C_{D,o}$	0.036	0.036
Takeoff Altitude	1525 m (ASL)	1500 m (ASL)	Oswald Efficiency Factor (e)	0.85	0.85
Mission Altitude	1525 m (ASL)	300 m (AGL)			

Building on Harmon's work, Hiserote examined a number of configurations for the HE-RPA power train, simulating three power configurations and three battery operational modes. Hiserote compared the performance of clutch start, electric start, and dual propeller configurations in combination with charge depletion, charge sustaining, and segmented ISR battery strategies. In the clutch start configuration, the electric motor and the mechanical clutch are used to restart the engine in flight. Shutting down the engine in flight reduces the fuel consumption and acoustic signature during loiter. The electric start system is similar; however it uses a separate electric starter to restart the engine and allows for a one-way mechanical clutch to couple the motor and engine shafts. In the dual propeller configuration the engine and motor are completely decoupled and each drives its own propeller.

Hiserote optimized each aircraft configuration using code similar to Harmon's. Based on his results, both the electric start and dual mode configuration carried significant weight penalties, the first from the starter weight and the second from inefficiencies of a wind milling propeller. Likewise, the charge depletion strategy required excessive battery weight for all configurations. Thus, for a single 3 hour loiter, Hiserote determined a charge sustaining, clutch start configuration was preferable and an increased payload capacity through battery reduction was attainable if segmented loiter was acceptable [**11**]. The design details of Hiserote's charge sustaining aircraft for a single three hour loiter are shown alongside Harmon's in Table 1.

Following Hiserote's work, the development project split in a number of research directions. AFIT professors Lt Col Frederick Harmon and Dr. David Jacques acquired Office of the Secretary of Defense and Air Force Research Laboratory (AFRL) funding to purchase airframes and equipment for the aircraft, and airframes were ordered from startup company CLMax Engineering. Meanwhile, several other students continued development of the propulsion system components; those contributions will be mentioned in the following discussion of aircraft components.

3. Hybrid System Components

Figure 5 illustrates a block layout of a hybrid-electric, parallel propulsion system for a RPA. The major components are: IC engine, electric motor, propeller, batteries, mechanical clutch, and engine controller. The following is a presentation of each component from two aspects: first, an overview of the component's operation including the modeling equations and second, a discussion of prior work on components for similarly sized RPAs by other researchers.

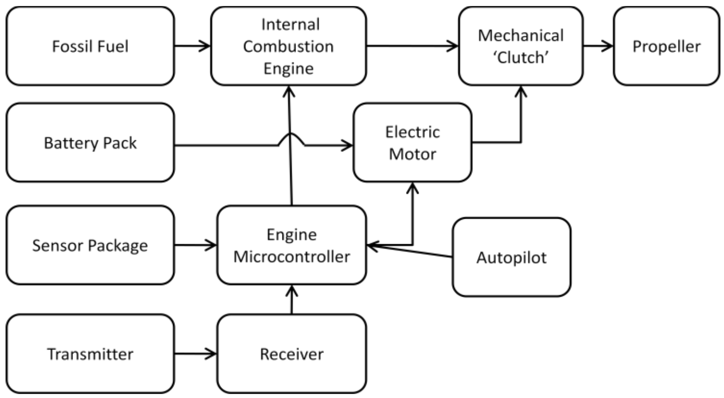

Figure 5: Components of HE-RPA propulsion system

3.1. Internal Combustion Engine

Internal combustion (IC) engines are one of the most common modern power sources. An IC engine harnesses the pressure and expansion of a gas from the combustion of fuel in order to drive a piston; it then converts the energy from linear motion to rotary motion to do work. Most large IC engines operate using the four-stroke Otto cycle depicted in Figure 6 [**40**]. As the name suggests, the cycle has four phases: air and fuel enter the cylinder, the mixture is compressed, the mixture ignites, combusts and expands, and finally, the combustion products are exhausted. Each revolution of the crankshaft only performs half of the cycle, and thus each cycle is two revolutions.

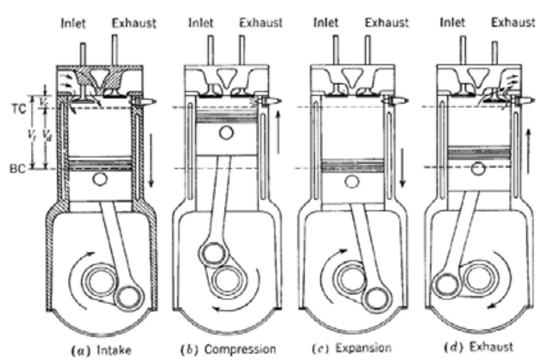

Figure 6: Four-Stroke Otto cycle for IC engine [**40**]

Many smaller IC engines use a two-stroke cycle, depicted in Figure 7 [**40**]. The two-stroke cycle combines the compression and intake strokes as well as the combustion and exhaust strokes resulting in one revolution per cycle. The cylinder head enables this combination by acting as a valve. As a result, two-stroke engines weigh less than comparable four-stroke engines and possess excellent power to weight ratios [**40**]. In return for their lower power to weight ratios, four-stroke engines offer better thermal efficiency, smoother operation, and lower torque spikes than their two-stroke counterparts [**15**].

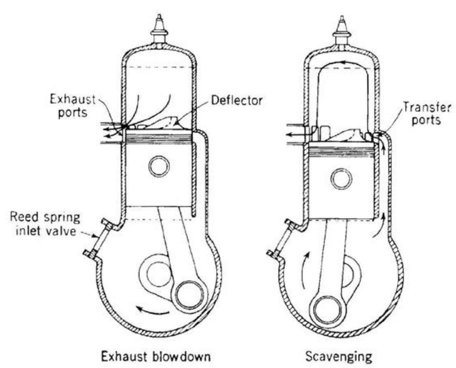

Figure 7: Two-Stoke cycle for IC engine [**40**]

An IC engine has a power conversion efficiency, η_f, expressed in Equation (1) as a function of specific fuel consumption, SFC, and the heating value of the fuel, Q_{HV} [**40**]. The specific fuel consumption is defined as the fuel consumption, represented by the mass flow rate of fuel, $\dot{m}_f$, per unit of shaft work represented by the power, P. Engine performance is frequently described using torque, Q, and power which are shown in Equations (3) and (4) where, MEP, is the mean effective pressure, V_d is the displacement volume of the cylinder, n_R is the number of strokes per cycle, and N and is the rotational speed [**40**]. However, since power and torque are dimensional quantities, mean effective pressure is commonly used to compare IC engines. As in Equation (5), MEP is the ratio of the per cycle work to the per cycle displacement. Larger values of MEP are indicative of increasing power to weight ratios. MEP can be calculated as in

Equation (5), using the volumetric efficiency, η_v, free stream air density, ρ_∞, and fuel to air ratio F/A [**40**].

$$\eta_f = \frac{1}{SFC \cdot Q_{HV}} \tag{1}$$

$$SFC = \frac{\dot{m}_f}{P} \tag{2}$$

$$\tau = \frac{MEP \cdot V_d}{2\pi \cdot n_R} \tag{3}$$

$$P = \frac{MEP \cdot N \cdot V_d}{n_R} \tag{4}$$

$$MEP = \frac{P \cdot n_R}{V_d N} = \eta_f \eta_v Q_{HV} \rho_\infty (F/A) \tag{5}$$

Most small RPAs use two stroke engines, capitalizing on their superior power to weight ratios. However, the reduced fuel economy due to higher specific fuel consumption is a costly tradeoff to save weight. Four-stroke engines provide clearly superior fuel efficiency, but with a lower power to weight ratio. Four stroke engines are also advantageous in a hybrid system containing a mechanical clutch since smoother operation reduces the wear on clutch plates and bearings.

Unlike electric motors, IC engine performance and efficiency are functions of air speed and altitude due to ram effect and air density. For the low speeds and altitudes of the RPA in this work, specific fuel consumption is relatively insensitive to changes in airspeed and ram effect [**41**]. Power, meanwhile, is drastically affected and Anderson suggests the following correction based on the free stream air density, where P_{SL} and ρ_{SL} denote the shaft power and the density at standard sea level, respectively.

$$\frac{P}{P_{SL}} = 1.132 \frac{\rho}{\rho_{SL}} - 0.132 \tag{6}$$

The prediction of small IC engine performance is inherently more empirical than electric motors, whose modeling equations are based on fundamental electricity equations with a handful of motor specific constants. This is due primarily to the elusive nature of sufficient theoretical models for small IC engines due to their complexity. Menon at University of Maryland has devoted a great deal of effort into developing a theoretical model for a small IC engine, including a complex combustion chemistry model, multiple heat transfer relations, and a fifth order Runge-Kutta solution of the differential equations [**42**]. Despite this effort, the calculated results differ wildly from testing, and thus hardware testing remains the best way to characterize small ICEs.

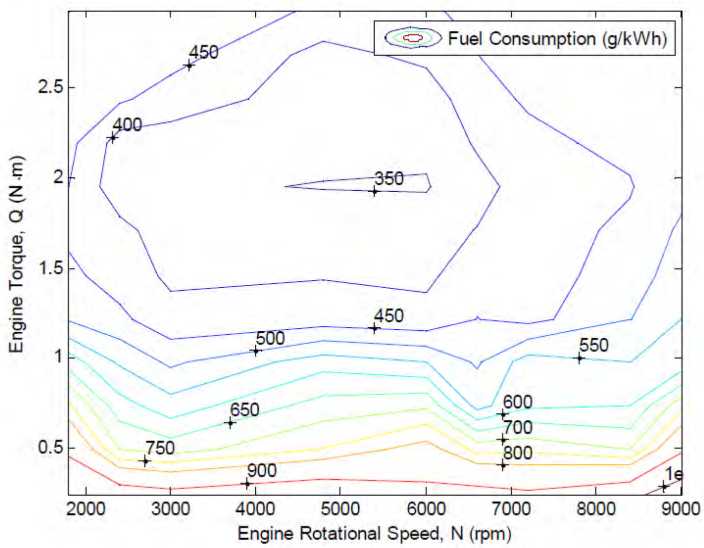

Figure 8: Sample engine efficiency map [**13**]

In any application, an IC engine should operate near its peak efficiency for a given power requirement and the relationship between torque, speed, and efficiency can be visualized in an engine efficiency map as shown in Figure 8 [**13**]. The plot shows torque plotted against speed with contours of constant fuel consumption. Ideally, the engine would operate in the 'island' which is less than full open throttle [**40**]. For a hybrid-electric system, this raises two points. First, the propeller speed and torque at cruise should fall in or near that maximum efficiency 'island' of the engine. Second, the engine controller should use the electric motor in power assist and recharge to keep the engine operating in or near the island if at all possible.

Finally, the engine's fuel, which is gasoline for many small IC engines, must be considered. While gasoline is the intended fuel for the AFIT aircraft, it may not be the ideal fuel in the long run. For example, the diesel cycle is similar to the Otto cycle, but uses heavier fuel, such as diesel, and a significantly higher compression ratio of up to 20:1 [**43**]. The fuel flash ignites due to temperature rise during compression; there is no spark plug. Studies have shown that a small diesel engine could double the fuel efficiency and thus endurance of a small aircraft [**7**]. However, small diesel engines have very poor power to weight ratios. Nevertheless, the Department of Defense continues to push military engines towards heavy fuels such as diesel and JP-8. These fuels have lower flashpoints than gasoline and are consequently safer to handle. Moreover JP-8 is also the standardized battle field fuel for both NATO and the Department of Defense, according to DoD Directive 4140.25 [**44**]. Therefore, while the current AFIT aircraft will run on gasoline, a future iteration could very well be a diesel electric hybrid.

3.2. Electric Motors

Relative to IC engines, electric motors are quiet and provide low speed, high torque power. This makes electric motors ideal for near-silent operation during endurance. Direct current (DC) electric motors are preferred over three phase alternating current (AC) motors for small aircraft since they are simpler to operate and because their power can be drawn directly from batteries without the use of a power inverter. However, some DC motors have low power to weight ratios, potentially making them too heavy for an airborne application. DC motors are divided into two categories: brushed and brushless. In a brushed DC motor, brushes, usually graphite, contact commutators on the rotor, completing a circuit through the windings on the armature. This circuit induces a magnetic field which repels the permanent magnets on the stator, causing the rotor to turn. As the rotor turns, the brushes transfer power to a different set of commutators, changing the magnetic field, and propagating the motion.

In a brushless motor, the electromagnets are mounted on the stator and permanent magnets are mounted on the rotor. A motor controller distributes power to the electromagnets, effectively switching the current and thus the magnetic field. In effect, the motor controller's distribution of power mimics a three phase AC motor. Brushless motors are further divided into two types: inrunner and outrunner. In an inrunner motor, the rotor is contained axially within the electromagnets and therefore the central shaft of the motor spins like a traditional brushed motor. In an outrunner, the permanent magnets on the rotor surround the electromagnets and the outer portion of the motor, including much of the casing spins. Inrunner motors provide exceptional speed but poor torque relative to outrunners. The lower speed and higher toque of outrunners make them ideal and commonly used for RC aircraft applications.

Brushless motors have fewer moving parts (no brushes) and are considered more reliable than brushed motors. Also, since they do not require a ferromagnetic core, brushless motors are significantly lighter and smaller than their brushed counterparts. However, while a brushed motor is controlled simply by setting its voltage and current, brushless motors required a speed controller, complicating their inclusion in a HE system [**45**]. Brushless motors also run at higher speeds than their brushed equivalents, potentially requiring additional gearing and mitigating some of the weight savings [**45**].

Figure 9 shows a model of an electric motor as presented by Lundström and similar to the model presented by Drela [**46**,**47**]. The Lundström model makes it clear that the current and voltage losses occur through the no load current, I_o, and in the internal resistance, R_m. Equations (7) through (11) are the classical linear equations for an electric motor. Equation (7) demonstrates that the motor torque, Q_m, is linearly proportional to the motor current, I, less losses, I_o, through the motor torque constant, k_t [**46**]. Equation (8) demonstrates an analogous relationship between the motor speed, ω_m, the voltage, V, and the voltage constant, k_v [**46**]. The shaft power, P_{shaft}, is the product of the motor speed and torque and the power into the motor, $P_{electric}$, is the product of the voltage and current [**46**]. The motor efficiency, η_m, is defined as the shaft power over the power into the motor [**46**].

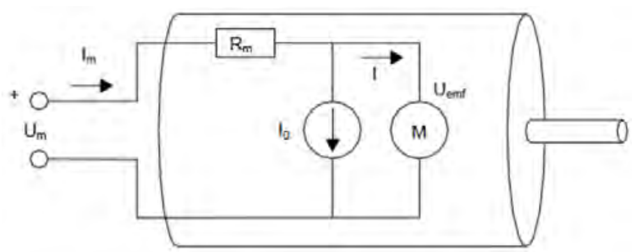

Figure 9: Model of an electric motor [**46**]

$$Q_m = (I - I_o) \cdot k_t \tag{7}$$

$$\omega_m = (V - I \cdot R_m) \cdot k_v \tag{8}$$

$$P_{shaft} = Q_m \cdot \omega_m \tag{9}$$

$$P_{electric} = I \cdot V \tag{10}$$

$$\eta_m = P_{shaft}/P_{electric} \tag{11}$$

Figure 10 shows typical motor torque, power, and efficiency curves as functions of speed and voltage, denoted by Drela as Ω [**48**]. The torque and efficiency diagrams are key when matching the electric motor to the propeller as discussed after the presentation of propellers. Lundström performed extensive testing on electric motors sized for 50-200W of power output, about 25% to 50% of the size required by the AFIT aircraft. He compared manufacturer data to test data and came to the following conclusions. First, and most importantly, motor manufacturer data is overly optimistic and actual efficiencies are typically several percent less than reported. Second, for smaller motors, the 'constant' motor parameters: k_v and k_t are not actually constant and instead demonstrate a positive linear relationship with voltage. Finally, he noted significant power losses in the electronic speed controller during low speed operation, due to actual power losses as well as switching losses in the generation of the PWM signal [**46**].

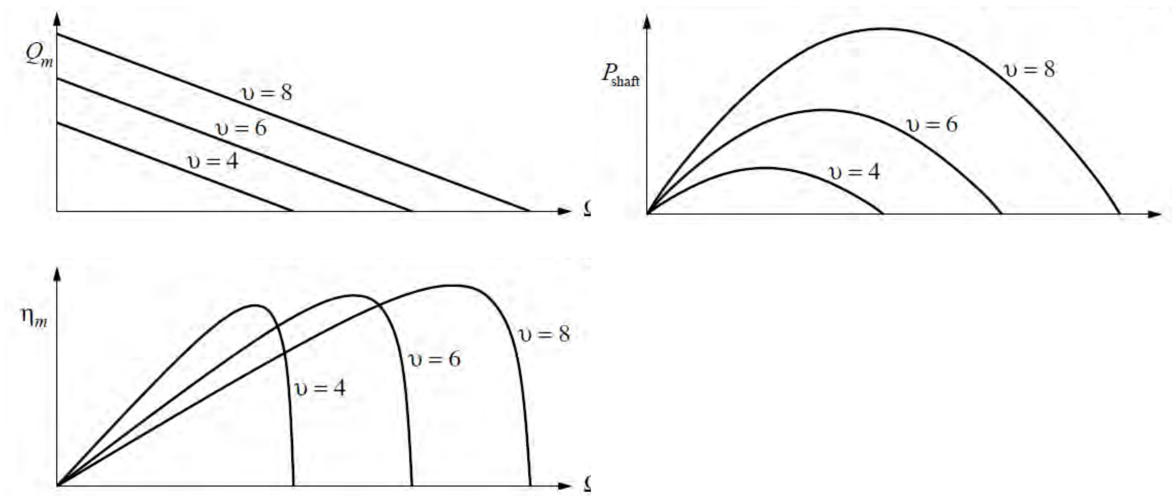

Figure 10: Characteristic motor variables as functions of speed and voltage [**48**]

3.3. Propellers

Unlike in an automobile, the shaft power in an RPA is delivered to a propeller, not a set of wheels, and the selection of a propeller is critical to efficient propulsion system design. A propeller is essentially an airfoil spun axially such that its lift generates thrust for the aircraft. The propeller power, P_{prop}, can be expressed by the power delivered to the propeller shaft, P_{shaft}, multiplied by the propeller efficiency, η_{prop}, or equivalently by the product of the flight velocity, V_∞, and the thrust, T, as presented in Equation (12) [**49**]. The efficiency of the propeller can be expressed in terms of the advance ratio, J, the thrust coefficient, C_T, and the power coefficient, C_P, shown in Equations (13) through (16) where D is the propeller diameter [**49**]. The torque coefficient, C_Q is listed for completeness in Equation (17) [**49**].

$$P_{prop} = P_{shaft} \cdot \eta_{prop} = T \cdot V_\infty \tag{12}$$

$$\eta_{prop} = J\frac{C_T}{C_P} \tag{13}$$

$$J = \frac{V_\infty}{\omega_{prop} \cdot D} \tag{14}$$

$$C_T = \frac{T}{\rho_\infty {\omega_{prop}}^2 D^4} \tag{15}$$

$$C_P = \frac{T}{\rho_\infty {\omega_{prop}}^3 D^5} \tag{16}$$

$$C_Q = \frac{Q}{\rho_\infty {\omega_{prop}}^2 D^4} \tag{17}$$

The advance ratio describes the ratio of the free stream air velocity to the advance of the propeller, which is the distance it would advance axially in one rotation. Propellers are usually denoted with two numbers: AAxBB where for a standard APC propeller, AA is the diameter in inches and BB is the propeller's advance in inches. The advance ratio, thrust coefficient, and torque coefficient are used to compare propellers of similar geometry.

Figure 11 shows characteristic plots of propeller torque, thrust, and efficiency as functions of flight velocity and rotational speed, which Drela denotes as Ω [**48**]. Such plots are generated from the plots of efficiency, torque coefficient, and thrust coefficient versus advance ratio (denoted as λ) by picking a flight velocity and varying the rotational speed to generate the curves. Thus, both the electric motor and the propeller have distinct efficiency characteristics that are functions of rotational speed as well as voltage for the motor and flight velocity for the propeller. From first principles, the propeller-motor system will operate where the torque provided by the motor is equal to that required by the propeller at the operating airspeed. In an ideal system the intersection would occur at or near the peak efficiency of both components [**48**]. Examples of both a well matched and a poorly matched system are shown below in Figure 12. Clearly, matching the propeller to the electric motor is critical for efficient vehicle operation and to extend the life of the batteries. Moreover, for a hybrid system, the propeller must also be matched to the IC engine, presenting an additional challenge for the aircraft designer. A variable pitch propeller may ease some of these issues for some additional cost and complexity.

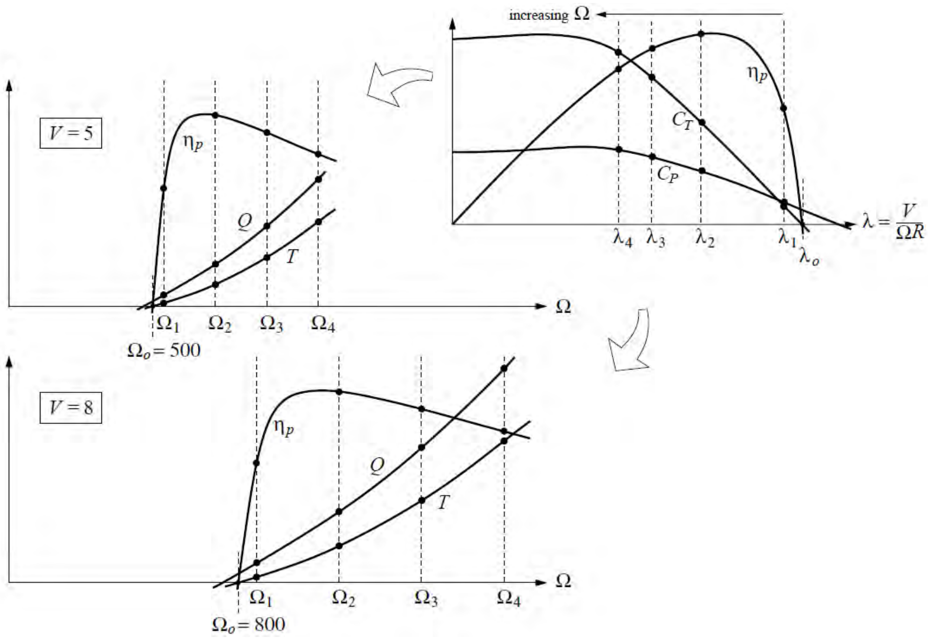

Figure 11: Characteristic propeller plots [**48**]

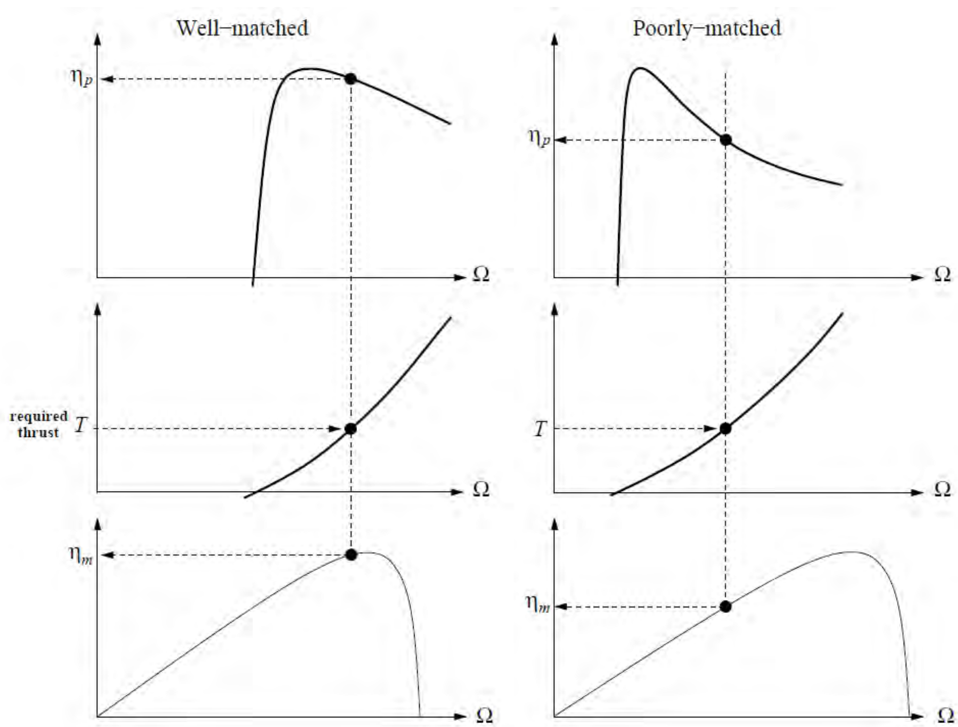

Figure 12: Well matched and poorly matched propeller-motor combinations

The rapid growth of the UAV market has been followed lock-step by propeller studies. Since 2006, Wichita State University has developed an extensive database of wind tunnel test data for propellers ranging from 6 to 24 inches in diameter using their Integrated Propulsion Test System [**49**]. AFIT graduate student Capt Todd Rotramel developed code to perform motor-propeller matching for the AFIT aircraft, which draws on this data [**13**]. In 2008, Deters and Selig at the University of Illinois Urbana-Champaign collected a large amount of data for micro UAV propellers in the 2 to 10 inch range. They found increasing propeller diameter and decreasing pitch produced the highest propeller efficiencies [**50**]. Selig and Uhlig studied the 3D effects on propellers due to twist and tip effects during stall, effects that led to significant discrepancies with modeling simulations using only 2d airfoil data. They determined while correction for the effects is possible, it requires propeller test data [**51**]. Also in 2008, Ol and Zeunne from the Air Force Research Laboratory collected propeller data, which they correlated with theoretical predictions based on blade sectioning techniques. They found blade sectioning (modeling the blade as finite slices) yields accurate results that improve as the Reynolds number increases [**52**]. Finally, in 2009 Gur and Rosen performed an extensive propeller optimization study aimed not only at maximizing the aerodynamic efficiency of the propeller, but also minimizing its acoustic signature and maximizing its structural integrity. As the acoustic requirement becomes more demanding, the propeller operational speed decreases, the pitch increases, and more power is required from the motor and engine [**53**]. Clearly, the propeller is both a complicated and crucial component of the HE-RPA.

3.4. Batteries

Batteries lie at the center of the technological push for hybrid-electric vehicles. A battery is defined as a closed system where chemical reduction-oxidation reactions at the anode and cathode generate electric energy [**54**]. In a battery, the reacting chemicals are contained in the cell unlike fuel cells where the chemicals are delivered to the cell. Batteries are characterized by their specific energy and specific power. Specific energy is the energy per unit mass in the battery and the specific power is the power output of the battery per unit mass. When plotted against each other, these parameters form a Ragone Plot, a sample of which is shown in Figure 13 [**55**]. Since the specific energy is directly related to the cell's endurance and specific power is related the cell's discharge rate, an ideal power source would lie in the top right corner of the Ragone plot.

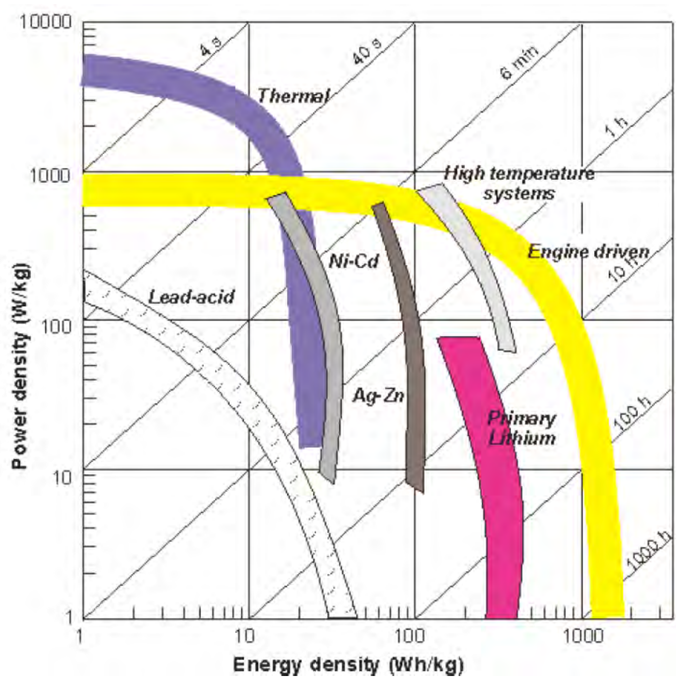

Figure 13: Ragone plot for common rechargeable batteries [**55**]

Batteries are advantageous for a hybrid system for multiple reasons: they provide high efficiency, on demand power without any pumps or filters and they are insensitive to physical orientation. However, their specific energies are less than 1/40th of fossil fuels, making battery weight the driving limitation on hybrid-electric vehicle endurance, especially for aircraft. Table 2 compares a variety of rechargeable battery chemistries and their specific energies. Lithium-ion (Li-Ion) and lithium-ion polymer (Li-Po) have largely replaced nickel-cadmium (Ni-Cd) and nickel-metal-hydride batteries (NiMH) batteries in the RPA industry due to their significantly higher specific energies. Additionally, Li-Ion and Li-Po batteries have no cell memory and do not self discharge, problems that plague the older chemistries.

Table 2: Comparison of typical rechargeable batteries [**56**,**57**,**12**]

	Ni-Cd	NiMH	Li-Ion	Li-Po	Li-S
Specific Energy (Wh/kg)	45-80	60-120	90-200	130-240	250-600
Cycle Durability	1500	300-500	300-1000	500-1000	100
Nominal Voltage per cell (V)	1.25	1.25	3.3-3.8	3.7	2.1

Unfortunately, lithium batteries are less stable than the older battery chemistries and require exacting charging procedures. Rechargeable batteries are characterized by a charging current called the C-rate, which is best illustrated by example. A 1000 mAh battery can provide 1 A of current for one hour at a 1C-rate. Or, the same battery can provide 2 A of current for 30 min at a 2C-rate. Either way, the battery then recharges at a 1C-rate, but it takes closer to three hours for a full charge; increasing current will not increase the rate of charge [**12**]. Furthermore, excessive charging current can cause the batteries to explode or ignite. These instabilities have lead to the prohibition of certain lithium chemistries in RPA competitions such as the AIAA, Cessna, and Raytheon Design, Build, and Fly Competition. Thus the charging characteristics of the batteries play a significant role, especially during recharge, in a hybrid-electric system.

Several groups have performed significant research on modeling and simulating lithium batteries for scale-up and inclusion in RPA systems. A team at Boundless Corporation in Boulder, Colorado developed battery controllers allowing safe inclusion of lithium batteries on a small RPA. Their system monitored individual packs for excessive temperature and cell polarity reversals and provided the operator with real time feedback and the capability to reallocate energy draw in the case of cell malfunction or overheating [**58**]. Meanwhile, several groups have developed mathematical models of Li-Ion and Li-Po battery discharge and recharge that are useful for scale-up and/or dynamic simulation of a hybrid-electric propulsion system [**59**,**60**]. Finally, companies like Sion power continue to push the envelope of battery chemistry to deliver higher energy density, longer battery life cycles, and more stable chemistries [**57**]. These improvements should increase the viability of hybrid-electric vehicles of all types, especially aircraft.

3.5. Mechanical Clutch

In a parallel hybrid system, a clutch is required to combine the power of the hybrid components, in this case the electric motor and the IC engine. There are two primary requirements imposed on such a mechanism. First, it must allow the electric motor to operate the propeller with the IC engine disengaged to facilitate endurance mode. Second, it should allow the electric motor to apply a torque to the IC engine shaft, enabling the midair restart of the IC engine, although this is not 100% critical at the proof-of-concept stage. There are three potential clutch mechanisms for an HE-RPA: an electromagnetic clutch, a centrifugal clutch, and a clutch bearing, each with its own advantages and disadvantages.

An electromagnetic clutch uses an induced magnetic field to transmit mechanical work. There are many different types of electromagnetic clutches, but the most common type is the single face clutch, which consists primarily of a coil, hub, armature, and rotor [**61**]. When there is no current passing through the coil, the armature and rotor rotate independently, and the clutch is disengaged. When a current is passed through the coil it induces a magnetic field, which attracts the magnets on the rotor and causes the rotor to spin and transmit torque. The equation for magnetic field strength, B, is shown in the Equation (18) which is a formulation of the Biot-Savart law where: μ_o is the magnetic dipole moment, I_{clutch} is the coil current, r is the distance from the coil element dl to the point of interest, and u is the angle between the coil element and the vector, r [**61**]. As the coil current increases the field strength increases, allowing for a greater transmission of torque. A schematic of an electromagnetic clutch is shown in Figure 14.

Electromagnetic clutches offer two way torque transmission and can be engaged or disengaged at any speed. However, they are typically too heavy or prohibitively expensive for an expedient prototype aircraft application.

$$B = \int \frac{\mu_o I_{clutch}}{4\pi} \cdot \frac{\sin u \, dl}{r^2} \tag{18}$$

Figure 14: Schematic of an electromagnetic clutch [**61**]

Centrifugal clutches are common in handheld gasoline powered tools such as weed whackers and chainsaws as well as golf carts. A chainsaw centrifugal clutch is shown in Figure 15 [**62**]. The centrifugal clutch has weighted arms that are pulled radially inwards by extension springs. When the shaft connected to the arms spins, the arms rotate and extend radially against the springs due to centrifugal motion. When the shaft extends far enough, the friction pads on the arms contact the housing and the clutch engages, transmitting torque to the second shaft. Centrifugal clutches are reliable and inexpensive, however, they can be heavy and generally do not provide two way engagement at low speeds. This could prevent in flight restart of the engine using the electric motor.

Figure 15: Centrifugal clutch from a chainsaw [**62**]

A third option to link the two shafts is a one-way bearing, formally referred to as a clutch bearing. A one-way bearing is shown in Figure 16 [**63**]. During rotation in one direction, the shaft rolls freely along the pins, just as in a roller bearing. When the inner shaft turns the opposite direction, the rollers press against the springs which bind them in place, stopping the inner shaft and transmitting torque to the shaft attached to the outside of the bearing [**63**]. Based on a brief market survey, one-way bearings of an appropriate size are very light weight and inexpensive compared to both electromagnetic and centrifugal clutches. However, clutch bearings have a number of drawbacks. First, they only engage in one direction, precluding a mid air restart of the IC engine. Second, they can be noisy at high speeds, a potential issue if employed on a silent aircraft. Finally, the torque spikes of the engine may cause premature fatigue failure of the springs in the one-way bearing, causing it to bind or become a two-way bearing. Nevertheless, their low cost and weight made one-way bearings the choice for the first flight test iteration of the AFIT hybrid-electric system.

Figure 16: Clutch bearing with metal springs [**63**]

3.6. Hybrid Controller

If an autopilot or flight computer is the brain of a modern aircraft, then the hybrid controller is the brain of a hybrid-electric system. While an autopilot stabilizes the aircraft and controls the heading and altitude, the hybrid controller converts throttle requests into control signals for the electric motor and IC engine. It is conceivable that as hybrid-electric systems advance, these control schemes will be programmed directly into the autopilot. For now, due to the limitation of commercially available autopilots, it is preferable from a coding standpoint to use two separate controllers. In the AFIT aircraft, the autopilot is a Procerus Technologies Kestrel and the intended hybrid controller is a custom controller implemented on a Microchip PIC32 microcontroller, both shown in Figure 17.

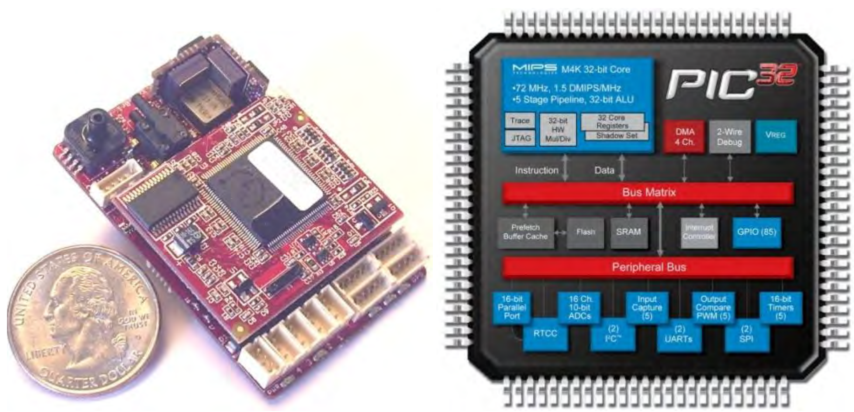

Figure 17: Procerus Technologies Kestrel autopilot (left), Microchip PIC32 Microcontroller (right) [**64**,**65**]

A comprehensive survey and explanation of control schemes, algorithms, and implementations is beyond the scope of this thesis. Thus, only the controller background specific to this project is presented. There are numerous different types of controllers; some of the most common are rule-based, fuzzy logic, and neural networks. Harmon's initial work was with neural networks applied to an HE-RPA [**14**]. Harmon also used rule based controllers to check/verify his neural networks, and those rule based controllers laid the groundwork for the AFIT RPA engine controller. Rule based controllers are simply a set of rules that establish criteria for switching between different operational states. The rule based switching between these states is referred to as a state machine and rule based controllers and associated state machines are easily represented in flow charts such as that shown in Figure 18, where the event (condition) button click, cycles between two states, 'on' and 'off'.

In his Master's Thesis at AFIT, Lt Collin Greiser combined Harmon's rule based control schemes with the ideal operating line as conceived and tested by Fransisco [**66**] and rule based control schemes for continuously variable transmissions from the work of Schurhoff [**67**]. The ideal operating line is the line on the torque map that represents the maximum fuel efficiency at each speed. In Fransisco's work, he proposed running the engine on its ideal operating line, making up for high demand with the electric motor and using surplus power to recharge the batteries during low demand. While Fransisco's work was originally on automobiles, these same principles can be applied to a hybrid-electric system in an aircraft. Meanwhile Schurhoff developed several control strategies for a continuously variable transmission including: sloped engagement, stepped engagement, and several torque split strategies [**67**]. For more details on these methods, see either Greiser's or Schurhoff's work [**17**,**67**].

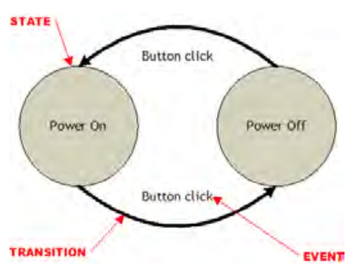

Figure 18: Simple state machine [**68**]

Greiser then implemented these rule based algorithms on a Microchip PIC32 microcontroller with custom firmware, developed specifically for this application. The firmware, referred to as The PIC32 Lightning project, was the work of John Hagen [**16**]. The firmware provides a layer of abstraction from the machine language native to the PIC32 allowing the user to write his or her state machine in 'English' as opposed to 'code'. The firmware also provides an assortment of useful functions, such as the ability to read in shaft rpm from a sensor without the user worrying about setting the controller pins, interrupts, and so forth. Greiser performed preliminary testing on his state machine for his thesis, but more testing is required, especially with the motor and engine running in combination. Such ground testing will be a prerequisite to flight test of the system.

4. Flight Test

There are two objectives of this work. The first goal is to complete and integrate a previously developed hybrid-electric system into an airframe. The second objective is to test that hybrid-electric system and compare its performance to the performance predicted using Hiserote's model [**12**]. When flight testing an RPA the instrumentation weight must be smaller than for a manned aircraft; meanwhile the measured quantities are also smaller requiring lower sensor ranges and higher accuracies. This section examines the key parameters the flight test should determine, the accompanying variables and instrumentation, and finally a brief overview of ground and flight test techniques.

4.1. Performance Parameters and Calculation Techniques

The critical parameters for the HE-RPA for this initial flight test focus on the operational capabilities unique to the aircraft, in this case the flight endurances, ranges, and velocities required to perform a near silent ISR mission. While normally that would include the aircraft's acoustic signature, such a project would be its own thesis and is beyond the scope of this work.

4.1.1. Cruise and Endurance Time

The three most important aircraft performance benchmarks for this project are the endurance time on target, the time (or range) available for one-way cruise to the target, and the acoustic signature of the aircraft, although the latter is out of scope for this work. The Flight Test

Handbook used at the United States Air Force Test Pilot School provides several basic techniques that are adaptable to a small HE-RPA. During cruise operation, the aircraft will run primarily on the IC engine, thus its range will be primarily a function of fuel burn. The Flight Test Handbook initially suggests simply measuring fuel flow rate, $\dot{m}_f$, while the aircraft is trimmed at its cruise condition and then extrapolating the range, R, based on the amount of fuel available, m_f, and the aircraft velocity as in Equation (19) [**69**]. Such a calculation assumes the weight of the aircraft is constant wherein reality the aircraft weight decreases as fuel is consumed. As the weight decreases the aircraft can be re-trimmed at a smaller angle of attack, decreasing its drag. Therefore an improved form of the calculation is the Breguet range equation for a propeller driven aircraft presented by both Payne and Anderson and shown in Equation (20), where W_1 and W_0 are the full fuel and no fuel aircraft weights, respectively, L/D is the lift to drag ratio, and c_{SFC} is the power specific fuel consumption as defined in Equation (21) as the rate of fuel consumption per unit shaft power [**41**,**69**]. Unlike the corresponding expression for a jet aircraft, the propeller range equation is not a function of air density. Also note that Equation (20) does not account for wind speed. Finally, observe that the most efficient cruise condition for a propeller driven aircraft occurs at $(C_L/C_D)_{max}$ [**41**].

$$R = \frac{m_f}{\dot{m}_f} V_\infty \tag{19}$$

$$R = \frac{\eta_{prop}}{c_{SFC}} \frac{L}{D} \ln \frac{W_0}{W_1} \tag{20}$$

$$c_{SFC} = -\frac{\dot{m}_f}{P} \tag{21}$$

Anderson and Payne also present the Breguet endurance equation, derived to maximize loiter time and shown in Equation (22), where E is the endurance time [**41**,**69**]. Like the range equation, the endurance equation accounts for fuel burn during loiter and suggests that endurance can be maximized by operating at $\left({C_L}^{3/2}/C_D\right)_{max}$. Equation (22) presents a conundrum for battery powered aircraft, which do not experience a decrease in weight during battery only operation: their endurance time, as per Equation (22) is zero. Thus a return to the original range strategy suggested by Payne is appropriate; by measuring the rate of battery drain at the endurance flight condition, the endurance time can be extrapolated based on a battery capacity, E_{bat}, as in Equation (23), where $\bar{I}$ and $\bar{V}$ are the average current and voltage draw, respectively [**69**]. Additionally, the velocity for maximum endurance during electric only operation will occur at the minimum power required.

$$t_{end} = \frac{\eta_{prop}}{c}\sqrt{2\rho_\infty S}\frac{{C_L}^{3/2}}{C_D}\left(\frac{1}{\sqrt{W_1}} - \frac{1}{\sqrt{W_0}}\right) \tag{22}$$

$$E = \frac{E_{bat}}{\bar{I}\bar{V}} \tag{23}$$

4.1.2. Velocities, Climb Rate, Turning

Secondary to the cruise range and endurance time are a number of operational velocities, the climb rate, and the turning radius of the aircraft. As described by Anderson, each of these can be determined graphically or analytically. This section covers both the graphical and analytical approaches, although it is restricted to steady flight as per the initial test objective of this work.

The graphical techniques are dependent on a plot of two curves: the power required by the aircraft and the power available to the aircraft, both as a function of velocity. The power required in steady flight, P_R, is simply the product of drag and velocity as in Equation (24) [**41**]. Thus the power required can be determined from the aircraft's drag polar, which is a function of the airframe and essentially independent of the propulsion system; the drag polar can be determined from a non-hybrid variation of the aircraft, before the hybrid version ever flies. Typically the drag polar is presented a shown in Equation (25), although some sources use a third linear term for improved fidelity [**41**]. $C_{D,o}$ and K are constants determined by flight test where $C_{D,o}$ is the zero lift drag coefficient. Once the drag polar is known, various ratios of ${C_L}^n/C_D$ can be calculated.

$$P_R = D \cdot V_\infty \tag{24}$$

$$C_D = C_{D,o} + K{C_L}^2 \tag{25}$$

The power available, P_A, represents the maximum capability of the engine-propeller combination at a given flight velocity, as presented in Equation (26) [**41**]. A sample plot of the power available and power required curves is shown in Figure 19; a similar plot uses thrust in lieu of velocity, and the difference is merely a factor of V_∞ [**70**]. Using these curves, Anderson describes methods for finding the maximum, stall, endurance, and cruise velocities as well as the rate of climb and a rough technique for turn performance, each of which will be described shortly. Clearly, determination of the drag polar and the power available is critical for aircraft evaluation.

$$P_A = \eta_{prop} P \tag{26}$$

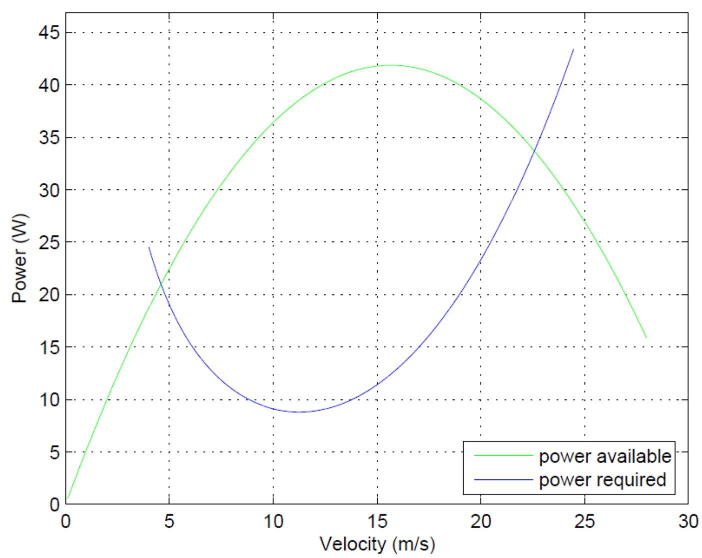

Figure 19: Sample power required and power available curves [**70**]

The maximum velocity occurs at the right intersection of the power available and power required curves and is the point where the aircraft lacks sufficient power to overcome any additional drag from an increase in speed. The maximum velocity may be calculated analytically as in Equation (27) (using the '+' from the ±) where $T_{A,max}$ is the maximum available thrust. The stall speed may occur at the left intersection of the power available and power required curves, and if that is the case, Equation (27) (using the '-' from the ±) provides the appropriate calculation [**41**]. Stall under Equation (27) implies the aircraft lacks sufficient power to fly any slower. However, one should also check the stall speed calculated using $C_{L,max}$ shown in Equation (28), which corresponds to stall due to insufficient lift [**41**]. The larger of the velocities from Equations (27) and (28) should be used as the stall velocity. The cruise velocity is the speed for maximizing range of the aircraft. To find it graphically, the power curves must be converted into thrust curves. The velocity for maximum range then occurs at the minimum thrust required, which is the $(C_L/C_D)_{max}$ condition for a propeller aircraft. The analytical expression of cruise velocity for a propeller aircraft is given in Equation (29) [**41**]. The endurance speed occurs at the minimum power required and corresponds to the maximum $\left(C_L{}^{3/2}/C_D\right)_{max}$ condition. Its analytical expression is given in Equation (30) [**41**].

$$V_{max/stall} = \sqrt{\frac{\frac{T_{A,max}}{W}\frac{W}{S} \pm \frac{W}{S}\sqrt{\left(\frac{T_{A,max}}{W}\right)^2 - 4C_{D,o}K}}{\rho_\infty C_{D,o}}} \tag{27}$$

$$V_{stall} = \sqrt{\frac{2}{\rho_\infty}\frac{W}{S}\frac{1}{C_{L,max}}} \tag{28}$$

$$V_{cruise} = \sqrt{\frac{2}{\rho_\infty}\frac{W}{S}\sqrt{\frac{K}{C_{D,o}}}} \tag{29}$$

$$V_{endurance} = \sqrt{\frac{2}{\rho_\infty}\frac{W}{S}\sqrt{\frac{K}{3C_{D,o}}}} \tag{30}$$

There are a number of ways to calculate the rate of climb and the simplest is for a steady, constant velocity climb. By assuming a climb angle of less than 15 degrees, one can assume the excess power is equal to the power available to climb [**41**]. The excess power is simply the power available less the power required. Divided by aircraft weight, the excess power yields the climb rate R/C as in Equation (31). The largest vertical distance between the power available and required curves will give the maximum rate of climb.

$$R/C = \frac{excess\ power}{W} = \frac{\eta_{prop}P - TV_\infty}{W} \tag{31}$$

A similar analysis can be used to find the minimum turning radius for a banked turn. Banking decreases aircraft lift, which essentially eats away at the excess power margin. Banking on the verge of stall gives the steepest possible bank angle and the minimum turning radius. Anderson presents the velocity for minimum turn radius and the corresponding radius as Equations (32) and (33) respectively, where T/W is the thrust to weight ratio at the flight condition [**41**]. The load factor, $n_{R,min}$, which should be considered to prevent structural damage to the aircraft, is given in Equation (34). If the load factor exceeds its maximum allowable value, permanent airframe deformation or even airframe failure will occur. Clearly, the drag polar, power available, battery voltage and current draw, and fuel usage are critical parameters to characterize aircraft performance and measurement techniques are discussed next.

$$V_{R,min} = \sqrt{\frac{4K(W/S)}{\rho_\infty(T/W)}} \tag{32}$$

$$R_{min} = \frac{4K(W/S)}{g\rho_\infty(T/W)\sqrt{1 - \frac{4KC_{D,o}}{(T/W)^2}}} \tag{33}$$

$$n_{R,min} = \sqrt{2 - \frac{4KC_{D,o}}{(T/W)^2}} \tag{34}$$

4.2. Measured Variables and Instrumentation

As mentioned in the engine controller section, the aircraft uses a Procerus Technologies *Kestrel Autopilot*. The *Kestrel* comes equipped to measure a variety of flight telemetry including airspeed, attitude, pressure (pitot static), battery current, and battery voltage [**65**]. While the *Kestrel* provides necessary data, noticeably absent in the basic Kestrel capability is the fuel usage, propeller shaft speed, and engine throttle position. Also, there is no capability to measure the thrust generated by the propulsion system, which will be discussed in Ground and Flight Testing. Procerus does provide a sensor expansion board for the *Kestrel*, but the limited slots may not provide sufficient instrumentation for the aircraft, especially since some of the channels may be dedicated to safety features such as an engine kill switch. Thus other telemetry options were explored.

Eagle Trees Systems are frequently used for remote controlled (R/C) aircraft and RPA telemetry. The company manufactures a wide variety of sensors and data logging chips that are an R/C hobbyist industry standard. In their work on small UAV flight test, Ostler et al utilized an Eagle Tree Systems *Seagull* instrumentation package in conjunction with a Procerus *Kestrel* [**71**]. The *Seagull* provides shaft rpm (optical and magnetic), battery voltage and current, pressure, airspeed, servo position, and a variety of other sensors [**72**]. Again note that there is no fuel flow measurement capability using the *Seagull*. When located, a suitable fuel sensor could be integrated into the *Kestrel*, *Seagull*, or even the engine controller. Most commercially available fuel flow sensors are not designed for small RPAs and their weight is prohibitive or their accuracy is too limited. Thus fuel instrumentation remains an untackled challenge for flight test instrumentation. Since fuel flow, throttle setting, and engine speed can be measured on the dynamometer and the throttle setting and engine speed can be measured in flight, the engine speed and throttle setting can be used with the engine map from bench testing to estimate the fuel burn rate and in turn the BSFC in flight.

4.3. Ground and Flight Testing

To calculate the desired performance parameters, the power required and the power available curves are the only two quantities that cannot be measured directly. Both require knowledge of the thrust or power the aircraft is using or capable of at a given flight condition. The flight velocity, altitude, density, angle of attack, and aircraft weight are all available from preflight measurement or from the *Kestrel*. The speed of the propeller shaft is measurable using the *Seagull*. Unfortunately, it is inordinately difficult to measure the torque delivered to the propeller shaft or the thrust of the aircraft directly. Oslter et al experienced this same issue during their flight test of electric MAVs. To circumvent the problem, they developed motor-propeller operation curves in a wind tunnel by plotting thrust as a function of airspeed and throttle position. They then matched the airspeed and throttle of the trimmed aircraft to the map to determine both the power required and power available at that speed [**71**]. The same basic analysis could be applied one step further if no wind tunnel was available for testing. The hybrid system could be tested independently on a dynamometer to generate performance curves for the hybrid system by plotting torque as a function of shaft speed and throttle setting. AFIT already has a dynamometer setup used by Lt Collin Greiser and Capt Isseyas Mengistu for their prior work on this project [**15**,**17**]. For a known operating condition, the torque from the map and the aircraft velocity could be matched to propeller data as described in Section 3.3. Thus the thrust, power required, and power available for the trimmed aircraft could be determined solely by measuring velocity, shaft speed, and throttle setting in the air and 'matching' it to data collected on the ground, which Oslter found provided excellent results [**71**].

Such a setup could even be taken one step further as done during test of a fuel cell hybrid system at the University of Colorado [**30**]. During the test, the hybrid system was placed on a dynamometer, which fed its torque signal into a computer running an aerodynamic simulation of the aircraft. The computer simulation generated a thrust request, which was sent to the engine controller, allowing the system to effectively flight test the propulsion system. Bradley refers to this as Hardware-in-the-Loop testing [**30**]. Since the aerodynamic coefficients for the computer simulation could be obtained from a non hybridized airframe with appropriate ballasting, such a test creates a new set of opportunities for testing the propulsion system in an environment more controlled, predictable, and repeatable than an actual flight test. Furthermore, such a setup with even manual control of the dynamometer provides a test bed for the engine controller as indicated. However, in this project, such testing will remain a means to an end: namely, integration to flight test.

III. Methodology: System Integration

1. Chapter Overview

This chapter examines the integration of COTS components into a HE propulsion system. The chapter begins with a detailed description of the objectives and a generic overview for the hybrid system along with a description of the intended airframe. The remainder of the chapter examines the selection, testing, and integration of each component, concluding with the final system for testing and validation.

2. System Objectives and Overview

2.1. System Objectives

The overall objective for the project is to instantiate, demonstrate, and validate a HE system for a small RPA; thus, there must be a set of objectives for the system itself. Those objectives are best described in the context of the mission concept presented in Chapter I, Figure 1. The system should leverage electric power for near silent endurance and ICE power for extended range. The ICE and EM should operate in tandem to provide boost power during demanding mission legs such as takeoff and climb. Using the EM to supplement the ICE during cruise should permit the ICE to operate at its most efficient point, tacitly improving the fuel economy of the aircraft. When engine power supply exceeds demand, the EM should act as an electric generator to recharge the batteries. Finally, it must be possible to reduce the acoustic signature of the ICE for near silent loiter, either with a mid air restart mechanism allowing the ICE to turn off during loiter or by idling the ICE during loiter if the ICE at idle is quieter than the propeller and airframe.

A final objective, not addressed in Chapter I for brevity and clarity, is the use of all commercial of the shelf (COTS) components when constructing the system. In the Department of Defense, there is an underlying and growing belief that COTS components reduce costs across the acquisition lifecycle and ease some of the logistical burdens of supply chain management.

Regardless of the veracity of the statement, COTS parts are faster and less expensive to obtain than their custom manufactured counterparts, making them preferable for an 18 month research effort. Therefore, this effort will use COTS parts as much as possible during the integration of the system and, to an extent, provide a case study in using COTS for a fast prototyping effort.

2.2. Generic HE System

Figure 20 shows the basic components of a HE propulsion system for a small RPA. The depicted setup is a parallel power train, meaning the ICE and EM can independently power the aircraft as described in Chapter II. Starting with the top power train, the ICE converts hydrocarbon fuel into mechanical energy, which is transmitted through a mechanical linkage to the propeller. In the second power train, the EM converts stored chemical energy in the batteries to mechanical energy which is also transferred through the mechanical linkage to the propeller.

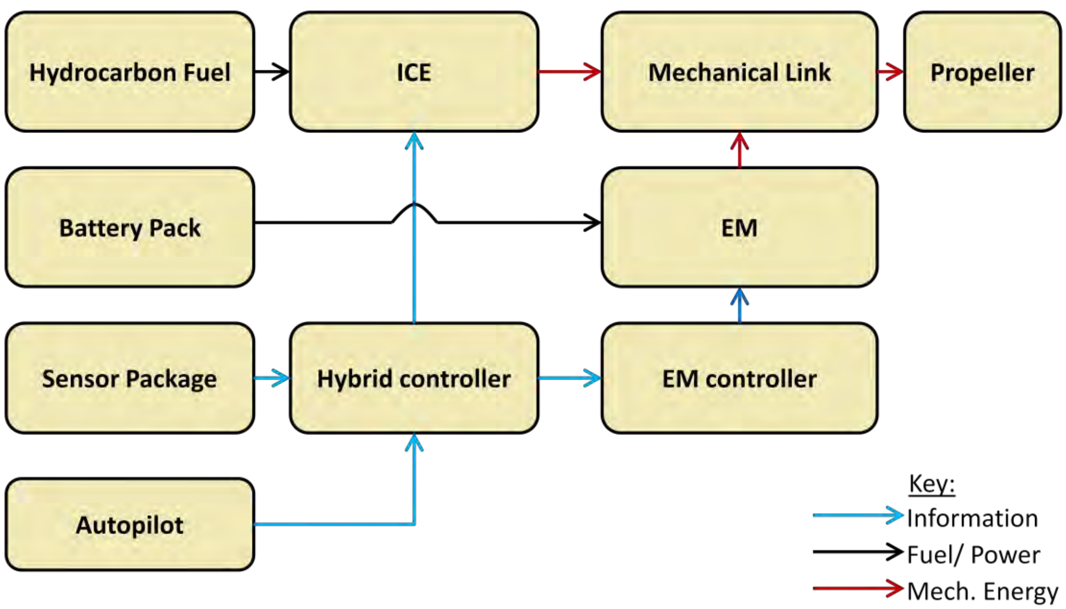

Figure 20: Components of a generic parallel HE propulsion system for a small RPA

When it is off, the ICE requires significant torque to turn since compression still occurs in the cylinder despite the absence of fuel, ignition, and combustion. Therefore, the EM must be capable of overrunning the ICE during electric only operation to avoid significant losses in propulsive efficiency and damage to the engine. Thus, the mechanical link must be a type of clutch mechanism. Meanwhile the ICE does not need to overrun the electric motor as the electric motor in the off state provides very little rotational resistance.

In the bottom of Figure 20, a number of electrical components are included, most of which fall in the avionics category. The key piece of equipment is the hybrid controller. The hybrid controller must accept a throttle input from the entity controlling the aircraft, autopilot or otherwise, and split it between the ICE and EM based on the flight mode. The autopilot is responsible for flying the aircraft when it is not under manual control, and the instrumentation system provides feedback to both the engine controller and the user. The last piece of equipment, the motor controller, is more closely associated with the EM than the ICE. Unlike an ICE which is controlled using a servo, an EM requires a device to control it by modulating the input power; for a brushless motor the device must also convert the battery supplied DC power into three phase AC power. When combined, these components form a parallel HE propulsion system. Prior to discussing component integration, it is worth detouring for a brief description of the intended airframe.

3. Air Frame Development

Early in the Condor Project (September or October 2010), the team decided to acquire a custom airframe from start-up RPA company CLMax Engineering. The team purchased two identical airframes. The first aircraft, referred to as the engine-only aircraft or AFIT-1, came with a 35cc, 4 stroke, Honda GX35 engine. The second aircraft, referred to as the HE aircraft, came with no engine to facilitate retrofit with the hybrid system. The name Condor is used to identify the airframe, regardless of the installed propulsion system. Figure 21 shows AFIT-1 during flight test in November 2011. The airframe uses an Eppler 210 airfoil, has a 0.305 m (1 ft) chord and a wingspan of 3.66 m (12 ft) or 4.57 m (15 ft) depending on the wing configuration. The aircraft is 1.83 m (6 ft) tip to tail and masses as little as 10.9 kg (24 lbs) in the engine-only configuration.

Figure 21: AFIT-1 during flight test at Camp Atterbury, November 2011

AFIT-1 allowed the team to tune the autopilot and familiarize themselves with the airframe's operational characteristics while the HE system was still in development. For more detail on the development and testing of AFIT-1, the reader is referred to Molesworth and English [**19**]; for additional information on the autopilot tuning, refer to Giacomo [**18**]. With the intended airframe presented, the chapter switches focus to the integration of the HE system. The presentation is by component; while the presentation is also somewhat chronological, the author often worked on multiple components in parallel, making a pure chronological presentation burdensome to the reader.

4. Internal Combustion Engine

Although the electric and combustion power trains are equally important from the standpoint of the hybrid concept, the ICE for this application is the dominant propulsion device. Its large size and weight relative to the rest of the propulsion system makes the ICE a convenient mounting point for the other propulsion components and for attaching the entire propulsion system to the airframe. Once selected, changing the ICE becomes increasingly difficult due to the time and money invested in the model specific mounting hardware, the notable non-COTS components of the project.

4.1. Engine Selection

In his thesis, Mengistu developed an engine test bench with a dynamometer and characterized both a Honda GX35 engine and a Fuji-IMVAC BF-25EI engine [**15**]. The Fuji engine was undesirable for this application for two reasons. First, the Fuji engine has an electronic ignition and requires a separate sparking system mounted alongside the engine. Second, Mengistu found the engine was difficult to start consistently [**15**] jeopardizing reliable mid-air restart. Meanwhile, the Honda GX35 engine has an integrated magneto in lieu of an electronic ignition, mounting to the airframe as a single package. The GX35 also started more reliably during testing [**15**].

Based on comparisons to the design simulations of Hiserote [**12**], the Honda GX35 is, on paper, overpowered for the airframe. The Honda manual states the engine can output 0.97 kW (1.3 hp) and Mengistu confirmed that value during dynamometer testing [**73**,**15**]. Meanwhile, Hiserote's simulation for a 13.6 kg (30 lb) aircraft with a 4.57 m (15 ft) wingspan calls for only 0.30 kW (0.4 hp) from the ICE for the climb and cruise flight segments. Therefore, the Honda GX25, the GX35's lighter counterpart with a maximum output of 0.75 kW (1.0 hp), was selected for the system. Table 3 compares the manufacturer specifications of both engines [**74**,**73**].

Table 3: Comparison of Honda GX25 and GX35 engines

Parameter	GX35 (Engine-only aircraft)	GX25 (HE aircraft)
Net Power Output	0.97 kW (1.3 hp) @7000 rpm	0.75 kW (1.0 hp) @7000 rpm
Net Torque	1.6 N-m (1.2 lb-ft) @5500 rpm	1.0 N-m (0.74 lb-ft) @5000 rpm
Dry Weight	3.3 kg (7.6 lb)	2.7 kg (6.8 lb)

The decision to pursue the GX25 engine was made in late 2010 while CLMAX Engineering was still designing the airframe. CLMax Engineering decided to power the engine-only aircraft with the GX35 engine, a decision supported by the author since the GX35 should provide power comparable to the combined EM and GX25, assuming the EM can provide 220 W (0.3 hp). For all EM and speed controllers under consideration at that point in the design, the electrical power output was limited by the speed controller not the EM itself. All considered speed controllers could sink at least 20 A at 28 V, or approximately 560 W. Assuming a speed controller power conversion efficiency of 80% and an EM efficiency of 86%, both conservative values [**12**], the EM would still provide 370 W (0.5 hp) at full power, bringing the maximum power output of the hybrid system to 1.12 kW (1.5 hp). Therefore, if the GX35 could fly the engine-only aircraft, it would validate the design power estimate for the HE system.

Once selected, the ICE narrows the design space since the associated mounting hardware is specific to the engine model. While the raw materials are not expensive, the design and manufacturing process is time consuming and potentially costly if the brackets are produced commercially. The initial set of system brackets were manufactured by two undergraduate students on the project, Carl Heinly and Andrew Koch from Cedarville University, in May and June of 2011. Upon completion of these brackets, the author resisted changing the ICE as a solution to integration issues. With the engine selected, the focus shifted to the electronics and avionics for the airframe, while engine testing itself was delayed until late June 2011 due to schedule availability.

4.2. Engine Testing

4.2.1. Engine Control and Instrumentation

As described in Chapter II, the author initially planned to operate the ICE using an IOL control strategy adapted from Harmon and based on the framework implemented by Greiser [**17**]. The IOL strategy defines the torque split between the EM and ICE during operation. The ICE is run at its most fuel efficient point and EM power supplements any additional the flight power requirements. If more thrust is required beyond what the EM can provide, the ICE adds power by operating beyond its IOL. Such a control strategy requires feedback to the hybrid controller and a map of the ICE's efficiency. To select the ideal operating point for the ICE, the hybrid controller matches the ICE's speed to the corresponding throttle setting via the IOL. Therefore, in addition to control over the ICE, the hybrid controller must be able to measure the ICE's speed.

Early in the avionics design, the author selected Eagle Tree's Seagull Flight Data Recorder as the flight telemetry system for reasons described later in the document. The Seagull provides optical and magnetic speed (rpm) feedback to the flight data recorder. While the magnetic sensor could track the magnet on the flywheel that drives the magneto, the author chose the optical sensor, focused on reflective tape on the engine flange, since other Seagull users complained of noise and erroneous readings when using the magnetic sensor on the magneto. Figure 22 shows the optical rpm sensor and the non reflective portion of the engine flange, circled for clarity. Feeding the telemetry from the Seagull optical sensor to the hybrid controller required a wire splice on the signal line to connect it to both the Seagull system and the controller. The signal itself is a standard 3.3 V rising edge where the interrupt frequency is the engine speed, if a single reflective stripe is used, as is the case on this setup.

The ICE is controlled using a regular sized Futaba metal gear servo connected to the carburetor. Hobbyist servos are highly interchangeable and such a connection is standard on nearly all remote controlled engines. The servos can be driven by any PWM signal allowing the use of a standalone controller in the laboratory, or a receiver and autopilot combination in the aircraft. Mounting and shielding the ICE servo proved to be the only significant obstacle and the mounting is discussed in Section 8.7 of this chapter.

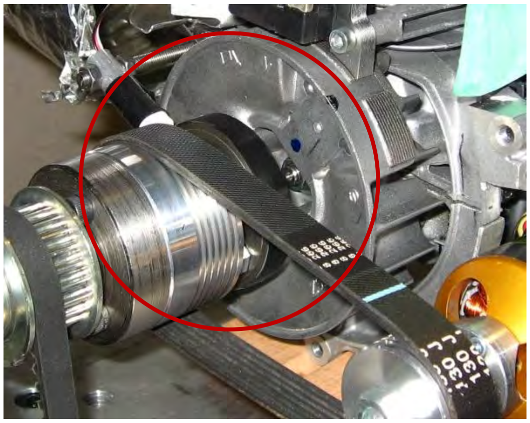

Figure 22: Hybrid system on dynamometer showing engine flange and optical RPM sensor

4.2.2. Dynamometer Setup

The next step in integrating the ICE was to generate torque maps of the engine and program those maps into the hybrid controller to effect IOL control. As discussed in Chapter II, by recording the engine's fuel consumption and torque for a grid of engine speeds and throttle settings, one can generate a map of brake specific fuel consumption as a function of throttle and speed. Plotting the most fuel efficient throttle setting against engine speed forms the operating line necessary to implement an IOL torque split strategy.

The engine was tested on the same dynamometer setup described in Mengistu's thesis [**15**]. Figure 23 shows the Honda GX25 mounted to the dynamometer inside of the test cell. The dynamometer is a DYNOmite Mini Eddy Dyno 96 V. An extension flange and gear bolted to the flywheel and a timing belt connected the engine to the 96 V direct current braking system, seen as the red coils in the bottom right of Figure 23. Data from the dynamometer is collected by the DYNOmite Pro Data Computer and Controller using a 28 channel wire harness. The controller transfers the data to the DYNO-MAX 2010 Pro Software Suite run on a standalone computer in the laboratory, where it can be recorded, saved, and exported for analysis. The software can also control the load the dynamometer applies to the engine or dynamically adjust the load to maintain a target engine speed. As already implied, the dynamometer can measure torque, speed, and power.

To mount the engine to the dynamometer, a plate the size and shape of the bulkhead for the aircraft was manufactured out of aluminum and mounted vertically on a 2.5 cm (1 in) thick aluminum slab. The slab was bolted directly to the dynamometer reaction cradle. The engine then mounted to an intermediate plate, attached to the simulated bulkhead with rubber vibration mounts.

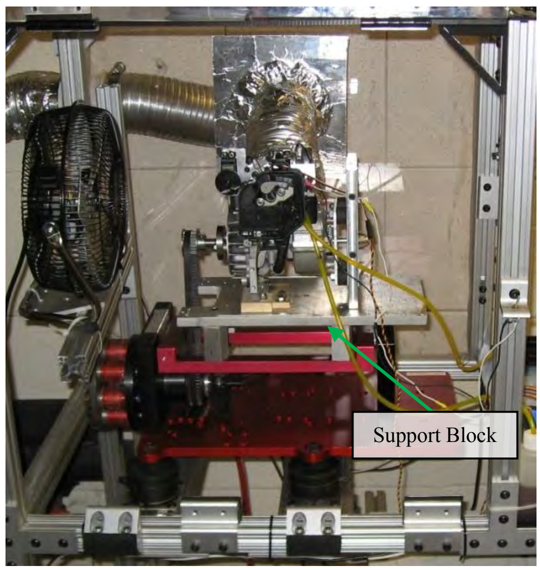

Figure 23: Dynamometer test setup with Honda GX25 engine, no pillow block, electric motor and starter motor not attached

As described and pictured in Figure 23, this set-up leaves the engine cantilevered from behind, as if it were mounted to the aircraft. In the aircraft, the ICE and EM power translates into axial thrust; the dynamometer provides a resistance torque and a corresponding force that pulls downward on the gear and subsequently the engine shaft. The moment arm of this torque, with the engine mounted only from behind, is substantial. Initial runs demonstrated that the moment from loading the dynamometer enhanced engine vibration causing the timing belt between the dynamometer and gear to slip. In a first attempt to overcome this issue, a wooden support block was added underneath the engine to reduce the moment arm of the belt on the engine assembly. The block can be seen under the flywheel in Figure 23.

The engine vibrated against the pine wedge, chipping away the wood and requiring a replacement block every 2-3 hours of operation. Therefore, a pillow block was added on the engine flange forward of the dynamometer belt to counter the moment produced by the load. This pillow block is shown schematically in Figure 24 and in a picture of the hybrid system mounted to the dynamometer in Figure 25. The pillow block significantly reduced engine vibration as well as variation in the measured torque. It also reduced the replacement frequency of the pine support block.

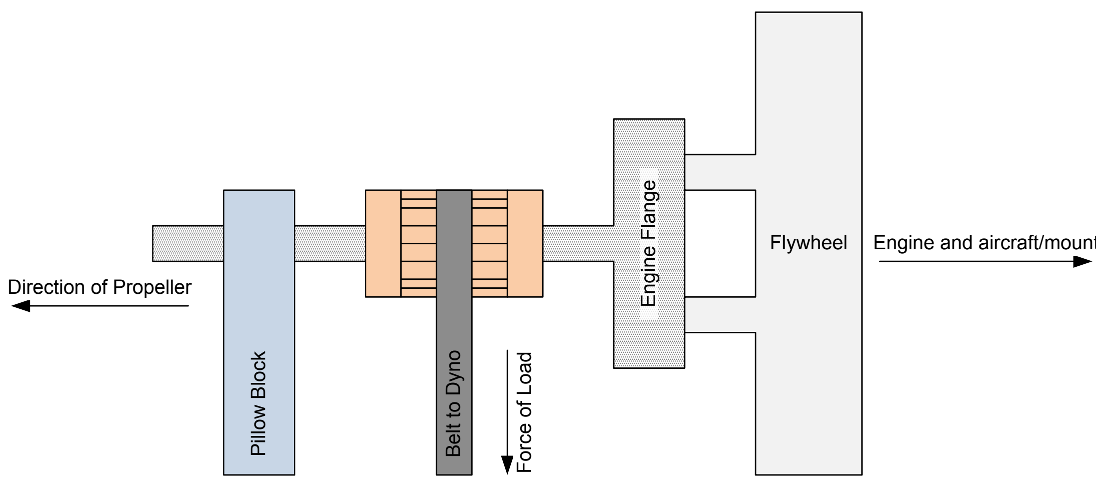

Figure 24: Schematic of pillow block location

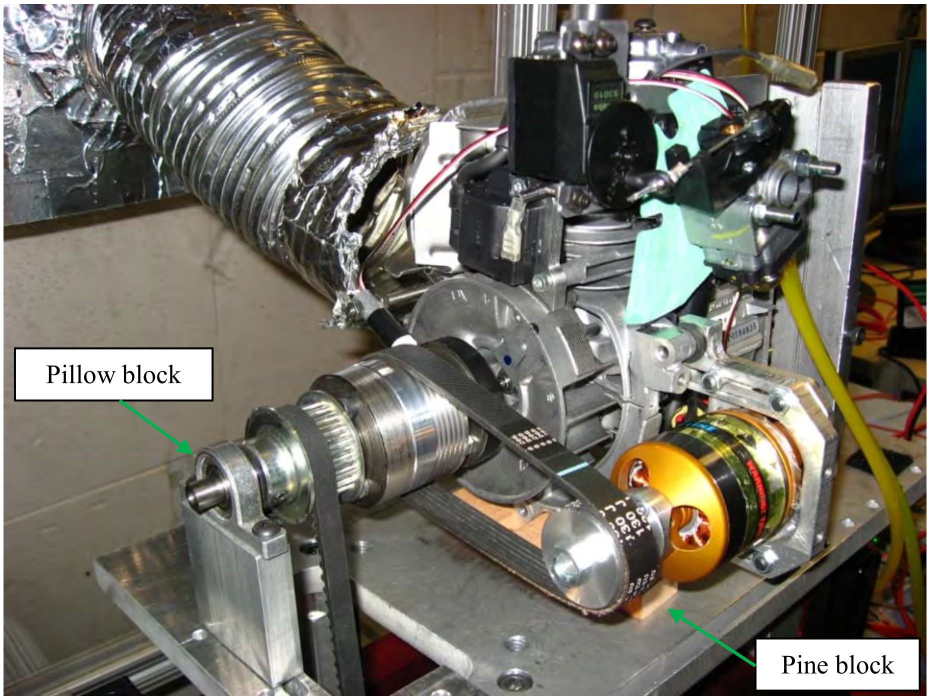

Figure 25: Hybrid system on dynamometer showing pillow block and pine support block

There are two other quantities necessary for the torque maps outside of those already mentioned: the ICE throttle setting and the fuel flow. Fuel flow was measured using a Max Machinery 213 piston helical flow meter. Designed specifically for low flow rates between 1 and 1800 mL per minute and non aqueous organic fluids such as gasoline, the Max 213 is ideal for this application. The flow meter uses a standard 5 V data signal with published gains, making it possible to hook the flow meter directly into the dynamometer's data acquisition system. The meter would not work for flow measurement on the airframe however; it has a mass of 0.6 kg and is sensitive to inertial orientation. The carburetor of the GX25 stores fuel in a small reservoir before mixing it with incoming air; over a several second period, the fuel flow to the engine is not constant. Thus, the fuel flow should be averaged over at least 30 seconds at a given throttle setting for useful results. One should also purge air from the fuel flow meter before taking data.

The throttle setting measurement was more complicated. The most accurate way to measure the throttle setting is by the position of the carburetor, shown with servo attached in the upper right corner of Figure 25. Initially, the throttle setting was measured with throttle position sensors designed to link with the dynamometer's data acquisition system. These throttle position sensors are spring loaded. Their force combined with the spring on the carburetor caused twitching in the servo position. Furthermore, the throttle position sensors had a 20-25% dead zone at either the high end or the low end. Heinley and Koch tried to create an analog gauge for the carburetor position, but the vibration of the engine during operation and the relatively short range of motion of the carburetor made it difficult to read accurately.

The position of the servo controlling the carburetor is easier to measure than the carburetor itself, but the servo must be calibrated so its range of motion matches the carburetor's range of motion. The servo was controlled via the PIC32 originally intended for use as the hybrid controller. By setting 0% throttle to the carburetor's fully closed position and 100% throttle to the fully open position in the controller's code, the PIC32 then adjusted the servo movement to match the offset and range of the carburetor. Typically, a servo's full range corresponds to a pulse width of 1 ms to 2 ms. However, to match the servo and carburetor, the that range was adjusted to 1 ms to 1.67 ms. The PIC controller calculated the pulse widths for the intermediate throttle settings. Even with the PIC32, changing the linkage between the servo arm and carburetor requires a recalibration of the servo, and thus the throttle setting is not perfectly repeatable. Using the throttle setting to kill the engine as a baseline, tracking the throttle servo is repeatable to within ±5% throttle, an acceptable value when torque map testing is performed in 10% throttle steps.

4.2.3. Initial Torque Maps

In July of 2011, the first set of torque maps for the GX25 engine were generated without the pillow block on the setup. The ICE was tested alone, without the EM mounted alongside. The engine was tested at 10% through 100% throttle in 10% increments. At each throttle setting, the engine was run from just above the stall speed to the no load speed in 250 rpm increments, remaining for 60 seconds at each speed. A sample test procedure is included in the Appendix E. The data from this first set of runs were compiled into a single spreadsheet and then plotted.

Figure 26 is the torque map for the GX25. The maximum torque of the engine occurs around 5500 rpm, but is only 0.8 N-m instead of the 1.0 N-m in the manufacturer's documentation. During testing, the vibration of the engine and tension in the dynamometer belt caused the timing belt to slip, reducing the load measured by the dynamometer. Therefore, without the pillow block, the measured torque is off by some scaling factor of slippage and a later torque map generated with the pillow block in place is presented in Chapter IV. That test also includes the EM mounted alongside the engine so that the drag of the powered off EM is taken into account. Figure 26 is presented at this point to justify a change in the control strategy for the engine that will become important during the discussion of the avionics. Figure 27 is the corresponding fuel burn for the engine during the tests. Combining the fuel burn and torque maps yields the IOL for the engine, shown in Figure 28. Initial estimates from Rotramel's code [**13**] indicate the expected operating speed for the system is between 4250 rpm and 6000 rpm. Over this range the most efficient throttle setting is 100% except for a single data point. At that data point, the differences in the BSFC at 80%, 90%, and 100% throttle are within 3%, a differentiation less significant than the measurement noise. Due to alignment issues with the engine on the dynamometer, only a single repeat trial was possible. Therefore, the point does not necessarily indicate an abnormality in engine operation; rather it could be an artifact of noise in the measurements.

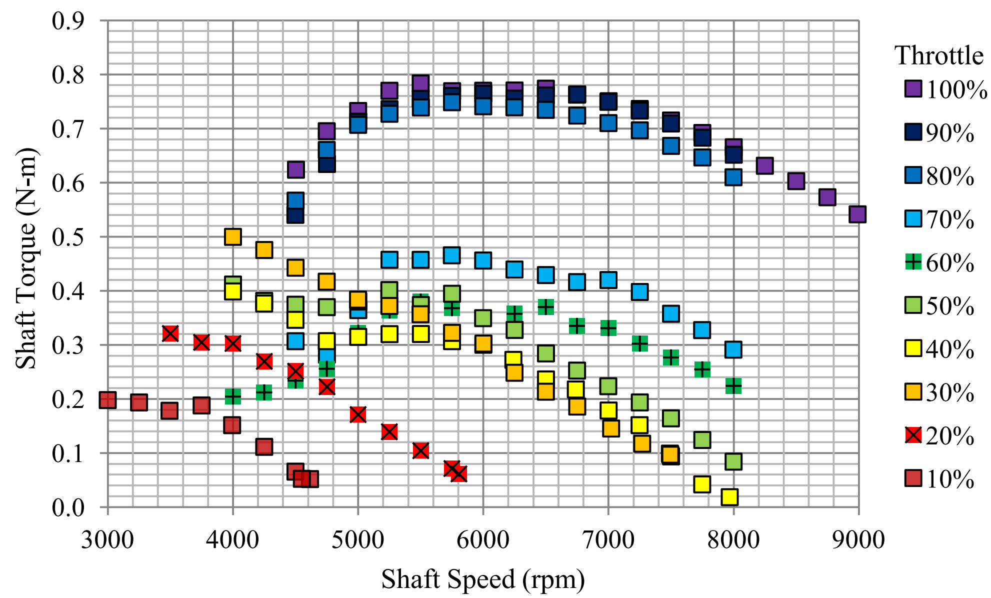

Figure 26: Torque map for Honda GX25 engine, no pillow block, no electric motor

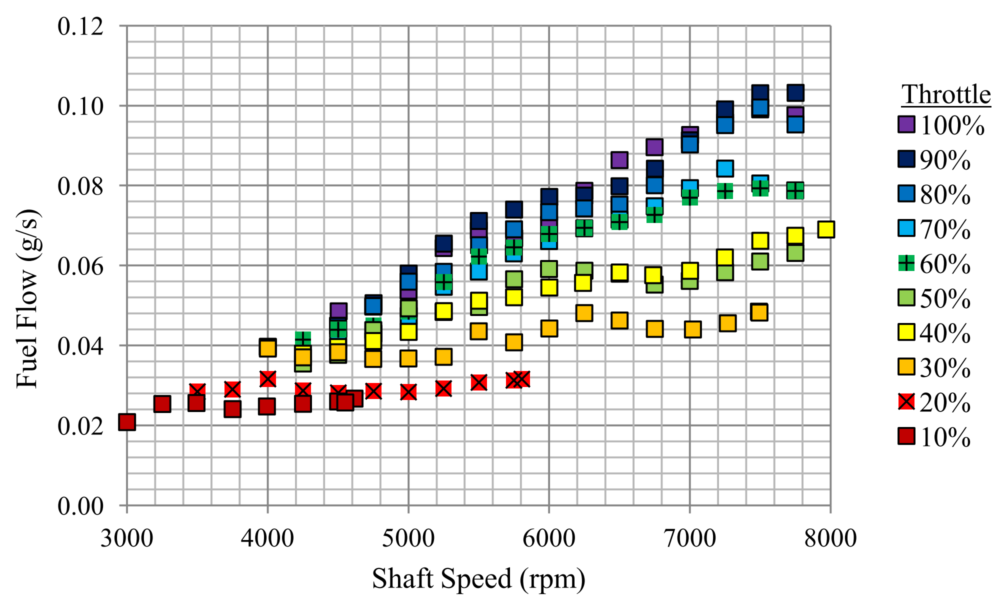

Figure 27: Fuel burn for Honda GX25 engine, no pillow block, no electric motor

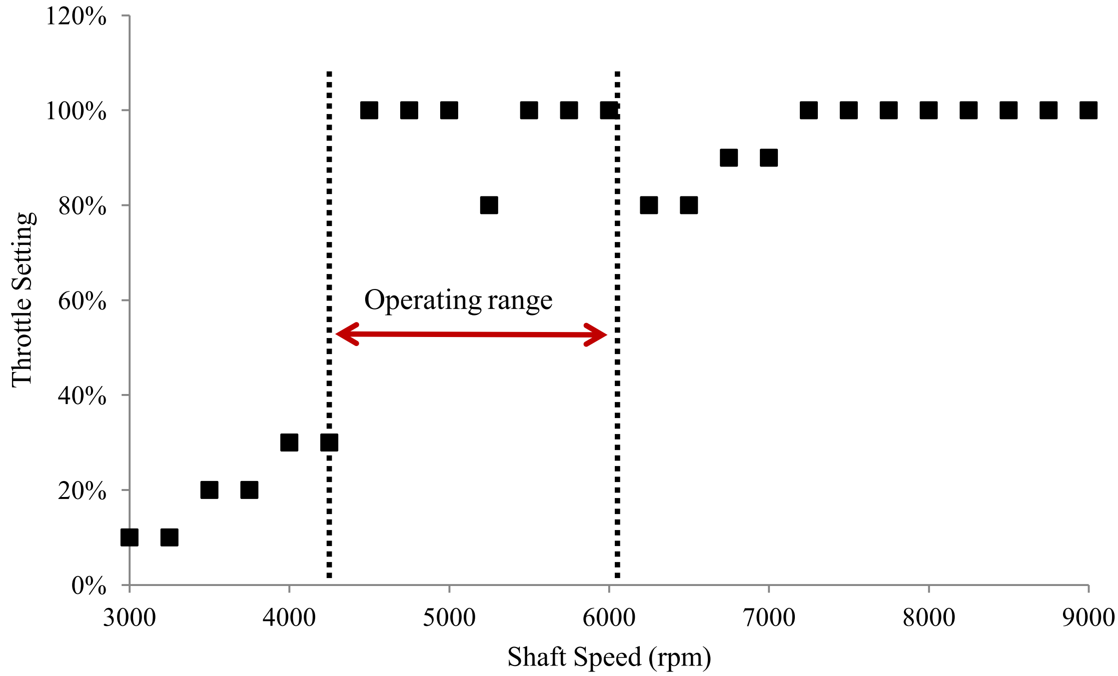

Figure 28: Ideal operating line for Honda GX25 engine, no pillow block, no EM

In an IOL configuration, the GX25 will go to 100% throttle before the EM engages. Thus, the EM would act more like a boost power device added when the ICE alone is insufficient to provide the power demanded from the propulsion system. In steady level flight the ICE would spend the majority of its time below 100% throttle since, based on simulation, less than full ICE power will be required for cruise. Since 100% throttle is likely overpowered for the steady level flight condition, the IOL strategy will only add EM power for high demand operations, limiting the fuel efficiency increases for IOL control with this engine carburetor combination. Some savings may be possible by fixing the ICE throttle in cruise to 5-10% below the power required for steady level flight and using the EM to make up the difference. By fixing (in lieu of constant trimming) the ICE throttle, fuel burn may decrease slightly.

There are other issues operating the GX25 continuously at full power. At 100% throttle, the GX25 can only operate for about 20 minutes on the bench without overheating. After approximately twenty minutes, smoke and oil/fuel were ejected from the carburetor air intake and the engine would throttle linearly from its current setting to off over 10 s to 15 s. The engine itself may have been overheating, or the carburetor could have been experiencing vapor lock. A fan was added in front of the engine to simulate airflow, but only gained an additional 4-5 minutes before overheating occurred. The stock engine on a yard tool would have a full plastic shroud delivering forced air cooling and would likely not be run at full open throttle for extended periods of time.

The efficiency results themselves may be more of a function of the carburetor than of the engine itself. The stock GX25 carburetor has no fuel air mixture adjustment. It has a needle valve that pulls a pin out of a fuel well and opens the airflow passage to the engine as the throttle increases. Therefore, the fuel air mixture is a fixed function of throttle setting. Over the last 40-50% of throttle, the mixture leans, increasing combustion temperature, fuel efficiency, and causing the engine to overheat. Ultimately, this warrants further study of carburetors, a potential topic for future work discussed in Chapter V.

Investigating new carburetors more appropriate for an IOL strategy was not the subject of this work. Still, these results allowed additional latitude in the engine control strategy. Since the IOL for the engine and carburetor combination is essentially a flat line at maximum power, a boost power configuration where the ICE is held at a constant power irrespective of speed and the EM is used to supplement power for efficient flight is justified. To prevent the engine from overheating, that constant power was selected well under full throttle. This modification to the control strategy became crucial in the avionics implementation discussed later in the chapter. The stock carburetor is shown in Figure 29 with the air intake and fuel well labeled.

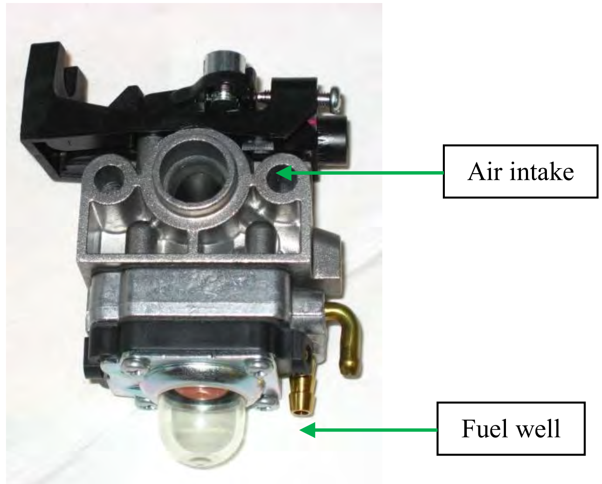

Figure 29: Stock Honda GX25 carburetor

4.2.4. ICE Mechanical Failures

Following the initial torque mapping, the author began a second set of maps with the pillow block installed and the EM mounted alongside the engine. Early in the 40% throttle test, the engine failed catastrophically making a grinding sound and halting in just under 4 seconds. Upon investigation, the crankshaft was found to be snapped in half and the timing belt connecting the crankshaft to the intake and exhaust valves was found to be stripped and torn. Initially, the failure was attributed to the stresses placed on the engine during testing without the pillow block. However, a new engine with less than 10 hours of operation failed shortly after testing resumed.

In the top of the Honda GX25 there is a cam connected to the timing belt that controls the intake and exhaust valves. On the cam there is an inertial speed governor that relieves cylinder pressure to make the engine easier to start. The cam and governor are circled in Figure 30. The governor is held to the cam on one side by a rivet pin and on the other side by a free floating pin. In the second engine, the rivet pin had loosened allowing the free floating pin to fall from its slot in the cam and to jam itself between the cam gear and the engine housing, seizing the engine.

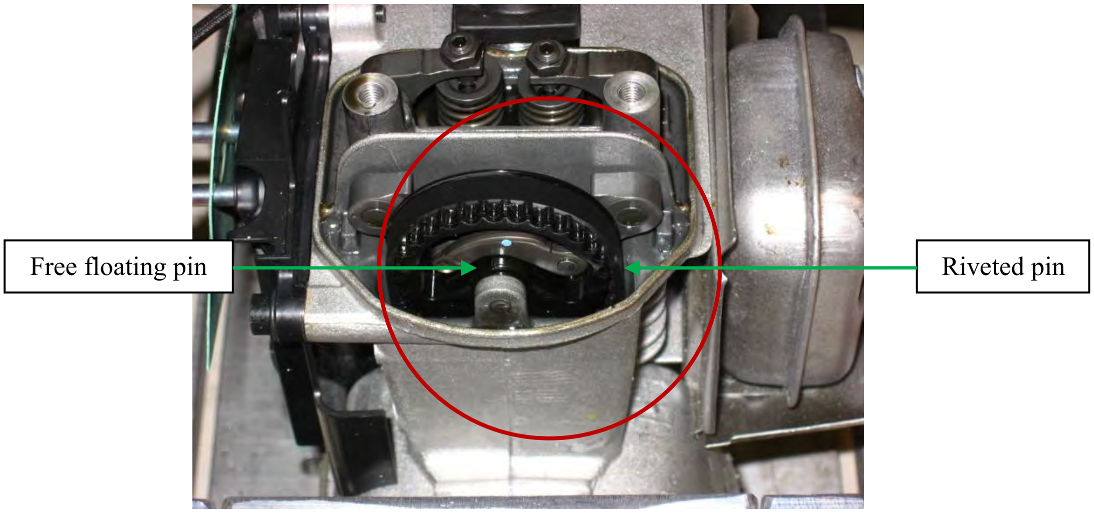

Figure 30: Cam gear and governor for pressure release in Honda GX25

A reexamination of the first broken engine found the same pin in the oil reservoir, sheared in half, implicating the pin as a probable cause of failure in the first engine. The cam gear assembly was replaceable. Upon further investigation, the replacement part had a different design than the original part included on the GX25 and the new part was backordered in the United States. This suggests that the issue with the cam was partially the manufacturer design, not the end user application, and two new gears were ordered from Honda. One replacement was for the second engine still intact except for the pin; the other was to replace the stock cam gear in a third engine intended for use on the airframe.

Following the failure of the second engine and prior to the discovery of the new cam gear, a 24 hour build up test was performed to determine what hybrid system components, if any, were loosening the governor retaining pin. Every six hours another part of the system was added, although the system was never connected to the dynamometer load. The test concluded the hybrid system itself, to include the EM and connecting belt, was not loosening the pin.

Before the cam gear failed on the second engine, running the EM and ICE in a dual mode to create additive torque had been demonstrated on the dynamometer. Testing also identified several concentricity issues; loading the full hybrid system with the dynamometer led to substantial vibrations. Most of the alignment troubles stemmed from GX25's aluminum cast flywheel, discussed in more detail in Section 6.2.2 of this chapter. By this point, torque maps were no longer essential to implement the EM and ICE control strategy after switching from an IOL torque split to a boost power configuration. Also, the buildup test did not eliminate the dynamometer as a potential contributing factor in the cam gear failure. Therefore, to avoid undue wear on and risk to the hybrid system, the Condor team opted to postpone further dynamometer testing. Instead the system was integrated onto the airframe where it could be tested with the propeller as the load. Loading the system with the propeller eliminates vibration from alignment discrepancies in the dynamometer mount. The test setup for the system on the airframe is described Section 9 of this chapter and the results are included in Chapter IV.

4.3. Starting Configurations

Connecting the EM and ICE with a clutch bearing so the EM overruns the ICE complicates the midair restart of the engine. With the help of Capt Cary Wilson at AFRL, the Condor team obtained a small starter motor that mounts to the pull start hub at the rear of the GX25. Figure 31 shows the starter motor assembly and gearing as well as the assembly mounted to the engine through the simulated bulkhead. The starter motor is made by FEMA, which is a small company located in Germany. The starter motor takes 12 V power and has a one-way bearing so that it can turn the engine, but the ICE will not drive the starter motor once started. There are limited options for COTS ICE starters in the appropriate size, and all of them, like the FEMA motor, require custom mounting hardware specific to end user's ICE. Therefore, when issues arose with the FEMA motor, other commercial choices were virtually non-existent.

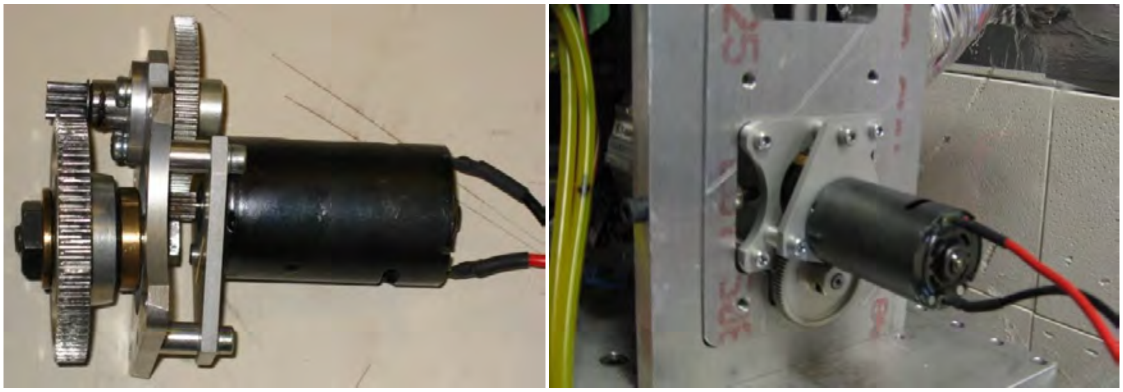

Figure 31: Starter motor assembly for Honda GX25 (left), starter motor mounted on ICE (right)

From a proof of concept standpoint, the starter motor is capable of starting the GX25 engine, which was demonstrated successfully on the bench. However, the setup has a number of issues identified in testing. First and most notably, the start/restart capability is unreliable. The starter motor only started the engine about 50% of the time during a 30 s attempt. To get even 50% reliability, the starter motor could not simply be supplied with a 12 V power source like that available from the step down converters intended for the avionics system. The starter motor consistently required power from a deep cycle lead acid battery with a full charge, 13.8 V, for an effective start. The starter motor assembly has a mass of 0.5 kg, making it a substantial weight addition to an approximately 13.6 kg (30 lb) aircraft. The starter motor would occupy the area directly behind the engine bulkhead, space dedicated to fuel and batteries. Although slim, the starter motor is directly in the middle of the space, making it difficult to fit fuel or batteries around it.

The Honda GX25 is not well equipped for a starter motor. The pull start shaft on the back of the GX25 is not concentric, even visually. This is of little consequence for a pull start which rotates the shaft only 2-3 times during the starting pull. It is a large issue for a starter motor which performs dozens of rotations. Over time, the alignment, or lack thereof, caused significant wear on the teeth of the large starter motor gear, wear that can be seen in a close inspection of Figure 31. Based on the manual starter used when the starter motor was not connected, it is the author's opinion that a faster motor, different gearing, or both would be required to reliably start the engine. After proving the starter motor concept on the dynamometer, the starter assembly was replaced with the cone and a manual starting motor like that used on hobbyist aircraft. As the cone was secured to the misaligned pull start shaft, vibration in the cone made manual starting challenging as the handheld motor would drift off of cone.

Due to the reliability issues, the Condor team decided to push mid-air restart to a future version of the aircraft and pursue a more reliable ground start only solution. This choice only eliminates testing one portion of the concept: mid air restart. To test EM-only power, the ICE can run in idle and the EM can propel the airframe. For an acoustic or loiter test, the engine could be killed and the aircraft could land under electric power. Obviously, to be fully operational, the ability to restart the engine to fly home would be required. Still, a starter motor is conceptually possible and the remainder of the concept could be tested more reliably without it.

Eliminating the starter motor is not as straightforward as just using a manual starter and an external battery. When the system is mounted to the aircraft, the operator is unable to access the rear of the engine to use a hand held starter. The one-way bearing eliminates the possibility of starting the engine from the front using a manual starter and propeller cone; spinning the propeller in the direction of starting the engine will overrun the engine due to the one-way bearing. Therefore, the author reverted to the manufacturer's recommended solution: use the pull start that comes with the engine. The CESI support contractors created a mount to fit the pull starter between the engine and aircraft bulkhead, allowing for pull start of the engine on the ground. The pull starter only moved the propulsion system 1.3 cm (0.5 in) forward since the mounting plate for the starter motor was eliminated in the process. The pull starter is more reliable and safer than even a traditional manual starting system since the operator can stay completely behind the plane of the propeller. The pull start allows the testing of all concept objectives except for mid-air restart itself, which is discussed as an objective for future work in

Chapter V. This concludes the discussion of ICE integration. The chapter continues with a discussion of the EM integration.

5. Electric Motor and Batteries

5.1. Motor Selection

Electric motors are almost exclusively voltage controlled; it is easier to regulate the effective voltage to a motor using a transistor or similar switch than it is to regulate current to the motor. Recalling the modeling equations in Chapter II, voltage control effectively controls the speed of the motor, which is not conducive to a torque split strategy. Since a torque splitting strategy divides the load between the EM and ICE based on the torque each provides to the system, controlling the current of the EM was the preferred approach in this project.

5.1.1. Initial Brushed Motor

Based on the work of Hagen [**16**], the Maxon RE50 200 W DC motor was initially selected as the driving electric component of the hybrid system based on matching it to the Honda GX25 manufacturer specifications using Rotramel's code [**13**]. Current control of the motor was accomplished using two NiQor NQ40 quarter brick DC-DC power converters, one to run the motor and one operate the motor as a generator to regenerate the batteries. Both the Maxon motor and the NiQor NQ40 are shown in Figure 32. Initial weight estimates of the brushed motor based electric system were prohibitively heavy. Alone, the Maxon motor masses 1.1 kg and the Synqor converters mass 84 g each. Initial testing indicated that the Synqor converters are highly sensitive to electro static discharge and that soldering wire of a sufficiently large gauge to handle the EM's 20+ A current draw to the pins is difficult. Based on these issues, the author consulted Justin Delmar and Benjamin Razidlo at Air Force Research Laboratory, Propulsion Directorate (AFRL/RZ) early in the effort concerning other possible motor configurations.

Brushless motors, specifically out runners, offered a significant weight savings compared to the in runner brushed DC motors like the Maxon RE50. However, they also came with a significant complication: brushless motors require a motor controller to turn the battery supplied DC power into three phase AC power. The conversion further complicates the pursuit of torque control via current control. Nevertheless, the weight savings offered by a brushless solution, upwards of 0.5 kg, warranted further investigation.

Figure 32: SynQor NiQor DC-DC converter (left) [**75**]; Maxon DC Motor: 370354 (right) [**76**]

5.1.2. Brushless Motor Selection

A market survey of available brushless motor brands in the relevant size returned the two main competitors in the United States: Neu Motors and AXI Model Motors. Neu brand motors are considerably more expensive than their comparable AXI equivalents. Neu Motors is also a much smaller company than AXI; in the author's past experience, this led to lead times up to six months on a single, standard motor. Thus, the AXI motor product line was investigated for an appropriate part.

Rotramel's simulation run with the Honda GX25 engine and power requirements estimated for a 13.6 kg (30 lb) aircraft with a 4.57 m (15 ft) wingspan using Hiserote's code suggested a motor with an operating range of 5000 ± 1000 rpm. Selecting a motor with a K_v value to deliver 5000 rpm at 30 volts under no load gives a K_v of 170 rpm/volt. This value is too low for the actual motor since loading will decrease the speed below the no load speed and the motor should not run at full power to merely catch the ICE. The AXI Gold Line 4130/20 motor has a K_v value of 305 and is one of the lightest Gold Line motors available in an applicable size range. The AXI 4130/20 has a mass of 409 g, much lighter than the Maxon RE50 [**77**]. It also has a conversion efficiency of 88%, comparable to the estimates used in Rotramel's code. Saving 700 g over the Maxon motor, the AXI motor was the clear choice, provided a workable motor controller.

5.2. Motor Controllers

Castle Creations controllers dominate the hobbyist market for electric propelled aircraft. Working with a Castle ICE75 in the laboratory, it is no mystery as to why. The controllers are plug-and-play. Batteries plug into one side, the motor plugs into the other. A standard cable connects the PWM throttle signal from the user's control device and the system is ready to fly. The simplicity is also the downfall of a Castle controller for this application; it lacks manufacturer supported configurability. Initially, it was unclear if the ICE75 or any other Castle controller could support regeneration of the batteries. Note that ICE75 refers to the 75 A version of the standard Castle controller. Hagen had investigated the possibility of battery regeneration and concluded that the setup would require circuitry to redirect power siphoned from the EM to a rectifier before reaching the Castle controller, essentially isolating the Castle controller from the circuit when regenerating the batteries. A schematic of a proposed setup is shown in Figure 33.

Due to the expected complications of using the Castle controller for regeneration, two different motor controller solutions were initially pursued. The primary solution was Elmo Motion Control's SimplIQ Whistle Solo controller. Elmo controllers can also act as full bridge rectifiers, eliminating the need for any additional circuitry to regenerate the batteries. The Elmo controllers also require an entirely custom code, written in Elmo Motion Control's proprietary SimplIQ language, similar to C. Delmar and Razidlo at AFRL/RZ agreed to help with the development of the Elmo while the author used the Castle controller in the laboratory.

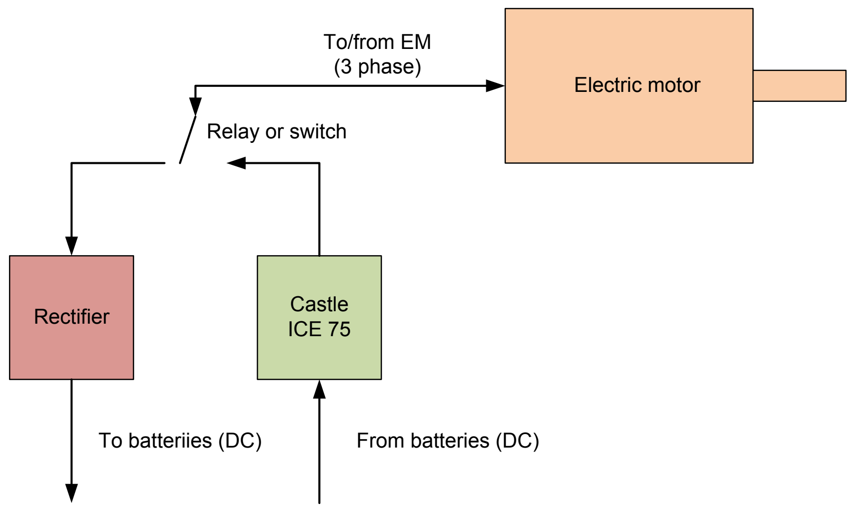

Figure 33: Circuit for power isolation of the Castle controller during battery regeneration

5.2.1. The Castle ICE 75

Since AFRL/RZ was developing the Elmo controller for this application in parallel, the Castle was only intended to act as a substitute until the Elmo controller was ready. In July 2011 when the EM had been mounted to the ICE, a Castle ICE75, shown in Figure 34, and a manual throttle control were used to determine if the ICE and EM could run together and not vibrate one another apart or damage the one-way bearing connecting the power trains. In tandem operation, the EM added torque to the output of the ICE as measured by the dynamometer. During startup the morning after the test, the ICE75 ceased function and caught fire. The author called Castle Creation's technical support line and spoke with two engineers at Castle Creations. The author was concerned that spinning the motor with the Castle controller inactive could have damaged the controller leading to the fire. If the free spinning motor were the culprit, it would have serious implications before even considering using the ICE75 for battery regeneration. Since the ICE always drags the EM, the Castle controller would have to be disconnected from the circuit when not in use, not just during regeneration.

Figure 34: Castle Creations ICE 75 controller [**78**]

The discussion with Castle's Technical Support yielded two important facts. First, the setup was not responsible for the destruction of the ICE75. Rather, a manufacturing defect in one of the transistors led to a short circuit that caused the fire. Secondly, one of the technical support operators stated that he uses a Castle controller as a full bridge rectifier to run the wind farm in his back yard; it uses power from a wind mill to regenerate the marine batteries used to power his porch lights. However, the controller requires custom programming and must be isolated from the circuit when the batteries are full to prevent overcharging. In the case of a lead acid battery, overcharging ruins the battery; in the case of a Li-Po battery, overcharging causes it to explode and catch fire. The Elmo controller does not require isolation circuitry, and, since AFRL/RZ was almost finished with the Elmo controller code, the Elmo controller became the clear choice for the integrated system.

5.2.2. The Elmo Motion Control Whistle Solo Controller

The Whistle Solo controller by Elmo Motion Control is a complex motor controller designed for large industrial applications, although the controller itself fits easily within a 5.7 cm (2.25 in) cube. A picture of the controller is shown in Figure 35. While there are numerous ports on the Elmo, only three are of concern for this project. For information beyond that included in this document, please refer Elmo Motion Control's official documentation [**79**].

Figure 35: Solo Whistle motor controller, Elmo Motion Control [**80**]

Figure 36 shows the port and pin layout for the Solo Whistle controller. Wires M1-M3 connect to the phases of the motor and are not considered a port for the Whistle model on the Condor. Ports J1, J2, and J4 are configured for the Condor application. A full list of the pin connections is available in Appendix B. Port J1 supplies power to the Elmo to run both the program and to supply power for the EM. The Solo Whistle is limited to 20 A and 95 V. Since the Solo Whistle also serves as a rectifier, the underside of the Solo Whistle acts as a heat sink and must remain clear during operation.

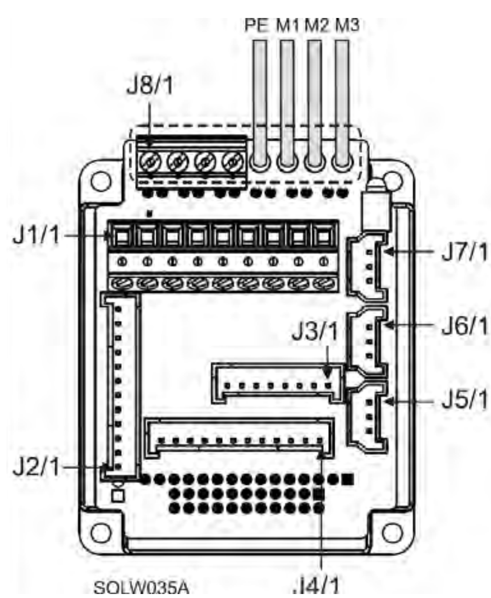

Figure 36: Pin layout for Solo Whistle controller [**79**]

Port J4 is the main feedback port for the Solo Whistle and it is where the motor encoder connects. The Solo Whistle requires position feedback provided by an E6 Optical encoder manufactured by US Digital, shown mounted to the EM in Figure 37. The specifications for the encoder and its associated cables are provided in the final section of this chapter. The Solo Whistle requires differential feedback; therefore the encoder requires a modified LD5 encoding chip that links to the standard 10 pin cable. This cable is spliced to the Solo Whistle J4 cable and the connection details are included in Appendix B. The selected encoder uses 500 counts per revolution, although Elmo Motion Control suggests a 2000 count per revolution encoder may ease the start up commutation issue discussed shortly. The position feedback allows the Solo Whistle to compare its position to the amount of power used to drive the EM, allowing it to determine how much torque it provided and effect torque control. The Solo Whistle's alternate control scheme is speed control, which also requires encoder feedback.

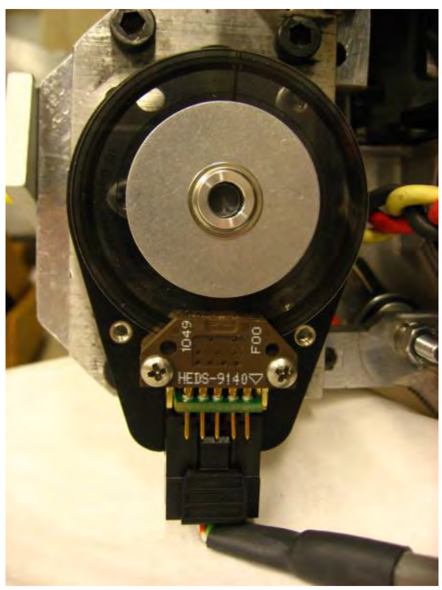

Figure 37: US Digital D6 encoder, 500 counts per revolution, differential feedback

Finally, port J2 provides the input and output line for the Solo Whistle to include 4 digital and 2 analog input lines. These lines allow the hybrid controller to control the EM throttle and the Solo Whistle's operating mode. The throttle is controlled using a 0-4 V analog signal corresponding to 0-100% throttle. The Solo Whistle's analog inputs are floating, necessitating the connection of the return line to ground for a proper reference voltage. AFRL programmed three digital lines, which accept a 5 V digital signal, to provide four operational modes for the Solo Whistle. These modes and their corresponding pin combinations are listed in Table 4. Note that Pin J2/1 is not digital 1 in the Solo Whistle coding.

Table 4: Solo whistle control mode and pin combinations

Mode	Pin: J2/1 (Digital 3)	Pin:J2/3 (Digital 5)	Pin:J2/4 (Digital 6)
Torque control	High (5 V)	Low (0 V)	Low (0 V)
Regeneration	High (5 V)	Low (0 V)	High (5 V)
Initialize	Low (0 V)	Low (0 V)	High (5 V)

The torque control mode is the standard EM drive mode. The EM power output increases with the analog throttle signal to the Solo Whistle. In regeneration mode the code reverse the sign of the throttle signal, allowing the Solo Whistle to take power from the rotating motor, rectify it, and return it to the main power bus. During regeneration the throttle signal should be limited so that the charging current does not exceed the C rate of the batteries, as shown in Equation (35). The third state, initialize mode, tares the analog voltage sensors. The signal combination for initialize mode should be the first signal combination the Solo Whistle receives when it is powered. Therefore, to start the Solo Whistle as programmed, J2/4 should be held high while the analog input is fed a zero throttle signal. After 0.4 s or longer, J2/4 should be grounded and the Solo Whistle may be switched to the user's mode of choice.

$$throttle\ [\%] = 100 * \frac{C[A]}{20} \tag{35}$$

AFRL/RZ also added two additional modes that have currently no activating pin combination. There is a speed control mode where the throttle setting will control motor speed between 0 and 8000 rpm. There is also a position mode where the Solo Whistle will use the motor encoder to return the EM to its starting position. A possible use for this mode is discussed in Chapter IV.

The Solo Whistle controllers are programmed using a RS232 Serial cable connected to Port J5 on the Elmo controller. Currently, only Delmar and Razidlo at AFRL/RZ have a copy of the code and the correct serial to J5 cable. Also, when the Solo Whistle is paired with a new motor or a new set of inductors, discussed shortly, it requires a new calibration performed using the SimplIQ software suite. Again, RFRL/RZ has the appropriate computer, cable, and software to perform the calibration.

Most of the issues with Solo Whistle integration were coding and wiring glitches. However, there are three unique issues with the Solo Whistle worthy of mention here. First, the Solo Whistle under unexpected load can dump power back onto the ground rail through its protective earth line. Protective earth is attached to ground in this application as the batteries are considered a non-isolated power supply. During testing with the PIC32 as the hybrid controller, having the PIC32 and Solo Whistle on a common ground caused noise on servos attached to the PIC32 and the burnout of multiple power converters on the PIC32 board. Therefore, the avionics wiring was altered so that the power supply for the EM and Solo Whistle is entirely isolated from the avionics power to avoid potentially harming the avionics, including the significantly more expensive Kestrel autopilot.

The second issue with the Solo Whistle is its start-up procedure. After the voltage sensor is zeroed, the Solo Whistle rotates the EM to check its zero position against the motor encoder. If there is no load on the EM this calibration is relatively straight forward. However, once integrated into the hybrid system, the belt connecting the EM to the ICE power train provides two very different loads. In the clockwise direction from the seat of a hypothetical pilot, there is only the inertial load of the propeller as the one-way bearing allows the EM to overrun the stationary ICE. In the counterclockwise direction, the EM pulls against the ICE. Several iterations of the starting parameters for the Solo Whistle's internal calibration algorithm yielded a set of values that allow it to commutate ~95% of the time on the first attempt. If the Solo Whistle is unable to commutate on startup the power must be cycled for another attempt; the Solo Whistle will not run without a successful commutation. The Solo Whistle should be initialized before starting the ICE so the Solo Whistle is the only device rotating the EM. It follows that a power loss in flight should be avoided as there is no guarantee the Solo Whistle will initiate correctly when power is restored if the EM is rotating due to the propeller or ICE.

Third and finally, the Solo Whistle is designed to work with motors larger than the AXI 4130/20 and thus motors with a larger inductance. To stabilize the Solo Whistle with the AXI 4130/20, inductors were added to each phase of the EM power lines. Each inductor should be 10 μH. After several months of back and forth testing between AFRL/RZ and AFIT, the author and Delmar had worked out all of the bugs in the Solo Whistle controller and the interface with the hybrid system. The electric power train was ready in the middle of November 2011. Before moving on to the mechanical integration of the hybrid system, the last sub section addresses the selection of batteries for the airframe.

5.3. Battery Selection

The selection of batteries was based on three factors: voltage, weight, and price. In order to ensure sufficient battery voltage for the EM to match the speed of the ICE and contribute torque, the author selected a minimum voltage threshold and determined for the commercially available battery packs which combination would provide the most power for the least weight and least price. The search was restricted to Li-Po batteries based on the information presented in the literature review.

In June 2011, the author and Delmar at AFRL/RZ performed a set of point tests to characterize the speed and load capabilities of the Solo Whistle and AXI 4130/20 pair using

AFRL/RZ's dynamometer test setup. The results from three no load and three maximum torque tests are presented in Table 5.

Table 5: Elmo voltage and load test results

Voltage (V)	**Load (N-m)**	**Speed (rpm)**
22	0.5	3000
26	0.5	4000
30	0.5	4000
22	0	5300
26	0	6300
30	0	7000

Assuming the optimal power range for the ICE is between 5000 rpm and 6000 rpm, anything less than 26 V from the batteries will be too low even with a 1:1 gear ratio between the ICE and EM as discussed later in Section 6.2.3. While the gear ratio was not the subject of this design decision, the pack voltage had to be sufficient that there was a workable gear ratio and propeller combination. Pushing the high end of the presented voltage range provides greater assurance that the EM will be able to match the engine in dual mode while still providing additive torque. Therefore, the author pursued a battery solution in the 30 V range.

Thunder Power is one of the market leaders in hobbyist Li-Po batteries, so the battery search began in Thunder Power's catalog. Battery price increases with discharge and charge rate, justifying the selection of 25C series batteries, the lowest discharge and charge rate available. According to the manufacturer, the batteries can discharge at 25C and charge at up to 5C with a load balancer. That means that a 3300 mAhr pack can discharge at 82.5 A, 4.1 times faster than the Solo Whistle can use the power even at full load. To charge above 1C, the battery charger must have a balancer. As there is no balancer on the aircraft and since there is no need for ground charging rates greater than 5C for this test application, 25C batteries were deemed acceptable.

The selection was then narrowed to pack combinations providing the required voltage. Three different combinations were candidates. The 8s packs provided 32 V nominal and 33.6 V at full charge. However, the packs are $10/pack more expensive than buying two 4s packs of the same capacity and linking them in series. The 7s packs provide 28 V nominal and 29.4 V at full charge. However, they require special battery pack balancers that are somewhat expensive. The Condor team already had balancers for batteries up to 6s. Therefore, the author selected the 4s packs which provide 16 V nominal and 16.8 V at full charge. Linking two 4s packs in series provides 32 V nominal and 33.6 V at full charge. Meanwhile the same packs in series drop to only 24 V at empty, keeping the battery voltage in the range suggested in the discussion with Table 5.

Next, each of the 4s battery capacities were compared using two figures of merit: the price per mAhr and the cost per mAhr. The results of this computation are shown in Table 6. The table also lists the endurance flight time per set of two packs. The endurance flight power is taken at 180 W based on Harmon's [**14**] and Hiserote's [**12**] simulations and is comparable to the 166 W predicted by CLMax Engineering. These simulations are discussed in Chapter IV. Based on Table 6, the 3300 mAhr packs were selected, despite the slightly better specific energy of the 2700 mAhr packs. Because of the higher capacity, 20% fewer 3300 mAhr packs were required to get the same endurance flight time. Since the team decided to buy 3 sets of batteries, 8-3300 mAhr batteries per set versus 10-2700 mAhr batteries per set significantly reduced the cost for a small loss in specific energy. The maximum battery load for the aircraft is six batteries packs, wired in three parallel sets. Each set consists of two packs in series.

Table 6: Figure of merit for Thunder Power 4s Li-Po 25C series battery packs

Capacity (mAhr)	Mass (g)	Price ($)	Cost metric ($/Ahr)	Weight metric (g/Ahr)	Endurance time (hr/per pack pair)
1350	122	44.99	34.60	90.0	0.24
2100	192	59.99	28.57	91.4	0.37
2700	238	79.99	29.60	88.2	0.48
3300	315	89.99	27.27	95.4	0.59
3900	362	109.99	28.20	92.8	0.69
4400	414	124.99	28.40	94.0	0.78
5000	471	134.99	27.30	94.2	0.89
5400	480	149.99	27.80	88.9	0.96
6600	623	179.99	27.27	94.0	1.17
7800	714	219.99	28.21	91.5	1.39

6. Mechanical Integration

The portion on mechanical integration focuses on physically joining the ICE and EM and their power trains to power the propeller both independently and in tandem. The integration is split into two topics: combining the power shafts from the ICE and EM and mounting the EM to the ICE. Figure 38 shows the system assembled on the airframe and Figure 39 is a schematic top view of the assembled hybrid propulsion system.

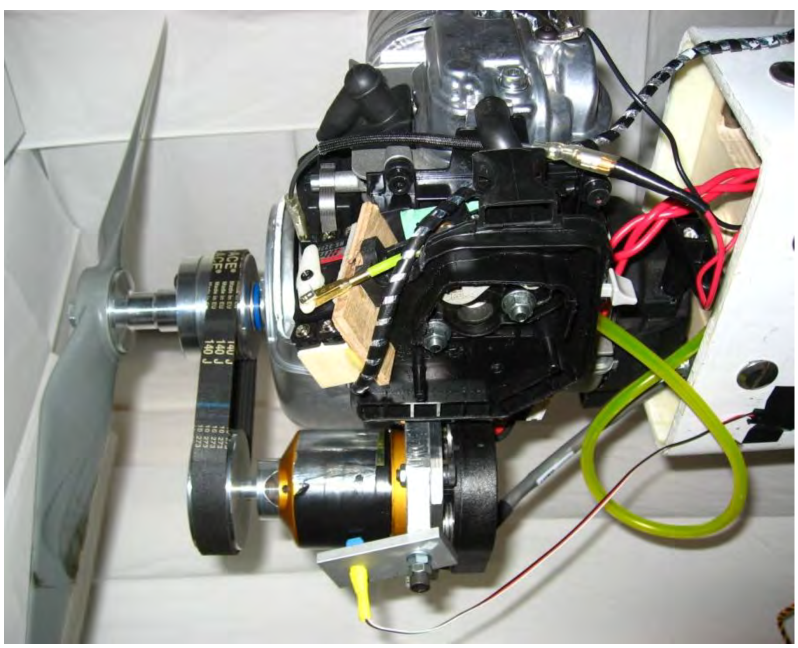

Figure 38: Assembled hybrid system on airframe

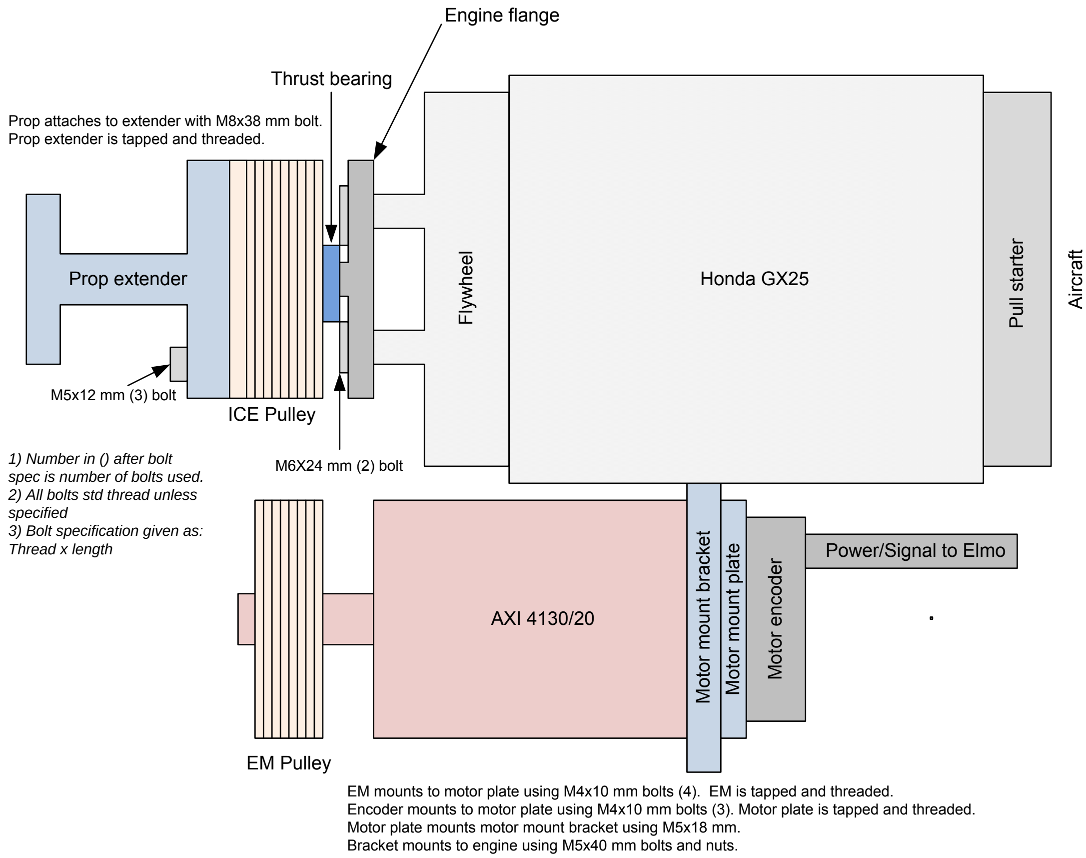

Figure 39: Top view sketch of combined EM and ICE

6.1. Motor Mount Bracket and Plate

The main mounting challenge was positioning the EM alongside the ICE so that the two drive shafts would be parallel to one another. It is desirable to mount the EM as far aft as possible to reduce the overall aircraft length and the moment arm of the EM in front of the aircraft's center of gravity. Since the EM is an outrunner, it must be secured from behind, complicating the mounting process. The left portion of Figure 40 shows the Honda GX25 stripped of all the extra weight unnecessary for operation. The best mounting points for any sort of bracket in this configuration are the three identified mounting holes for the flywheel shroud. The flywheel shroud is shown attached to the engine in the right portion of Figure 40. The mounting points for the fuel tank are also available, since the fuel will be carried internal to the aircraft. The engine shroud is where one would normally secure the attachment shaft for a weed whacker or similar application. Two flanges on the flywheel hold the shoes of a centrifugal clutch, and the clutch's housing, bolted to the four indicated holes on the shroud, carries the circular clutch plate.

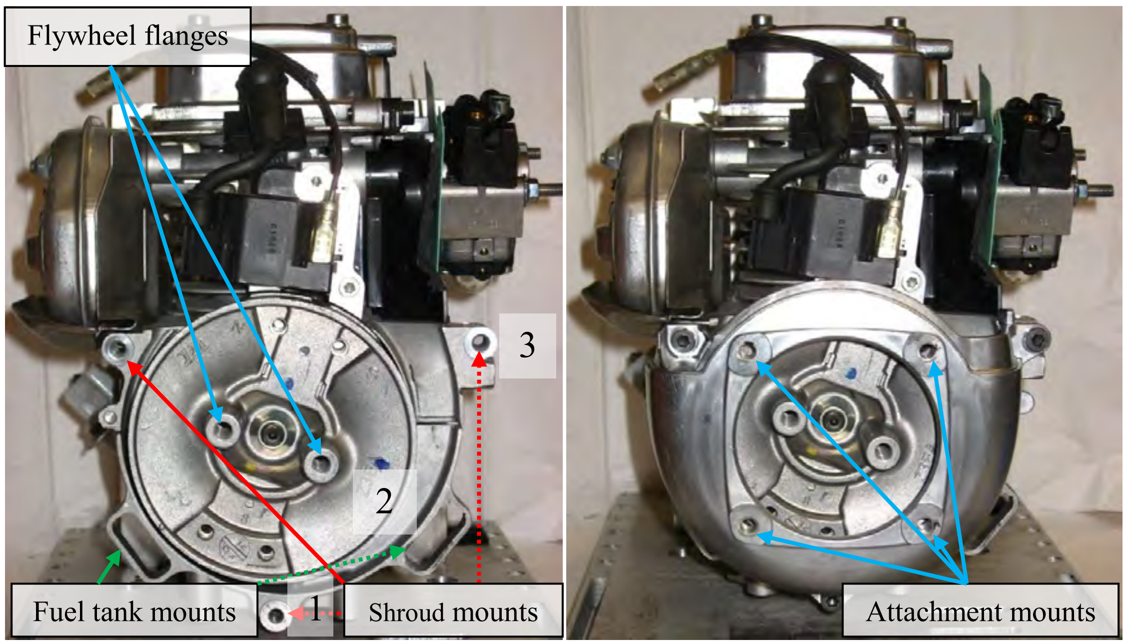

Figure 40: Stripped Honda GX35 without flywheel shroud (left), with flywheel shroud (right); dashed lines indicated slected mouting points for EM bracket

The mount was designed so the engine shroud could be removed for flight, lightening the aircraft. In order to mount the EM as far aft as possible, a bracket, termed the motor mount bracket, was created. The bracket attaches to the rear surface of the mounting holes indicated by dashed lines in Figure 40. Since the engine casing is cast aluminum, the rear sides of these mounting surfaces are not precision ground and therefore not in the same plane. In hindsight, it may have been prudent to move the EM forward 1.3 cm (0.5 in) and mount the motor mount bracket to the forward side of these points. The fronts of the two of the mounting points that hold the shroud are precision ground to the same plane to ensure proper alignment of the commercial accessory shaft. Then only the fuel tank mount would need washers to bring it into the correct plane. With the associated pulleys and flanges completed prior to this realization, the author instead squared the motor mount bracket using a sequence of spacing and rubber washers between the motor mount bracket and the engine. The specification of washers for each of the three mounts is given in Appendix D.

The next challenge was mounting the EM to the bracket. The EM is designed to mount to a metal plate, flat on the back, with the motor shaft extending through the plate to the optical encoder. The optical encoder mounts to the opposite side of the same plate. This motor mount plate then attaches to the motor mount bracket using four M5 bolts and nuts. The attachment point on the motor mount bracket is slotted so that EM may slide toward or away from the ICE to tension the belt connecting the drive shafts. Figure 41 shows a sketch of the motor mount plate and bracket, highlighting the engine mounting points as well as slot location to adjust the belt. Figure 42 shows the actual bracket and plate.

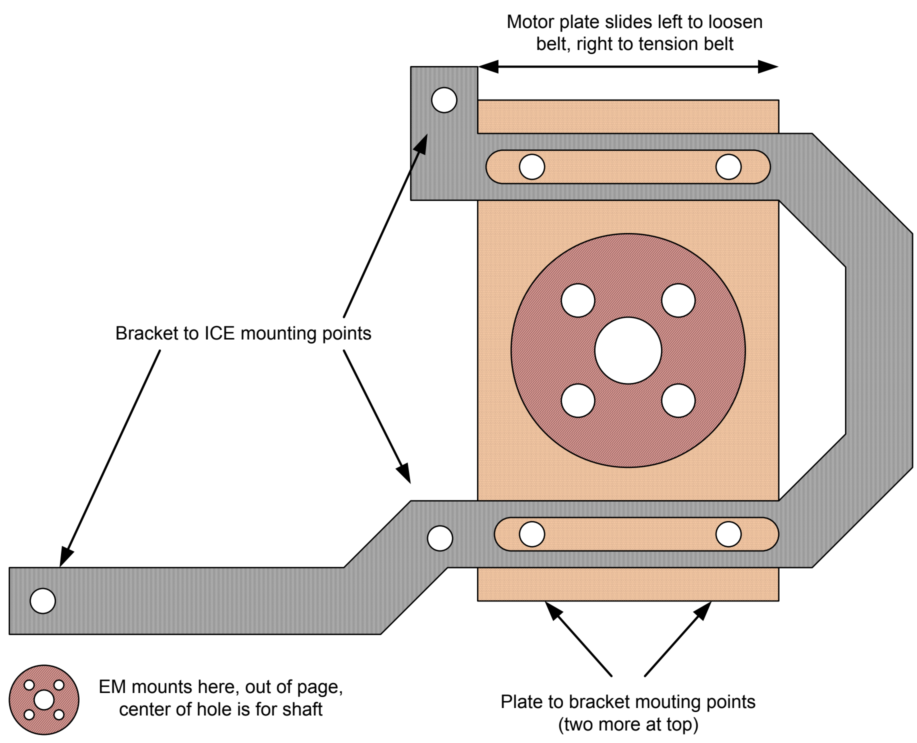

Figure 41: Schematic of motor mount bracket and plate

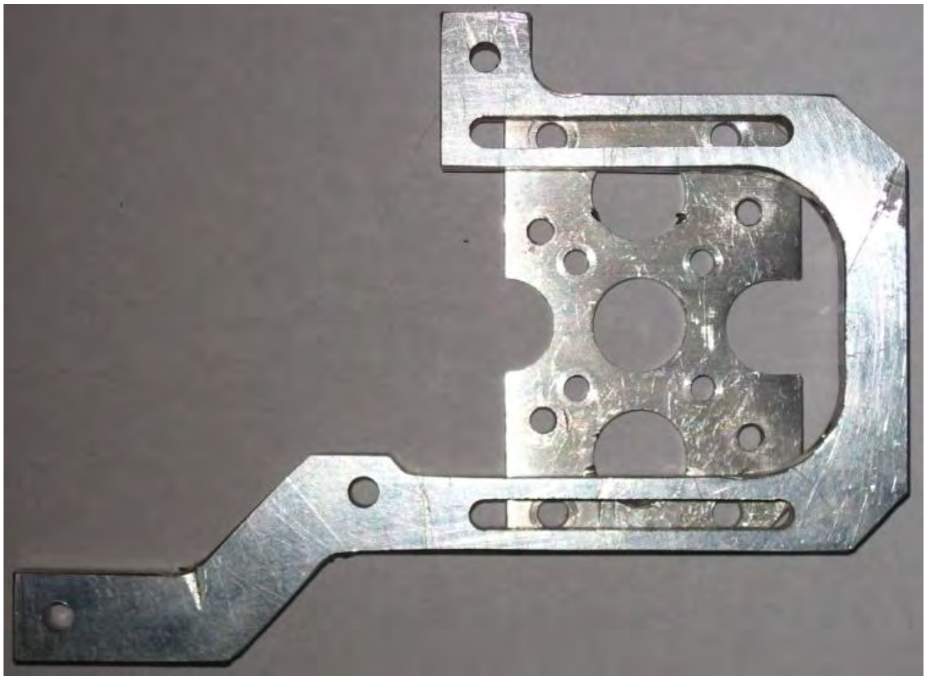

Figure 42: Motor mount bracket and motor plate

Figure 43 is a close up of the assembled bracket and plate mounting system with both the motor and encoder attached. Drawings of the plate and bracket are included in Appendix C.

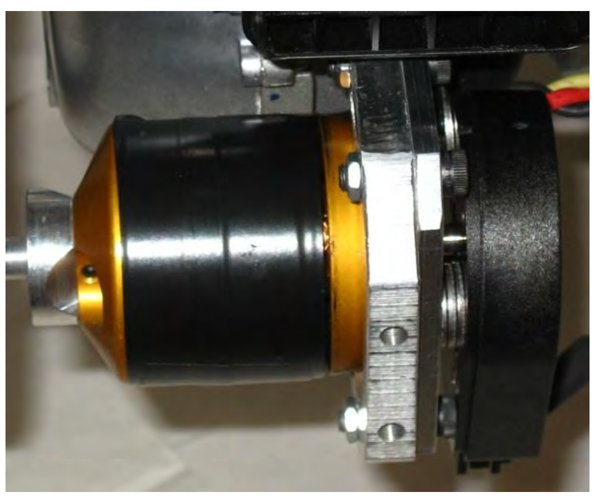

Figure 43: AXI 4130/20 mounted to motor plate and motor mount bracket, all attached to Honda GX25

Initially, the author envisioned a tensioning system to tighten the belt connecting the EM and ICE. A 6 Rib belt was selected due to concerns about wear on a timing belt. A 6 Rib belt would also provide some damping of torque spikes from the ICE before they reached the EM. The first operation of the hybrid system demonstrated that the belt could be sufficiently hand-tightened by pulling the EM and motor plate assembly away from the ICE with the bolts loosely in the slots on the bracket. When the belt reached the desired tension, the bolts were tightened. In fact, the EM could be pulled far enough from the ICE to cause the front of the EM to bend toward the ICE, bending the outside edge of the motor mount bracket forward. The bending forces are shown schematically in Figure 44.

The bending forces lead to an issue first identified during ICE testing with the EM unpowered, but connected. When the belt is under tension, it creates the same reaction forces as in Figure 44. If the bracket bends far enough, the misalignment between the pulleys on the ICE and EM is sufficient that the belt will come off of the EM pulley. Figure 44 shows a suggested cable tensioning device to counteract the belt tension. However, further testing demonstrated that the belt only derails at speeds over 9000 rpm, well above the ICE's operational range on the aircraft. The tensioning cables to prevent the belt from coming off of the pulley during high speed operation were therefore tabled. Thus, while both a belt tightening mechanism and a system to prevent bending of the motor mount bracket are designed for the hybrid system; they are not implemented on the prototype aircraft.

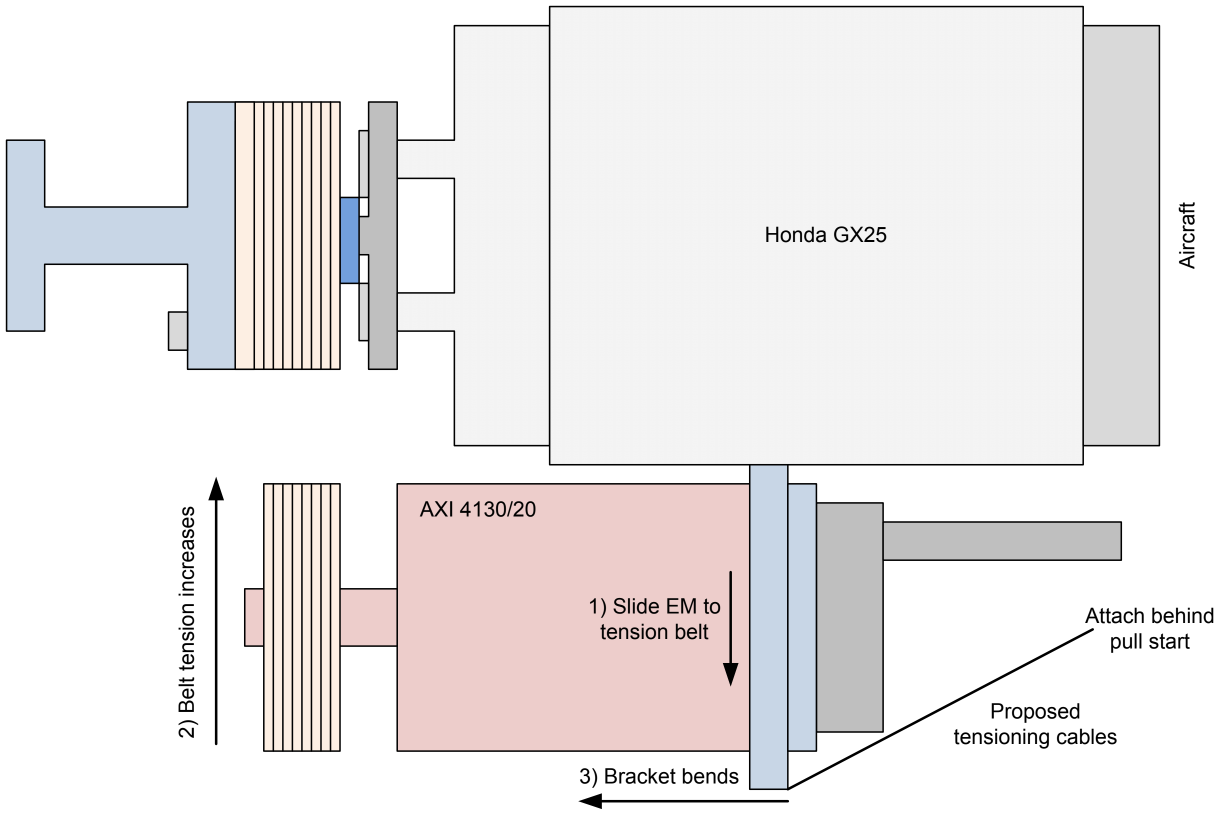

Figure 44: Proposed tension cables to prevent bracket from bending and causing the 6 Rib belt to come off of the EM pulley

6.2. Shaft Power Integration

Once the EM was mounted to the ICE, the next task was joining the drive shafts of the ICE and EM. During the bracket sizing and placement, the author ensured that the EM's drive shaft was far enough forward so that there was overlap with the region in front of the ICE flywheel. Then a pulley on the ICE and a pulley on the EM with teeth in the same plane could tie the power systems together with the aforementioned 6 Rib J-belt. As the ICE pulley contains a one-way bearing and attaches the propeller to the airframe, it was designed first.

6.2.1. The ICE Pulley

The ICE pulley was sized to hold two bearings and the propeller. On the ICE side, the one-way bearing is pressed into the pulley and rides on the engine flange bolted to the flywheel where the clutch pads would normally attach. The engine flange required several iterations and is discussed next. The one-way bearing is a Boca Bearing RC081208 FS. The bearing's race, rollers, and springs are made from stainless steel; it can handle speeds up to 17000 rpm and has a maximum rated torque of 8.85 N-m [**63**], about 10 times the rate torque of the ICE. The bearing fits a 1/2 in shaft and its mass is merely 9.36 g.

On the propeller side of the pulley is a Boca Bearing 1/2-TP thrust bearing. The thrust bearing transfers the thrust generated by the propeller to the engine flange while allowing the ICE pulley to overrun the ICE and drive the propeller when the aircraft operates in EM-only mode. A 1/4-20 in bolt passing through the thrust bearing and into the center of the engine flange ties the entire system together. Torque Transmissions, a machine and tool company in Ohio, manufactured three of the pulleys to the drawing provided in Appendix C.

Originally the author intended to bolt the propeller directly to three holes tapped into the front of the ICE pulley. Discussing the plan with the flight support contractor revealed that drilling three holes through the hub of the propeller carried a substantial risk of compromising the structural integrity of the propeller, leading to failure in flight. Therefore, the ICE pulley was adapted to mount to a Fuji IMVAC 42 mm BT-32A propeller extender flange. To facilitate this modification, new holes were tapped to match the Fuji part and a lip was turned on the pulley's front edge to seat the propeller extender. The inner bore of the pulley was enlarged by 0.254 cm (0.010 in) so that damaged one-way bearings could be easily pressed out of the pulley. These aftermarket modifications are noted on the drawing in Appendix C.

Figure 45 shows a sketch of the ICE pulley and engine flange assembly. The additional thrust bearing between the ICE pulley and engine flange ensures the pulley does not rub on the bolts holding the engine flange to the flywheel. The propeller, held to the prop extender with a single bolt, is not shown. Figure 46 shows the actual ICE pulley and the engine flange, with the one-way bearing pressed into the pulley.

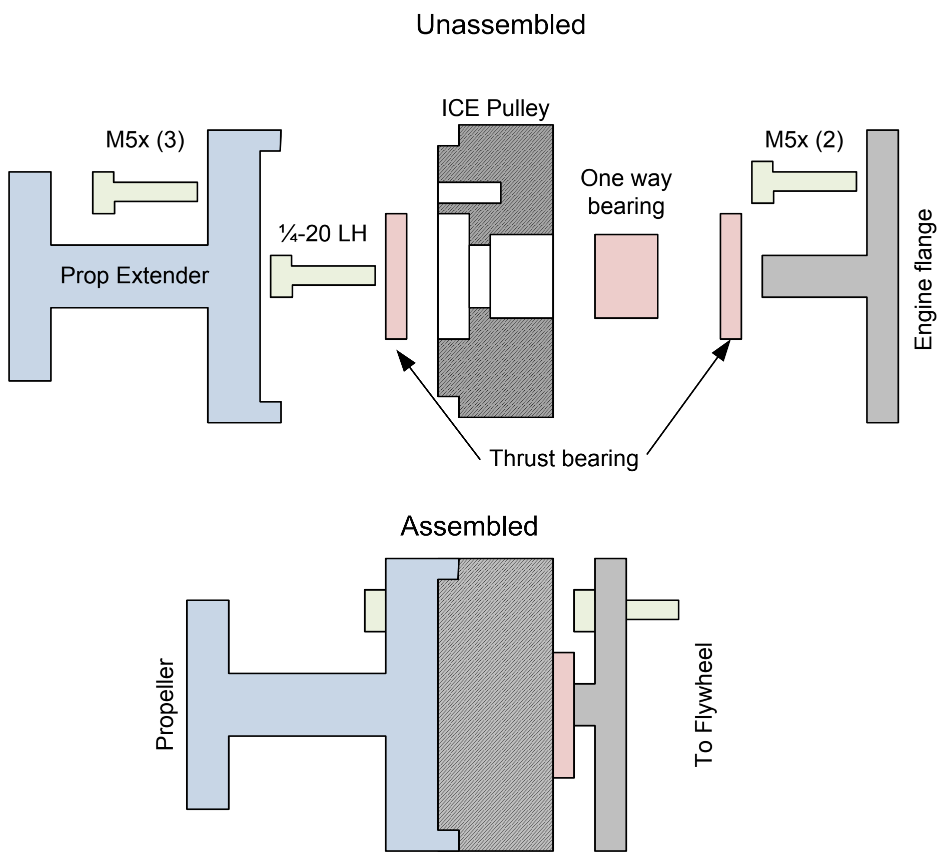

Figure 45: Assembly sketch of the ICE pulley and engine flange (patent pending)

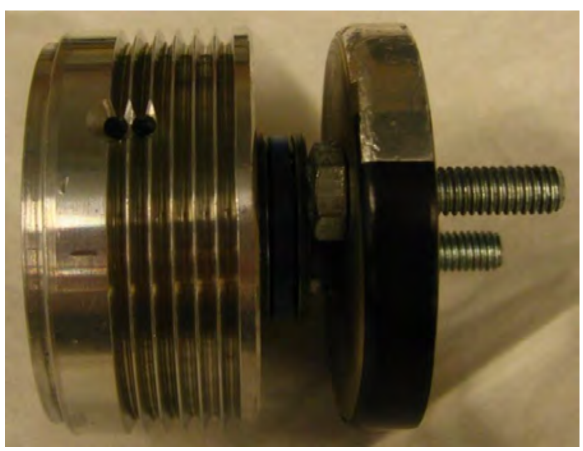

Figure 46: ICE pulley and engine flange

6.2.2. ICE Flange

The engine flange has two responsibilities. First, it holds the propeller and ICE pulley on the aircraft with a bolt that extends though the thrust bearing in the front of the ICE pulley. Second, it provides a race for the one-way bearing in the ICE pulley, allowing the ICE to transmit torque to the propeller. Manufacturing the engine flanges to connect the ICE to the dynamometer was straightforward, although the parts were stainless steel instead of aluminum to handle the torsion loads. Heinly and Koch made the first engine flange in early July 2011. After several hours of testing on the dynamometer the one-way bearing seized. Testing continued on the ICE to complete the torque maps with the attached EM; after all, the goal of the torque maps was to characterize the power available from the ICE on the airframe.

During the break-in testing when the first Honda GX25 failed, the ICE pulley and engine flange were disassembled. During the removal of the ICE pulley, the remnants of the one-way bearing carved groves in the warped metal of the engine flange. Discussions with the AFIT machine shop revealed a likely cause. The engine flange was not precision ground so the bearing was running on a relatively rough surface, ±250 μm (±0.01 in) surface finish. The engine flange was only stainless steel, no harder than the rollers in the bearing. The combination of heat, friction, and materials led to failure of the engine flange.

The machine shop technicians recommended and manufactured a new flange, this time from A2 tool steel. After manufacturing, the new flange was vacuum heat treated to a 60-62 Rockwell hardness and then the surface was precision ground to a ±2.50 μm (±0.0001 in) surface finish. The new flange was attached to the propulsion system in time for the 24 hr ICE buildup test discussed in Section 4.2.4. After 24 hours of operation and another 2-3 hours of testing in various modes, the new flange showed no wearing and the one-way bearing looked essentially new. It should be noted that while the one-way bearings come pre-packed with grease, one-way bearing grease was added and the flange was cleaned every time the pulley was disassembled.

With the system mounted to the airframe the propeller was added as a load to avoid potential system damage due the difficulties with aligning the dynamometer. Adding the propeller created an entirely new issue. When the EM or ICE was turned on, the propeller, extender, and ICE pulley assembly detached from the front of the system. The 1/4-28x3/4 in bolt holding the ICE pulley to the engine flange was right handed as is the propeller. The thrust and spinning of the propeller, accompanied by the vibration of the engine, was sufficient to break loose medium strength LockTite and back the bolt out of the engine flange. It should be noted that one cannot simply crank down on the bolt as doing so would crush the thrust bearing.

The machine shop added a cotter pin through the flange to hold the bolt in place. While the cotter pin successfully retained the bolt, it introduced another issue. The entire ICE pulley, extender, and propeller assembly rides on the 1.3 cm (0.5 in) length of the thrust bearing. If the tightness of the bolt holding the pulley to the flange is not exact, the assembly wobbles even below 2000 rpm. The cotter pin only allows one tightness, and it was not the correct tightness for vibration free operation. Therefore, the author pursued the only available recourse, short of a system redesign. The author ordered a new flange from the machine shop, this time with 1/4-20 left hand threads. A left hand thread tightens in the direction of propeller rotation and should not back out during operation. A drawing for the revised engine flange is available in Appendix C. After running the ICE with the new flange for an hour at various throttle settings between 20% and 100%, there was no loosening of the bolt, indicating the changes in thread orientation were effective.

There is a final note on the engine flange worth mentioning. The GX25 flywheel is cast aluminum and the concentricity of the mounting points is off by ±1.3 mm (±0.05 in) on all three engines in the laboratory. The manufacturer assumes that the centrifugal clutch will take up the slop when it engages the clutch plate in the aftermarket attachment. In this application, this alignment issue causes the engine flange and propeller to be slightly off center from the ICE's rotational centerline. While the vibration was bearable for this prototype, the alignment issue presents an argument for a centrifugal clutch in a future iteration, discussed in Chapter V.

6.2.3. EM Pulley

The EM pulley attaches to the threaded shaft on the front of the AXI 4130/20. The only real design question for the pulley is its diameter to achieve a suitable gear ratio between the EM and ICE. For reference, the ICE pulley has an outer diameter of 5.08 cm (2.00 in). The author used Rotramel's code [**13**] to run a variety of simulations using the AXI 4130/20 and Honda GX25 manufacturer specifications for a nominal 30 V battery pack. In Rotramel's simulation, battery pack voltage only influences endurance flight time, not the optimization of the gear ratio. The code assumes the pack voltage is sufficient to provide the required EM speeds. In each run, the gear ratio between the EM and ICE was optimized to match the selected propeller, ICE, and EM. The gear ratio is the ICE pulley diameter divided by the EM pulley diameter. A gear ratio greater than unity indicates the EM will spin faster than the ICE pulley and propeller. The two bladed 18x8 and 18x12 propellers were selected to bracket the 18 inch propeller market. Discussion of the propeller selection is in Section 7 of this chapter.

The primary concern was that the EM had to be capable of meeting the endurance power requirements, specifically the speed and torque. A lesser concern was the EM's capability to match the ICE speed and provide torque during dual mode operation. Table 7 summarizes the simulation results for the endurance operation of the aircraft.

Table 7: Summary of optimal endurance operational speed and torque for AXI 4130/20

EM Speed (rpm)	EM Torque (N-m)	Prop Speed (rpm)	Prop Torque (N-m)	Gear Ratio (ICE/EM)	Propeller (in x in)	Battery Voltage (V)
6450	0.31	4220	0.45	1.53	18x8	30
5450	0.38	3560	0.57	1.53	18x12	30
4200	0.49	4200	0.49	1.0	18x8	30
6120	0.33	3560	0.56	1.72	18x12	30

Referring back to Table 5 in Section 5.3, the Solo Whistle and AXI 4130/20 combination struggles above ~6000 rpm where the motor speed is pushed using gear ratios greater than 1.5 or the 18x8 propeller. Propellers with diameters and pitches larger than the 18x12 or smaller than the 18x8 would have similar effects. Therefore, the author ordered EM pulleys in two gear ratios: 1.5:1 and 1:1 to provide options after the final propeller selection. The EM pulleys were ordered from Torque Transmissions and the drawings are available in Appendix C.

7. Propeller Selection

The propeller selection was based on a several simulations using Rotramel's code. The 1:1 and 1.5:1 pulley ratios were simulated for two different propellers: the APC 18x8 and the APC 18x12. These propellers were selected as a first estimate based on the simulations run during the battery and the EM pulley selections described in Sections 5.3 and 6.2.3. Additional propeller testing was precluded by a lack of available data for Rotramel's code and the available results bracketed a workable solution. The simulation was run at 600 m above sea level on a standard day using the Solo Whistle controller, AXI 4130/20, and battery specifications as described so far in this chapter. The key results are summarized below in Table 8. Table 8 also includes the optimal gear for both propeller sizes.

Table 8: Simulation summary for initial propeller selection for Condor at 600 m ASL

		Endurance			Cruise			
Propeller (in x in)	**Gear ratio (ICE/EM)**	**EM Speed (rpm)**	**EM Torque (N-m)**	**Flight Velocity (m/s)**	**ICE Speed (rpm)**	**ICE Torque (N-m)**	**Flight Velocity (m/s)**	**Endurance time (hr/set of 2 packs)**
18x8	1:1	4220	0.49	15.5	5334	0.71	22.1	0.196
18x12	1:1	3560	0.56	15.5	4466	0.81	22.1	0.172
18x8	1.5:1	6330	0.33	15.5	5334	0.71	22.1	0.284
18x12	1.5:1	5340	0.38	15.5	4466	0.81	22.1	0.250
18x8	1.47:1*	6240	0.33	15.5	5334	0.71	22.1	0.281
18x12	1.71:1*	6123	0.33	15.5	4466	0.81	22.1	0.383
**Optimized gear ratio*								

The data in Table 8 show that the 1.5:1 gear ratio is closer to the optimal value to maximize the endurance of the aircraft. The ratio would drive the EM to 7750 rpm just to match the ICE at 5500 rpm during dual operation. The AXI 4130/20 and Solo Whistle combination is capped at 8000 rpm so the 1.5:1 gear ratio may be too high for proper dual mode operation. Switching to the 1:1 gear ratio significantly decreases the endurance time for a given set of battery packs, but is likely necessary for matching the EM and ICE in dual mode. For either gear ratio, any propeller with a diameter or pitch larger than the 18x12 would drive ICE speeds well below 4000 rpm. Meanwhile any propeller with a diameter or pitch smaller than 18x8 would increase ICE speeds above 6000 rpm and make it difficult for the EM to catch the ICE in Dual mode operation, even with a 1:1 gear ratio. Therefore, the author ordered 18x8, 18x10, and 18x12 propellers, intending to start with the 18x10 propeller as a compromise between the lower speed of the 18x12 and higher endurance efficiency of the 18x8.

8. Avionics

The avionics are responsible for splitting the throttle signal from the autopilot or manual transmitter between the EM and ICE depending on the flight mode. Table 9 summarizes those modes. This section focuses on the electronics necessary to control that mode as well as the throttles of the two power trains. Note that while the Procerus Kestrel autopilot factored into the avionics design and is responsible for the control of the aircraft, this paper does not cover the programming and tuning of the autopilot. For details on autopilot tuning and stability for the Condor, consult Giacomo [**18**].

Table 9: Hybrid propulsion system operating modes

Mode	Description	Use	Required for testing?	Implemented in final system?
EM-only	The EM provides all power for the aircraft. The ICE is at idle or off.	Loiter	Yes	Yes
ICE-only	The ICE provides all power for the aircraft. The EM is off.	Cruise, Ingress, Egress	Yes	Yes
Dual	The EM and ICE both provide power for the aircraft.	Takeoff, climb	Yes	Yes
Regen	The EM acts as a generator to recharge the batteries.	Battery regeneration	Yes	Yes
Start	The EM and ICE throttles are set to a combination conducive ICE starting.	ICE startup	No, but included on PIC to facilitate bench testing.	No
Test	EM and ICE throttles are set to fixed values.	Bench testing	No, but included on PIC to facilitate bench testing.	No

8.1. Design 1: The PIC32 Hybrid Controller

8.1.1. Concept Overview

The avionics design explained herein assumes the *a priori* selection of the Solo Whistle and AXI4130/20. Realistically, there were several iterations of the avionics prior to the first presented design, but those iterations became obsolete with the selection of the Solo Whistle and AXI 4130/20. The first avionics system design revolves around the PIC32MX795F microcontroller as the hybrid controller. The PIC32 is described in Chapter II Section 3.6 as the PIC32 Lightning developed by Hagen [**16**]. Ideally, a fully operational aircraft would self select between the different flight modes depending on battery charge, flight condition, and so forth. For this instantiation, it was more feasible to implement a state machine on the PIC32 Lightning where the user, through some form of input, sets the flight mode. The PIC32 Lightning then splits the throttle signal appropriately between the ICE and EM. Figure 47 shows the initial layout of the avionics. The PIC32 Lightning receives a raw throttle signal from the Kestrel as well as two signals to select the flight mode. The raw throttle is a PWM signal corresponding to 0-100% throttle. The mode signals are two PWM sliders, explained momentarily. The PIC32 also receives the ICE's rotational speed from a signal tap on the Seagull Flight Data Recorder.

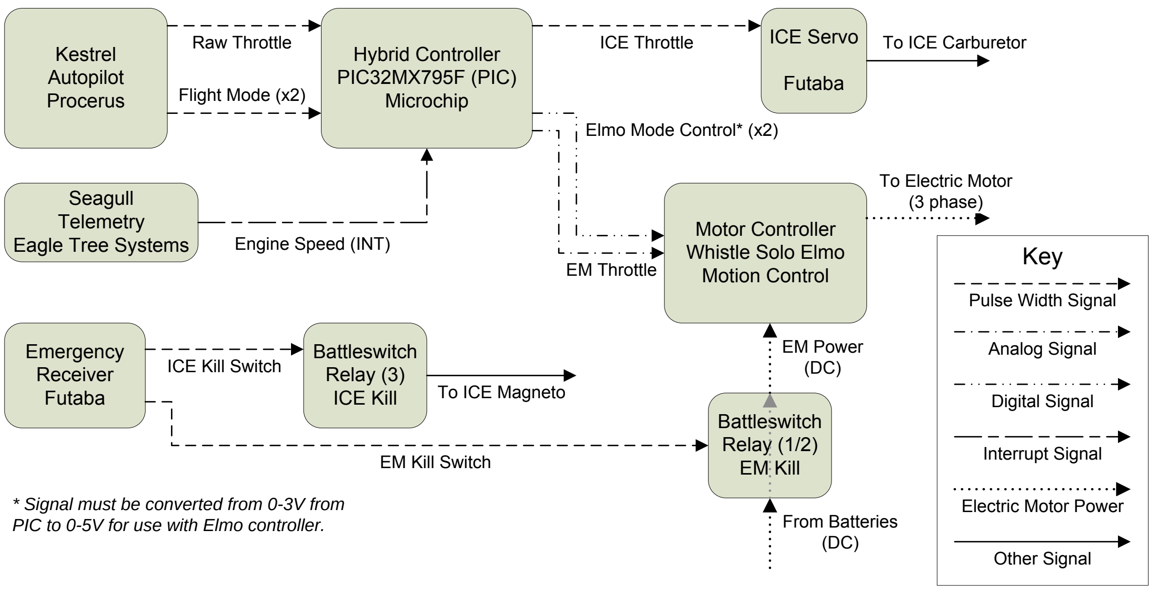

Figure 47: Avionics design 1: PIC32 Lightning as hybrid controller

8.1.2. Code Layout

The code on the hybrid controller is split into two portions. The first portion of the main program executes once on startup, setting all of the port identification and other predefined variables. The second portion is a continuous *while(1)* loop that performs two actions. First, it interprets the mode signal using the *SetPropulsionState()* function. Second, it uses the code specific to that state to execute the throttle split using the *PropulsionControlStateMachine()* function. There are a number of other housekeeping functions that are beyond the scope of this discussion and the interested reader should refer to Hagen for details [**16**]. The specific throttle splitting equations for each mode are provided in Appendix E and a copy of the controller code is provided in Appendix G. The code requires the ICE IOL and ICE maximum torque lines as well as the EM's maximum torque. These values are preprogrammed into the PIC32.

After calculating the throttle split, the hybrid controller provides the analog throttle and digital mode signals to the Solo Whistle and a PWM throttle signal to the ICE servo. The *while(1)* loop then repeats, executing the entire mode selection and throttle setting process at over 100 Hz. Meanwhile, BattleSwitch relays, discussed in Section 8.4, provide independent emergency kill switches for both the ICE and EM.

8.1.3. Mode Control Signals

The author explored several options for the operating mode signal supplied to the hybrid controller, initially planning to use BattleSwitch relays to convert a set of four PWM signals from the Kestrel autopilot into a set of binary digital signals. Due to the semi-proprietary nature of the Procerus code, there are insufficient PWM signals available that can be simultaneously changed. If the signals were changed one at a time at a rate 1/3 sec/signal, the hybrid controller would momentarily 'glitch' into another mode when the partially changed combination matched another flight mode. In the best case, the hybrid controller would default to idle; in the worst case the glitch would kill the ICE, EM, or both.

The Kestrel's gimbaled camera does have two signals that change simultaneously, which the author converted to use for mode control. Each signal is used as a ternary slider which is decoded by the PIC32, creating a total of nine different modes. The signal combinations for the operating states are listed in Appendix H. While this design was phased out for reasons discussed in the next section, this exercise did yield one important conclusion: the Kestrel autopilot and Virtual Cockpit ground station software can be altered to allow the user to control the propulsion state, in this case by redirecting signals intended for the gimbaled camera. The ability to redirect servo signals facilitated the second design, discussed in Section 8.3.

8.2. PIC32 and Procerus Kestrel Incompatibilities

Linking the Kestrel autopilot to the PIC32, exposed an array of incompatibilities. First, connecting the PWM mode signals from the Kestrel to the PIC32 introduced 600 Hz noise on top of the 50 Hz PWM signal yielding rapid and erratic mode switching. Normally the electro mechanical nature of a servo would damp and eliminate this noise. Second, the Kestrel and PIC32 could not share a power rail since the Kestrel requires a dedicated ground. Placing the components on the same ground created additional noise on the signal lines and in the analog signal to the Solo Whistle controller. These issues could have been overcome with filtering and independent battery packs. However, there was one untenable issue: when the Kestrel autopilot signal lines were connected to the PIC32, the ICE control servo received noise spikes causing 40% jumps in throttle. These jumps were sufficiently rapid to kill the engine. Several attempts to shield the lines and to filter the noise were unsuccessful.

By this point in the design, a boost power configuration was acceptable and two controllable PWM signals were available from the gimbaled camera. Therefore, with some programming assistance from Capt Molesworth, the author decided the best course of action was to port the hybrid system control entirely to the Kestrel. The move trades the relatively open source, configurable nature of the PIC32 coding for the relatively rigid semi-proprietary Kestrel code. It is the author's opinion that the PIC32 is still the preferable system for bench testing due to its rapid configurability and HE system code for the PIC32 is included in Appendix G. The code contains a number of features in addition to the hybrid system control algorithms that streamline torque mapping. Despite the advantages of the PIC32, given the choice between a new autopilot for the aircraft and attempting to port the absolutely necessary components of the hybrid control scheme to the existing autopilot, the latter seemed a superior course of action. It would allow proof of concept testing on the airframe and take little enough time that flight testing before March 2012 would still be within reach.

8.3. Vision 2: Kestrel

Figure 48 shows the second avionics design with the Kestrel autopilot acting as the hybrid controller. In this configuration, the raw throttle signal from the Kestrel is automatically transmitted to the ground control station with other flight telemetry. Custom code inserted into the gimbaled camera control function opens the flight telemetry packet and extracts the raw throttle signal. It checks the user interface in Virtual Cockpit for the flight mode, which the user selects using a radio button, shown in Figure 49.

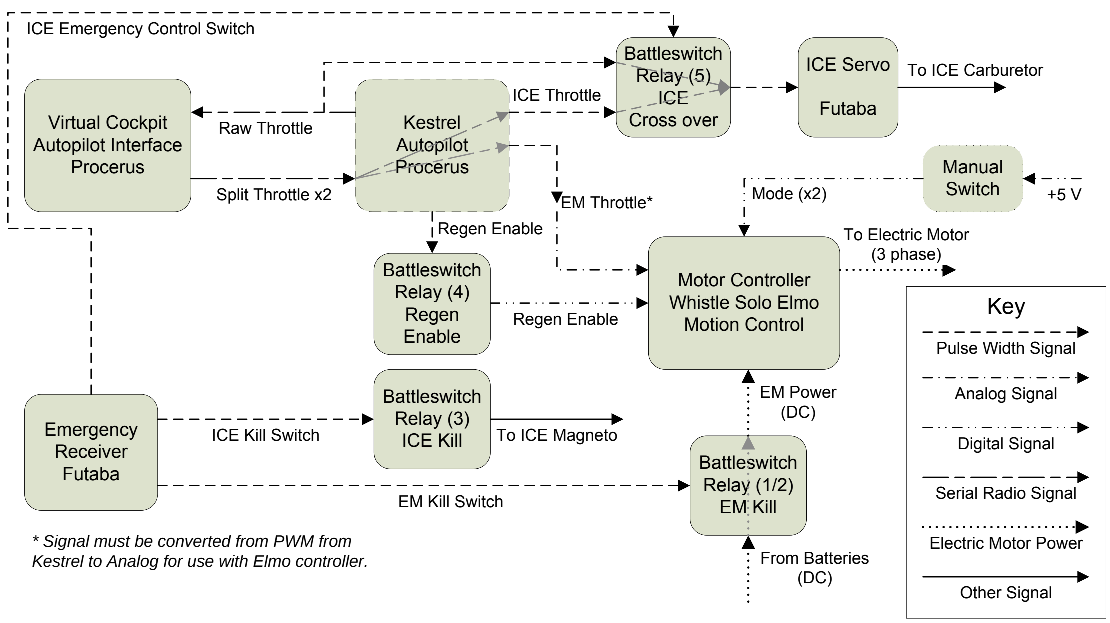

Figure 48: Avionics design 2: Kestrel autopilot as hybrid controller

The inserted code then calculates the throttle split and sends the throttle signal to the gimbaled camera servo packet, repackages the packet, and sends it back to the Kestrel autopilot on the airplane. The entire downlink, calculation, and uplink happens at 6 Hz. This time also includes the conversion of the throttle signals from a percentage to 0-2π, as the gimbaled camera servo packets are programmed in radians. A sample of the inserted code is included in Appendix I. The ICE servo and EM control lines then plug into the gimbaled camera while the raw throttle line is plugged into an emergency relay, explained in Section 8.4.

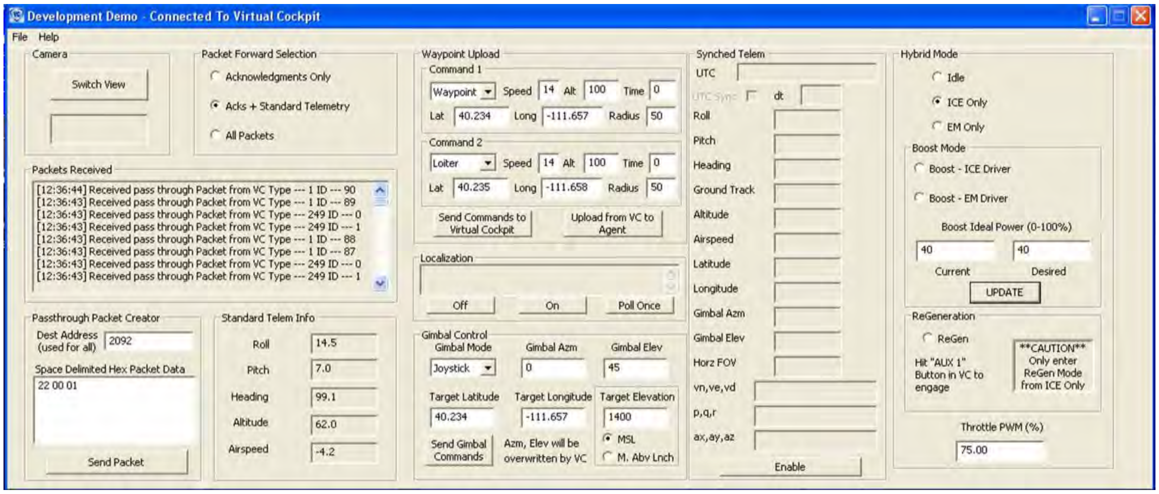

Figure 49: Virtual Cockpit user interface showing mode selection buttons

The Procerus programming language is a modified form of C++ and is advanced enough to use an IOL torque split strategy. As discussed in Section 4.2, there is no need for an IOL strategy with the Honda GX25 and the stock carburetor. Therefore, in dual mode either the ICE or EM is set to a user defined throttle setting and the other component fulfills the remaining power requirement to maintain the flight condition. The user may select which component is held fixed, also useful for testing purposes.

Once the servo signals carried in the gimbaled camera packet reach the aircraft, the signal for the ICE is passed directly to the ICE control servo. The EM signal passes through a PWM to analog conversion board which translates the EM signal from a 1-2 ms PWM to the 0-5 V analog signal required by the Solo Whistle. Note that 80% throttle from the Kestrel corresponds to the Solo Whistle's maximum throttle of 4 V. Therefore, the EM throttle is scaled by a factor of 0.8 before leaving Virtual Cockpit. The PWM to analog board is manufactured by Blue Point Engineering; it is designed specifically for R/C servo signals. The board is pictured in Figure 50.

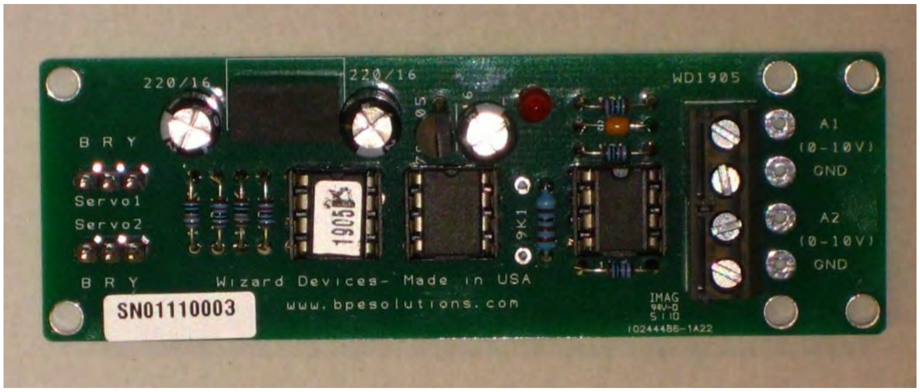

Figure 50: R/C Servo to analog conversion board by Blue Point Engineering

Eliminating the PIC32 complicates control of the Solo Whistle's operating modes. A single PWM line from the Kestrel is converted to a digital signal that controls the 'regeneration' line. A manual toggle switch alternates a 5 V signal between the 'torque control' and 'initialize' lines. The user switches the toggle to 'initialize' when the Solo Whistle is initially powered. Then, the user switches the toggle to 'torque control' where it stays during operation.

8.4. BattleSwitch Relays and Safety Measures

Since the throttle control as described depends on an uplink between the aircraft and Virtual Cockpit, a number of safety features were added using BattleSwitch relays. A BattleSwitch is a relay that is triggered using a standard R/C servo signal. The relays are dipole; in the off position, the common pin, SC, connects to S1 and in the on state SC connects to S2. The relays are manufactured by Dimension Engineering and a picture of a BattleSwitch along with its wiring diagram is shown in Figure 51. At 34 g and approximately a cubic inch the relays are ideal for an aircraft application. When the relay receives a R/C PWM signal greater than 50%, it throws to the on position; it turns off when the signal drops below 50%. The author originally planned to use the BattleSwitches to convert a set of PWM signals from the Kestrel to a set of digital signals to select the flight mode. Instead, the relays are used in the avionics system as safety measures.

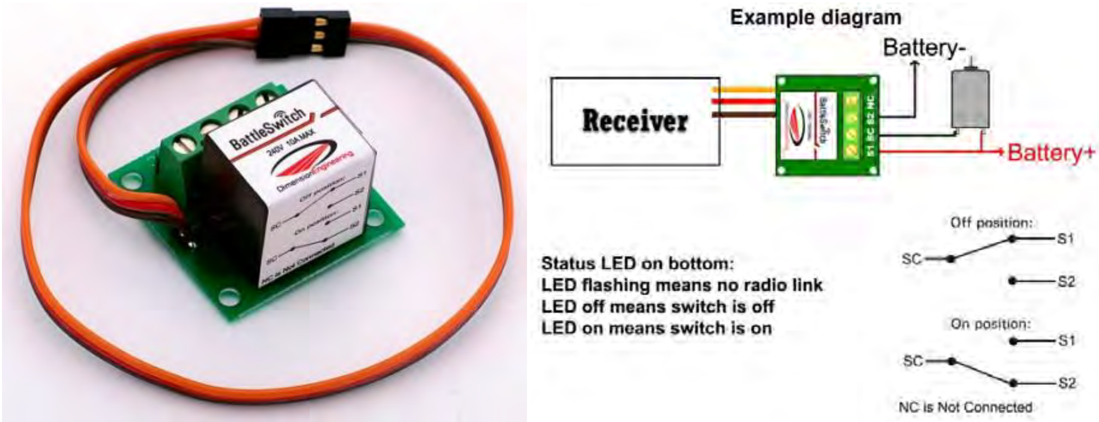

Figure 51: BattleSwitch relay and wiring diagram by Dimension Engineering [**81**]

Table 10 lists the BattleSwitch relays used in the final system. Except for the regeneration switch, the BattleSwitches are triggered by the emergency receiver and are independent of the Kestrel autopilot. The first two switches cut power to the Solo Whistle controller and EM. This is useful for cycling power to the system if commutation fails on start-up. It can also function as a safety kill to prevent a runaway aircraft in the event the autopilot fails or loses communication with Virtual Cockpit. Two switches are used to handle the 20 A draw of the Solo Whistle; each switch is rated at 10 A.

The third switch grounds the magneto on the ICE, effectively killing the engine. The switch can cut the engine for silent operations, to test EM-only mode, or again, to prevent a runaway aircraft. Without mid-air restart implemented, once the ICE is killed the aircraft will have to land on electric power or under glide. The fourth switch, not controlled by the emergency receiver, controls Pin J2/3 to the Solo Whistle and enables regeneration mode.

Table 10: BattleSwitch relay connections and channels

#-Function	S1	SC	S2	On function	Off function	Receiver
1 - EM Kill	Solo Whistle	Battery Power	NC	Solo Whistle Unpowered	Solo Whistle Powered	Channel 7 Switch C
2 - EM Kill	Solo Whistle	Battery Power	NC	Solo Whistle Unpowered	Solo Whistle Powered	Channel 7 Switch C
3 - ICE Kill	NC	Magneto	Magneto	Kill ICE	none	Channel 8 Switch D
4 - Regen Enable*	GND	Solo Whistle Pin J2/3	+5V	Disable Regen	Enable Regen	Channel 5 Switch A
5 - ICE crossover	Kestrel ICE camera	ICE control servo	Kestrel raw throttle	ICE Throttle	Raw throttle	Channel 6 Switch B

**Regeneration mode is controlled by the Kestrel autopilot in the aircraft*

The last switch was implemented specifically due to the nature of the code inserted into Virtual Cockpit. In a normal loss of communication situation where the Kestrel loses contact with Virtual Cockpit, the Kestrel would continue to fly the aircraft since its throttle would be directly connected to the ICE (or EM) control servo (or controller). The hybrid setup disconnects this throttle and routes it through Virtual Cockpit at the ground station and then back to the aircraft as discussed in Section 8.3. If communication is lost, no throttle signal is transmitted to either the ICE or EM and, the Kestrel has no control of the propulsion system. The fifth switch connects the raw throttle from the Kestrel to the ICE control servo bypassing the throttle split in Virtual Cockpit. This setup was tested using a BattleSwitch to perform the cross over and there are no discernible issues; the throttle is passed with no additional delay or hysteresis. Thus if communication is lost, the Kestrel can control the ICE and fly the aircraft to a rally point or perform any other lost communication protocol. In a future iteration, the control of the fifth switch should probably be changed to the Kestrel autopilot and triggered immediately on loss of communication. This concludes the discussion of the avionics for the hybrid aircraft where system control is concerned. The remainder of the section discusses instrumentation and several miscellaneous electronics issues.

8.5. Seagull Flight Data Recorder and Instrumentation

As mentioned in Section 4.2.1, a Seagull Flight Data recorder was selected as the instrumentation on the aircraft. A single Seagull unit can provide two rotational speed measurements, up to four servo measurements, battery voltage, battery current, as well as altitude and airspeed if hooked up to the Pitot probes on the aircraft. Since the Kestrel provides airspeed as well as ground track velocity in the flight telemetry packet down linked to and logged in Virtual Cockpit, the Seagull is used only to monitor the hybrid system.

In the setup, the Seagull is powered from the Kestrel servo power rail since the voltage of the EM battery packs exceeds the tolerance of the Seagull. To measure the voltage of a battery, the Seagull must have a common ground with the battery pack it is measuring. To connect the Seagull to the EM battery pack ground requires a splice that disables the Seagull's capability to measure PWM signals. Therefore, the author had to choose between monitoring the battery voltage for the EM and the PWM signals to the hybrid system throttles. Since the Seagull data streams live to a handheld unit or computer on the ground, the author opted to measure battery voltage to avoid overcharging the batteries while testing regeneration mode. Virtual Cockpit tracks the two throttle signals and the raw throttle down linked from the Kestrel, so the choice provides the largest number of monitored variables. If desired, a second Seagull system could, redundantly, monitor the PWM signals.

8.6. Avionics Box Concept

Another consideration that arose during integration was fitting the electronics into the aircraft while maintaining modularity to facilitate tweaks, changes, and debugging. To solve this problem, the author conceptualized an avionics box constructed from 1/8 in Plexiglas or similar that would hold all of the different circuit boards. The box could slide in and out of the aircraft and the wires external to the box could be quickly attached with quick disconnects. Heinley and Koch manufactured two such boxes. Due to late changes in the avionics and unanticipated changes in the internal aircraft space, the author opted to attach the electronics to individual boards, one for each wall of the aircraft, as shown in Section 9 of this chapter. Nevertheless, for a final aircraft design, the box concept has significant merit as it would simplify field maintenance of the electronics. It could also make the entire avionics system modular and replaceable.

8.7. Engine Servo Issues

After the elimination of the PIC32 from the avionics, there was still a noise problem on the ICE control servo. The servo is mounted above the flywheel and EM and next to the magneto. Therefore, it is exposed to several magnetic fields and twitches even when the EM is powered on, but not rotating. Mounting the servo behind the ICE bulkhead did not solve the problem; the long control cable acted like an antenna, creating additional electromagnetic interference. The connection also had significant hysteresis due to the length of the cable run. Therefore the servo was moved to the forward mounting position shown in Figure 38 to shorten the control cable to a 3.8 cm (1.5 in) control rod, introducing the electromagnetic interference in the process. The standard hobbyist solution for interference on servo wires is to twist the servo wire. However, twisting the servo wire did not solve the issue. Therefore, wire mesh shielding was added to the servo wire, effectively eliminating the noise.

9. Final Integrated Configuration

This section summarizes the final hybrid propulsion system as integrated onto the Condor airframe in preparation for the validation and testing discussion in the subsequent chapter. Where possible, it will reference previously presented figures to avoid repetition. Table 11 lists the COTS components in the final airframe along with their manufacturer and price as of the writing of this document. Figure 52 revisits the generic hybrid system presented in Figure 20, filled in with the selected COTS components and modified so the autopilot also serves as the hybrid controller. Wire and cabling is not included. Figure 39 and Figure 38, already presented, depicted the final layout of the ICE and EM in schematic and picture form, respectively. Figure

48 shows the signal layout of the avionics while the full wiring diagram is in Appendix A and the Solo Whistle wiring specification is in Appendix B.

Table 11: COTS components in integrated propulsions system

Part	Manufacturer	Model or Part Number	Approximate Cost
Electric Motor	AXI Model Motors	AXI 4130/20	$150 [**82**]
Internal Combustion Engine	Honda Motor Company	Honda GX25	$195 [**83**]
ICE Servo	Futaba	S310	$25/ea [**78**]
Batteries	Thunder Power RC	TP3300-4SPL25	$90/pack [**84**]
Electric motor controller	Elmo Motion Control	Solo-Whistle	~$1042 [**85**]
Inductors	Digikey	M8879-ND	$4/ea [**86**]
Elmo motor cables	Elmo Motion Control	CBL-MLXFDBK	$27/ea [**87**]
Optical encoder	US Digital	E6 Optical Encoder E6-500-236-I-D-D-D-B	$90/ea [**88**]
Motor encoder cable	US Digital	CA-FC10-SH-NC-2	$15/ea [**88**]
Motor encoder chip	US Digital	LD5	$16/ea [**88**]
Serpentine belt	Belt Palace	140 J6	$16/ea [**89**]
One-way bearing	Boca Bearing	RC081208 FS One-way Bearing	$15/ea [**63**]
Thrust bearing	Boca Bearing	1/2-TP Thrust Bearing	$7/ea [**63**]
Seagull flight data recorder (includes sensors, transmitter)	Eagle Tree Systems	SEA-FLIGHT-24-02	$520 [**90**]
Electric expander (100A)	Eagle Tree Systems	ELE-EXP-100	$40 [**90**]
PWM to analog converter	Blue Point Engineering	R/C Servo to Analog Converter	$85 [**91**]
BattleSwitch relays	Dimension Engineering	BattleSwitch	$25/ea [**81**]
Propeller	APC Propellers	18x10 Sport	$22/ea [**92**]
Propeller extender	Fuji Engines	Fuji IMVAC Prop Flange Short 42.5 mm BT-34A	$70/ea [**78**]

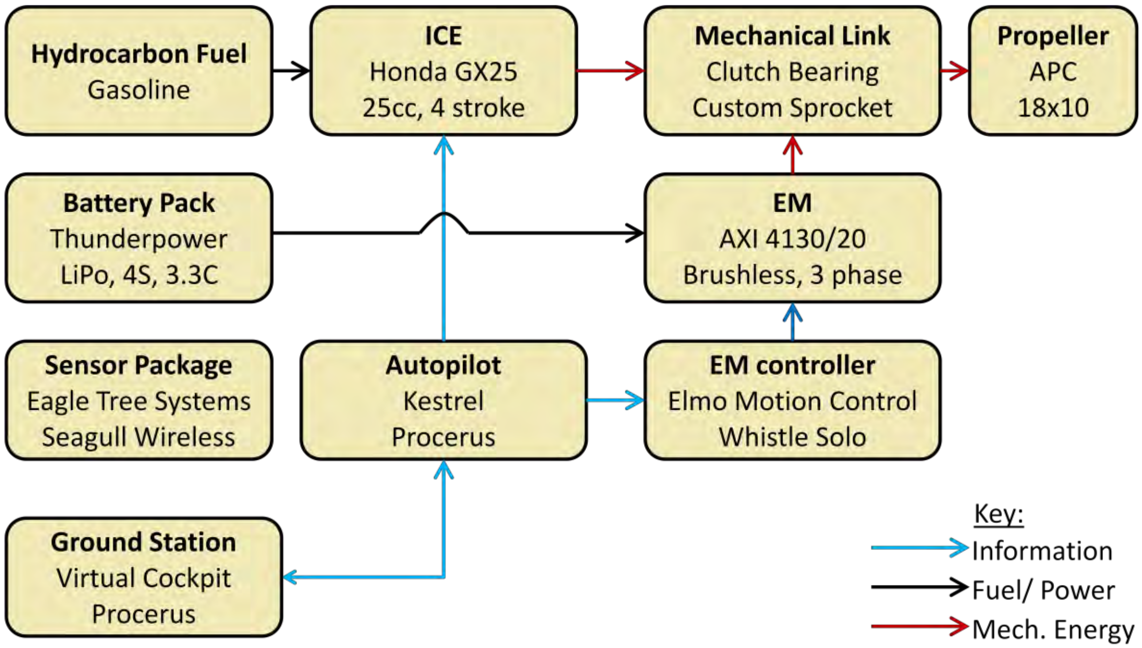

Figure 52: Generic hybrid system with selected COTS parts listed for each component

Figure 53 shows the layout of the hybrid system components in the airframe. The propulsion system attaches to the front bulkhead of the aircraft. Behind the bulkhead is the 1.78 L (60 fl oz) fuel tank. The inductors for the Solo Whistle and EM are sandwiched between the fuel tank and the top of the fuselage. Behind the fuel tank under the removable wing root are the batteries, mounted to the interior of the aircraft using hook and loop fastener. Up to 3 sets of two 4s 3.3C Li-Po batteries may be carried at this location. Behind the batteries on the floor of the fuselage is the Kestrel autopilot.

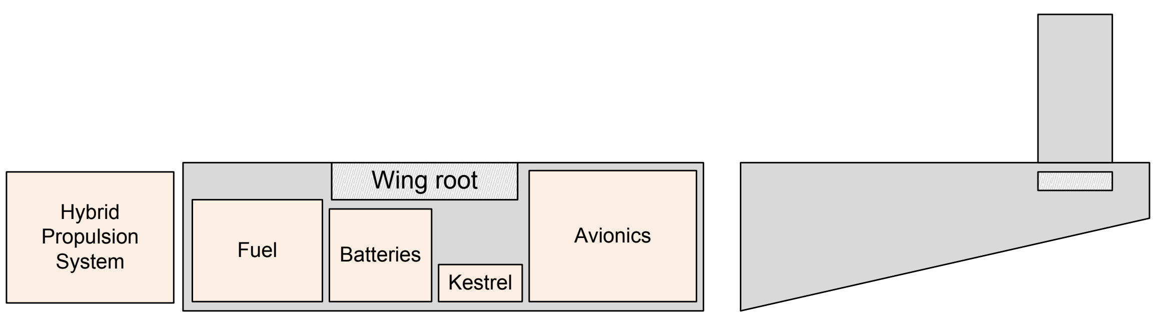

Figure 53: Aircraft layout

In the section behind the wing root and forward of the tail joint, the avionics and electrical components are mounted to 1/8 in thick plywood plates attached to the walls and floor of the fuselage using hook and loop fastener. The components attach to the plates using 4-40 nylon screws. Figure 54 shows the components mounted to each panel. The tail of the aircraft is empty except for servos and wires for the control surfaces. A set of batteries may be moved to the tail to adjust the center of gravity of the airframe, if necessary.

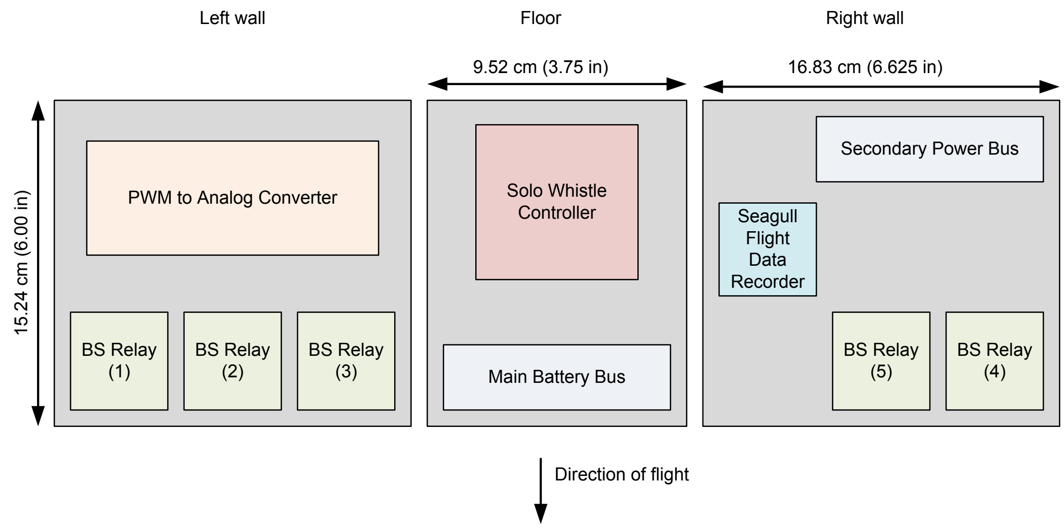

Figure 54: Avionics layout

The system is testable in three different configurations. First, the hybrid propulsion system can be removed from the aircraft and mounted to the dynamometer cradle; the avionics then sit alongside on the dynamometer stand. Second, the system can be mounted to and inside of the aircraft and the wingless fuselage mounted inside the dynamometer test stand. This allows the exhaust vent to remove fumes from the ICE and the safety shield to protect operators from the propeller, allowing indoor testing of the system on the airframe. Third, the fuselage may be removed from the test stand, fitted with its wings and empennage surfaces, and used for ground and flight testing of the hybrid system. A combination of these setups was used to generate test data for comparison to the design simulations as discussed in the next chapter. The text will specify the configuration used to generate the test data. A significant portion of ICE testing was performed using the PIC32 to control the servos and throttle signals. The same testing could be accomplished using any servo control setup since the throttle signals were held static or changed in step increments for the testing. With the final configuration presented, the focus of this work now shifts to the results of testing and the comparison with the simulations used to design the aircraft.

IV. Results and Analysis: Validation and Testing

1. Introduction

With the integration of the propulsion system complete, the focus of the paper now shifts to testing and validation. The first section of the chapter focuses on comparing the implemented aircraft and propulsion system to Hiserote's [**12**] and Rotramel's [**13**] design simulations. The second section of the chapter presents the bench, ground, and flight test results of the final system that were available at the time of publication.

2. Design Simulation Comparisons and Component Test Data

2.1. Comparison of Condor to Hiserote's Design Simulation

As mentioned previously, the Condor team ordered an engine-only aircraft using a Honda GX35 engine to allow the team to vet the airframe independently of the HE propulsion system. This section first compares the engine-only aircraft to the optimized aircraft design from Hiserote's and Harmon's simulations [**11**,**10**]. Then, the engine-only aircraft parameters are fed through Hiserote's code, which predicts the power requirements for the aircraft and HE system. These requirements are compared to the manufacturer and bench test data for the components. Finally, the weight allocations predicted by the code for the both the engine-only and the HE aircraft are compared to the weights estimated by the simulation.

2.1.1. Comparison of Constructed Aircraft to Initial Design

Table 12 lists the key design parameters for the Condor aircraft alongside the initial designs of Harmon and Hiserote for a clutch start, charge sustaining aircraft configuration as discussed in Chapter II Section 2.4 [**11**,**10**]. The Condor has a slightly smaller wing both in span and total area and a higher aircraft weight, leading to a larger overall wing loading at takeoff. Initially, the Condor was designed with a 4.57 m (15 ft) wingspan to match the aircraft envisioned by Hiserote [**12**]. Due to concerns about the strength of the wing material, the main wing of the

Condor was reduced to a 3.66 m (12 ft) span with the option of adding an additional 0.91 m (3 ft) of wing using outboard wing extensions.

During the November 2011 flight test of AFIT-1 using the Honda GX35 engine with the aircraft ballasted to 15.9 kg (35 lbs), a wind gust hit the aircraft in flight with the 4.57 m (15 ft) wing span configuration. The increased lift and resulting wing deflection cracked the fiberglass wing coating approximately 0.6 m (2 ft) from the wing root. Aside from the structural concerns, the 4.57 m (15 ft) configuration was difficult to handle in the air and was prone to sudden upwards pitching. The stability analysis in [**18**] also indicated lateral instabilities with the 4.57 m (15 ft) wing span. The larger wing was difficult to handle on the ground and the wing tips were prone to touching the ground during the taxi and takeoff rolls. Based on the experience with AFIT-1, the Condor team decided to pursue the 3.66 m (12 ft) wingspan for testing the HE propulsion system.

Table 12: Comparison of Condor aircraft to initial design estimates

Physical Dimensions	**Harmon**	**Hiserote**	**Condor**
Aspect Ratio	14.6	14.42	12
Wing Loading	90 N/m^2	90 N/m^2	140 N/m^2
Wing Area (S)	1.48 m^2	1.48 m^2	1.115 m^2
Wing Span (b)	4.65 m	4.62 m	3.6576 m
Wing Chord (c)	0.32 m	0.321 m	0.3048 m
Aircraft Mass (Takeoff)	13.6 kg	13.6 kg	15.9 kg
Mission Parameters	**Harmon**	**Hiserote**	**Condor**
Takeoff Altitude	1525 m (ASL)	1500 m (ASL)	300 m (ASL)
Mission Altitude	1525 m (ASL)	300 m (AGL)	300 m (AGL)
Endurance time	1 hr	3 hr	1 hr*
Aerodynamic Parameters	**Harmon**	**Hiserote**	**Condor**
$C_{L,max}$	1.25	1.25	1.507**
$C_{D,o}$	0.036	0.036	0.040**
Oswald Efficiency Factor (e)	0.85	0.85	0.85 (estimated)
** Reduced from 3 hours due to poor specific energy of COTS batteries within project budget constraints.* *** estimated based on airfoil data* [**93**].			

The Eppler 210 airfoil has a greater $C_{L,max}$ than the NACA 4412 airfoil used in the initial design simulations. While the aircraft itself uses an Eppler 210 airfoil, data on the Eppler 210 is difficult to find. In its place, both the author and Giacomo used the NACA 4412 data. The NACA 4412 airfoil is similar to the Eppler 210; the main difference is that near the trailing edge the Eppler 210 has slightly more under camber than the NACA 4412. This minor difference gives the NACA 4412 slightly lower induced drag as well as a slightly lower lift coefficient. It is the author's experience that once manufactured, the two airfoils are interchangeable in operation. Manufacturing inaccuracies wash out the theoretical difference between the foils, justifying the substitution of NACA 4412 data in the absence of Eppler 210 data.

Table 12 lists a larger takeoff weight than the ideal aircraft. At the time of the AFIT-1 flight test, the weight of the hybrid system was not finalized. However, based on the selected components, the 15.9 kg (35 lbs) was identified as an upper limit driven primarily by the extra structure, batteries, and avionics of the HE propulsion system. To verify the airframe could handle the increased weight, AFIT-1 was ballasted to 15.9 kg (35 lbs) using simulated payload. For the purpose of simulation, the hybrid system payload capacity is assumed to equal to the difference between the takeoff weight and the 15.9 kg (35 lbs) limit, even though the aircraft was not ballasted for the initial hybrid-electric ground and flight testing.

In his design, Hiserote assumed a battery specific energy of 200 Whr/kg, a high end value for COTS Li-Po batteries. Despite the optimistic battery estimates, Hiserote's optimized aircraft still struggled to perform a simulated 3 hr continuous loiter in some configurations [**12**]. Meanwhile, the batteries for the Condor are closer to 132 Whr/kg. The Condor batteries were constrained significantly by budget, leading to performance 30% to 40% lower than the technological cutting edge for Li-Po batteries. Furthermore, other chemistries such as Li-S offer specific energies upwards of 300-600 Whr/kg as discussed in Chapter II, Section 3.4 [**57**].

The endurance time of the aircraft is directly proportional to the specific energy of the batteries. From initial estimates, Hiserote's 3 hr loiter [**11**] was too aggressive for the Li-Po batteries within the ~$2000 battery budget for the project. Therefore, the objective value was decreased to Harmon's 1 hr loiter [**10**]. Thus, while the Condor falls short of the 3 hr loiter time, additional funding for top-end batteries on the current market as well the future advancements in battery technology could increase the energy capacity of the Condor allowing it to perform loiter missions approaching the 3 hr time frame suggested by Hiserote. The reported loiter time estimates for the Condor should be interpreted as the performance of an airframe constrained by budget and current COTS technology and not as a limit on the possible performance of the airframe under different budget or technological conditions.

Lastly, the designated mission for the actual aircraft has changed slightly from the missions envisioned by Hiserote [**12**]. The mission altitudes have been decreased to reflect the flight test location at Camp Atterbury, IN. Despite all of the changes from the initial optimized design, the Condor airframe is relatively true to the optimized design, recognizing discrepancies in wingspan and weight primarily due to optimistic design constraints and battery performance predictions.

2.1.2. Simulated Flight Maneuver and Component Power Requirements

While Hiserote's code was originally intended to optimize an HE-RPA, the optimization routine in the code can be hardcoded with a designed aircraft and will instead output the power requirements of the system and components to meet the specified aircraft performance. The analysis also calculates the weight fractions for both the non-hybridized and hybridized versions of the aircraft. Those weight fractions are the topic of Section 2.1.4. The simulation is based on a number of performance parameters in addition to the aircraft weights and geometries listed in Table 12. These performance parameters are summarized in Table 13. To match the implemented Condor aircraft as closely as possible, the clutch start configuration and charge sustaining strategy were chosen from the available simulations in Hiserote's code. The hard-coded clutch mass remained at Hiserote's value of 0.600 kg [**12**] as an approximation for the engine flange, ICE pulley, EM pulley, and one-way bearing.

Table 13: Condor performance parameters for Hiserote's simulation

Parameter	Value	Parameter	Value
Power-to-weight ratio EM	3130 W/kg	Empty weight fraction	0.700
Power-to-weight ratio ICE	392 W/kg	Payload mass	3.488 kg
Cruise SFC	2.07E-6 N/W/s	Clutch mass	0.600 kg
Endurance SFC	2.90E-6 N/W/s	Endurance time	1 hr
Rate of climb	2 m/s	One way cruise	1 hr
Cruise velocity	20.11 m/s	Payload power*	0 W
Maximum velocity	30.0 m/s	Avionics power*	0 W
Stall Safety margin	1.54 m/s		
** Avionics and payload batteries are separate from EM battery packs and thus do not deplete the endurance power.*			

The power-to-weight ratios were calculated based on the manufacturers' power specifications for each component and the weight of the component with all parts not required for flight removed. The payload and empty mass fractions are based on the simulated payload (ballast) and fuel loads flown in the 15.9 kg (35 lbs) AFIT-1 flight test. The SFC and stall safety margin were left at the nominal values used in the initial design simulation. The aircraft rate of climb was set at 1 m/s. The maximum velocity was set at 30 m/s, just short of the 30.9 m/s maximum speed AFIT-1 achieved during flight test. The cruise velocity was set to 20.1 m/s to match the cruise velocity used for AFIT-1 in the 15.9 kg (35 lb) configuration flight test. The endurance and cruise legs were reduced to match Harmon's original concept [**10**]. Finally, the avionics and payload run on a separate battery pack from the EM. That pack's weight is lumped into the empty weight of the airframe. Therefore, the avionics and payload power consumptions are set to zero since they do not contribute to power draw of the EM battery packs.

Table 14 lists the power requirements and their corresponding velocities using Hiserote's simulation. The maximum velocity is the driving aircraft power requirement and is more than twice the next highest power requirement. Hiserote's code sizes the hybrid system by selecting the ICE to meet the cruise power requirement and the EM to meet the endurance power requirement. It then checks to see if the system will meet the other power requirements to include the maximum velocity. Meanwhile the projected ICE size for the engine-only aircraft is based solely on the maximum power required instead of the cruise power. Therefore, the ICE the code selects for the original aircraft will always be able to meet all power requirements in Table 14; the hybrid system is only guaranteed to meet the endurance and cruise requirements.

The preceding explanation highlights an issue with the code's treatment of performance requirements for the HE design. The code sizes the propulsion system to meet the projected cruise and endurance requirements. However, the code will reject the design if it cannot achieve the maximum flight velocity of the original, engine only, airframe. The operational concept for the HE aircraft is near silent loiter and efficient operation. Failure to meet the maximum velocity of the original aircraft is not necessary to fulfill that concept. Therefore, the HE design may be acceptable even if it falls somewhat short of the maximum velocity requirement since that requirement is derived from the performance of the engine only airframe, not the operational concept. When comparing the designed system to the power requirements from the code, the maximum velocity should be treated as an objective value, not a threshold value.

Table 14: Simulated flight maneuver power requirements for Condor at 15.9 kg (35 lb)

Velocity	Simulated Power Required (W)	Theoretical Velocity (m/s)	Condor Velocity (m/s)
Climb	307	Rate of climb: 1.0	
Cruise	268	20.1	20.1
Endurance	166	15.1	
Maximum velocity	735	30.0	30.9*
Stall	151	13.5	9.0
**Maximum velocity achieved by AFIT-1 during flight test.*			

During flight testing, the stall velocity of the 15.9 kg (35 lb) Condor was identified as 9.0 m/s, about 4 m/s lower than that predicted by Hiserote's code. Hiserote's simulation is based on thin airfoil theory, which depends on an airfoil that is both thin and lacks significant under camber [**41**]. The Eppler 210 is neither, leading to a mismatch between predicted and actual performance as the calculation diverges from the CL_{max} point. In this instance, the extra under camber provides a slight boost in lift compared to the simulation, reducing the airframe's actual stall speed. For all gliders Harmon and Hiserote have simulated to date, a lower actual stall speed facilitates better endurance speeds while maintaining a safety margin above stall, arbitrarily 1.54 m/s (5 kts) [**11**]. For the Condor, the 4.7 m/s difference between the best predicted endurance velocity, 11.1 m/s (and below predicted stall), and the simulated endurance velocity, 15.1 m/s (and 1.54 m/s above predicted stall), changes the endurance power requirement from 141 W to 166 W. If the airframe actually stalls at 9.0 m/s, then the endurance leg could be flown at 11.1 m/s while maintaining the 1.54 m/s safety margin and adding about 17% to the endurance time for a fixed battery capacity.

Table 15 shows the simulated power requirements for each propulsive component. While the requirements from Table 14 represent the aerodynamic power required at the propeller, the values in Table 15 are for the individual components. They reflect nominal motor, propeller, and shaft efficiencies, selected conservatively by the author to match manufacturer data. The unmodified airframe requires a 943 W engine to meet all performance requirements. Meanwhile the ICE and EM sized for the hybrid system meet all performance requirements except for the maximum flight velocity, where they fall about 200 W short. This shortcoming accounts for the 30% difference between the power for the engine-only variant and the combined power of the ICE and EM. Recall based on the earlier discussion that the HE system may be satisfactory even if it does not match the maximum velocity of the engine only aircraft. Furthermore, these projections are only optimal sizing estimates. Since the actual components are COTS parts, not custom parts designed for the simulated power output, they may be more powerful allowing the hybrid to actually meet all performance requirements. Also, this simulation does not reflect shaft speeds and component matching which is the subject of Section 2.2 of this chapter.

Table 15: Simulated component power requirements for Condor at 15.9 kg (35 lb)

Component	Simulated Power Required	Driving Flight Condition
Engine-only ICE	943 W	Maximum velocity (30.9 m/s)
HE ICE	432 W	Cruise velocity (20.1 m/s)
HE EM	208 W	Endurance velocity (15.1 m/s)
Battery Capacity	248 Wh	Endurance time

2.1.3. Comparison of Simulated Component Power Requirements to Manufacturer Data and Component Bench Tests

Table 16 compares the simulated power requirements to the manufacturer specifications for each component. At first glance it seems the GX35 may be underpowered for the airframe. However, the power requirement is driven by the maximum velocity, as discussed previously. Thus while the GX35 is, on paper, barely capable of meeting the maximum velocity requirement, it should be more than capable of performing all other flight maneuvers. The parts selected for the hybrid ICE and EM both exceed their estimated power requirement based on Hiserote's code. Therefore, the actual HE system should be capable of meeting all performance requirements, even though the simulated HE system designed for endurance and cruise falls short of the maximum velocity requirement.

Table 16: Simulated and manufacturer component power requirements for Condor airframe at 15.9 kg (35 lb)

Component	Simulated Power Required	Part #	Manufacturer Max Power
Engine-only ICE	943 W	GX35	970 W
HE ICE	432 W	GX25	746 W
HE EM	208 W	AXI 4130/20	640 W
Battery Capacity	248 Whr	6xTP3300-4S	211.2 Whr

Compared to the simulated power required in Table 16, the AXI 4130/20 is over three times the maximum power required for the application. The EM was selected based on three criteria. First, the EM had to match the speed range of the ICE. Second, the EM was selected with enough torque to turn over and start the engine since it was chosen prior to considering a separate starter motor or pull start. Third, the ICE to EM gear ratio is limited to less than 2:1 for mechanical and weight considerations, further limiting the speed and torque ranges of the EM. These three criteria narrowed the EM selection to two candidate AXI motors. The lightest motor, the 4130/20 was selected for the application. In a future instantiation of the system, a smaller EM could be chosen if the torque requirements are relaxed in the absence of clutch starting the ICE.

As described in Chapter III, dynamometers at AFIT for the Honda GX35 and at AFRL/RZ for the AXI 4130/20, were used to characterize the power available from the propulsive components. The Honda GX35 used on AFIT-1 was tested by Mengistu; his thesis includes more detailed results [**15**]. Based on his testing, the maximum power available from the GX35 is 950 W, which is in good agreement with the manufacturer's value and sufficient to fly the aircraft.

Figure 55 shows the power map for the Honda GX25 engine as tested on the dynamometer setup at AFIT. Due to heating issues on the test stand, as described in Chapter III Section 4.2.3, the testing only includes 20% to 80% throttle. However, the 510 W maximum power available from the engine at 80% throttle is more than sufficient to meet the 432 W requirement from the simulation. Considering that an additional 20% throttle is available beyond the capability in Figure 55, it is safe to conclude the GX25 should meet the cruise power requirements.

Figure 56 is a plot of the maximum power output of the AXI 4130/20 at 20 A and two nominal voltages that reflect 8 cells (32 V) and 6.5 cell (26 V) packs, respectively. Note that packs do not come with partial cells and the 6.5 cell count is given purely as a reference for the reader. The 20 A current represents the limit of the Solo Whistle Controller. The maximum developed power is 358 W, again, more than sufficient to meet the power requirements for the components as predicted by the simulation.

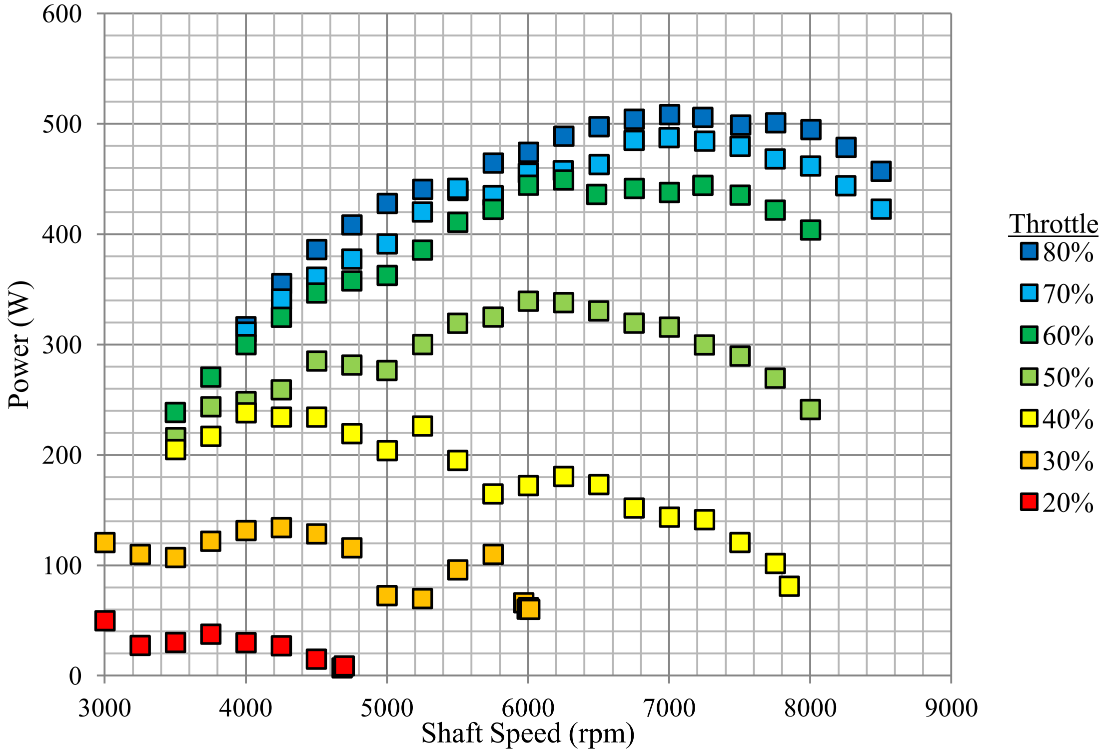

Figure 55: Power map of Honda GX25 ICE, EM with belt mounted alongside and off

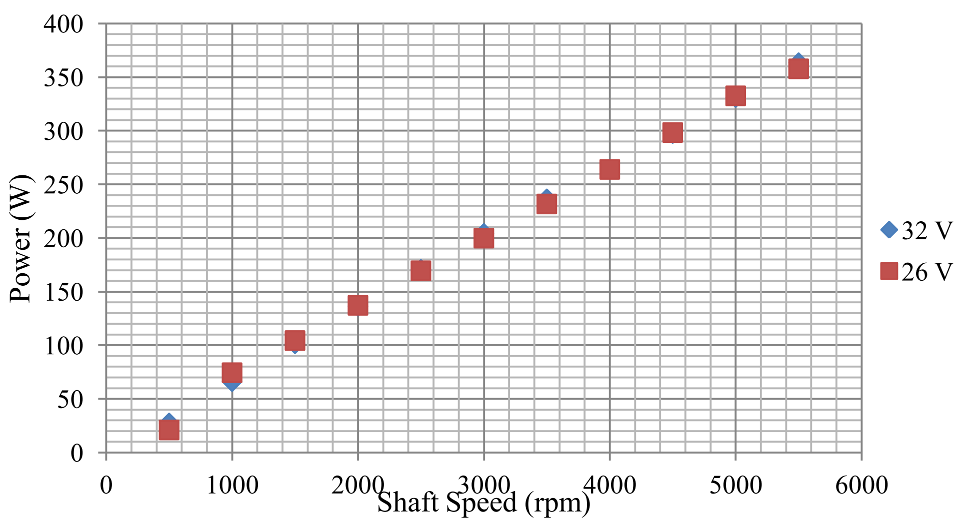

Figure 56: Maximum power of AXI 4130/20, courtesy of Justin Delmar, AFRL/RZ

Table 17 compares the bench test results to the simulation and manufacturer data. From the bench test results, the HE system should meet all of the performance requirements in Table 14 with the possible exception of the maximum velocity requirement. Based on the November 2011 flight test, the GX35 engine is able to keep AFIT-1 airborne at just over idle throttle and cruise at 55% throttle. Calculating the maximum power available from the EM and ICE using the manufacturer documentation, the total power of the HE system exceeds the power of the GX35 determined by the Mengistu [**15**] by nearly 70%. Based on the maximum power available from the EM and ICE from dynamometer testing, the HE components only sum to 91% of the tested GX35 power, although the GX25 bench testing concludes 20% under full throttle. The limitations of the Solo Whistle Controller, discussed in Chapter V Section 3.5, contribute significantly to this difference between the manufacturer and tested HE system power output.

So far, this analysis has not addressed mechanical losses in the clutch mechanism and the belt. The design code includes a mechanical loss term for the clutch, set at 95% for the simulation. If actual losses are greater than 5%, the margin between the simulated component power requirements and the tested component power outputs will decrease. If one includes 5% losses between the ICE and EM, the combined tested power is reduced to 86% of the GX35. The losses are a function of several variables including belt tension, alignment, and temperature. If the system alignment is questionable, 95% efficiency may be a generous estimate.

The preceding discussion is based only on the tested power of the components. Based on a separate test, the EM can deliver an additional 92 W at 7000 rpm and 157 W at 8000 rpm, in addition to the 358 W it delivers at 5500 rpm. An additional 20% throttle is available from the ICE. Even so, the tested hybrid system will not deliver significantly more power than the GX35, and will probably deliver less power once clutch losses are included. While the components deliver the power required from the simulation to fly the airframe in cruise and endurance, a small combined power shortcoming could cause problems during the aircraft takeoff roll. A similar analysis to determine if the speed and torque ranges of the EM, ICE, and propeller match was completed using Rotramel's code and is included in Section 2.2 of this chapter.

Table 17: Simulated power requirements and available component power for Condor airframe at 15.9 kg (35 lb)

Component	**Simulated Power Required**	**Part #**	**Manufacturer Max Power**	**Bench Test Max Power**
Engine-only ICE	953 W	GX35	970 W	953 W
HE ICE	432 W	GX25	746 W	508 W*
HE EM	208 W	AXI 4130/20	640 W	358 W*
Battery Capacity	248 Whr	6xTP3300-4S	211.2 Whr	Not Tested

** These test results are not the maximum possible power for the component, just the maximum power of the ranges tested for each component.*

Table 17 also contains the manufacturer information for the Condor EM battery packs. The manufacturer data indicates the selected set of 6 packs is underpowered for the endurance time. However, the power draw in the batteries is a strong function of the propeller efficiency at the endurance flight condition. Hiserote's code uses a very basic propeller efficiency model [**12**]. Meanwhile, Rotramel's code uses actual propeller data to estimate the efficiency based on component speeds [**13**]. Therefore, a more in depth discussion of batteries will be postponed until Section 2.2 of this chapter.

2.1.4. Comparison of Aircraft Mass Allocation to Simulation

Hiserote's code also uses the weight breakdown from the original, engine-only, aircraft to estimate the component masses of the hybrid airframe. The propulsive component masses are based on typical component specific energies while the battery and fuel masses are based on providing the power necessary to meet the cruise and endurance time requirements.

Table 18 summarizes the estimated aircraft masses and compares them to the actual masses for the engine-only and HE airframes. A complete breakdown of the masses for both aircraft is available in Appendix J. The simulation was based on AFIT-1 ballasted with simulated payload to a mass of 15.9 kg (35 lb). Therefore, the simulation empty weight matches perfectly with AFIT-1. The code considers the empty weight of the aircraft to be the airframe and all components less the fuel and payload. The propulsion system mass is the combination of the ICE, propeller, and propeller flange as well as the EM and batteries for the HE system. The mass for avionics, wiring, and mounting brackets is not calculated in the code, but is included in Table 18 for both aircraft.

Table 18:Simulated and actual aircraft masses

	Predicted Mass (kg)	**Actual Mass (kg)**
Engine–only Aircraft (AFIT-1)		
Fuel	0.85	1.28
Payload (sand bags - ballast)	3.91	3.49
Total Stores (fuel and payload)	4.76	4.77
Propulsion	2.82	2.67
Mounting brackets, avionics, and wiring	0.00	0.42
Total Empty (includes airframe, not listed)	11.13	11.13
Total Aircraft (Empty + 'cargo')	15.90	15.90
HE Aircraft (AFIT-2)		
Fuel	0.63	0.47
Payload (sand bags - ballast)	3.79	0.19
Total Stores (fuel and payload)	4.42	0.66
Propulsion	3.18	5.39
Mounting brackets, avionics, and wiring	0.00	1.79
Clutch Mass	0.60	0.41
Total Empty (includes airframe, not listed)	11.48	15.41
Total Aircraft (Empty + 'cargo')	15.90	15.90

AFIT-1 matches the simulation relatively well. The largest deviation is a 0.5 kg trade of payload weight for additional fuel, driven the by the team’s decision to completely fill the fuel tank for the flight test. In an operational implementation, that mass could be traded back to payload. The 0.42 kg of brackets, avionics, and wiring is mostly absorbed in the simulation's overestimate of propulsion system mass. Thus, for an engine-only configuration with minimal avionics, the lack of a bracket, avionics, and wiring term does not significantly impact the simulation's validity.

The mass prediction for the HE airframe does not match the actual aircraft as well as the engine-only variant. The propulsion system is almost 70% heavier than predicted by the simulation, in part due to overdesigning the ICE and EM compared to the simulated power requirements. The code bases the ICE and EM masses on generic component specific energies and the power required for cruise and endurance, respectively. Since the actual ICE and EM are significantly more powerful than the code estimates, it follows that the code mass estimate will also be too small. If the power predications of the code are verified during the flight test, a future iteration could use an ICE and an EM which are both smaller and lighter than those in the current hybrid system.

The code does not estimate the mass of avionics, wires, and mounting brackets and these parts amount to over 2 kg for the HE system. Meanwhile, the EM pulley, ICE pulley, bearings, and engine flange making up the clutch mechanism have a mass of 0.41 kg, 0.19 kg under the clutch mass used in the simulation. Therefore, while much of the payload in the HE configuration is traded for avionics, wiring, and bracket mass not accounted for by the code, the HE aircraft retains about 0.19 kg available for payload. Since the payload can tap the avionics or even EM batteries, 0.19 kg would allow for a camera and possibly a small microphone or other sensor, permitting the hybrid aircraft to complete a number of missions using its near silent loiter capability.

2.1.1. Comparison of Component Mass Allocation to Simulation

Table 19 breaks out the mass estimate for the major propulsive components. The EM and ICE are more powerful than those predicated by the code; because the code sizes those components using their specific energy, it follows that their masses are heavier in implementation than prediction. The code estimate for fuel is relatively close to the amount of fuel that can be carried on the HE aircraft for a 15.9 kg (35 lb) load out. A small amount of fuel has been traded to make up for the additional propulsive system mass not anticipated by the code. Due to budget constraints discussed earlier in Section 2.1.1, the batteries for the HE system have 17% less energy capacity than required for a 1 hr loiter and they are nearly twice the weight estimated using Hiserote's code . Therefore, in addition to the other tweaks to the code recommended in Chapter V, one should also consider adjusting the battery specific energy to a number realistic for the actual purchased batteries.

Table 19: Estimated and actual component masses for HE system

	Predicted Mass (kg)	Actual Mass (kg)
EM	0.07	0.41
ICE	1.10	2.09
Batteries	1.24	2.34
Fuel	0.63	0.47

2.2. Propulsion Component Comparison to Rotramel's Component Matching Code

Hiserote's simulation only addresses the power requirements for the components; it does not examine whether or not the speed and torque ranges of the ICE, EM, and propeller are compatible. In that regard, Rotramel's component matching code picks up where Hiserote's code leaves off. Rotramel's code takes the aircraft flight power estimates from Hiserote's code as well as empirical propeller test data from Wichita State University and calculates the optimal component speed and torque requirements for cruise and endurance operation. The optimal speed is the speed at which the propeller and component efficiencies are maximized. The code is also capable of optimizing the gear ratio and other parameters, as discussed in Chapter III Sections 6.2.3 and 7.

Although the 18x10 propeller was selected for this application, 18x10 propeller data was unavailable from Wichita State University. In the absence of better data, the author interpolated between the results for the 18x8 and 18x12 propellers, and the results are listed alongside the interpolated values in Table 20.

Table 20: Simulated endurance and cruise shaft speed and torque requirements

Propeller (APC, 2 bladed)	**18x8**	**18x10***	**18x12**
Endurance (EM) shaft speed (rpm)	4200	3870	3550
Endurance (EM) shaft torque (N-m)	0.491	0.528	0.566
Cruise (ICE) shaft speed (rpm)	5330	4900	4470
Cruise (ICE) shaft torque (N-m)	0.711	0.761	0.811
**18x10 results are linearly interpolated between 18x8 and 18x10 due to lack of propeller data.*			

During the tests to generate the power maps of the ICE in Figure 55 and the EM in Figure 56, data was collected for torque and speed as well. For more details on the data collection, reference Section 2.1.3 of this chapter. Figure 57 shows the torque map for the Honda GX25 at 20% to 80% throttle. Figure 58 displays the maximum torque available from the AXI 4130/20 capped at 20 A maximum current draw. Note that the torque available from the motor is roughly a constant, validating Greiser's decision not to use a torque map for the EM in his implementation of the torque split equations [**17**].

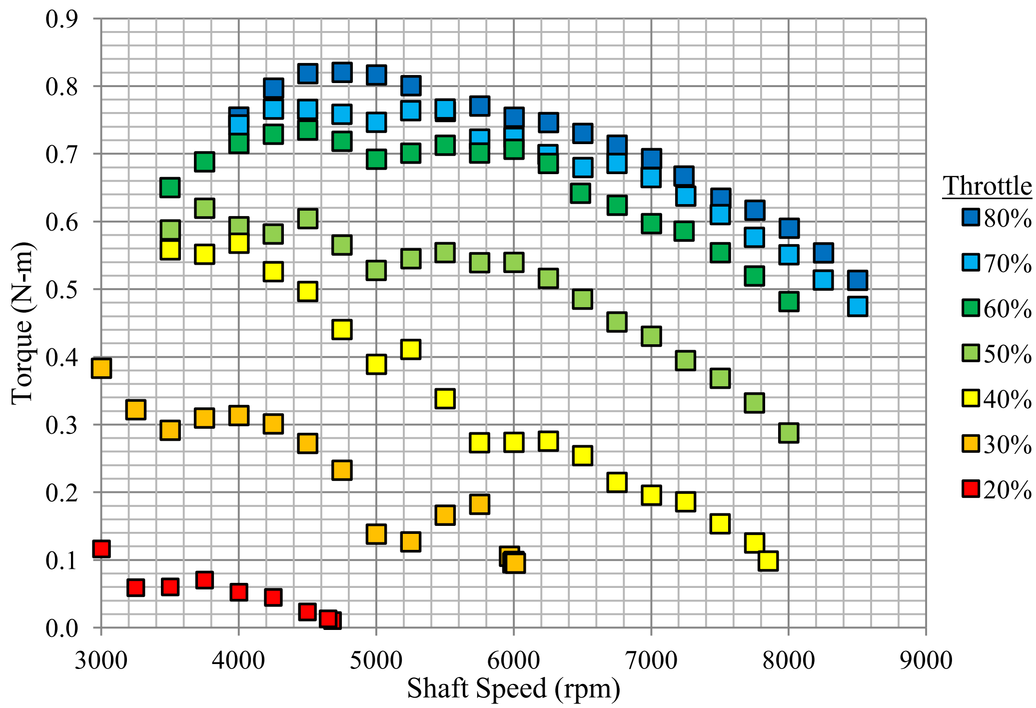

Figure 57: Torque map for Honda GX25 engine, EM with belt mounted alongside and off

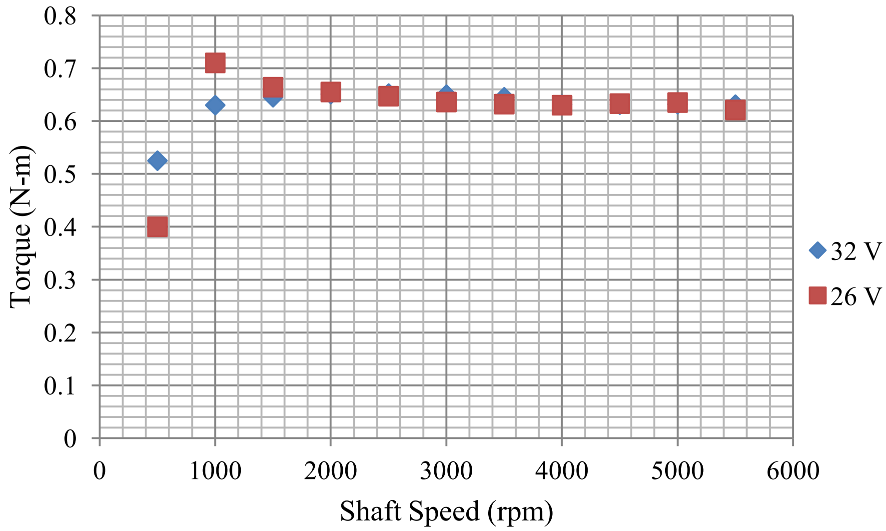

Figure 58: Maximum torque of AXI 4130/20 at 20 A, courtesy of Justin Delmar, AFRL/RZ

Table 21 shows the maximum available component torque at each simulated speed alongside the projected torque requirement from Rotramel's simulation. Both the Honda GX25 and the AXI 4130/20 are capable of meeting the requirements predicted by the simulation, although the excess torque margins are much smaller than the excess power margins from Hiserote's code. Until the aircraft is flown and the component speeds are monitored in both cruise and endurance operation, it is not possible to validate the prediction from the code. At this point, the only conclusive result is that the EM and ICE should meet the speed and torque requirements to fly the aircraft based on the simulation.

Table 21: Comparison of simulated endurance and cruise shaft speed and torque requirements to component bench test results

Propeller	**18x8**	**18x10***	**18x12**
Endurance (EM) shaft speed (rpm)	4200	3870	3550
Endurance (EM) shaft torque (N-m)	0.49	0.53	0.57
Maximum tested component torque (N-m)	0.63	0.64	0.64
Cruise (ICE) shaft speed (rpm)	5330	4900	4470
Cruise (ICE) shaft torque (N-m)	0.71	0.76	0.81
Maximum tested component torque (N-m)	0.80	0.82	0.82
**18x10 results are linearly interpolated between 18x8 and 18x10 due to lack of propeller data.*			

Rotramel's code also predicts the endurance time from the number of batteries in the airframe and the endurance power draw. While Hiserote's design code predicts 0.85 hr of endurance for the intended battery payload, Rotramel's code predicts only 0.51 hr (18x12 propeller) to 0.68 hr (18x8 propeller). The discrepancy originates in the gear ratio between the EM and ICE, which is not considered in Hiserote's analysis. As discussed in Chapter III Section 6.2.3, the optimal gear ratio for the system ranges from 1.5 for the 18x8 propeller to 1.7 for the 18x12 propeller. However, a 1:1 gear ratio between the EM and ICE was chosen to ensure the EM could catch the ICE during dual mode operation. Therefore, the EM and propeller combination operates at less than maximum efficiency at the endurance condition, leading to higher power consumption and decreased loiter time. Refinement of the gear ratio in a future iteration could significantly increase the loiter time for the HE aircraft.

3. Bench, Ground, and Flight Testing

3.1. Introduction

So far the results have focused on comparing the hybrid system components and the integrated system design to the design simulations of Hiserote and Rotramel. Dual mode operation and the system in various states of assembly were tested several times during system integration. However, a rigorous bench test of the system was delayed until the mechanical integration of the system was completed in January of 2012 with the delivery of the left hand threaded engine flange. With the completely assembled system, the project transitioned entirely from integration and validation activities to testing activities, starting with a bench test of the integrated system with ground and flight testing to follow, weather permitting.

The assistance of both Capt English and Capt Molesworth was critical in completing the test planning and testing in a time efficient manner. The testing sequence was designed to validate the system on the bench and on the ground before flying it for the first time. The bench and ground test procedures were designed to mirror the flight test procedures both to check the functionality of the system and to provide the operators with two practice runs before executing the test cards with a flying airframe. The test plan in Appendix L provides an overview of the planned testing while Appendix M provides a copy of the test cards developed by Molesworth and the author. The remaining subsections present the results from testing completed as of the writing of this document.

3.2. Bench Test Results

3.2.1. Testing Outline and Hybrid System Configuration

For the bench tests, the hybrid system was attached to the fuselage and secured in the dynamometer test stand, with the dynamometer removed. An 18x10 propeller functioned as the load for the system, so all data represents a static ground test. The Seagull instrumentation system was used to monitor propeller speed as well as battery current and voltage. The hybrid system was controlled with the Kestrel autopilot. Fuel usage was measured with a stop watch and an external fuel tank mounted on a digital balance with a resolution of 5 g. The dynamometer test stand facilitated indoor testing while allowing the system to be held in place, the exhaust gasses to be vented to the outdoors, and the operators to be protected from a possible propeller failure by bullet-resistant polycarbonate glass.

The overarching objective of the bench test was to validate the function of the HE system, including the control procedures intended for use in flight. The remainder of this section summarizes the bench tests and analyzes the results. For the fully detailed test cards, the reader is referred to Appendix M.

3.2.2. Results from Bench Testing

Table 22 lists the bench test objectives and results for each of the bench tests. All test objectives were completed successfully. Moreover, none of the issues that required multiple attempts were the result of a HE system malfunction. Figure 59 shows the aircraft mounted to the test stand for bench testing.

Table 22: Hybrid system bench test objectives and results

Test #	Objective	Result
BT-01	Verify functionality of system in ICE only mode.	Successful
BT-02	Verify Functionality of system in EM only mode	Successful
BT-03	Verify mode transition from EM only to ICE only mode works.	Successful
BT-04	Verify mode transition from ICE only to EM only mode works	Successful
BT-05, BT-06	Verify both dual modes function. BT-05 verifies the ICE can operate at a constant set point while the EM throttle is varied. BT-06 verifies the EM can operate at a constant set point while the ICE throttle is varied. Both tests also check that set point of the constant component may be changed.	Successful
BT-07	Verify the ICE kill switch functions and that the EM still operates after the ICE is killed.	Successful
BT-08	Verify the EM kill switch functions and that the ICE still operates after the ICE is killed.	Successful
BT-09	Verify the ICE crossover switch to pass ICE control from the Gimbaled Camera line to the Kestrel throttle line during an emergency functions properly.	Successful
BT-10	Verify that Regen mode works properly.	Successful

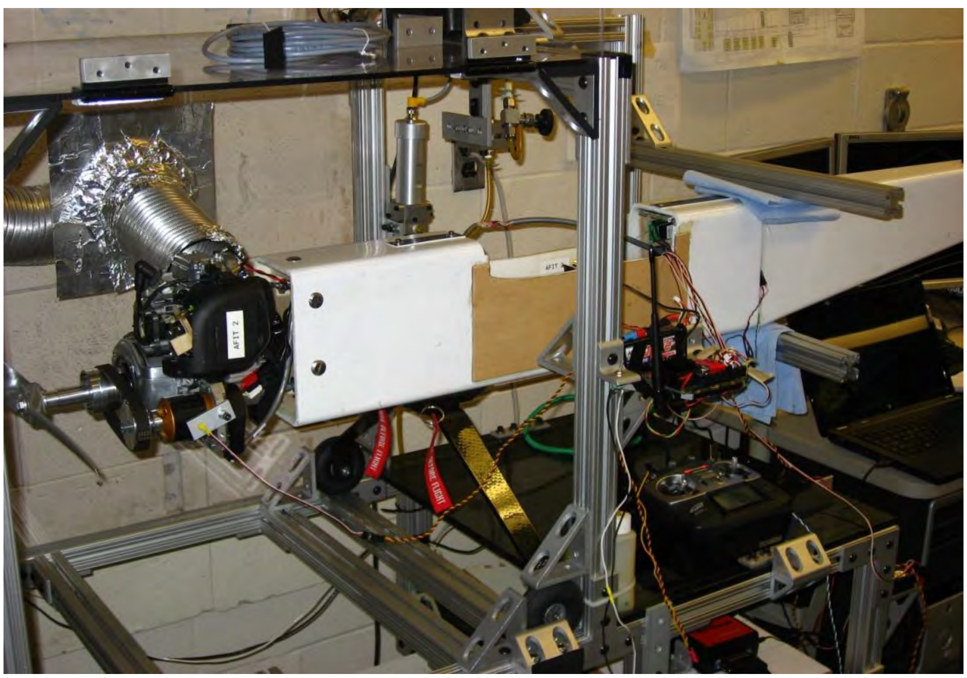

Figure 59: HE aircraft mounted to test stand for bench testing

During BT-01, the full throttle range of the ICE was tested. Note that the range is less than 0-100% due to the idle cutoff of the ICE on the low side and the throttle range of the Kestrel exceeding the throw of the ICE servo on the high side. During the test, the ICE idle shutoff was determined and set at 22%. Table 23 contains the throttle and propeller speed data from the bench test. At cruise velocity, Rotramel's code predicts a propeller speed of 4900 rpm for the 18x10 propeller as listed in Table 21. The speeds in Table 23 are for static conditions. In cruise, the oncoming air flow will reduce the torque per rotation for the propeller (a function of advance ratio) and the propeller speed for a given throttle setting will, in general, increase. Therefore, the static data indicates the ICE will be able to deliver propeller speed and torque sufficient to meet the cruise power requirements predicted using Rotramel's simulation.

Table 23: Propeller speed and throttle data for ICE only bench test

Throttle (%)	**Propeller speed (rpm)**
22 (idle)	3050
30	3970
40	4600
50	5150
60	5290
70	5340
80	5380

A 20 minute test of the ICE at 30% throttle was also performed to simulate the cruise fuel burn. The 30% throttle setting was selected to minimize vibration of the airframe in the test stand and may be short of the cruise power requirement, although the GX35 can fly the Condor at just beyond idle power. Over the 20 minute time frame, the engine consumed 50 g of fuel, or about 0.4 g/s. Figure 60 shows the fuel burn for the GX25 from the torque map testing discussed in Section 2.2 of this chapter. The 0.4 g/s estimate at 4050 rpm falls in the 30-50% throttle range indicating the single point bench test is in agreement with the dynamometer data. Note that the throttle offset of the Kestrel makes the 30% throttle used for the cruise test correspond more closely to 38% throttle on the fuel burn map in Figure 60.

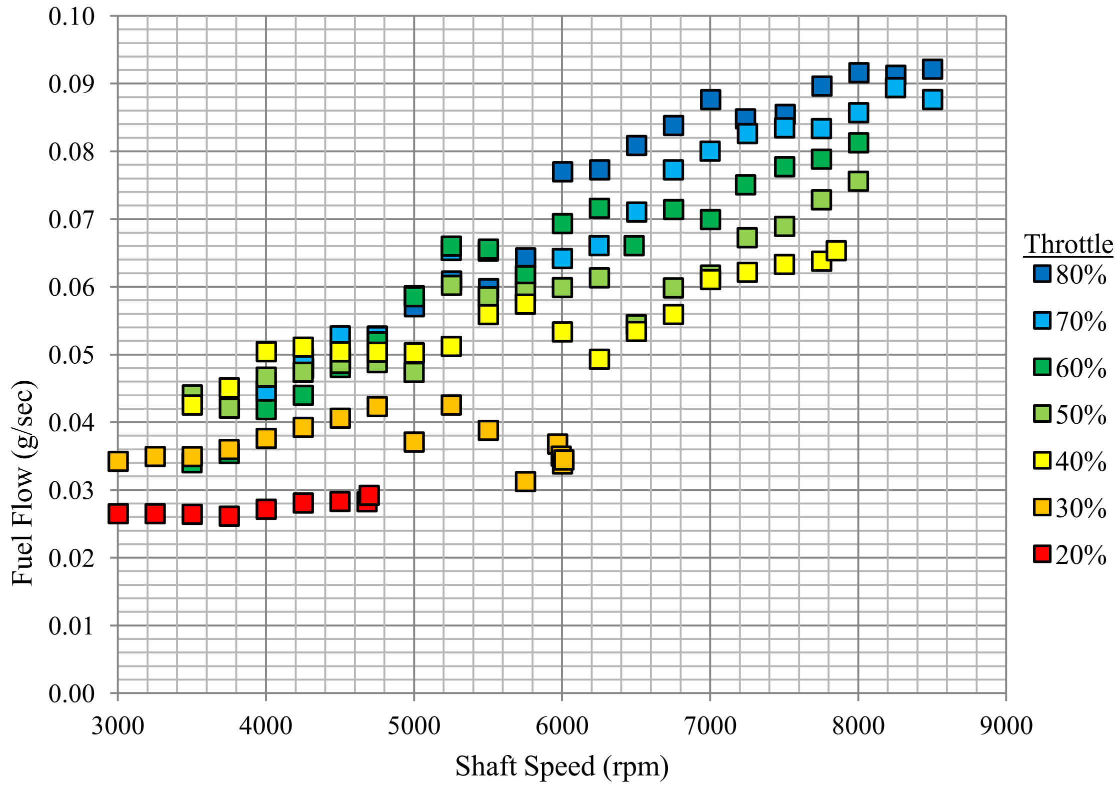

Figure 60: Fuel burn for Honda GX25 engine, EM with belt mounted alongside and off

From the fuel consumption and engine speed, it is possible to use the power map in Figure 55 to estimate the SFC at 3.1x10^{-6} N/Ws±20%. Hiserote's simulation estimates the cruise SFC at 2.1 x10^{-6} N/Ws. Considering the cruise condition from the bench test may be less than the most fuel efficient throttle setting, the similarity of the two values provides confidence in the initial estimate used during the aircraft design.

BT-02 entailed a test of the EM similar to BT-01. The EM was run with the ICE off instead of at idle. Table 24 shows the throttle, propeller, and electric data for the EM only test. Like the ICE in BT-01, the EM is near maximum power to achieve the propeller speed predicted at the endurance velocity using Rotramel's code. Again, since this test is static, the propeller speed will increase for the same throttle setting when the aircraft is traveling at the endurance velocity. Thus the test verifies the EM should fly the aircraft during endurance operations.

Table 24: Propeller speed and throttle data for EM only bench test

Throttle (%)	**Propeller speed (rpm)**	**Pack voltage (V)**	**Pack current (A)**	**Energy for 30 s (mAhr)**
21	1150	32.9	0.1	2
30	1630	32.9	0.7	3
40	2120	32.9	1.4	4
50	2490	32.8	2.5	10
60	2860	32.8	3.6	18
70	3160	32.5	4.8	27
80	3420	32.5	6.0	33
90	3710	32.5	7.7	46
96	3900	32.3	8.7	45

One might notice the pack currents are somewhat lower than the 20 A current limit of the Solo Whistle controller. The Solo Whistle's limit is based on the current delivered to the EM at the operating voltage (a function of speed) and power, which causes it to differ significantly from the pack current draw at maximum throttle and these speeds. It is clear that the Solo Whistle sources far less power than the battery packs can supply or than the motor can use. Therefore, if one desired to increase the power output of the electric system, a motor controller better matched to the system power ranges would be a good starting point.

BT-03 and BT-04 tested the transition between ICE only mode and EM only mode. The two main concerns were the throttle down of the ICE to idle and the commutation of the Solo Whistle controller. Due to the somewhat abrupt change in throttle when switching the ICE directly to idle, there was a possibility that transitioning from ICE only mode to EM only mode would kill the engine. However, the ICE throttled to idle without incident. Likewise, there was a chance that changing from EM only mode to ICE only mode would cause the EM to lose its commutation. Again, the EM switched modes without incident.

BT-05 and BT-06 addressed dual mode operation of the system. First, the tests verified that switching between the two different types of dual modes worked well. Second, the tests demonstrated that the EM and ICE could provide additive torque during dual mode operation.

While the torque of the system cannot be directly measured, the propeller speed increases with torque. Thus the propeller speed trend serves as a proxy for the torque trend. Based on the throttle steps and speed changes, it is safe to conclude that while the torque is additive, there are mechanical losses in the system. Without torque measurements or additional propeller data for the 18X10 propeller, these losses while present, cannot be quantified.

Table 25 lists the throttle settings, propeller speeds, and pack voltages for the dual mode tests. Both throttle control and set point changes function correctly using the EM as the throttle device with the ICE at a set point and vice versa. The propeller speeds indicate that torque changes in the same direction as the throttle to either component, verifying that the ICE and EM can provide additive torque across the one-way bearing mechanism.

Table 25: Propeller speed and throttle data for Dual mode bench test

EM throttle (%)	**ICE throttle (%)**	**Propeller speed (rpm)**	**Pack current (A)**
EM Driver (EM Boost), ICE at setpoint			
31	30	4460	2.5
43	30	4670	4.0
43	40	5260	4.2
ICE Driver (ICE Boost), EM at setpoint			
30	19	3508	1.9
30	30	4500	2.4
50	30	4800	5.2

The test also indicates that the EM never manages to completely overrun the ICE during the test. Therefore, if the ICE remains at idle during electric only operation, it will still provide some amount of power to the aircraft. Thus the results from an EM only flight test with the ICE in idle will not reflect the true performance of the electric system in an application with midair restart where the ICE may be turned off entirely for loiter. Nevertheless, the Dual mode test demonstrated that the additive torque across the one-way bearing was functional, which was one of the largest technical risks in the HE implementation. As of this test, the one-way bearing had 5 hours of operation without any signs of significant wear.

Tests BT-07, BT-08, BT-09 all checked operational fail safes on the system. BT-07 ensured that the ICE kill switch worked as intended and verified that the EM would still function after the ICE was killed. BT-08 provided a similar test, ensuring the ICE would still operate after a successful EM kill. BT-09 checked the ICE crossover switch that provides throttle authority to the Kestrel in the event of a loss a communication with Virtual Cockpit. All tests were successful, although BT-09 required several attempts while a servo range setting issue in Virtual Cockpit that caused the engine to spool up during crossover was resolved.

The last bench test, BT-10, tested the Regen capability of the propulsion system. For this test, only two batteries, 1 set, were used to mitigate damage in the event of a serious charging malfunction. Over 22 minutes, the Solo Whistle used the EM as a generator to charge the set of batteries from 31.5 V to 32.0 V at an average rate of 0.3 C. Operationally, a charge rate of 1C could be used, cutting the recharge time by a factor of three. Table 26 shows the throttle settings, propeller speeds, and pack voltages for the Regen test. Increasing the recharge rate to 1 C would quicken the charging. The test demonstrates the Solo Whistle can in fact function as a rectifier and charge battery packs. Therefore, a number of mission profiles and configurations including segmented loiter, battery top off during ingress, and high power draw payloads are now viable.

Table 26: Propeller speed and throttle data for Regen bench test

EM throttle (%)	**ICE throttle (%)**	**Propeller speed (rpm)**	**Pack current (A)**
Off	30	4130	0.0
Regen	30	4050	1.15

The bench test of the hybrid system on the airframe verifies all implemented system functionality. Moreover, the only operational functionality missing at this point is mid-air restart capability. With the hybrid system, mode controls, and emergency fail safes verified, the hybrid-electric Condor was ready to progress to a full-scale ground test.

3.3. Ground Test Results

Initially, the author intended to do a full scale ground test that mirrored the planned flight test procedures, as indicated by the test cards included in Appendix M. The testing was planned for the range located behind the United States Air Force Museum, about 1/2 mile from AFIT. Figure 61 shows the aircraft without the outboard wings during ground testing on 15 February 2012. Immediately after starting the aircraft at the range, the team noticed a simultaneous twitching of the control servos to include the throttle signal to both the ICE and EM. The team also observed radio interference with the Seagull flight instrumentation system. After several hours of troubleshooting, the team concluded the interference was due to ambient noise in the 900 MHz band used by both the Kestrel autopilot and the Seagull instrumentation system. Previous tests had demonstrated that the Kestrel and Seagull do not interfere with one another and that the observed servo noise was not present in the somewhat shielded environment of the AFIT laboratory. Moreover, according to the CESI support contractors, the museum range is known for having radio interference issues.

Figure 61: HE aircraft on runway behind United States Air Force Museum for ground testing

The instrumentation and radio interference precluded the initially planned ground test. However, the team successfully demonstrated all of the operational modes (except regen) and transitions of the HE system as well as ground control of the aircraft. The ICE can taxi the aircraft at slightly more than 20% throttle and the EM can taxi the aircraft at 80-90% throttle when the ICE is turned off. The 80-90% EM throttle is for a faster-than-walking speed taxi; 50-60% throttle will keep the aircraft rolling. Dual mode operation works using either the EM or the ICE as the driver with the other component at a setpoint. The test also demonstrated that the mode and throttle transitions were smooth and did not cause the aircraft to tip or roll. Despite concerns about the transmission delay of throttle information from the aircraft to Virtual Cockpit and back, the pilot said the aircraft was controllable, albeit somewhat sluggish. Several ICE boost mode practice takeoff rolls with the EM set to 40% showed that the aircraft should have enough power to takeoff and that it should be controllable during the ground roll.

The team found one servo issue that should be noted to avoid future repetition. The tail wheel steering servo and rudder servo share a channel in the HE aircraft. Normally, servos that share a channel such as elevators or ailerons are matched to provide symmetry for the aircraft. In the HE aircraft, the tail servo was an analog servo while the rudder servo was digital. This mismatched caused twitching on the tail wheel servo. The team replaced the tail wheel servo with a digital servo and the twitching stopped. The learned lesson then, is that analog and digital servos should not be mixed on a signal channel as they can and will interfere with one another.

According to the CESI support contractors, the Camp Atterbury range has fewer radio interference issues. Therefore, since all aircraft functionality had been demonstrated in the abbreviated ground test and rigorously on the bench, the Condor team decided to push forward with flight testing at Camp Atterbury. While the shortened ground test did not provide significant quantitative data for the HE system, is did provide a qualitative checkout of the system. With the system qualitatively vetted, the team believed that acquiring flight test data at a range with less interference was a more prudent use of time and resources than continuing to battle interference for ground test data at the local range.

Flight Test Results

As of the writing of this document, the HE aircraft flight test is planned for the end of February 2012, but was not completed in time for this version of the publication. If testing results are not available by the publication deadline for this document, the results will be included in a paper planned for the 48th AIAA/ASME/SAE/ASEE Joint Propulsions & Exhibit and International Energy Conversion Engineering Conference during the summer of 2012. The test cards for the planned flight testing are included in Appendix M. Figure 62 shows the fully assembled aircraft in the laboratory prior to flight testing.

Figure 62: Fully assembled HE aircraft prior to flight test

V. Conclusions and Recommendations

1. Chapter Overview

This chapter begins with conclusions from the project. The chapter concludes by highlighting key issues with the Condor system and providing recommendations for future work to address those issues. The discussion includes a comparison of the implemented system's capabilities to the operational concept envisioned at the onset of the effort.

2. Conclusions

The goal of this effort was to integrate and demonstrate an HE propulsion system for a small RPA capable of the mission concept presented in Chapter 0, namely near silent loiter capability. In addition to demonstrating the hybrid electric system, the research also aimed to compare single point static tests of the system to the designs codes. Despite the lack of a flight test event, the bench and ground testing has shown that the hybrid-electric system is clearly functional and for the first time in the history of the Condor project, there is an integrated system capable of operating on an airframe. This section addresses the important conclusions about the simulation codes and the tested hybrid system.

As indicated in the Abstract, there are three unique aspects of this system that set it apart from other parallel hybrid projects and directly contributed to the success of the system. First, the component selection was based on sizing and optimizing the propulsive components for the integrated system using the design codes developed specifically for this application by Hiserote [**12**] and Rotramel [**13**]. Second, torque control of the EM and ICE permitted stable and repeatable additive torque in dual mode operation. Even though a full IOL strategy is not implemented in this design, the underlying framework for such a strategy is in place. Furthermore, the EM is torque controlled which stabilizes its operation even when used in a boost power capacity. Third, the one-way bearing clutch mechanism (patent pending) was crucial to combining the electric and combustion power trains into a synergistic hybrid system.

2.1. System Evaluation Based on Test Results

Based on the bench and ground testing, the designed HE system functions in EM only mode, ICE only mode, Dual mode, and Regen mode. In EM only mode, the EM can deliver 260 W, about 20% more power than required for endurance flight based on simulation. Ground testing demonstrated that the aircraft is controllable in all operational modes and that the transitions between modes are smooth. During operation, the one-way bearing clutch mechanism allowed the EM to overrun and add torque to the ICE enabling EM only mode and Dual mode, respectively. The hybrid system control implemented on the Kestrel autopilot facilitated boost power operation using either component on the primary throttle with the other component at a set point. The regeneration mode functions, allowing the HE system to recharge the batteries in flight with the ICE. Testing all mode switching permutations showed that the system can switch between all modes without losing the Solo Whistle's commutation, stalling the ICE, or becoming uncontrollable.

Amidst the successes, there remain a number of areas for improving the system. Future work should revisit the acoustics of the airframe. This work suggested mid air restart as one way to decrease the acoustic signature of the aircraft during loiter operations. If mid air restart is not desired on the aircraft, improved mufflers for the ICE could also reduce the ICE's signature. The mechanical implementation, while functional, could benefit from another design iteration to improve the alignment, reduce vibration, and decrease bracket mass, freeing mass for additional payload or fuel capacity. Most of all, improving the specific energy of the batteries would allow the system to realize longer loiter times. The recommendations are discussed in more detail in Section 3.

2.2. Code Validation

2.2.1. Experimental Comparison to Hiserote's Code

The aerodynamic predictions of Hiserote's code are well in line with the test results from this project. However, the sizing calculations fall short of in several regards. First and foremost, the calculations include no term for the mass of wiring, brackets, and avionics, probably because this weight is difficult to estimate *a priori*. However, for a hybrid system built from COTS components, these masses contribute significantly to the aircraft mass, cutting heavily into the payload capacity.

Additionally, the code assumes that the propulsive components are scalable in infinitely small increments, while the available COTS components tend to fall into finite power ranges. In the case of the hybrid system, the smallest feasible COTS ICE and EM were nearly double the code's requirement, leading to a mismatch in predicted and actual weight. Adding capability for the code to select from a user defined selection of COTS components and then optimizing the system within that design space would make the code more effective from an initial design standpoint. Likewise, the user should tweak the constraints to fit the available technology. In the case of this aircraft design, the initial design assumed a feasible aspect ratio of 15, while the technological limit of the Condor is closer to 12.

Finally, the code may mislead the user on the viability of a given hybrid design. When the code sizes the ICE and EM to the cruise and endurance power requirements, the resulting components may not meet the maximum velocity and climb requirements for the original airframe. The code then states that the hybrid system does not meet the requirements, even if matching those particular performance metrics is outside of the project objective. For example, the objective of the HE Condor is near silent loiter. A small loss of maximum velocity as a result of a HE system is not a critical issue. Thus, Hiserote's design code executes the power prediction portion of the design well, but could use some tweaking to improves the fidelity of the propulsion system sizing and mass estimates.

2.2.2. Experimental Comparison to Rotramel's Code

Since the speed ranges of the ICE and EM selected using Rotramel's code work well together and the gearing ratio is, so far, acceptable, the propeller, ICE, and EM matching code seem to function adequately for the design and initial system validation. So far, there are two identified weaknesses in the code. First it depends on the availability of test data for the user's propeller of choice. The data available to AFIT is currently very sparse and contacting Wichita State University for every desired propeller is tedious. Secondly, the code as written does not work well with the Solo Whistle controller. The code assumes the EM and batteries, not the EM controller, will be the electrically limiting factors. In the case of the HE Condor where the Solo Whistle Controller is the limiting component, the code over predicts the capability of the EM system. While one could rightfully argue this is more of an issue with the Solo Whistle than the code, custom speed controllers capable of current, and thus torque, control may be more limiting than the standard hobbyist speed controllers. Thus future users should be careful to ensure the EM controller can meet the code's expectations based on the batteries and EM.

3. Recommendations for Future Work

This section highlights and crystallizes key issues with the HE system and recommends future work to resolve them. The issues center on deviations between the implemented system and an operational system capable of completing the envisioned operational concept.

3.1. Carburetors, Hybrid Propulsion Controller, and Control Strategies.

During ICE testing, the author found that the stock GX25 carburetor was not conducive to an IOL control strategy, as the IOL for the ICE carburetor combination was 100% throttle over the vast majority of the intended operating range. Therefore, when the PIC32 and Kestrel autopilot integration failed, a boost power strategy was implemented on the Kestrel without losing any real functionality from the system. The IOL strategy would have simplified to a boost power configuration, even if carried out on a separate controller.

Such an implementation, while functional, falls short of several of the ultimate goals for the system. First, the hybrid system as built is unable to capitalize on fuel efficiency mapping, IOL or otherwise, to tap the potential for more fuel efficient cruise flight. Additionally, the boost power implementation on the Kestrel is less than elegant and incurs significant delay from the transmission of the throttle signal to Virtual Cockpit and back to the aircraft.

Therefore, there are two possible steps to improve the hybrid control on a future version of the system. First, additional carburetors should be investigated to find one that provides for efficient flight at a throttle setting reasonable for cruise operation. This in turn would provide real motivation for an IOL control strategy over a boost power strategy. Second, the control of the hybrid system should be reworked in one of two ways. One solution is to use an autopilot that is able to function without interfering with the PIC32 controller. The PIC32 is highly configurable in a laboratory setting and easy to port to an airframe application. The second, and preferable solution in the author's opinion, would be to find an autopilot, more configurable than the Kestrel, capable of controlling the aircraft and hybrid system. The new autopilot should have configurable loops and gains to allow for multiple throttle controls and some number of analog and digital outputs to control the throttle to the Solo Whistle Controller and the flight modes, respectively. The new autopilot should also carry out the throttle split on the aircraft to avoid signal delay and other complications associated with processing the calculation on the ground. Such changes to the carburetor and hybrid system control would allow the system to realize true seamless hybrid functionality instead of being a flying collection of manually controlled flights modes.

3.2. Mid Air Restart and Airframe Acoustics

The most significant functionality of the original system sacrificed in this version is the mid air restart. Mid air restart would allow the ICE to be turned off during electric only loiter and then turned back on for egress. Without mid air restart, the ICE must be idled during loiter operations. Further testing should be performed to determine if the idling ICE is sufficiently quiet for loiter operations. If further acoustic reductions are required, there are two possible solutions: mid air restart of the ICE and an improved muffler.

During the integration, a starter motor that could restart the ICE was successfully demonstrated. However, the starter motor required more current than the step down converters on the aircraft could provide to the 12 V power rail and aligning the starter motor assembly on the engine was difficult. Still, the starter motor was capable of cold starting the engine, demonstrating the viability of such a setup. If a future effort uses a starter motor for midair restart, the Honda GX25 engine is well suited for the application, provided alignment issues can be resolved. On the GX25 the speed governor on the cam gear opens a valve at the top of the cylinder, lowering the pressure in the cylinder during start up. Once the engine is started, the valve closes. The valve mechanism significantly reduces the starting torque of the GX25 relative to similarly sized engines.

Alternatively, a new aftermarket muffler could decrease the acoustics signature of the ICE. The Lockheed YO-3A Quiet Star, deployed by the Army towards the end of the Vietnam War used improved mufflers and quiet props that made it acoustically undetectable at 1200 ft [**94**]. NWUAV Propulsion Systems is currently working on similar quieter mufflers for small RPA applications [**95**]. Therefore, if mid air restart is not desired on the aircraft, a quieter muffler may be able to provide any necessary reductions in acoustic signature.

3.3. Engine Flange and Alignment

The engine flange and pulley assembly is critical to the function of the hybrid system; it enables electric only and dual mode operation. While the current design clearly worked during testing, there is definite room for improvement. Specifically, the author suggests three refinements. First, the engine flange and pulley interaction length should be extended to allow a second bearing, clutch or roller. Currently, all propeller loads in the plane of rotation, to include most of the vibration, rides on the 1.3 cm (0.5 in) length of the one-way bearing. Extending the surface of contact between the flange and pulley with another bearing would reduce radial stresses on the one-way bearing and reduce vibration at the propeller.

Second, the engine flange should be refined so that the surface on which the one-way bearing runs is concentric with the engine's center of rotation. The current engine flange was designed assuming the mounting posts on the flywheel were equidistant from the engine's axis of rotation. As discussed in Chapter III Section 6.2.2, they are not. Bringing the engine flange and in turn the ICE pulley into alignment with the engine would also reduce vibration and wear on the system.

Third, the EM mounting bracket should be reworked to mount to the front of its current mounting points. As discussed in Chapter III Section 6.1, moving the bracket to the front of the current points would provide two mounting points precision ground into the same plane. This would make aligning the EM with the engine far simpler and reduce the potential for the belt to derail during operation.

3.4. New Electric Motor and Gear Ratio

As discussed in Chapter IV Section 2.2, the choice of EM to ICE gear ratio below the optimal gear ratio led to a significant reduction in the endurance time of the aircraft. Thus, an easy way to increase the loiter time would be to alter the gear ratio between the EM and ICE. A gear ratio of 1.5:1 to 1.75:1 would be appropriate for the 18x10 propeller selection. If the EM is not fast enough to catch the ICE with these gear ratios, there remain three available options. First, a lower gear ratio between 1:1 and 1.5:1 could be used to realize some improvement in endurance time. Second, the batteries could be reconfigured to increase the pack voltage to the Solo Whistle to increase the speed range of the EM. Third, the AXI 4130/20 could be exchanged for a different EM that meets the speed and torque ranges for the system with the new gear ratio. One should avoid a gear ratio greater than 2:1 as the size mismatch between the J-belt pulleys will lead to substantial slipping and possible derailment of the belt.

3.5. Solo Whistle Commutation and Power Limitations

Currently, the Solo Whistle controller must be manually commutated during system power-up as described in Appendix K. This procedure precludes an emergency restart of the EM in the air in the case of a user initiated kill or a power interruption since the Solo Whistle must be the only dynamic force acting on the EM during commutation. From a testing standpoint, commutating the Solo Whistle at the start of a test is mildly annoying. From an operational standpoint, it would severely detract from the viability of the system. The commutation takes an amount of finesse and patience that infrequently extends from the laboratory into field operations. Therefore, in future iterations targeted at pre-operational prototypes, a more rigorous EM control solution should be investigated. The solution may be as simple as swapping the Solo Whistle controller for a Castle Creations controller and trading the mass of the Solo Whistle's inductors for the mass of isolation circuitry for the Castle controller.

Another possible reason to exchange the Solo Whistle controller for another motor controller is the power limitations of the Solo Whistle. While the AXI 4130/20 can handle up to 640 W of output power, the Solo Whistle is capped between 250W and 300W in the current setup. If more power is required from the EM for stable operation in endurance mode, the only viable solution is to exchange the motor controller since the Solo Whistle is operating at its current limit in this instantiation. A new motor controller would require configuration to facilitate current (and thus torque) control. It may also require isolation circuitry as previously discussed for the Castle controller.

3.6. Gear Weight and Skid Landing

During the initial design of the airframe, there was discussion about dropping the gear after takeoff and skid landing to cut down on the in flight mass of the airframe. The gear mass is nearly 0.5 kg. One concern with a belly landing is the potential to damage the propeller. The Solo Whistle is capable of returning the EM to its starting location and holding it in place. If there were positive position control, such as a timing belt, between the EM and propeller, this functionality would allow the Solo Whistle to align the propeller parallel to the ground for a dead stick landing. If a return to a gearless glider is desired, such capability should be considered if selecting a different EM controller based on the discussion in the previous section.

3.7. Improved Battery Specific Energy

Finally, as per the discussion in Chapter IV Section 2, the batteries used in the current design fall short of initial expectations, primarily due to economic constraints on the project. As battery technology advances, battery designs and chemistries delivering better specific energy for lower prices should become available on the market. Even on the current market, the increased specific energy of Li-S batteries may be worth the increased price and shortened lifespan relative to Li-Po batteries for an operational instantiation of the concept. With a lifespan of approximately 300 cycles, Li-S [**57**] batteries could be sufficiently rechargeable to be economically viable for operational use. Even in the Li-Po battery market, there are batteries available that would improve the endurance time of the system relative to the current battery selection. Thus changes in battery selection could significantly improve the potential loiter time for the HE system.

4. Final Thoughts

To the best of the author's knowledge, the Condor project's HE aircraft is the first and only functional parallel HE-RPA prototype in existence, although several groups are close behind on their own somewhat different designs. The Condor distinguishes itself from those efforts with the focus on selecting the components to optimize the integrated system, the use of torque control for dual mode operation, and the one-way bearing clutch mechanism (patent pending) linking the power trains. With the plethora of applications for an operational HE-RPA, the future of the field holds promise. Whether the HE system is leveraged for improved efficiency, silent loiter, or remote landing, delivery, and restart, the combination of combustion and electric power offers a unique and, now, viable solution to expand the mission capabilities of small RPAs.

Appendix A. Avionics Wiring Diagram for Installed System

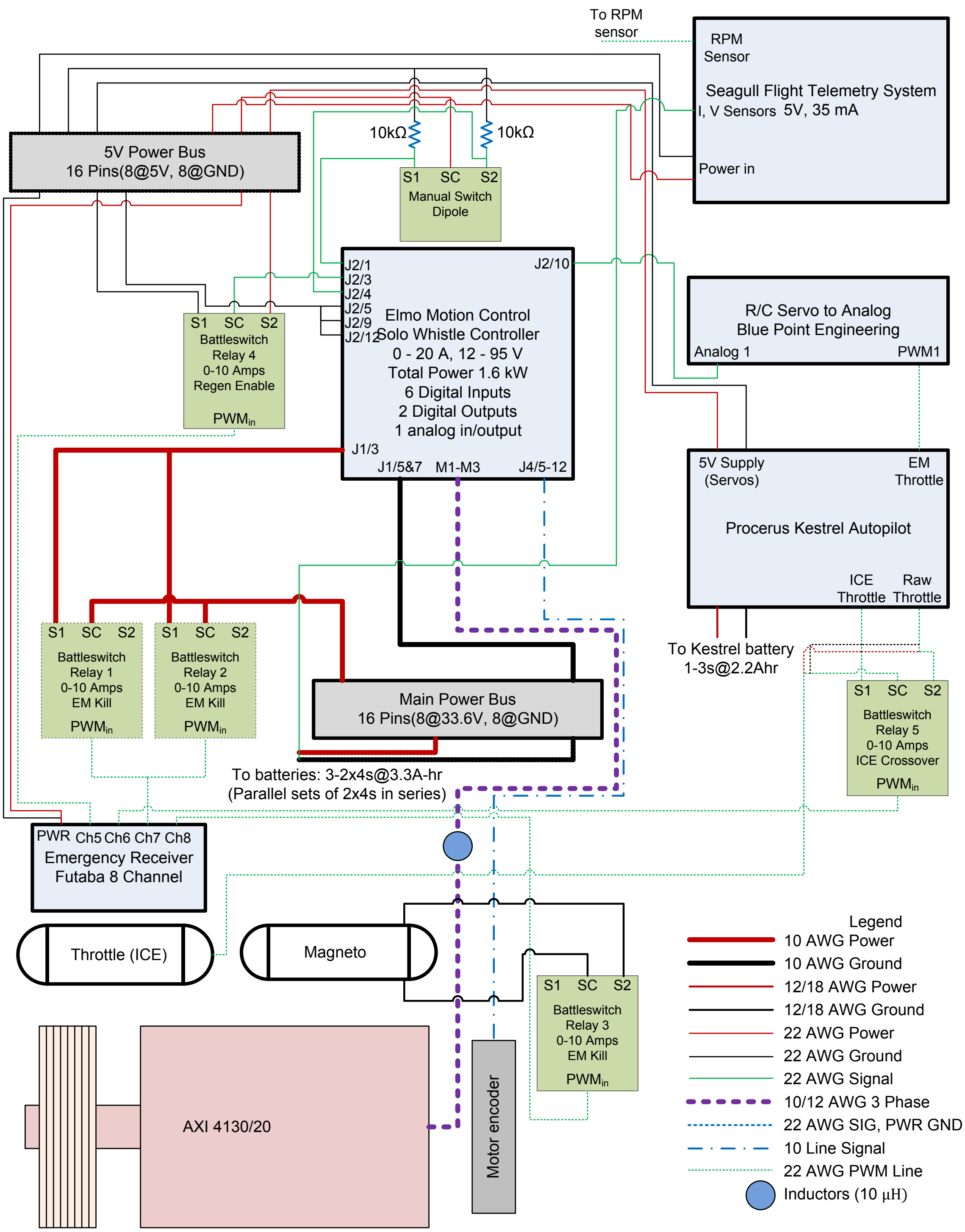

Figure A-1: Wiring diagram for avionics as installed in test aircraft

Appendix B. Elmo Motion Control Solo Whistle Wiring Connections

Table B–1: Elmo Motion Control Solo Whistle Port J1 wiring

Elmo Port/Pin	Name	Connects to
J1/1	Auxiliary power supply	NC
J1/2	Auxiliary GND	NC
J1/3	Positive power input	Battery power
J1/4	Positive power input	NC
J1/5	Ground	Battery ground rail
J1/6	Ground	NC
J1/7	Protective earth	Battery ground rail
J1/8	NC	NC
J1/9	NC	NC
Port J1 provides power to the Solo Whistle and EM.		

Table B–2: Elmo Motion Control Solo Whistle Port J2 wiring

Elmo Port/Pin	Wire Color Elmo	Name	Connects to
J2/1	Green	Digital 3	Manual switch
J2/2	Yellow	Digital 4	NC
J2/3	Pink	Digital 5	Remote battle switch
J2/4	Gray	Digital 6	Manual switch
J2/5	White	Digital Input GND	GND
J2/6	Brown	Digital output 2	NC
J2/7	Blue	Digital output GND 2	NC
J2/8	Red	Digital output 1	NC
J2/9	Black	Digital output GND 1	GND
J2/10	Purple	Analog input 1	EM throttle
J2/11	Orange	Analog input 2	NC
J2/12	Cyan	Analog GND	GND
Port J2 provides the Solo Whistle with throttle and mode signals.			

Table B–3: Elmo Motion Control Solo Whistle Port J4 wiring

Elmo Port/Pin	Wire Color Elmo	Name	Connects to	Wire Color
J4/1	Green	N/A	NC	N/A
J4/2	Yellow	N/A	NC	N/A
J4/3	Pink	N/A	NC	N/A
J4/4	Gray	N/A	NC	N/A
J4/5	White	Supply return	Encoder cable	Green (white stripes)
J4/6	Brown	5 V	Encoder cable	White (green stripes)
J4/7	Blue	I-	Encoder cable	White (orange stripes)
J4/8	Red	I+	Encoder cable	Orange (white stripe)
J4/9	Black	B-	Encoder cable	White (brown stripes)
J4/10	Purple	B+	Encoder cable	Brown (white stripes)
J4/11	Orange	A-	Encoder cable	White (blue stripes)
J4/12	Cyan	A+	Encoder cable	Blue (white stripes)
Port J4 provides the Solo Whistle with differential position feedback from the motor encoder. Color specification assumes Elmo Motion Control Cable CBL-MLXFDBK and US Digital Cable CA-FC10-SH-NC-2.				

Additional Notes:

1) M1-M3 connect to the phases of the EM.

2) Port J5 provides a serial connection for hooking the Solo Whistle to the PC for programming and calibration purposes.

3) All digital signals are 5 V signals.

4) Refer to Figure 36 for pin location

Appendix C. Drawings

All drawings are in inches unless otherwise noted. In house drawings are by Andrew Koch and Carl Heinley, Cedarville University.

1. Engine Flange

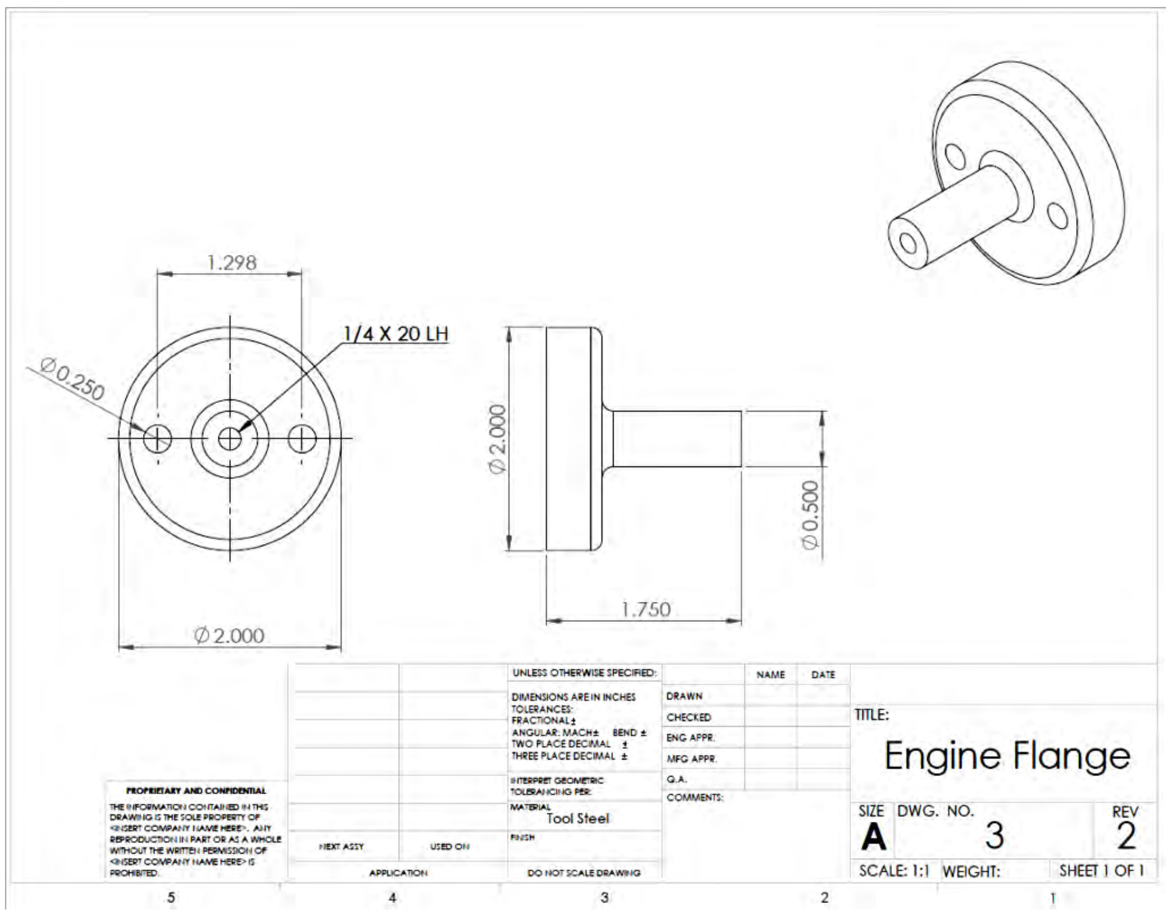

2. ICE Pulley

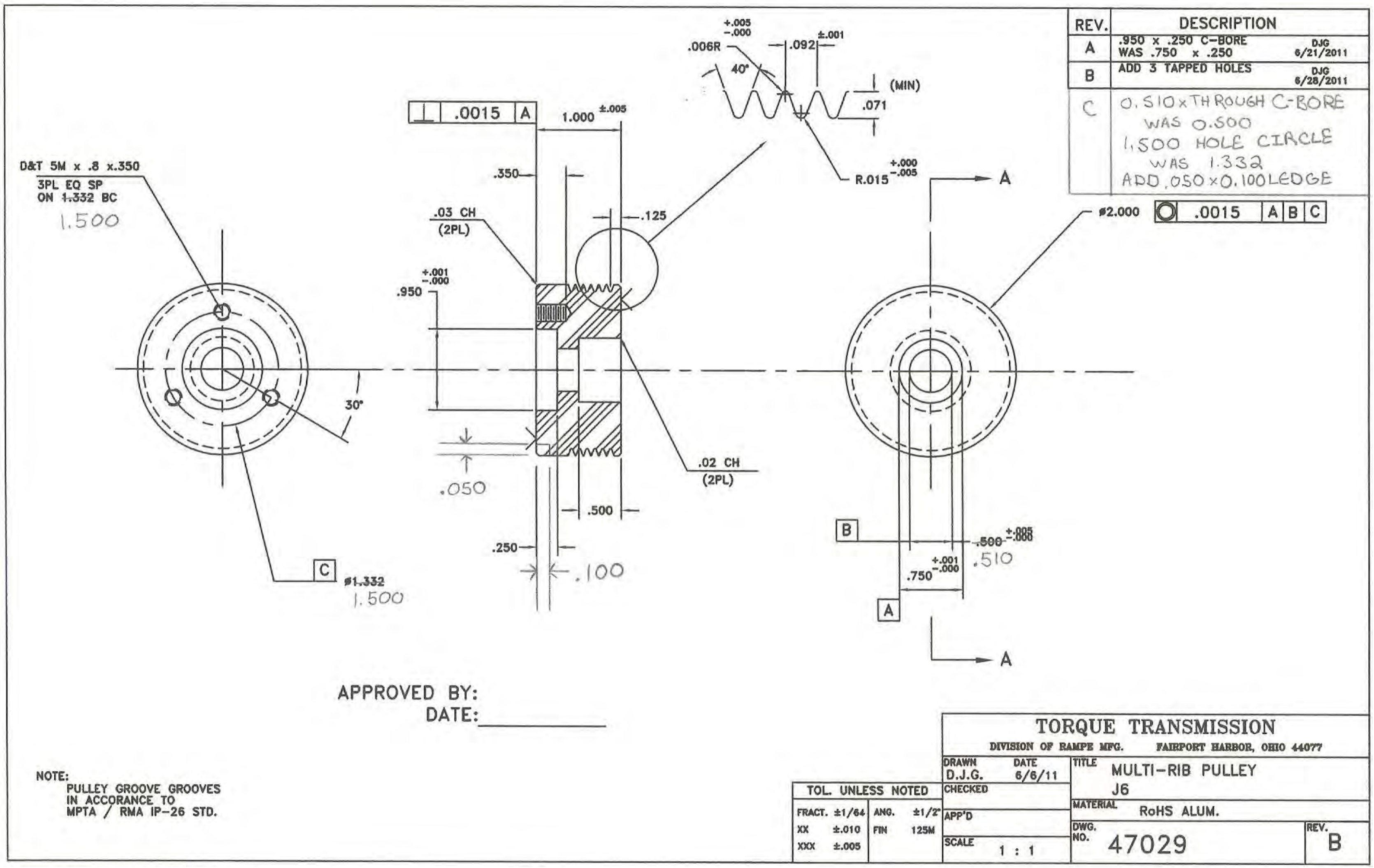
REV. | DESCRIPTION
A | .950 x .250 C-BORE WAS .750 x .250 | DJG 6/21/2011
B | ADD 3 TAPPED HOLES | DJG 6/28/2011
C | 0.510 x THROUGH C-BORE WAS 0.500 1,500 HOLE CIRCLE WAS 1.332 ADD .050 x 0.100 LEDGE
D&T 5M x .8 x.350
3PL EQ SP
ON 1.332 BC
1.500
30°
C ø1.332
1.500
.0015 A
1.000 ±.005
.350
.03 CH (2PL)
.950 +.001 -.000
.050
.250
.100
.500
.125
.006R +.005 -.000
.092 ±.001
40°
(MIN)
.071
R.015 +.000 -.005
.02 CH (2PL)
A
ø2.000 .0015 A B C
B
.500 +.005 -.000
.510
.750 +.001 -.000
A
APPROVED BY:
DATE:
NOTE:
PULLEY GROOVE GROOVES IN ACCORANCE TO MPTA / RMA IP-26 STD.
TORQUE TRANSMISSION
DIVISION OF RAMPE MFG. FAIRPORT HARBOR, OHIO 44077
DRAWN D.J.G. DATE 6/6/11
TITLE MULTI-RIB PULLEY J6
CHECKED
MATERIAL RoHS ALUM.
APP'D
TOL. UNLESS NOTED
FRACT. ±1/64 ANG. ±1/2°
XX ±.010 FIN 125M
XXX ±.005
SCALE 1 : 1
DWG. NO. 47029
REV. B

3. EM Pulley, Small (Not Used)

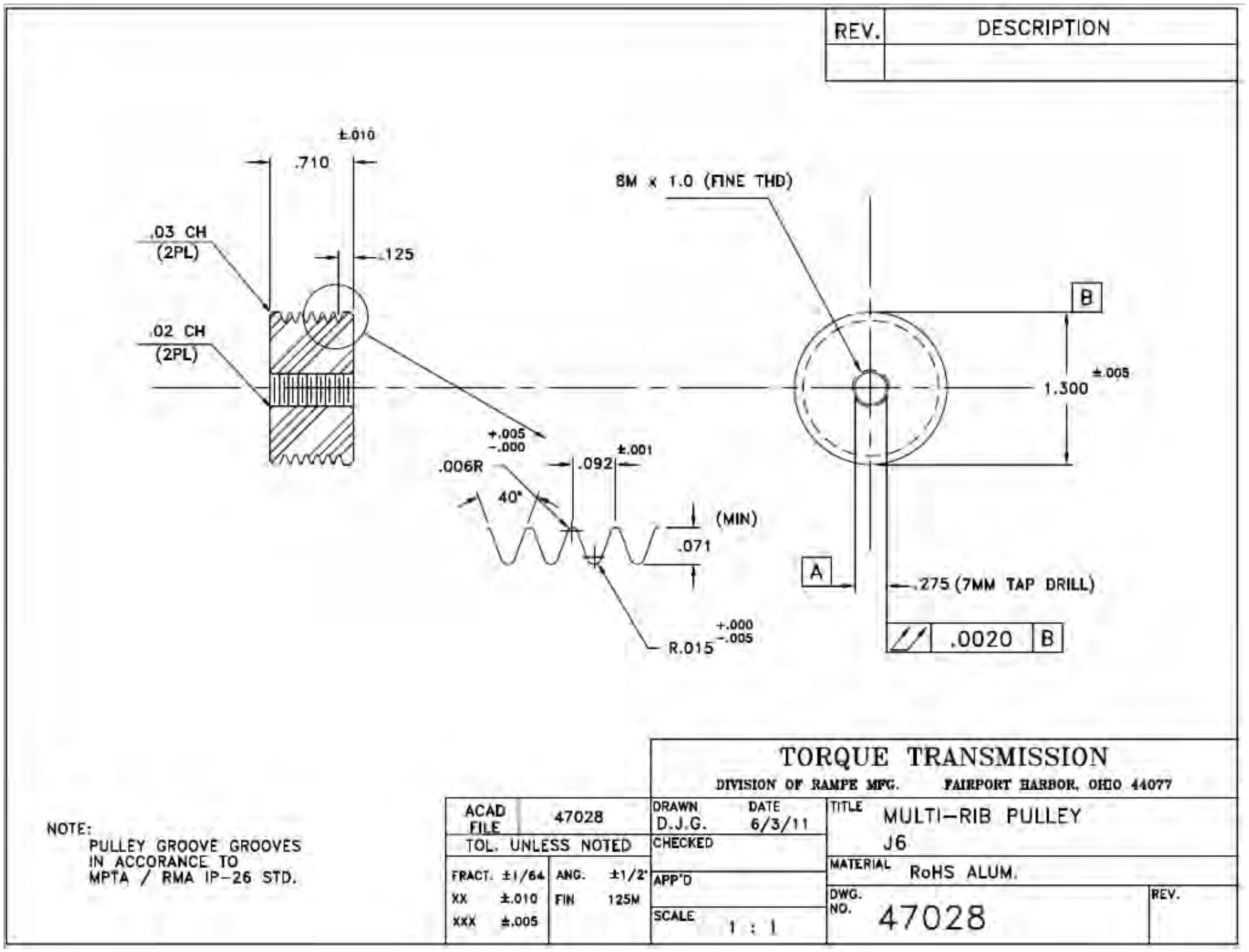

4. EM Pulley, Large (Currently Used)

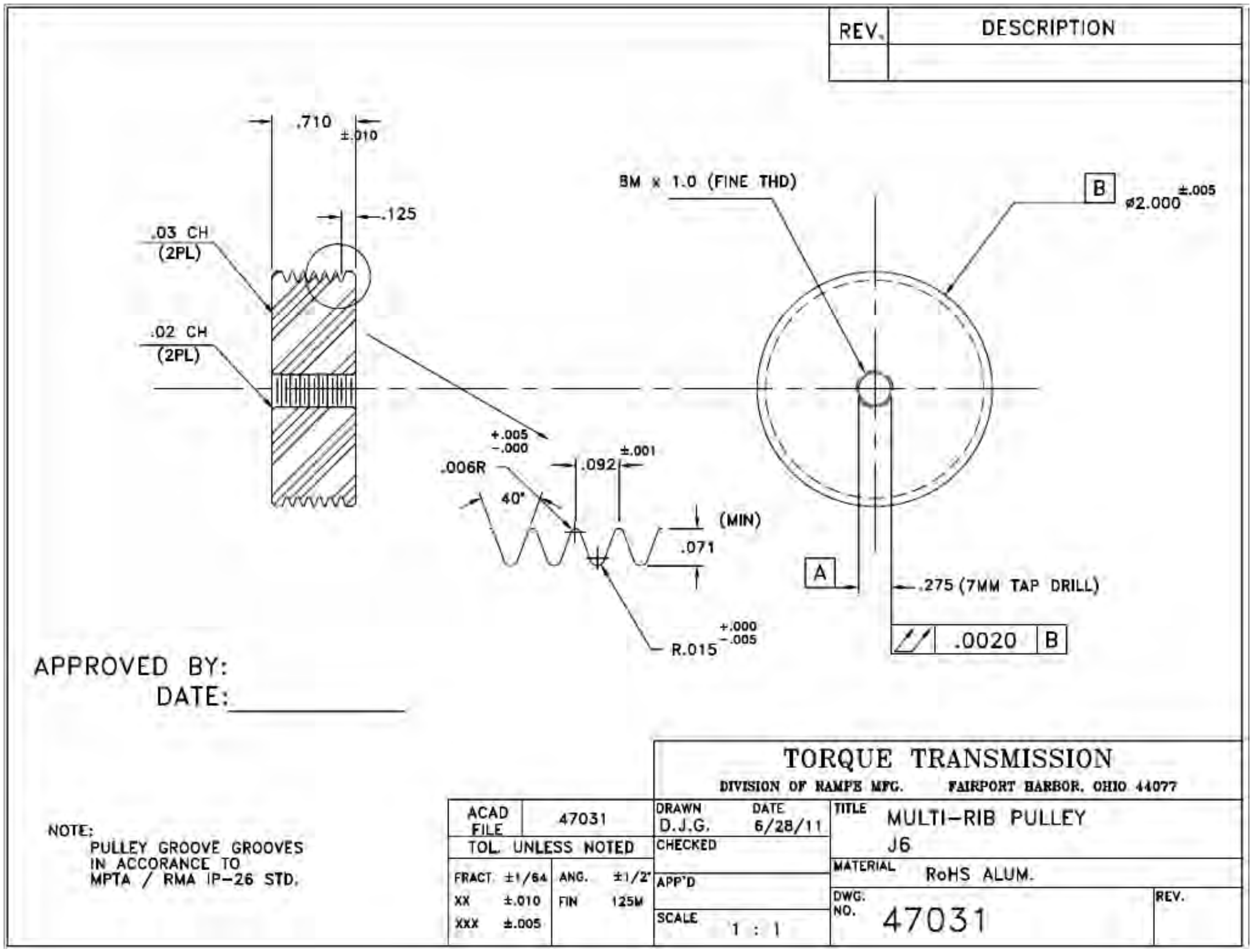

5. Motor Mount Bracket:

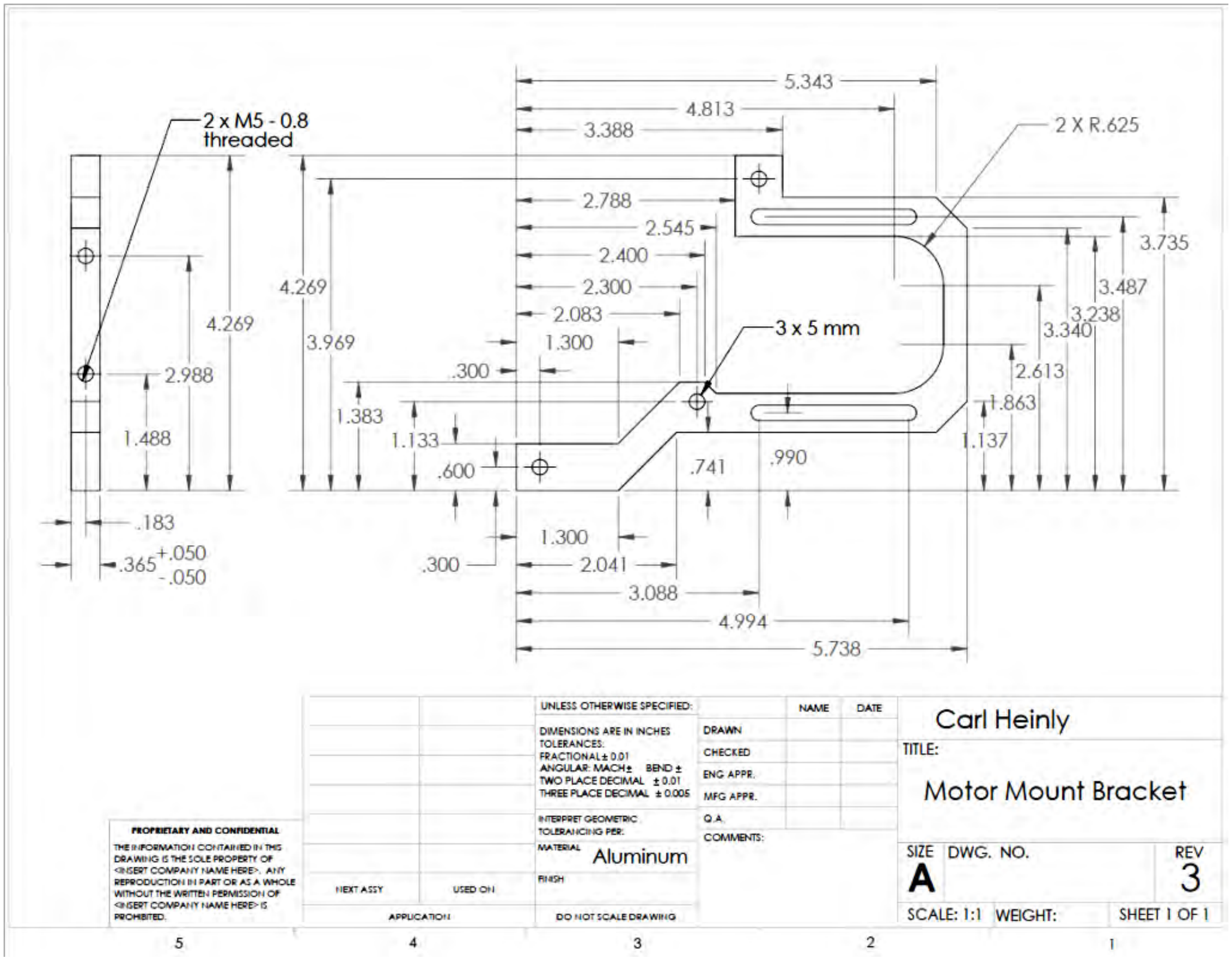

6. Motor Mount Plate

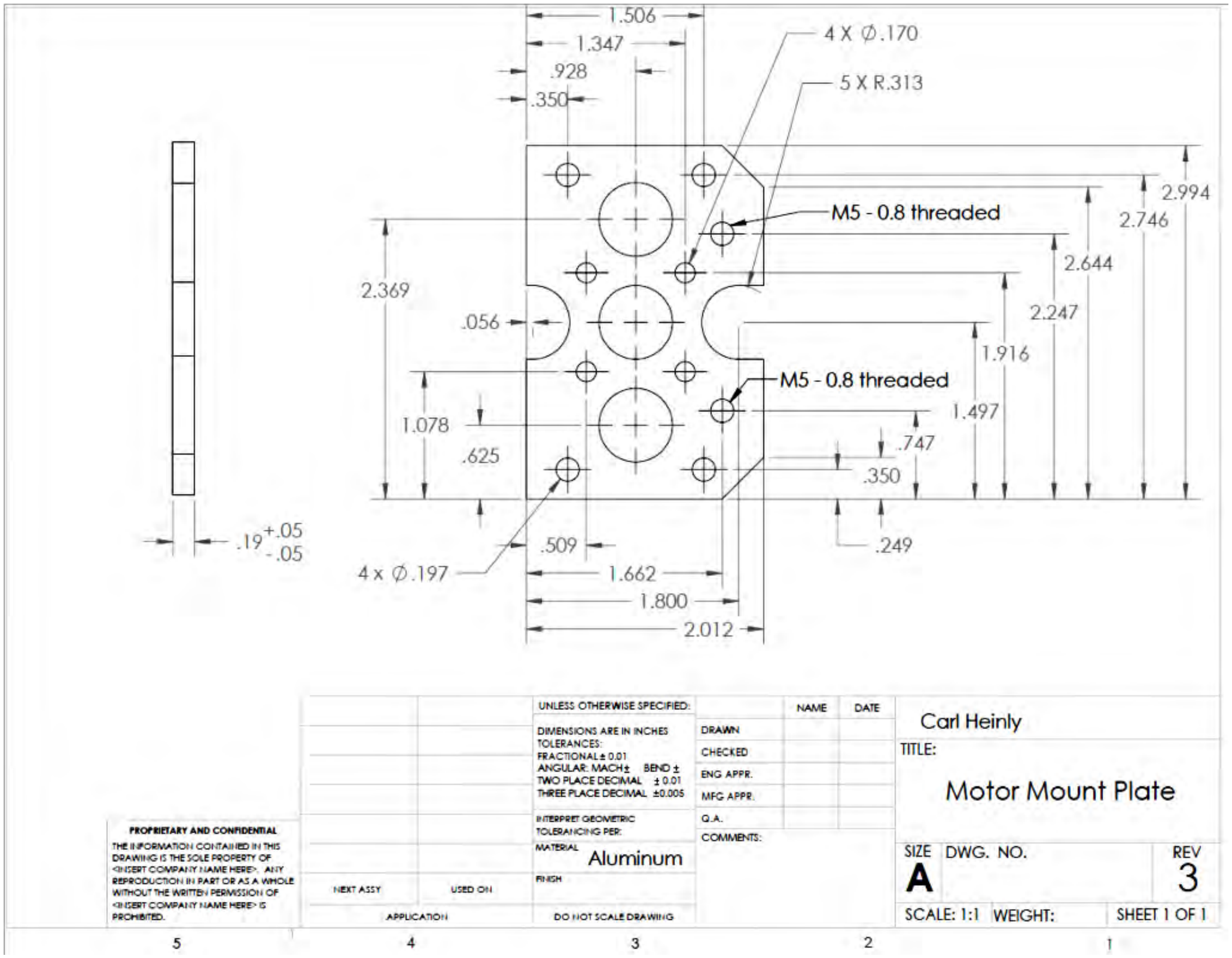

Appendix D. Bolt and Connector Specifications

Table D–1 provides the bolt specifications to assemble the hybrid propulsion system. All bolts are right handed American Standard threads unless otherwise noted. Where nuts are not included, the receiving component has a hole tapped to the proper thread specification. Each hex standoff for mounting electronics takes two bolts, one to secure the standoff to the component and one to secure the standoff to the plate.

Table D–1: Bolt specifications

Connection	Thread	Length	# Bolts	# Nuts
Propeller adapter to ICE pulley	M5 std	12 mm	3	0
ICE flange to flywheel	M6 std	24 mm	2	0
AXI 4130/20 to EM pulley	5/16 fine	N/A	0	1
Motor bracket to ICE*	M5 std	40 mm	3	3
AXI 4130/20 to motor plate	M4 std	10 mm	4	0
Propeller to propeller adapter	M8 std	38 mm	1	0
Motor mount plate to motor mount bracket	M5 std	20 mm	4	4
ICE pulley to ICE flange	1/4-20 LH	3/4"	1	0
Electronics standoffs	4-40	1/4"	8/component	4/component**

** list of washers include in*
*** electronics use hex standoffs to elevate components*

Table D–2 lists the washers used to square the motor mount bracket to the engine so the EM and ICE pulleys are parallel and the 6 Rib belt connecting the power trains does not derail. The connection numbers correspond to the mounting locations in Figure 40 of the main text.

Table D–2: Washer order for bolts securing motor mount bracket to ICE

Connection	Order (from head of bolt)
1 (bottom)	Bolt head > shroud (if used) > engine > rubber washer > metal washer > motor mount bracket > lock washer > nut
2 (middle)	Bolt heat > metal plate* > engine > metal washer > rubber washer > metal washer > rubber washer > metal washer > motor mount bracket > lock washer > nut
3 (top)	Bolt head > shroud (if used) > rubber washer > rubber washer > motor mount bracket > lock washer > nut

** The metal plate acts as bolt hole since the mounting location is larger than the bolt head.*

Appendix E. Torque Split Equations:

This appendix summarizes the torque split equations for the IOL control strategy. In this implementation the same throttle request should deliver the same output torque to the propeller regardless of operating mode, provided the propulsion system can generate sufficient torque with the active components. This code is implemented in the PIC32.

1. Requested Torque

The requested torque is the product of the throttle request from the autopilot or manual controller multiplied by the maximum torque available from the propulsion system as a function of speed in rpm.

$$Requested\ Torque = Throttle\ Request \cdot Maximum\ Torque(rpm) \tag{E–1}$$

2. Maximum Torque

The maximum torque is the sum of the maximum torque from the EM, assumed a constant over the range of speeds, and the maximum torque from the ICE read from the torque map at the current speed.

$$Maximum\ Torque = EM\ Max\ Torque \cdot ICE\ MAX\ Torque(rpm) \tag{E–2}$$

3. ICE Only Mode

In ICE only mode EM throttle is zeroed while the ICE provides the requested torque.

$$ICE\ Throttle = \frac{Requested\ Torque}{ICE\ Max\ Torque(rpm)} \tag{E–3}$$

$$EM\ Throttle = 0 \tag{E–4}$$

4. EM Only

In EM only mode the ICE throttle is zeroed or idled while the EM provides the requested torque.

$$EM\ Throttle = \frac{Requested\ Torque}{EM\ Max\ Torque} \quad \text{(E–5)}$$

$$ICE\ Throttle = 0\%\ or\ idle \quad \text{(E–6)}$$

5. Dual Mode

Dual Mode operation is split into three cases.

5.1. **Case 1**

When the requested torque is less than the IOL Torque of the ICE at the speed as read from the torque map, the ICE provides the power for the aircraft.

$$ICE\ IOL\ Torque(rpm)\ >\ Requested\ Torque$$

$$ICE\ Throttle = \frac{Requested\ Torque}{ICE\ Max\ Torque(rpm)} * 100\% \quad \text{(E–7)}$$

$$EM\ Throttle = 0\% \quad \text{(E–8)}$$

5.2. **Case 2**

In this case the requested torque is provided by the ICE at its IOL point supplemented by the EM.

$$ICE\ IOL\ Torque(rpm) + EM\ Max\ Torque >\ Requested\ Torque > ICE\ IOL\ Torque(rpm)$$

$$ICE\ Throttle = \frac{ICE\ IOL\ Torque}{ICE\ Max\ Torque(rpm)} * 100\% \quad \text{(E–9)}$$

$$EM\ Throttle = \frac{Requested\ Torque - ICE\ IOL\ Torque}{EM\ Max\ Torque} * 100\% \quad \text{(E–10)}$$

5.1. **Case 3**

In this case the torque is provided by the EM operating at full capacity and the ICE operating above its IOL point for the given speed.

$$Requested\ Torque > ICE\ IOL\ Torque(rpm) + EM\ Max\ Torque$$

$$ICE\ Throttle = \frac{Requested\ Torque - EM\ Max\ Torque}{ICE\ Max\ Torque(rpm)} * 100\% \tag{E–11}$$

$$EM\ Throttle = 100\% \tag{E–12}$$

**Note, there is also a mode programmed in the PIC32 to pass the throttle command directly to the ICE or EM in ICE-only or EM-only mode respectively.*

Appendix F. Torque Map Test Procedure

1) Turn on cooling fan, exhaust fan

2) Turn on servo controller, check that 100% throttle is fully open, 0% throttle is fully closed

3) Set engine to starting throttle setting

4) Turn on auxiliary instrumentation (i.e. Seagull)

5) Set up the test profile in DYNOmite Software Suite

i) Record torque at 10 Hz every 250 rpm until engine is unable to meet the next increase in speed

ii) The initial step down to the first speed should be gradual, no more than 50 rpm per second

6) Ensure dynamometer load cell is off

6) Start the engine, allow it to warm up for 4-5 minutes*

7) Set engine throttle to desired test setting**

8) Turn on the dynamometer load cell

9) Begin running the test

10) Upon completion of test, save dynamometer data

*If the EM is mounted to the engine, it may need to be run at 20-30% power while the engine is started, especially if using a starter motor for the engine

**If testing a dual mode of the system, set the EM throttle to the desired setting during step 7 as well

Appendix G. Sample Controller Code for PIC32 as Hybrid Controller

This appendix contains sample code for the PIC32 microcontroller to run the designed hybrid-electric system. This section only includes the *main.c*, *HybridPropulsionControl.c,* and *HybridPropulsionControl.h* files. The *main.c* file contains the main code that initializes the PIC32 and executes the functions to set the operating mode, perform the torque split, and control the ICE and EM throttle signals. The user must select which set of mode inputs is used, digital or PWM slider, in the configuration section of *HybridPropulsionControl.c*. The configuration section also allows the user to set the torque split type, input torque maps, and control a variety of other operational parameters. The *HybridPropulsionControl.h* file contains all of the pin assignments when using the PIC32 Lightning breakout board as designed by Hagen [**16**].

The board and code will only function with the PIC32MX795F512L set into Revision 26 of the USB 32 Bit Whacker PIC32MX795 development board sold by Sparkfun Electronics. For more information on the breakout board and pin numbering please consult [**16**]. To function, the three files should be compiled in a fresh implementation of the Lightning v1.50 source code available from Hagen [**16**] or from the Condor team. Also consult Hagen's documentation [**16**] for details on how to write new programs using the Lightning firmware.

The hybrid propulsion code written by the author is heavily commented and the details are too extensive to explain here. The commented code should be self explanatory for a user with basic experience programming in C and with microcontrollers. All code including the Lightning firmware compiles in Microchip's MPLAB v8.50 or higher and Hagen's documentation explains how to compile a project in MPLAB. For a user new to the MPLAB and C programming environment, the author recommends reading both Hagen's documentation [**16**] in its entirety for an introduction to the programming environment and Greiser's thesis for an explanation of the basic state machine framework. Please contact the author with questions about the hybrid propulsion code.

1. main.c

```
/****************************************************************
FileName:         main.c
Author:                 Joseph Ausserer
Project:                HE-RPA
Description:            Main file for the propulsion state machine.
***************************************************************/

/** CONFIGURATION- PIC32MX795 **********************************/
#pragma config FVBUSONIO = OFF            // OFF: VBUS_ON pin is controlled by the Port Function
#pragma config FUSBIDIO = OFF             // OFF: USBID pin is controlled by the Port Function
#pragma config FCANIO   = ON              // ON: Default CAN IO Pins
#pragma config FETHIO   = ON              // ON: Default Ethernet IO Pins
#pragma config FMIIEN   = ON              // ON: MII enabled
#pragma config FSRSSEL  = PRIORITY_7      // SRS Interrupt Priority Level 7
#pragma config FPLLODIV = DIV_1           // PLL Output Divider
#pragma config UPLLEN   = OFF             // OFF: USB PLL Enabled off
#pragma config UPLLIDIV = DIV_2           // USB PLL Input Divider
#pragma config FPLLMUL  = MUL_20          // PLL Multiplier
#pragma config FPLLIDIV = DIV_2           // PLL Input Divider
#pragma config FWDTEN   = OFF             // Watchdog Timer
#pragma config WDTPS    = PS1             // Watchdog Timer Postscale
#pragma config FCKSM    = CSDCMD          // Clock Switching & Fail Safe Clock Monitor
#pragma config FPBDIV   = DIV_1           // Bootup Peripheral Clock divisor
#pragma config OSCIOFNC = OFF             // CLKO Enable
#pragma config POSCMOD  = HS              // Primary Oscillator
#pragma config IESO     = OFF             // Internal/External Switch-over
#pragma config FSOSCEN  = OFF             // Secondary Oscillator Enable (KLO was off)
#pragma config FNOSC    = PRIPLL          // Oscillator Selection
#pragma config CP       = OFF             // Code Protect
#pragma config BWP      = OFF             // Boot Flash Write Protect
#pragma config PWP      = OFF             // Program Flash Write Protect
#pragma config ICESEL   = ICS_PGx2        // ICE/ICD Comm Channel Select
#pragma config DEBUG    = ON              // Background Debugger Enable
/** CONFIGURATION- PIC32MX795 **********************************************/
```

```
#include <GenericTypeDefs.h>
#include <LightningIO.h>
#include <LightningStream.h>
#include <LightningCommand.h>
#include <LightningDrive.h>
#include <LightningFlash.h>
#include <LightningScreen.h>
#include "User/HybridPropulsionControl.h"

/** PRIVATE PROTOTYPES *****************************************/

/** PRIVATE PROTOTYPES *****************************************/

int main(void)
{
      // Firmware
      SetupIO();
      InitializeFlash();
      InitializeScreen();
      ClearScreen();
      // Hardware
      ElmoInit();
      ConfigureHybridController();  // Setup up the inputs and outputs
      ScreenInit();

      while(TRUE)
      {
            // Firmware
            ProcessIO();
            LightningCommand();           // Uses UART1
            // Hardware
            SetPropulsionState();   // Always read the state before setting the propulsions system.
            //SetTestMode();
            PropulsionControlStateMachine(); // Executes the main controller code, repeatedly
            ScreenUpdate();
      }
      return;
}
```

2. HybridPropulsionControl.h

```
/*******************************************************************
FileName:        HybridPropulsionControl.h
Author:                      Collin Greiser & John Hagen
Project:               Hybrid Electric UAV
*******************************************************************/

#ifndef HYBRIDPROPULSIONCONTROL_H
#define HYBRIDPROPULSIONCONTROL_H

/** PUBLIC PROTOTYPES ***********************************************/
void PropulsionControlStateMachine();
void ConfigureHybridController();
void SetPropulsionState();
void SetTestMode();
void ElmoInit();
void SetElmoState(int elmoState);
void ScreenInit();
void ScreenUpdate();
double InterpolateVector1D(double yValues[], int length, double xStart, double xStep, double inputX);

/***** NUMERICAL CONSTANTS ******************************************/
// Digital Pins

// Mode Switches (input) (Takeoff/Idle and Manual Clutch not connected or used)
//#define RunKillSwitchPort              DIO1PORT    // G13; TRUE = Run, FALSE = Kill (which makes the
                                         name somewhat confusing)
//#define RunKillSwitchPin               DIO1PIN
#define RunKillSwitchPort                DIO16PORT   // G13; TRUE = Run, FALSE = Kill (which makes the
                                         name somewhat confusing)
#define RunKillSwitchPin                 DIO16PIN
#define RunKillKestrelSwitchPort         DIO15PORT   // Kestrel control signal *** wire this high when
                                         the kestrel is not in use
#define RunKillKestrelSwitchPin          DIO15PIN
#define ICEOnlySwitchPort                DIO2PORT    // Channel 5, SA (A7)
#define ICEOnlySwitchPin                 DIO2PIN
```

```
#define EMOnlySwitchPort                  DIO3PORT    // Channel 6, SB (A6)
#define EMOnlySwitchPin                   DIO3PIN
#define DualModeSwitchPort                DIO4PORT    // Channel 7, SC (G0)
#define DualModeSwitchPin                 DIO4PIN
#define StartSwitchPort                   DIO5PORT    // Channel 8, SD (G1)
#define StartSwitchPin                    DIO5PIN
//Elmo Mode Control Switches (output)
#define CurrentControlSwitchPin           DIO6PIN           // Elmo 3
#define CurrentControlSwitchPort          DIO6PORT
#define SpeedControlSwitchPin             DIO7PIN           // Elmo 4
#define SpeedControlSwitchPort            DIO7PORT
#define PropellerOrientSwitchPin          DIO8PIN           // Elmo 5
#define PropellerOrientSwitchPort         DIO8PORT
#define RegenerationSwitchPin             DIO9PIN           // Elmo 6
#define RegenerationSwitchPort            DIO9PORT
// Magneto Control Line
#define MagnetoControlPin                 DIO10PIN
#define MagnetoControlPort                DIO10PORT
// Starter Motor Control Line
#define StarterMotorSwitchPin             DIO11PIN
#define StarterMotorSwitchPort            DIO11PORT

// PWM Output Channels
#define ICEThrottleServo                  OCPORT1     // D0, Channel 3, J3
#define EMThrottleSignal                  OCPORT2     // Allows the EM signal to be read by the seagull
                                          and to control the EM in direct mode with a non-elmo
                                          controller
#define ICEChokeServo                     OCPORT3           // D1, Channel 1, SA

// Analogue In Channels
#define BatteryVoltagePort                AIPORT1
#define EngineTempPort                    AIPORT3
#define MotorTempPort                     AIPORT5
#define BatteryTempPort                   AIPORT9

// Analogue Out Channels
#define ElmoCurrentSpeedPort              AOPORT1
```

```
//Interrupt pins
#define ICESpeedPort                INTPORT1    // E8
#define EMSpeedPort                 INTPORT2    // E9

// PWM Input Channels
#define AutopilotThrottle           ICPORT1     // D8, Channel 3, J3 *singal line only

//Propulsion States
#define RESET_PROP                  0     // Kill Switch Off or Kestrel kill switch off.
#define ICEONLY_PROP                1     // Kill Switch On; ICE = T, EM = F, Dual = F, Start = F
#define EMONLY_PROP                 2     // Kill Switch On; ICE = F, EM = T, Dual = F, Start = F
#define ICEANDEM_PROP               3     // Kill Switch On; ICE = T, EM = T, Dual = T, Start = F
#define ICEONLYGENERATION_PROP      4     // Kill Switch On; ICE = T, EM = T, Dual = F, Start = F
#define IDLE_PROP                   5     // Kill Switch On; ICE = F, EM = F, Dual = F, Start = F
#define START_PROP                  6     // Kill Switch On; ICE = F, EM = F, Dual = F, Start = T
#define TEST_PROP                   8     // Kill Switch On; ICE = F, EM = F, Dual = T, Start = T
// Unused and unimplemented states
#define CATAPULT_PROP               7     // Not Implemented)
#define DEFAULT_PROP                IDLE_PROP   //    Default State

// ElmoStates
#define ElmoOff                     0     //    Defaults to Current Control Mode
#define ElmoCurrentControlMode      1     //
#define ElmoSpeedControlMode        2     //
#define ElmoRegenerationMode        3     //
#define     ElmoOrientPropMode      4     //

// Choke States
#define ChokeOpen                   1     //
#define ChokeClosed                 0     //

// ICE/EM Throttle Modes
#define DirectControl               0     // Bypass the controller logic and control the servo directly
#define TorqueControl               1     // Use the torque setting scheme developed by Grieser

// LCD Screen locations
#define propulsionStateX            6
#define propulsionStateY            0
```

```
#define elmoModeX                   16
#define elmoModeY                   0
#define ICEThrottleModeX            6
#define ICEThrottleModeY            1
#define EMThrottleModeX             16
#define EMThrottleModeY             1
#define normalizedICETorqueX        6
#define normalizedICETorqueY        2
#define normalizedEmTorqueX         16
#define normalizedEMTorqueY         2
#define ICESpeedX                   5
#define ICESpeedY                   3
#define EMSpeedX                    15
#define EMSpeedY                    3

// Shared Custome Memory Locations
#define SCMPropulsionState          1
#define SCMElmoState                2
#define SCMICEThrottleMode          3
#define SCMEMThrottleMode           4
#define     SCMNormalizedICETorque  5
#define SCMNormalizedEMTorque       6
#define SCMICESpeed                 7
#define SCMEMSpeed                  8
#define SCMBatteryVoltage           9

// Digital States
#define ON                          1
#define OFF                         0

// EM States
#define EMOFF                       0

/***** NUMERICAL CONSTANTS*************************************************/

#endif // HYBRIDPROPULSIONCONTROL_H
```

3. HybridPropulsionControl.c

```
/*******************************************************************************************************
FileName:                     HybridPropulsionControl.c
Author:               Collin Greiser & John Hagen & Joseph Ausserer
Project:                      Hybrid Electric RPA
Description:          Implements the state machine required to control the HE-RPA.  Includes a number of functions for such
control.  PropulsionControlStateMachine includes the operation modes for the RPA.  ConfigureHybridController handles the port
initialization.  SetPropulsionState uses a relay signal from the transmitter to switch between states.  All other functions are
private.

Public prototypes: (in header)
void PropulsionControlStateMachine();
void ConfigureHybridController();
void SetPropulsionState();
void SetTestMode();
void ElmoInit();
void SetElmoState(int elmoState);
void ScreenInit();
void ScreenUpdate();

There is no main code in this file.  It only offers the function definitions, the main one of which is the state machine which is s
giant switch statement controlled by the variable propulsion state.
*******************************************************************************************************/

/***** PRIVATE PROTOTYPES *************************************************/
double GetTorqueRequest();
double GetMaxICETorque();
double GetICEIOLTorque();
double GetMaxEMTorque();
double GetTotalAvailableTorque();
double GetThrottleRequest();

void SetNormalizedICETorque(double normalizedTorque);
void SetNormalizedEMTorque(double normalizedTorque);
void SetMagneto(char setHigh);
void SetChoke(char setHigh);

double GetThrottleSetting();
double GetBatteryVoltage(unsigned char BatteryPort);

double SaturateICESignal(double normalizedTorque);
double SaturateEMSignal(double normalizedTorque);
/***** PRIVATE PROTOTYPES ************************************************/
```

```
/***** NUMERICAL CONSTANTS************************************************/
#define IdleThrottle          0.20   // This value may not be appropriate, may need 20% to avoid stall
#define OffThrottle           0.0
#define StartICEThrottle      0.30
#define StartEMThrottle       0.30

#define InvertThrottle TRUE
#define InvertICEServo TRUE
#define InvertEMServo  FALSE

#define GearRatio             1.0

#define EngineMapLength       5
#define EngineMapWidth        11
#define MotorMapLength        5
#define MotorMapWidth  5

#define ICECountsPerRev 1
#define EMCountsPerRev        1

const char BatteryNumCells = 8;
const double BatteryCRate = 3.3;                     //
const double normalizedEMChargeTorque = 0.165;
const double BatteryCellMinVoltage = 3.2;            // V 3.0 volts is the real min, this allows 0.2V of safety for potential
                                                     balance issues, etc.
const double BatteryCellMaxVoltage = 4.0;            // V 4.2 volts is the real max, this allows 0.2V of for potential balance
                                                     issues, etc.
double MinimumPackVoltage = 25.6;
double MaximumPackVoltage = 32.0;
const double EMTakeoff = 0.1;                        //  Add 10% to ICE power to allow for EM to regenerate batteries
double PackVoltage;

double MaxEMTorque = 0.5;

double ICEMapYValues[] = {1.1, 1.3, 1.3, 1.4, 1.4, 1.4, 1.4, 1.3, 1.2, 1.1, 1.0};
const int ICEMapLength = 11;                         // Number of values MUST match ICEMapLength
const double ICEMapXStart = 4000.0;
const double ICEMapXStep = 500.0;

double IOLMapYValues[] = {0.2, 0.45, 0.632, 0.85, 0.95, 1.05, 1.15, 1.1, 1.0, 0.9, 0.7};
const int IOLMapLength = 11;                         // Number of values MUST match IOLMapLength
const double IOLMapXStart = 1000.0;
const double IOLMapXStep = 500.0;

/***** NUMERICAL CONSTANTS************************************************/

/***** INCLUDED HEADER FILES**********************************************/
```

```
#include <GenericTypeDefs.h>
#include "..\Lightning\LightningScreen.h"
#include "..\Lightning\LightningIO.h"
#include "..\Lightning\LightningDrive.h"
#include "..\Lightning\LightningStream.h"
#include "HybridPropulsionControl.h"
#include "math.h"
/***** INCLUDED HEADER FILES*********************************************/

/***** TEST PARAMETERS **************************************************/
char TestElmo = ElmoCurrentControlMode;
double TestEMThrottle = 0.00;
double TestICEThrottle = 0.60;
char TestStaterMotor = FALSE;
/***** TEST PARAMETERS **************************************************/

/***** VARIABLE DECLARATIONS********************************************/
BOOL EMOnlyModeSwitch;
BOOL ICEOnlyModeSwitch;
BOOL DualModeSwitch;
BOOL RunKillSwitch;
BOOL RunKillKestrelSwitch;
BOOL StartSwitch;

// These will be declared globally so they can be written by the LCD function without passing
double normalizedICETorque = IdleThrottle;
double normalizedEMTorque = 0;

int propulsionState = RESET_PROP;
int elmoState = ElmoOff;

int ICEThrottleMode = DirectControl;
int EMThrottleMode = DirectControl;

double throttleSetting = 0;
/***** VARIABLE DECLARATIONS *******************************************/


/***** FUNCTION DEFINITIONS ********************************************/

/***** PUBLIC FUNCTIONS ************************************************/

void ConfigureHybridController()
{
       // Mode inputs
       ConfigureDigitalIO(RunKillSwitchPort, RunKillSwitchPin, SETINPUT);
       ConfigureDigitalIO(RunKillKestrelSwitchPort, RunKillKestrelSwitchPin, SETINPUT);
```

```
        ConfigureDigitalIO(ICEOnlySwitchPort, ICEOnlySwitchPin, SETINPUT);
        ConfigureDigitalIO(EMOnlySwitchPort, EMOnlySwitchPin, SETINPUT);
        ConfigureDigitalIO(DualModeSwitchPort, DualModeSwitchPin, SETINPUT);
        ConfigureDigitalIO(StartSwitchPort, StartSwitchPin,  SETINPUT);

        // Elmo Mode Control Outputs
        ConfigureDigitalIO(CurrentControlSwitchPort, CurrentControlSwitchPin, SETOUTPUT);
        ConfigureDigitalIO(SpeedControlSwitchPort, SpeedControlSwitchPin, SETOUTPUT);
        ConfigureDigitalIO(RegenerationSwitchPort, RegenerationSwitchPin, SETOUTPUT);
        ConfigureDigitalIO(PropellerOrientSwitchPort, PropellerOrientSwitchPin, SETOUTPUT);

        // Magneto Pin
        ConfigureDigitalIO(MagnetoControlPort, MagnetoControlPin, SETOUTPUT);

        // Starter Motor
        ConfigureDigitalIO(StarterMotorSwitchPort, StarterMotorSwitchPin, SETOUTPUT);
        SetDigitalOutput(StarterMotorSwitchPort, StarterMotorSwitchPin, FALSE);

        // Set initial state for ICE - Idle with engine one to avoid stopping engine during intialization
        propulsionState = IDLE_PROP;
        SetNormalizedICETorque(IdleThrottle);
        SetChoke(ChokeOpen);
        SetMagneto(ON); //(TRUE grounds the spark plug)

        // Set initial state for Elmo - may not match eventual selection of idle condition
        elmoState = ElmoOff;
        SetElmoState(elmoState);      // Turn the Elmo to the off/default state to prevent issues during system off operation

        //Throttle PWM
        ConfigureMinMaxDutyCycle(ICEThrottleServo, 0.055, 0.10);
}


void PropulsionControlStateMachine()
{
        switch(propulsionState)
        {
                case RESET_PROP:
                        // Reset_prop state is the default "dead" state for all components.  This is not appropriate for an
                        initializing state.
                        // 0: Kill Switch Off

                        // Turn off the engine, close the choke, ground the spark plug
                        normalizedICETorque = OffThrottle;
                        SetNormalizedICETorque(normalizedICETorque);
                        SetChoke(ChokeClosed);
                        SetMagneto(OFF);
```

```
        // Turn off Elmo
        elmoState = ElmoOff;
        SetElmoState(elmoState);

        // Turn off starter motor
        SetDigitalOutput(StarterMotorSwitchPort, StarterMotorSwitchPin, FALSE);

break;


case ICEONLY_PROP:
// ICE Only operating mode
// 1: Kill Switch On; ICE = T, EM = F, Dual = F, Start = F

                              // Open the choke, enable the magneto
        SetChoke(ChokeOpen);
        SetMagneto(ON);

        // Turn Off Elmo
        elmoState = ElmoOff;
        SetElmoState(elmoState);

        // Turn off starter motor
        SetDigitalOutput(StarterMotorSwitchPort, StarterMotorSwitchPin, FALSE);

        //  Allow for torque request control of the throttle or allow the throttle command to be directly sent to
        // the servo
        switch(ICEThrottleMode)
        {
                case DirectControl: // Pass the throttle setting
                // Set to pass the throttle command directly, read torque back to user

                        throttleSetting = GetThrottleRequest();
                        normalizedICETorque = throttleSetting;               // use to monitor output
                                                                     without require excess
                                                                     code
                        normalizedICETorque = SaturateICESignal(normalizedICETorque);       // Saturate the signal

                break;

                case TorqueControl:    // Use the torque request strategy
                // Use the torque normalized to the maximum possible torque based on the torque maps

                        normalizedICETorque = GetTorqueRequest() / GetMaxICETorque();       // Normalize torque
                                                                                    request for throttle input
                        normalizedICETorque = SaturateICESignal(normalizedICETorque);       // Saturate the signal
```

```
                break;
        }

        SetNormalizedICETorque(normalizedICETorque);

break;


case EMONLY_PROP:
// Electric Motor Only Operation
// 2: Kill Switch On; ICE = F, EM = T, Dual = F, Start = F

        // Set the ICE to idle
        normalizedICETorque = IdleThrottle;
        SetNormalizedICETorque(normalizedICETorque);
        SetChoke(ChokeOpen);
        SetMagneto(ON);

        // Turn the Elmo to current control mode
        elmoState = ElmoCurrentControlMode;
        SetElmoState(elmoState);

        // Turn off starter motor
        SetDigitalOutput(StarterMotorSwitchPort, StarterMotorSwitchPin, FALSE);

        //  Allow for torque request control of the throttle or allow the throttle command to be directly sent to
        // the servo
        switch(EMThrottleMode)
        {
                case DirectControl: // pass the throttle setting

                        throttleSetting = GetThrottleRequest();
                        normalizedEMTorque = throttleSetting;        // Use to monitor output without require excess
                                                                     code
                        normalizedEMTorque = SaturateEMSignal(normalizedEMTorque);

                break;

                case TorqueControl:    // use the torque request strategy

                        normalizedEMTorque = GetTorqueRequest() / GetMaxEMTorque();
                        normalizedEMTorque = SaturateEMSignal(normalizedEMTorque);

                break;
        }
```

```
        SetNormalizedEMTorque(normalizedEMTorque);

break;


case ICEANDEM_PROP:
// Dual Power mode operation, both ICE and EM
// 3: Kill Switch On; ICE = T, EM = T, Dual = T, Start = F

        // Ensure the choke is open, magneto is on
        SetChoke(ChokeOpen);
        SetMagneto(ON);

        // Turn the Elmo to current control mode
        elmoState = ElmoCurrentControlMode;
        SetElmoState(elmoState);

        // Turn off starter motor
        SetDigitalOutput(StarterMotorSwitchPort, StarterMotorSwitchPin, FALSE);

        /*** Basic Program, runs the engine up to IOL and then uses the electric motor for the remaining
         ***/

        // Read these in once to prevent instability during code execution
        double requestedTorque = GetTorqueRequest();
        double IOLICETorque = GetICEIOLTorque()*1.05;        // Add 10% band for IOL operation
        double maxICETorque = GetMaxICETorque();
        double maxEMTorque = GetMaxEMTorque();               // Lower case indicates this is NOT the global variable
                                                             that is defined previously as I may make this more
                                                             accurate given enough time

        if(requestedTorque <= IOLICETorque)
        {
                // ICE
                normalizedICETorque = requestedTorque / maxICETorque;
                normalizedICETorque = SaturateICESignal(normalizedICETorque);
                // EM
                normalizedEMTorque = 0; // Turn off the EM
        }
        else if( (requestedTorque - IOLICETorque) <= maxEMTorque)   // Motor can provide enough boost power at
                                                                     engine IOL
        {
                // ICE
                normalizedICETorque = IOLICETorque / maxICETorque;
                normalizedICETorque = SaturateICESignal(normalizedICETorque);
                // EM
                double remainingTorque = requestedTorque - IOLICETorque;
```

```
                normalizedEMTorque = remainingTorque / maxEMTorque;
                normalizedEMTorque = SaturateEMSignal(normalizedEMTorque);
        }
        else if( (requestedTorque - IOLICETorque) >= maxEMTorque)
        {
                // ICE
                double remainingTorque = requestedTorque - maxEMTorque;
                normalizedICETorque = remainingTorque / maxICETorque;
                normalizedICETorque = SaturateICESignal(normalizedICETorque);
                // EM
                normalizedEMTorque = 1.0;     // Set Em to full power
        }

        // Set the servo and Elmo
        SetNormalizedEMTorque(normalizedEMTorque);
        SetNormalizedICETorque(normalizedICETorque);

        // Advanced program avilable at the end of the code

break;


case ICEONLYGENERATION_PROP:  // TODO: program this mode
// Uses the ICE to recharge the electric motor
// 4: Kill Switch On; ICE = T, EM = T, Dual = F, Start = F

        // Ensure the choke is open, magneto is on
        SetChoke(ChokeOpen);
        SetMagneto(ON);

        // Turn off starter motor
        SetDigitalOutput(StarterMotorSwitchPort, StarterMotorSwitchPin, FALSE);

        PackVoltage = GetBatteryVoltage(AIPORT1);

        if((PackVoltage < MaximumPackVoltage) && (PackVoltage > MinimumPackVoltage)) //safe to charge
        // Do not charge if battery voltage drops below the 3.0 V min. or goes above 4.2V maximum,  this assumes a
        // max of 4.1V and a minimum of 3.1V
        {
                // Turn the Elmo to current control mode, regen
                elmoState = ElmoRegenerationMode; //
                SetElmoState(elmoState);
                //  Allow for torque request control of the throttle or allow the throttle command to be directly
                // sent to the servo
                switch(ICEThrottleMode)
                {
                        case DirectControl: // Pass the throttle setting
```

```
                // Set to pass the throttle command directly, read torque back to user

                        throttleSetting = GetThrottleRequest();
                        normalizedICETorque = throttleSetting + EMTakeoff;          // use to monitor output
                                                                                    without require excess
                                                                                    code
                        normalizedICETorque = SaturateICESignal(normalizedICETorque);       // Saturate the
                                                                                            signal

                break;

                case TorqueControl:    // Use the torque request strategy
                // Use the torque normalized to the maximum possible torque based on the torque maps

                        normalizedICETorque = GetTorqueRequest() / GetMaxICETorque() + EMTakeoff;
                        // Normalize torque request for throttle input
                        normalizedICETorque = SaturateICESignal(normalizedICETorque); // Saturate the signal

                break;
        }
                SetNormalizedICETorque(normalizedICETorque);
                SetNormalizedEMTorque(normalizedEMChargeTorque);
}
else // Not safe to charge
{
        elmoState = ElmoOff; //
        SetElmoState(elmoState);
        //  Allow for torque request control of the throttle or allow the throttle command to be directly
        // sent to the servo
        switch(ICEThrottleMode)
        {
                case DirectControl: // Pass the throttle setting
                // Set to pass the throttle command directly, read torque back to user

                        throttleSetting = GetThrottleRequest();
                        normalizedICETorque = throttleSetting;
                        // use to monitor output without require excess code
                        normalizedICETorque = SaturateICESignal(normalizedICETorque); // Saturate the signal

                break;

                case TorqueControl:    // Use the torque request strategy
                // Use the torque normalized to the maximum possible torque based on the torque maps

                        normalizedICETorque = GetTorqueRequest() / GetMaxICETorque();
                        // Normalize torque request for throttle input
                        normalizedICETorque = SaturateICESignal(normalizedICETorque); // Saturate the signal
```

```
                        break;
                }
                        SetNormalizedICETorque(normalizedICETorque);
        }

break;


case IDLE_PROP:
// Default propulsion state with the electric motor off and the engine in idle
// 5: Kill Switch On; ICE = F, EM = F, Dual = F, Start = F

        // ICE
        normalizedICETorque = IdleThrottle;
        SetNormalizedICETorque(normalizedICETorque);
        SetChoke(ChokeOpen);
        SetMagneto(ON); //(TRUE grounds the spark plug)

        // EM
        elmoState = ElmoOff;
        SetElmoState(elmoState);      // Turn the Elmo to the off/default state to prevent issues during system off
                                      operation

        // Turn off starter motor
        SetDigitalOutput(StarterMotorSwitchPort, StarterMotorSwitchPin, FALSE);

break;


case START_PROP:
// Allows for manual start of the motor TODO: Expand to allow use of the starter motor
// 6: Kill Switch On; ICE = T, EM = T, Dual = F, Start = F

        // ICE
        normalizedICETorque = StartICEThrottle;
        SetNormalizedICETorque(normalizedICETorque);
        SetChoke(ChokeOpen);
        SetMagneto(ON); //(TRUE grounds the spark plug)

        // EM
        elmoState = ElmoCurrentControlMode;
        SetElmoState(elmoState);      // Eliminate the mtor as a load during startup
        normalizedEMTorque = StartEMThrottle;
        SetNormalizedEMTorque(normalizedEMTorque);

        // Turn off starter motor
```

```
                SetDigitalOutput(StarterMotorSwitchPort, StarterMotorSwitchPin, TRUE);

        break;



        case CATAPULT_PROP:     //TODO: Program this state
        // State for a catapult style takeoff
        // 7: Not Implemented
                break;


        case TEST_PROP:
        // Used to do propulsion system testing in the event the controller is not available
        // 8:

                // ICE
                        normalizedICETorque = TestICEThrottle;
                        SetNormalizedICETorque(normalizedICETorque);
                        SetChoke(ChokeOpen);
                        SetMagneto(ON);

                        // EM
                        elmoState = TestElmo;
                        SetElmoState(elmoState);      // This may change to eliminate the motor as a load during startup
                        normalizedEMTorque = TestEMThrottle;
                        SetNormalizedEMTorque(normalizedEMTorque);

                        // Starter Motor
                        SetDigitalOutput(StarterMotorSwitchPort, StarterMotorSwitchPin, TestStaterMotor);

                break;
        }
}


void SetPropulsionState()
{
        //Read the State of the switches and set them to true and false

        if(!GetDigitalInput(RunKillSwitchPort, RunKillSwitchPin))
        {
                RunKillSwitch = FALSE;
        }
        else
        {
                RunKillSwitch = TRUE;
```

```
}

if(!GetDigitalInput(RunKillKestrelSwitchPort, RunKillKestrelSwitchPin))
{
	RunKillKestrelSwitch = FALSE;
}
else
{
	RunKillKestrelSwitch = TRUE;
}

if(!GetDigitalInput(ICEOnlySwitchPort, ICEOnlySwitchPin))
{
	ICEOnlyModeSwitch = FALSE;
}
else
{
	ICEOnlyModeSwitch = TRUE;
}

if(!GetDigitalInput(EMOnlySwitchPort, EMOnlySwitchPin))
{
	EMOnlyModeSwitch = FALSE;
}
else
{
	EMOnlyModeSwitch = TRUE;
}

if(!GetDigitalInput(DualModeSwitchPort, DualModeSwitchPin))
{
	DualModeSwitch = FALSE;
}
else
{
	DualModeSwitch = TRUE;
}

if(!GetDigitalInput(StartSwitchPort, StartSwitchPin))
{
	StartSwitch = FALSE;
}
else
{
	StartSwitch = TRUE;
}
```

```
	//Uses transmitter to manually control propulsion states
	//See header file for channel and switch listings
	if((RunKillSwitch == FALSE) || (RunKillKestrelSwitch == FALSE))
	{
		propulsionState = RESET_PROP;
	}
	else if((ICEOnlyModeSwitch == FALSE) && (EMOnlyModeSwitch == FALSE) && (DualModeSwitch == FALSE) && (StartSwitch == FALSE))
	{
		propulsionState = IDLE_PROP;
	}
	else if((ICEOnlyModeSwitch == FALSE) && (EMOnlyModeSwitch == FALSE) && (DualModeSwitch == FALSE) && (StartSwitch == TRUE))
	{
		propulsionState = START_PROP;
	}
	else if((ICEOnlyModeSwitch == TRUE)  && (EMOnlyModeSwitch == FALSE) && (DualModeSwitch == FALSE) && (StartSwitch == FALSE))
	{
		propulsionState = ICEONLY_PROP;
	}
	else if((ICEOnlyModeSwitch == FALSE) && (EMOnlyModeSwitch == TRUE) && (DualModeSwitch == FALSE) && (StartSwitch == FALSE))
	{
		propulsionState = EMONLY_PROP;
	}
	else if((ICEOnlyModeSwitch == TRUE) && (EMOnlyModeSwitch == TRUE) && (DualModeSwitch == TRUE) && (StartSwitch == FALSE))
	{
		propulsionState = ICEANDEM_PROP;
	}
	else if((ICEOnlyModeSwitch == TRUE) && (EMOnlyModeSwitch == TRUE) && (DualModeSwitch == FALSE) && (StartSwitch == FALSE))
	{
		propulsionState = ICEONLYGENERATION_PROP;
	}
	else if((ICEOnlyModeSwitch == FALSE) && (EMOnlyModeSwitch == FALSE) && (DualModeSwitch == TRUE) && (StartSwitch == TRUE))
	{
		propulsionState = TEST_PROP;
	}
	else
	{
		propulsionState = IDLE_PROP;
	}
}

void SetTestMode()
{
	propulsionState = TEST_PROP;
}
```

```
void ElmoInit()
{
	SetAnalogOutput(ElmoCurrentSpeedPort,0.00);
	SetDigitalOutput(RegenerationSwitchPort, RegenerationSwitchPin, TRUE);
	WaitUs(4100); // Ensure the Elmo has time to zero itself
}


void SetElmoState(int elmoState)
{
	double ZeroVoltage = 0.000;

	if((elmoState == ElmoOff) || (elmoState == ElmoCurrentControlMode))
	{
		SetDigitalOutput(CurrentControlSwitchPort, CurrentControlSwitchPin, TRUE);
		SetDigitalOutput(SpeedControlSwitchPort, SpeedControlSwitchPin, FALSE);
		SetDigitalOutput(PropellerOrientSwitchPort, PropellerOrientSwitchPin, FALSE);
		SetDigitalOutput(RegenerationSwitchPort, RegenerationSwitchPin, FALSE);
		if (elmoState == ElmoOff)
		{
			SetAnalogOutput(ElmoCurrentSpeedPort,ZeroVoltage);
			normalizedEMTorque = EMOFF;
			SetNormalizedEMTorque(normalizedEMTorque);
		}
	}
	else if(elmoState == ElmoSpeedControlMode)
	{
		SetDigitalOutput(CurrentControlSwitchPort, CurrentControlSwitchPin, FALSE);
		SetDigitalOutput(SpeedControlSwitchPort, SpeedControlSwitchPin, TRUE);
		SetDigitalOutput(PropellerOrientSwitchPort, PropellerOrientSwitchPin, FALSE);
		SetDigitalOutput(RegenerationSwitchPort, RegenerationSwitchPin, FALSE);
	}
	else if(elmoState == ElmoRegenerationMode)
	{
		SetDigitalOutput(CurrentControlSwitchPort, CurrentControlSwitchPin, TRUE);
		SetDigitalOutput(SpeedControlSwitchPort, SpeedControlSwitchPin, FALSE);
		SetDigitalOutput(PropellerOrientSwitchPort, PropellerOrientSwitchPin, FALSE);
		SetDigitalOutput(RegenerationSwitchPort, RegenerationSwitchPin, TRUE);
	}
	else if(elmoState == ElmoOrientPropMode)
	{
		SetDigitalOutput(CurrentControlSwitchPort, CurrentControlSwitchPin, FALSE);
		SetDigitalOutput(SpeedControlSwitchPort, SpeedControlSwitchPin, FALSE);
		SetDigitalOutput(PropellerOrientSwitchPort, PropellerOrientSwitchPin, TRUE);
		SetDigitalOutput(RegenerationSwitchPort, RegenerationSwitchPin, FALSE);
	}
}
```

```
void ScreenInit()
{
	WriteScreenString("PSTAT",0,0);
	WriteScreenString("ELMDE",10,0);
	WriteScreenString("ICTMD",0,1);
	WriteScreenString("EMTMD",10,1);
	WriteScreenString("NRMIC",0,2);
	WriteScreenString("NRMEM",10,2);
	WriteScreenString("IRPM",0,3);
	WriteScreenString("ERPM",10,3);
}


void ScreenUpdate()
{
	// LCD
	WriteScreenString("  ", propulsionStateX, propulsionStateY);
	WriteScreenInteger(propulsionState, propulsionStateX, propulsionStateY);
	WriteScreenInteger(elmoState, elmoModeX, elmoModeY);
	WriteScreenInteger(ICEThrottleMode, ICEThrottleModeX, ICEThrottleModeY);
	WriteScreenInteger(EMThrottleMode, EMThrottleModeX, EMThrottleModeY);
	WriteScreenString("   ", normalizedICETorqueX, normalizedICETorqueY);
	WriteScreenFloat(normalizedICETorque*100, 0, normalizedICETorqueX, normalizedICETorqueY);
	WriteScreenString("   ", normalizedEmTorqueX, normalizedEMTorqueY);
	WriteScreenFloat(normalizedEMTorque*100, 0, normalizedEmTorqueX, normalizedEMTorqueY);
	WriteScreenFloat(GetGenericRPM(ICESpeedPort, ICECountsPerRev) , 0, ICESpeedX, ICESpeedY);
	WriteScreenFloat(GetGenericRPM(EMSpeedPort, EMCountsPerRev) , 0, EMSpeedX, EMSpeedY);

	// Shared Custom Memory
	SetSharedCustomMemoryInteger(SCMPropulsionState, propulsionState);
	SetSharedCustomMemoryInteger(SCMElmoState,elmoState);
	SetSharedCustomMemoryInteger(SCMICEThrottleMode, ICEThrottleMode);
	SetSharedCustomMemoryInteger(SCMEMThrottleMode, EMThrottleMode);
	SetSharedCustomMemoryFloat(SCMNormalizedICETorque, normalizedICETorque);
	SetSharedCustomMemoryFloat(SCMNormalizedEMTorque, normalizedEMTorque);
	SetSharedCustomMemoryFloat(SCMICESpeed, GetGenericRPM(ICESpeedPort, ICECountsPerRev));
	SetSharedCustomMemoryFloat(SCMEMSpeed, GetGenericRPM(EMSpeedPort, EMCountsPerRev));
	SetSharedCustomMemoryFloat(SCMBatteryVoltage, GetBatteryVoltage(BatteryVoltagePort));
}


/***** PUBLIC FUNCTIONS *************************************************/

/***** PRIVATE FUNCTIONS ************************************************/
```

```
double GetTorqueRequest()
{
	double throttleSetting = GetThrottleRequest();		// Will return 0-1.0
	double totalTorque = GetTotalAvailableTorque();
	return throttleSetting * totalTorque;
}


double GetMaxICETorque()
{
	int currentICERPM = GetGenericRPM(ICESpeedPort, ICECountsPerRev);
	return InterpolateVector1D(ICEMapYValues, ICEMapLength, ICEMapXStart, ICEMapXStep, currentICERPM);
}


double GetICEIOLTorque()
{
	int currentICERPM = GetGenericRPM(ICESpeedPort, ICECountsPerRev);
	return InterpolateVector1D(IOLMapYValues, IOLMapLength, IOLMapXStart, IOLMapXStep, currentICERPM);
}


double GetMaxEMTorque()
{
	return MaxEMTorque;
}


double GetTotalAvailableTorque()
{
	return GetMaxEMTorque() + GetMaxICETorque();
}


double GetThrottleRequest()
{
	if (InvertThrottle == TRUE)
	{
		return 1 - GetRCDutyCycle(AutopilotThrottle); // inverts the signal
	}
	else
	{
		return GetRCDutyCycle(AutopilotThrottle);
	}
}
```

```
void SetNormalizedICETorque(double normalizedTorque)
{
	double servoSetting;

	if (InvertICEServo == TRUE)
	{
		servoSetting = 1 - normalizedTorque;
	}
	else
	{
		servoSetting = normalizedTorque;
	}

	SetPWMDutyCycle(ICEThrottleServo, servoSetting);
}


void SetNormalizedEMTorque(double normalizedTorque)
{
	double servoSetting;
	double MaxVoltage = 4.096;
	double torqueSetting = MaxVoltage * normalizedTorque;
	SetAnalogOutput(ElmoCurrentSpeedPort,torqueSetting);
	if (InvertEMServo == TRUE)    // This is the signal output for the EM read by the seagull or for use with the Castle
Creations Controller
	{
		servoSetting = 1 - normalizedTorque;
	}
	else
	{
		servoSetting = normalizedTorque;
	}
	SetPWMDutyCycle(EMThrottleSignal,(servoSetting));           // Requires an inversion to work with Castle Creations
Controller
}


void SetChoke(char setHigh)
{
	if (setHigh == ChokeOpen) // Choke is open
	{
		SetPWMDutyCycle(ICEChokeServo, 0.0);
	}
	else if (setHigh == ChokeClosed)
	{
		SetPWMDutyCycle(ICEChokeServo, 1.0);
	}
```

```
}

void SetMagneto(char setHigh)
{
        if (setHigh == ON)
        {
                SetDigitalOutput(MagnetoControlPort, MagnetoControlPin, FALSE); //(TRUE grounds the spark plug)
        }
        else if (setHigh == OFF)
        {
                SetDigitalOutput(MagnetoControlPort, MagnetoControlPin, TRUE); //(TRUE grounds the spark plug)
        }
}

double GetBatteryVoltage(unsigned char BatteryPort)  // Voltage divider: 10k high, 1k low giving a 11:1 voltage to signal ratio
{
        char i;
        double rawVoltage;
        double batteryVoltage = 0;
        for(i = 0; i<10; i++)
        {
                rawVoltage = GetAnalogInput(BatteryPort);
                batteryVoltage = batteryVoltage + rawVoltage*11;
        }
        return batteryVoltage/10;
}

double SaturateICESignal(double normalizedTorque)
{
        // Saturate signal 0.0 - 1.0
        if(normalizedTorque >= 1.0)
        {
                normalizedTorque = 1.0;
        }
        else if(normalizedTorque <= IdleThrottle)
        {
                normalizedTorque = IdleThrottle;
        }
        else if(normalizedICETorque < 1.0 && normalizedTorque > 0.95)
        {
                normalizedTorque = 0.95;
        }
        else if(normalizedTorque < 0.95 && normalizedTorque > 0.90)
        {
```

```
		normalizedTorque = 0.9;
	}
	else if (normalizedTorque < 0.9 && normalizedTorque > 0.85)
	{
		normalizedTorque = 0.85;
	}
	else if(normalizedTorque < 0.85 && normalizedTorque > 0.8)
	{
		normalizedTorque = 0.8;
	}
	else if(normalizedTorque < 0.8 && normalizedTorque > 0.75)
	{
		normalizedTorque = 0.75;
	}
	else if(normalizedTorque < 0.75 && normalizedTorque > 0.7)
	{
		normalizedTorque = 0.7;
	}
	else if(normalizedTorque < 0.7 && normalizedTorque > 0.68)
	{
		normalizedTorque = 0.68;
	}
	else if(normalizedTorque < 0.68 && normalizedTorque >= 0.65)
	{
		normalizedICETorque = 0.65;
	}
	else if(normalizedTorque < 0.65 && normalizedTorque > 0.6)
	{
		normalizedICETorque = 0.6;
	}
	else if(normalizedTorque < 0.6 && normalizedTorque > 0.55)
	{
		normalizedICETorque = 0.55;
	}
	else if(normalizedTorque < 0.55 && normalizedTorque > 0.53)
	{
		normalizedTorque = 0.53;
	}
	else if(normalizedTorque < 0.53 && normalizedTorque >= 0.5)
	{
		normalizedTorque = 0.5;
	}
	else if(normalizedTorque < 0.5 && normalizedTorque > 0.45)
	{
		normalizedTorque = 0.45;
	}
	else if(normalizedTorque < 0.45 && normalizedTorque > 0.42)
```

```
        {
                normalizedTorque = 0.42;
        }
        else if(normalizedTorque < 0.42 && normalizedTorque >= 0.4)
        {
                normalizedTorque = 0.4;
        }
        else if(normalizedTorque < 0.4 && normalizedTorque > 0.35)
        {
                normalizedTorque = 0.35;
        }
        else if(normalizedTorque < 0.35 && normalizedTorque > 0.3)
        {
                normalizedTorque = 0.3;
        }
        else if(normalizedTorque < 0.3 && normalizedTorque >= 0.25)
        {
                normalizedTorque = 0.25;
        }
        else if(normalizedTorque < 0.25 && normalizedTorque >= 0.20)
        {
                normalizedTorque = 0.20;
        }
        else if(normalizedTorque < 0.2 && normalizedTorque >= 0.15)
        {
                normalizedTorque = 0.15;
        }
        else if(normalizedTorque < 0.15 && normalizedTorque >= 0.10)
        {
                normalizedTorque = 0.10;
        }
        else if(normalizedTorque < 0.10 && normalizedTorque >= 0.05)
        {
                normalizedTorque = 0.05;
        }
        else if(normalizedTorque < 0.05 && normalizedTorque >= 0.0)
        {
                normalizedTorque = 0.0;
        }
        else if(normalizedTorque <= 0.0)
        {
                normalizedTorque = 0.0;
        }
        return normalizedTorque;
}
```

```
double SaturateEMSignal(double normalizedTorque)
{
	// Saturate signal 0.0 - 1.0
	if(normalizedTorque >= 1.0)
	{
		normalizedTorque = 1.0;
	}
	else if(normalizedICETorque < 1.0 && normalizedTorque > 0.95)
	{
		normalizedTorque = 0.95;
	}
	else if(normalizedTorque < 0.95 && normalizedTorque > 0.90)
	{
		normalizedTorque = 0.9;
	}
	else if (normalizedTorque < 0.9 && normalizedTorque > 0.85)
	{
		normalizedTorque = 0.85;
	}
	else if(normalizedTorque < 0.85 && normalizedTorque > 0.8)
	{
		normalizedTorque = 0.8;
	}
	else if(normalizedTorque < 0.8 && normalizedTorque > 0.75)
	{
		normalizedTorque = 0.75;
	}
	else if(normalizedTorque < 0.75 && normalizedTorque > 0.7)
	{
		normalizedTorque = 0.7;
	}
	else if(normalizedTorque < 0.7 && normalizedTorque > 0.68)
	{
		normalizedTorque = 0.68;
	}
	else if(normalizedTorque < 0.68 && normalizedTorque >= 0.65)
	{
		normalizedICETorque = 0.65;
	}
	else if(normalizedTorque < 0.65 && normalizedTorque > 0.6)
	{
		normalizedICETorque = 0.6;
	}
	else if(normalizedTorque < 0.6 && normalizedTorque > 0.55)
	{
		normalizedICETorque = 0.55;
	}
```

```
else if(normalizedTorque < 0.55 && normalizedTorque > 0.53)
{
        normalizedTorque = 0.53;
}
else if(normalizedTorque < 0.53 && normalizedTorque >= 0.5)
{
        normalizedTorque = 0.5;
}
else if(normalizedTorque < 0.5 && normalizedTorque > 0.45)
{
        normalizedTorque = 0.45;
}
else if(normalizedTorque < 0.45 && normalizedTorque > 0.42)
{
        normalizedTorque = 0.42;
}
else if(normalizedTorque < 0.42 && normalizedTorque >= 0.4)
{
        normalizedTorque = 0.4;
}
else if(normalizedTorque < 0.4 && normalizedTorque > 0.35)
{
        normalizedTorque = 0.35;
}
else if(normalizedTorque < 0.35 && normalizedTorque > 0.3)
{
        normalizedTorque = 0.3;
}
else if(normalizedTorque < 0.3 && normalizedTorque >= 0.25)
{
        normalizedTorque = 0.25;
}
else if(normalizedTorque < 0.25 && normalizedTorque >= 0.20)
{
        normalizedTorque = 0.20;
}
else if(normalizedTorque < 0.2 && normalizedTorque >= 0.15)
{
        normalizedTorque = 0.15;
}
else if(normalizedTorque < 0.15 && normalizedTorque >= 0.10)
{
        normalizedTorque = 0.10;
}
else if(normalizedTorque < 0.10 && normalizedTorque >= 0.05)
{
        normalizedTorque = 0.00;
```

```
        }
        else if(normalizedTorque < 0.05 && normalizedTorque >= 0.0)
        {
                normalizedTorque = 0.0;
        }
        else if(normalizedTorque <= 0.0)
        {
                normalizedTorque = 0.0;
        }
        return normalizedTorque;
}
```

Appendix H. Propulsion State Signal Combinations

Table H–1 lists the operating mode signal combinations implemented on the PIC32. The PWM signals are for a two line slider setup, the digital signals are for a four line binary setup. The PWM column gives the duty cycle range that will trigger the combination. Note that the PIC32 also has a kill switch that will kill both the ICE and EM. The switch is listed in the header file, but not in Table H–1.

Table H–1: Digital and PWM signal combinations for PIC32 Lightning

	Digital Combination				**PWM Combination**	
Signal ID	ICE	EM	Dual	Start	PWM 1	PWM 2
PIC32 Pin	DIOPIN2	DIOPIN3	DIOPIN4	DIOPIN5	INT3	INT4
Mode						
Idle	OFF	OFF	OFF	OFF	0-55%	0-55%
ICE-only	ON	OFF	OFF	OFF	55-72%	0-55%
EM-only	OFF	ON	OFF	OFF	0-55%	55-72%
Dual	ON	ON	ON	OFF	55-72%	55-72%
Regen	ON	ON	OFF	OFF	55-72%	72-100%
Start	OFF	OFF	OFF	ON	72-100%	0-55%
Test	OFF	OFF	ON	ON	72-100%	72-100%

Appendix I. Throttle Redirect Code: Procerus Kestrel Autopilot

This appendix contains a sample of the code used in Virtual Cockpit to implement propulsion system control on the Kestrel. The sample code shows the packet intercept to split the throttle between the ICE and EM based on flight mode. It also shows the code used for capturing the throttle signal from the telemetry downlink stream. These two code sections must be added to the Procerus Kestrel code in the correct locations with the correct variable declarations to function properly. Please contact a member of the Condor team for more information on using this sample code.

1. Throttle Capture Code

```
//Throttle
                       unsigned char TempUChar;
                       float rawThrottle;
                       memcpy(&TempUChar, &NewPkt->PktData[39],1);
                       rawThrottle = (TempUChar);
```

2. Mode And Throttle Splitting Code

```
//Throttle Command sent via Gimbal Command Packet

        sVCPacket GimbalPkt;
        CString EditStr;

        GimbalPkt.VCPacketType = VC_GIMBAL_CMD;
        GimbalPkt.DataSize = sizeof(sGimbalPacket);

        //Fill up the data
        sGimbalPacket GimbalCmd;
        GimbalCmd.DestAddr = m_UAVAddress;
        GimbalCmd.GimbalMode = 0; //GIMBAL MODE JOY MSL

///////////////////////
//Mode Selection Code//
///////////////////////
        int regen;

        //Determine Hybrid Mode Selection
        if(((CButton*)GetDlgItem(IDC_IDLE))->GetCheck())
        {
        GimbalCmd.GimbalAzm = 0.4f;  //set idle to 20% throttle
        GimbalCmd.GimbalElev = 0.0f; //set servo position to off in radians
        regen = 0;
        }

        else if(((CButton*)GetDlgItem(IDC_ICE))->GetCheck())
        {
        GimbalCmd.GimbalAzm = rawThrottle/63.7f;  //convert throttle signal in % to
radians for servo
        GimbalCmd.GimbalElev = 0.0f; //set servo position to off in radians;
        regen = 0;
        }
```

```
        else if(((CButton*)GetDlgItem(IDC_EM))->GetCheck())
        {
        GimbalCmd.GimbalAzm = 0.0f;  //set servo position to off in radians
        GimbalCmd.GimbalElev = (rawThrottle * 0.9f) / 63.7f; //convert throttle signal (0-
100%) to 0-80% to limit PWM output to 4V instead of 5V
        regen = 0;
        }

//Boost Mode::ICE driver, Constant EM//
        else if(((CButton*)GetDlgItem(IDC_BOOST))->GetCheck())
        {
        GetDlgItem(IDC_IDEAL)->GetWindowText(EditStr);
        float IdealPower = (float)atof(EditStr);
        GimbalCmd.GimbalElev = (IdealPower * 0.90f) / 63.7f;  //Constant EM-convert
throttle signal in % to radians for servo
        GimbalCmd.GimbalAzm = rawThrottle / 63.7f;  //convert throttle signal in % to
radians for servo
        //GimbalCmd.GimbalElev = 0.785f; //set servo position to 50% in radian for EM
        regen = 0;
        }

//Boost Mode::EM driver, Constant ICE//
        else if(((CButton*)GetDlgItem(IDC_BOOST2))->GetCheck())
        {
        GetDlgItem(IDC_IDEAL)->GetWindowText(EditStr);
        float IdealPower = (float)atof(EditStr);
        GimbalCmd.GimbalAzm = IdealPower / 63.7f;  //Constant ICE-convert throttle signal
in % to radians for servo
        //GimbalCmd.GimbalAzm = 0.628f;  //set servo position to 40% in radian for ICE
        GimbalCmd.GimbalElev = (rawThrottle * 0.90f) / 63.7f; //convert throttle signal
(0-100%) to 0-80% to limit PWM output to 4V instead of 5V
        regen = 0;
        }

        else if(((CButton*)GetDlgItem(IDC_REGEN))->GetCheck())
        {
        GimbalCmd.GimbalAzm = (rawThrottle / 63.7f) * 1.1f;  //Add 10% to throttle signal
        GimbalCmd.GimbalElev = 0.251f; //set servo position to 16% in radians
        regen = 1;
        }

                else // Ensure Idle Mode if default fails
                {
        GimbalCmd.GimbalAzm = 0.4f;  //set idle to 20% throttle
        GimbalCmd.GimbalElev = 0.0f; //set servo position to off in radians
        regen = 0;
        }

        GimbalCmd.TrgtLat = 40.0f;
        GimbalCmd.TrgtLong = 40.0f;
        GimbalCmd.TrgtElev = 40.0f;

    //Now that we have our structs filled copy the structs to the VC packet that will be
sent
        memcpy(GimbalPkt.PktData, &GimbalCmd, sizeof(sGimbalPacket));

        //Finally send the packet
        m_VCConnector->SendData(&GimbalPkt);
```

Appendix J. Aircraft Mass Breakdown

Table J–1: Hybrid electric Condor weight breakdown for 15.9 kg (35 lb) configuration

Hybrid Aircraft:	**15876**	**Propulsion System**	**3969**	**Electric System**	**572**
Propulsion System	***3969***	***Electric System***	***572***	AXI 4130/20	409
Airframe	***7788***	***Combustion System***	***2381***	Motor encoder (& IC/screws)	44
Avionics	***1262***	***ICE Pulley and Flange***	***315***	Motor mount plate (no bolts)	35
Batteries	**2388**	EM Pulley	90	Motor mount bracket (no bolts)	84
Fuel	**468**	Propeller (& bolt)	167	Other (bolts, etc):	0
Payload	1	Propeller extender (& bolts)	68		
		Belt	18	**Combustion System**	**2381**
		Other (bolts, etc):	349	Honda GX25 (stripped, w/oil)	2086
Mass without payload	15875			Carburetor	120
		Airframe	**7788**	ICE servo	40
		Wings (x2, w/servos, wires)	2724	ICE servo mount	35
		Empennage (surfaces, servos)	627	Pull starter	100
		Rear fuselage (with tail gear)	1033	Other (bolts, etc):	0
		Forward fuselage (w/ fuel tank)	1437		
		Center wing sections	1538	**ICE Pulley and Flange**	**315**
		Gear	429	ICE pulley	
		Other (pins, etc)	0	ICE flange	
				One-way bearing	9

Avionics	**1262**	Thrust bearing (rear)	9
Kestrel Assembly	***422***	Thrust bearing (forward)	9
Instrumentation	***50***	Other (bolts, etc):	16
Solo whistle controller	84		
PWM to Analog Board	21	**Kestrel Assembly**	**422**
Battleswitches (x5)	105	Kestrel autopilot	34
Mounting boards	134	Kestrel battery	192
Power busses (x2)	90	Kestrel breakout board	67
Inductor assembly	277	Mounting board	78
Wiring	65	Transmitter and reciever	51
Emergency receiver	14	Other (wires, etc)	0
Batteries (input #)	**2388**	**Instrumentation**	**50**
6	2388	Seagull Unit	23
* 2 packs per set		RPM sensor	6
		Current/voltage sensor	6
Fuel (input oz)	**467.6**	Transmitter	15
22	467.6		
(719.7 kg/m^3) - Gasoline			
(60 oz = full tank)			
For all items where there are multiples, the shown mass is the total for all such items on the aircraft.			

Table J–2: Engine only Condor weight breakdown for 15.9 kg (35 lb) configuration

ICE Only Aircraft	**15876**	**Propulsion System**	**2903**	**Combustion System**	**2668**
Propulsion System	***2903***	***Combustion System***	***2668***	Honda GX35 (stripped, w/oil)	2373
Airframe	***7788***	Propeller (& bolt)	167	Carburetor	120
Avionics	***422***	Propeller extender (& bolts)	68	ICE servo	40
Fuel	***1275***	Other (bolts, etc):	0	ICE servo mount	35
Payload	3488			Pull starter	100
		Airframe	**7788**	Other (bolts, etc):	0
		Wings (x2, w/servos, wires)	2724		
		Empennage (surfaces, servos)	627	**Kestrel Assembly**	**422**
Mass without payload	12388	Rear fuselage (with tail gear)	1033	Kestrel autopilot	34
		Forward fuselage (w/ fuel tank)	1437	Kestrel battery	192
		Center wing sections	1538	Kestrel breakout board	67
		Gear	429	Mounting board	78
		Other (pins, etc)	0	Transmitter and reciever	51
				Other (wires, etc)	0
		Avionics	**422**		
		Kestrel Assembly	422		
		Wiring (best guess)	30		
		Fuel (input oz)	**1275**		
		60	1275.27		
		(719.7 kg/m^3) - Gasoline			
		(60 oz = full tank)			

Appendix K. Hybrid System Startup Procedure

1) Connect fuel lines.
2) Connect power to Kestrel autopilot.
3) Safety the magneto and Solo Whistle controller using kill switches.
4) Connect all EM battery packs. Connect two packs at a time. Keep all male ends from power bus covered until you are ready to connect a battery to them. If two male ends touch after the first set of batteries is connected, there will be a fire.
5) Set Solo Whistle to initialization mode using the two way switch.
6) Set Virtual Cockpit to EM only mode, zero throttle.
7) Toggle the EM kill switch to power on the Solo Whistle controller.
8) Use the two way switch on the aircraft to switch the Solo Whistle controller from initialize mode to run mode. The EM should twitch.
9) Adjust the throttle to ensure the EM will spin up and the Solo Whistle commutated. If the EM does not move even at 100% throttle, the Solo Whistle probably did not commutate. Kill the EM using the kill switch and return to Step 5. (If you have trouble commutating, make sure the ICE is at a point in its rotation where it provides relatively little resistance against the EM.)
10) Return to ICE only mode in Virtual Cockpit. Set throttle to 40-50% for ICE start.
11) Prime the engine with 3 full squirts of fuel from the primer bulb.
12) Close the choke.
13) Attempt two pulls on the engine. If it does not start, open the choke half way and try two more pulls. The engine should start. If not, repeat step 13) until it starts.
14) Switch the ICE to idle.
15) Proceed with operation.

Appendix L. Bench, Ground, and Flight Test Plan

Bench, Ground, and Flight Test Plan

Unless otherwise noted, the following information applies to all tests.

1) All testing will use the 18x10 Propeller.
2) The tested system will include all parts intended for use in flight tests, assembled in the same manner as during flight test.
3) The system must remain intact throughout the test for the test to be considered successful. Failure of the system or any component is considered a test failure and the test must be repeated if it is on the critical path.
4) For all tests, a portable handheld weather station will be used to record atmospheric conditions including: temperature, humidity, wind speed (if outside), and barometric pressure.

Instrumentation:

1) An Eagle Tree Systems Seagull Flight Telemetry system will be used to monitor system voltage, current, and speed. Information will download on a 2.4 GHz channel to a handheld flight data recorder or laptop.
2) The Kestrel will be used to monitor the system throttle settings and aircraft flight telemetry data. The information will downlink into Virtual Cockpit.
3) Ambient weather conditions will be monitored using a portable handheld weather station.

Bench Testing:

For all bench testing, the propulsion system will be mounted to the aircraft, secured inside the test stand in the laboratory. Each test may be run separately or in tandem with the previous test.

Safety:

1) All fumes will be vented using the test stand exhaust.
2) Propeller shield must remain closed at all times, except when starting the ICE manually
3) All emergency kill switches will be in place (emergency kill switches are listed at the end of the document).

Prerequisites: none

Tests:

Table L–1: Condor bench test plan

Bench Testing						
Tag	**Name**	**Description**	**Success Criteria**	**Collected data**	**Depends on**	**Critical path**
BT1	ICE Only	ICE is started in ICE only mode. EM is not powered. ICE is stepped through full throttle range in 10% increments, holding for 30 seconds at each step.	1) ICE completes test at each increment	1) Throttle Fuel flow 2) Engine speed	none	Yes
BT2	EM Only	EM is started in EM only mode. ICE is turned off. EM is stepped through full throttle range in 10% increments, holding for 30 seconds at each step.	1) EM completes test at each increment	1) Throttle Pack voltage 2) Solo Whistle current draw 3) Motor speed	none	Yes

BT3	ICE Only to EM Only Transition	ICE is operating 10-20% above idle. EM is off, but initialized. Propulsion system is switched to EM only mode, with the EM running at 20-30% throttle, and the ICE reduced to idle.	1) ICE power backs off to idle without stalling the ICE 2) EM successfully engages	1) Throttle	BT1, BT2	Yes
BT4	EM Only to ICE Only Transition	EM is operating at 20-30% throttle. ICE is at idle. Propulsion system is switched to ICE only mode, with the ICE running 10-20% above idle and the EM off.	1) EM turns off (measured as current to Solo Whistle) 2) ICE successfully powers up from idle	1) Throttle	BT1, BT2	Yes
BT5.1	Dual Mode from ICE only	ICE is operating at fixed throttle setting (30%-50%). EM is initially off. EM power is adjusted from 0% to 100% in 10% increments, holding for 30 seconds at each step. (This test demonstrates dual mode where the EM provides boost power)	1) EM increases system speed at each setting. 2) EM and ICE both function for entire test.	1) Throttle 2) Fuel flow 3) Engine speed 4) Pack voltage 5) Solo Whistle current draw	BT1, BT2	Yes
BT5.2	Dual Mode from EM only	EM is operating at fixed throttle setting (30%-50%). ICE is initially at idle. ICE power is adjusted from 0-50% in 10% increments, holding for 30 seconds at each step. (This test demonstrates dual mode where ICE provides boost power. It is unlikely we will use this mode.)	1) ICE increases system speed at each setting. 2) EM and ICE both function for entire test.	1) ThrottleFuel flow 2) Engine speed 3) Pack voltage 4) Solo Whistle current draw	BT1, BT2	Yes

BT6	Dual mode crossover test	The ICE and EM are operating in Dual mode with both the ICE and EM at 20%. Throttle control is directed to the ICE. The ICE power is varied by ±10% to verify throttle control of ICE. The EM power set point is switched from 20% to 10% and back to verify EM set point function. The Dual mode is then switched to a set ICE and throttle control of the EM. The EM is varied by ±10% to verify throttle control. The ICE set point is altered by 10% to verify set point control	1) Throttle and set point controls work on ICE and EM as expected in both modes	1) Throttle 2) Fuel flow 3) Engine speed 4) Pack voltage 5) Solo Whistle current draw	BT1, BT2, BT5.1, BT5.2	Yes
BT7	ICE Emergency kill	ICE is operating at any throttle above idle. ICE kill switch is activated.	1) ICE stops. 2) EM still functions after ICE stops.	None	BT1, BT2	Yes
BT8	EM Emergency kill	EM is operating at any throttle setting. ICE is at idle. EM kill switch is activated.	3) EM turns off (measured as current to Solo Whistle) 1) ICE is still idling after EM turns off.	None	BT1, BT2	Yes
BT9	ICE crossover test	ICE is receiving throttle signal from the redirected gimbaled camera line at 30-40% throttle. ICE crossover switch is activated and ICE receives throttle directly from Kestrel, preferably at 30%-40%.	1) ICE continues to operate.	None	BT1	Yes
BT10	Regen test	ICE is operating at 40%-50% power. EM is initially off. Battery packs are at least 2 V under full charge. Propulsion system is switched to regeneration mode, until battery pack voltage increases by 0.5 V.	1) Battery pack voltage increases.	1) Throttle Fuel flow 2) Engine speed 3) Pack voltage 4) Solo Whistle current draw	BT1, BT2, BT5	No

Ground Testing:

For all ground testing, the propulsion system will be mounted to the aircraft, without wings (mid section only). Testing will take place outdoors on an asphalt or concrete surface.

Safety:

1) Operator starting the aircraft will remain behind the plane of the propeller at all times.
2) Wings will not be attached to the airframe so there is no possibility of the airframe taking flight.
3) All observers and testers will remain clear of the aircraft velocity vector except when absolutely not possible.

Prerequisites: All Phase 1 tests require the successful completion of the Critical Path Bench Tests. All Phase 2 tests require the successful completion of all Phase 1 Critical Path Ground Tests.

Tests:

Ground Test Phase 1: Ground Test Phase 1 checks all of the emergency procedures for the propulsion system. This phase will be performed statically, with the aircraft held in place from behind the wing by an operator.

Table L–2: Condor ground test plan, phase 1

Ground Testing Phase 1: Emergency Tests						
Tag	**Name**	**Description**	**Success Criteria**	**Collected data**	**Depends on**	**Critical path**
GT1ET1	ICE Kill Check	Aircraft is operating in ICE only mode. EM kill switch is activated.	1) ICE is stopped.	none	BT Critical Path	Yes
GT1ET2	EM Kill Check	Aircraft is operating in EM only mode. ICE is at idle. EM kill switch is activated.	1) EM is stopped (verify with current draw).	1) Solo Whistle current draw	BT Critical Path	Yes
GT1ET3	ICE Crossover Check	1) Aircraft is in ICE only mode. EM is off, but initialized. 2) ICE is switched from Gimbaled camera redirect signal to direct Kestrel input.	1) Throttle control transitions successfully.	1) Throttle	BT Critical Path	Yes

Ground Test Phase 2: Ground Test Phase 2 simulates the different flight tests. During each specified lap, the aircraft will travel in a racetrack like path with at least 50 m straight-aways.

Table L–3: Condor ground test plan, phase 2

Ground Testing Phase 2: Simulated Flight Tests						
Tag	**Name**	**Description**	**Success Criteria**	**Collected data**	**Depends on**	**Critical path**
GT2SF1.1	Mode Checkout	1) Aircraft begins in ICE only mode with the EM initialized, but turned off. 2) In ICE only mode the aircraft completes 4 laps. 3) Aircraft is switched to EM only mode, ICE is reduced to idle. 4) In EM only mode the aircraft completes 4 laps. 5) Aircraft is switched to dual mode with ICE 10%-20% above idle setting. 6) In dual mode aircraft completes 4 laps using only the EM for throttle control. 7) Aircraft returns to ICE Only for 1 lap to simulate approach and landing. (This test simulates the mode checkout flight test)	1) Aircraft completes mission	1) Throttle 2) Engine speed 3) Pack voltage 4) Solo Whistle current draw	BT&GT1 Critical Paths	Yes

GT2SF1.2	Takeoff contingency operations	1) Aircraft begins in Dual mode with throttle control of the ICE and an EM set point. The EM is set to 20%. 2) Aircraft completes 1 lap using the ICE for throttle control. 3) Dual mode switches to an ICE set point 10% less than that used in GT2SF1.1, step 2. EM receives direct throttle control 4) Aircraft completes 4 laps using EM for throttle control. (This mode simulates using ICE boost power for takeoff and EM boost power in flight for cruise.)	1) Aircraft completes mission	1) Throttle 2) Engine speed 3) Pack voltage 4) Solo Whistle current draw	BT&GT1 Critical Paths. GT2SF1.1	Yes
GT2SF2	Cruise fuel burn	1) Aircraft is weighed prior to startup. 2) Aircraft begins in ICE only mode with the EM initialized, but turned off. 3) In ICE only mode the aircraft completes laps for 10 minutes. 4) Aircraft is shut down and weighed again to compute fuel burn. (This test simulates the flight test to estimate the cruise fuel burn of the aircraft)	1) Aircraft completes mission	1) Throttle 2) Engine speed 3) Pack voltage 4) Solo Whistle current draw 5) Initial and final aircraft weight	BT&GT1 Critical Paths	Yes

GT2SF3	Endurance power consumption	1) Aircraft begins in EM only mode with the ICE at idle. 2) In EM only mode, aircraft completes laps for 10 minutes.	1) Aircraft completes mission	1) Throttle 2) Engine speed 3) Pack voltage 4) Solo Whistle current draw	BT&GT1 Critical Paths	Yes
GT2SF4	Regen	ICE is operating at 40%-50% power. EM is initially off. Battery packs are at least 2 V under full charge. Propulsion system is switched to regeneration mode, until battery pack voltage increases by 0.5 V. Aircraft completes laps during recharge period.	1) Battery pack voltage increases.	1) Throttle 2) Engine speed 3) Pack voltage 4) Solo Whistle current draw	BT&GT1 Critical Paths, BT10	No
GT2SF5	ICE kill for Silent EM	1) Aircraft is operating in ICE only mode. 2) Aircraft performs 4 laps. 3) Aircraft switches to EM only mode. 4) ICE Kill switch is activated. 5) Aircraft performs 2 laps under EM only power.	1) Aircraft successfully completes test.	1) Throttle 2) Engine speed 3) Pack voltage 4) Solo Whistle current draw	BT&GT1 Critical Paths	No

Flight Testing:

For all flight testing, the propulsion system will be mounted to the aircraft. Each test will begin with aircraft using ICE only mode for takeoff. If ICE power is not sufficient for takeoff, then dual mode will be used.

Safety:

1) Operator starting the aircraft will remain behind the plane of the propeller at all times.
2) All observers and testers will remain clear of the aircraft velocity vector except when absolutely not possible.
3) All loss of communication protocol and emergency kill switches will be implemented.

Prerequisites: All flight tests require the successful completion of the Critical Path Bench Tests and Critical Path Ground Tests.

Tests:

Flight Test: During each specified lap, the aircraft will travel in a racetrack like orbit designed to keep the aircraft in visual and communications range over the airstrip.

Table L–4: Condor flight test plan

Flight Tests						
Tag	**Name**	**Description**	**Success Criteria**	**Collected data**	**Depends on**	**Critical path**
FT1	Mode Checkout	1) Aircraft uses ICE or Dual mode to achieve flight under manual control. 2) Aircraft switches ICE only mode with the EM initialized, but turned off. 3) In ICE only mode the aircraft completes 4 laps under manual control. 4) Aircraft is switched to EM only mode, ICE is reduced to idle. 5) In EM only mode the aircraft completes 4 laps under manual control. 6) Aircraft is switched to dual mode with ICE 10% less than required power during step 3. 7) In dual mode, aircraft completes 4 laps using only the EM for throttle control; the throttle is under manual control.	1) Aircraft completes mission	1) Throttle setting 2) Engine speed 3) Pack voltage 4) Solo Whistle current draw	BT&GT Critical Paths	Yes
FT2	Cruise fuel burn	1) Aircraft is weighed prior to startup. 2) Aircraft uses ICE or Dual mode to achieve flight under manual control. 3) Aircraft switches to ICE only mode with the EM initialized, but turned off. 4) In ICE only mode, the aircraft completes laps for 10 minutes at ideal cruise velocity from simulation. Autopilot control is preferred to maintain velocity. 5) Aircraft, lands, is shut down and weighed again to compute fuel burn. (This test simulates the flight test to estimate the cruise fuel burn of the aircraft)	1) Aircraft completes mission	1) Throttle setting 2) Engine speed 3) Pack voltage 4) Solo Whistle current draw 5) Initial and final aircraft weight	BT&GT Critical Paths	Yes

FT3	Endurance power consumption	1) Aircraft uses ICE or Dual mode to achieve flight under manual control. 2) Aircraft is switched to EM only mode with ICE throttled to idle. 3) In EM only mode, aircraft completes laps for 10 minutes, using autopilot control if possible. Flight velocity is the ideal endurance speed or the stall speed plus 5 knots, whichever is greater. 4) Aircraft lands under electric power, using ICE power in Dual mode if required.	1) Aircraft completes mission	1) Throttle setting 2) Engine speed 3) Pack voltage 4) Solo Whistle current draw	BT&GT Critical Paths	Yes
FT4	Regen	1) Aircraft uses ICE or Dual mode to achieve flight under manual control. Flight battery packs are at least 2 V less than full charge. 2) Aircraft is switched to ICE only mode with EM off. Autopilot is in control. 3) Propulsion system is switched to regeneration mode until battery pack voltage increases by 0.5 V. Aircraft flies standard race track in the interim. 4) Regeneration mode is disabled. 5) Aircraft lands.	1) Battery pack voltage increases.	1) Throttle setting 2) Engine speed 3) Pack voltage 4) Solo Whistle current draw	BT&GT Critical Paths, BT10, GT2SF4	No
FT5	ICE kill for silent EM operation	1) Aircraft uses ICE or Dual mode to achieve flight under manual control. 2) Aircraft switches to EM only power under manual control. 3) ICE is killed using ICE kill switch. 4) Aircraft performs 4 laps under electric only power. 5) Aircraft lands. (This test allows a ground observer to listen to the aircraft in silent mode, as if there were a restart for the ICE on the aircraft.)	1) Aircraft successfully completes test.	1) Throttle setting 2) Engine speed 3) Pack voltage 4) Solo Whistle current draw	BT&GT1 Critical Paths	No

Safety Switches:

In addition to the standard safety protocols, the following safety switches are in place on a separate (from the Kestrel) 2.4 GHz receiver transmitter.

1: ICE Kill switch: Direct control of ICE magneto. Kills the ICE in less than 1 second.

2: EM Kill switch: Cuts the positive power line to the EM Speed controller, killing the EM in less than 2 seconds.

3: ICE Crossover switch: Returns throttle authority of the ICE directly to the throttle line of the Kestrel instead of the gimbaled camera redirect.

Appendix M. Bench, Ground, and Flight Test Cards

This appendix contains all of the test cards for the bench, ground, and flight testing. The cards were developed by Molesworth and edited by the author to support the testing plan laid out in Appendix L. Completed test cards are annotated with the test data. Notes and observations from during the test are also included.

1. BT-01: CONDOR HE ICE Only Bench Test Card

Completed: 31 January 2012, Attempt 1

Preconditions:
Aircraft secured in test stand, HE system passed functional check, and Autopilot installation and ground configuration procedures accomplished as described in Section 1 through Section 2.1 of the Procerus Installation and Configuration Guide Document Version 2.0, dated 10/27/08. Autopilot mode control add-in verified via HE functional check. Ensure adequate support and safety measures in place.

Note: Mission requires a Safety Observer (SO), HE System operator (HEO), and Virtual Cockpit operator (VCO). The entire test will be conducted in Manual Mode

CONDOR Configuration: No wings, N/A–lbs, 18x10 2-blade prop

Objective:
Verify performance of integrated HE system in ICE Only mode under manual control

BT-01: PROCEDURES	Notes: **Duration:** 30 min
<u>ICE Throttle Response</u>	
1. **SO:** Ensure fire safety and test stand safety measures in place	
2. **HEO:** Verify RC Mode (control boxes grayed out) and in “Manual Mode”	
3. **HEO:** Record **starting fuel level**	**Starting Fuel Level:**1.825 kg
4. **VCO:** Ensure VC and VC HE add-in loaded	
5. **HEO:** Power-up and initiate HE system	
6. **VCO:** Switch to RC Mode	
7. **VCO:** Verify RC Mode (control boxes grayed out) and in **“Manual Mode”**	
8. **VCO:** Set VC add-in **ICE Only** Mode	**ICE Start Time:**12:13:03
9. **VCO:** Set ICE throttle to 50% for start-up	**% Throttle for Idle:**22%, 3050 rpm
10. **HEO:** Start HE system & Record **ICE start time**	**Throttle Position (%):** 30, 40, 50,
11. **HEO:** Verify ICE system operating correctly	60, 70, 80
12. **VCO:** Adjust throttle to **identify idle** position; restart if required	**Engine Speed (rpm):** 3970, 4600, 5150, 5290, 5340, 5380

BT-01: PROCEDURES	Notes: **Duration:** 30 min
13. **VCO:** Increase throttle 10% hold 30 sec 14. **HEO:** Record **engine speed** 15. **HEO/VCO:** Repeat steps 13-14 until 100% throttle; stop if unacceptable vibration develops 16. **VCO:** Reduce throttle to 30% to simulate cruise, hold 20 min; Record starting **Fuel Level** & end fuel level for test point 17. **VCO:** Reduce throttle to 0%, Place **VC into SAFE mode,** Record **ICE Stop time** 18. **HEO:** Ensure HE system properly shut down 19. **VCO/HEO/SP:** Proceed to **Card BT-02**	**ICE Start Time:** 12:19:30 **ICE Stop Time:** 12:39:30**;** **Engine Speed:** 4020 rpm **Fuel Level:** **Start:** 1.780 kg, **End:** 1.730 kg **Notes/Observations:** Test accomplished successfully on first attempt. Aircraft is capable of ICE only operation. Solo Whistle maintained commutation and alignment during entire test, although this was not a test objective.

2. BT-02: CONDOR HE EM Only Bench Test Card

Completed: 1 February 2012, Attempt 1

Preconditions:
Aircraft secured in test stand, HE system passed functional check, and Autopilot installation and ground configuration procedures accomplished as described in Section 1 through Section 2.1 of the Procerus Installation and Configuration Guide Document Version 2.0, dated 10/27/08. Autopilot mode control add-in verified via HE functional check. Ensure adequate support and safety measures in place.

Note: Mission requires a Safety Observer (SO), HE System operator (HEO), and Virtual Cockpit operator (VCO). The entire test will be conducted in Manual Mode

CONDOR Configuration: No wings, N/A–lbs, 18x10 2-blade prop

Objective:
Verify performance of integrated HE system in EM only mode under manual control

BT-02: PROCEDURES	Notes: **Dur:** 30 min
<u>**EM Throttle Response**</u>	
1. **SO:** Ensure fire safety and test stand safety measures in place	
2. **HEO:** Verify RC Mode (control boxes grayed out) and in "Manual Mode"	
3. **VCO:** Ensure VC and VC HE add-in loaded	
4. **HEO:** Power-up and initiate HE system; Start EM (commutate)	
5. **VCO:** Switch to **Manual Mode**	
6. **VCO:** Verify RC Mode (control boxes grayed out) and in "**Manual Mode**"	
7. **VCO:** Set VC add-in **EM Only Mode**	
8. **VCO:** Set EM throttle to 0% for start-up	**% Throttle for min EM run position:** 15%
9. **HEO:** Verify HE system operating correctly (ICE will be at 0%)	**Throttle Position (%):** 21, 30, 40, 50, 60, 70, 80, 90, 96
10. **VCO:** Adjust throttle to identify min **EM run position** (EM idle)	
11. **VCO:** Increase throttle 10% hold 30 sec	**Pack Voltage (V):** 32.9, 32.9, 32.9, 32.8, 32.8 32.5, 32.5, 32.5,
12. **HEO:** Record battery **pack voltage** & **current draw & cumulative power & motor**	

BT-02: PROCEDURES

speed

13. **HEO/VCO:** Repeat steps 13-14 until 100% throttle
14. **VCO:** Reduce throttle to 0%, Place **VC into SAFE mode**
15. **HEO:** Ensure HE system properly shut down
16. **VCO/HEO/SP:** Proceed to **Card BT-03**

Notes: **Dur:** 30 min

32.3

Current Draw (A): -0.6, 0.0, 0.74, 1.8, 2.9, 4.1, 5.3, 7.0, 8.0

Cumulative Power (mAhr): **Initial:** 14 16, 19, 23, 33, 51, 78, 111, 157, 202

Motor Speed (rpm): 1550, 1630, 2120, 2490 2860, 3160, 3420, 3710, 3900

Notes/Observations: Test accomplished successfully on first attempt. Aircraft is capable of EM only operation. Operational speeds (rpm) were lower than expected based on simulation, as were current draws from the batteries. This is more likely due to the performance limits of the Solo Whistle controller than the motor or batteries. The system should still be capable of endurance flight based on power draw from the batteries. Pack current was not zeroed at the begining of the test. There is a -0.7 A offset in the data.

3. BT-03: CONDOR HE ICE to EM Bench Test Card

Completed: 1 February 2012, Attempt 2

Preconditions:
Aircraft secured in test stand, HE system passed functional check, and Autopilot installation and ground configuration procedures accomplished as described in Section 1 through Section 2.1 of the Procerus Installation and Configuration Guide Document Version 2.0, dated 10/27/08. Autopilot mode control add-in verified via HE functional check. Ensure adequate support and safety measures in place.

Note: Mission requires a Safety Observer (SO), HE System operator (HEO), and Virtual Cockpit operator (VCO). The entire test will be conducted in Manual Mode

CONDOR Configuration: No wings, N/A–lbs, 18x10 2-blade prop

Objective:
Verify HE can transition from ICE mode to EM mode in manual control and then operate in EM mode

BT-03: PROCEDURES	Notes: **Dur:** 30 min
<u>**HE Mode Response**</u> 1. **SO:** Ensure fire safety and test stand safety measures in place 2. **HEO:** Verify VC in "Safe Mode" 3. **VCO:** Ensure VC and VC HE add-in loaded 4. **HEO:** Power-up and initiate HE system; commutate EM 5. **VCO:** Switch to **Manual Mode** 6. **VCO:** Verify RC Mode (control boxes grayed out) and in "**Manual Mode**" 7. **VCO:** Set VC add-in **ICE Only Mode** 8. **VCO:** Set ICE throttle to 50% for start-up 9. **HEO:** Start HE system 10. **HEO:** Verify HE system operating correctly 11. **VCO:** Adjust throttle to 10-20% above ICE idle 12. **VCO:** Set VC add-in **EM Only Mode**	**EM Response Verification:** (throttle settings, propeller speed, and pack current draw) ICE: Idle; EM: 42%; 3.6 A 4350 rpm ICE: Idle; EM: 35%; 2.8 A 4160 rpm ICE: Idle; EM: 54%; 5.0 A 4700 rpm **HE System Operating Correctly:** Yes **EM at throttle:** Yes **ICE at Idle:** Yes **Notes/Observations:** EM is not overrunning ICE, even

BT-03: PROCEDURES	Notes: **Dur:** 30 min
13. **HEO:** Verify EM running at correct throttle setting 14. **HEO:** Verify ICE reduced to idle 15. **VCO/HEO/SP:** Proceed to **Card BT-04**	with ICE at idle throttle. **Attempt 1:** During the first attempt, the ICE turned off instead of going to idle throttle. The coding for idle throttle in Virtual Cockpit had been set to 0% instead of 22% as determined during BT01. After correction, attempt 2 was successful.

4. BT-04: CONDOR HE EM to ICE Bench Test Card

Completed: 1 February 2012, Attempt 1

Preconditions:
Aircraft secured in test stand, HE system passed functional check, and Autopilot installation and ground configuration procedures accomplished as described in Section 1 through Section 2.1 of the Procerus Installation and Configuration Guide Document Version 2.0, dated 10/27/08. Autopilot mode control add-in verified via HE functional check. Ensure adequate support and safety measures in place.

Note: Mission requires a Safety Observer (SO), HE System operator (HEO), and Virtual Cockpit operator (VCO). The entire test will be conducted in Manual Mode

CONDOR Configuration: No wings, N/A–lbs, 18x10 2-blade prop

Objective:
Verify HE can transition from EM mode to ICE mode in manual control

BT-04: PROCEDURES	Notes: **Dur:** 30 min
<u>**HE Mode Response**</u>	
1. **SO:** Ensure fire safety and test stand safety measures in place	
2. **HEO:** Verify VC in "Safe Mode"	
3. **VCO:** Ensure VC and VC HE add-in loaded	
4. **HEO:** Power-up and initiate HE system; Commutate EM	
5. **VCO:** Switch to **Manual Mode**	
6. **VCO:** Verify RC Mode (control boxes grayed out) and in "**Manual Mode**"	
7. **VCO:** Set ICE throttle to 50% for start-up	
8. **HEO:** Start HE system	
9. **HEO:** Verify HE system operating correctly	
10. **VCO:** Set VC add-in **EM Only Mode,** adjust throttle (EM) to 30% to ensure control	**Throttle controlling EM:** Yes
11. **HEO:** Verify ICE goes to idle	**ICE to Idle:** Yes

BT-04: PROCEDURES	Notes: **Dur:** 30 min
12. **VCO:** Switch to **ICE Only Mode** 13. **HEO:** Verify EM off 14. **HEO:** Verify ICE at set throttle 15. **VCO/HEO/SP:** Proceed to **Card BT-05, BT-06**	**EM turns off:** Yes **Throttle controlling ICE:** Yes **Notes/Observations:** Throttle verification performed by watching for a change in propeller speed (rpm) as throttle was adjusted by a 10% step.

5. BT-05, BT-06: CONDOR HE Dual Mode Bench Test Card

Completed: 1 February 2012, Attempt 1

Preconditions:
Aircraft secured in test stand, HE system passed functional check, and Autopilot installation and ground configuration procedures accomplished as described in Section 1 through Section 2.1 of the Procerus Installation and Configuration Guide Document Version 2.0, dated 10/27/08. Autopilot mode control add-in verified via HE functional check. Ensure adequate support and safety measures in place.

Note: Mission requires a Safety Observer (SO), HE System operator (HEO), and Virtual Cockpit operator (VCO). The entire test will be conducted in Manual Mode

CONDOR Configuration: No wings, N/A–lbs, 18x10 2-blade prop

Objective:
Verify HE can transition to dual mode (EM driver and ICE driver) in manual control

BT-05, BT-06: PROCEDURES

Notes: **Dur:** 30 min

EM Driver Test: BT-05

1. **VCO:** Set Dual Mode (ICE) value at 10-30%
2. **VCO:** Set VC add-in to **Dual Mode (EM Boost)**
3. **VCO:** Decrease throttle (EM) to 0%
4. **HEO:** Verify EM powers down & ICE remains at 10-30% setting
5. **VCO:** Increase throttle (EM) to 30% hold 30 sec
6. **HEO:** Verify EM powers up
7. **VCO:** Increase throttle (EM) to 40%
8. **HEO:** Verify EM powers up
9. **VCO:** Change ICE set point to 40%
10. **HEO:** Verify ICE powers up

EM Driver Response Verification:
(throttle settings, propeller speed, and pack current draw)

Initial:

ICE: 30%;	EM: 31%; 3.6 A	4460 rpm

Adjust Dual Mode throttle:

ICE: 30%;	EM: 43%; 4.0 A	4670 rpm

Adjust ICE Set point:

ICE: 40%;	EM: 43%; 4.2 A	5360 rpm

ICE Driver: BT-06

ICE Driver Response Verification:
(throttle settings, propeller speed, and pack current

BT-05, BT-06: PROCEDURES

11. **VCO:** Set throttle (EM) at 50%, ICE set point at 30%
12. **VCO:** Switch to ICE driver
13. **HEO:** Verify EM switches to 30% setting & ICE powers up to 50%
14. **VCO:** Decrease throttle (ICE) to 20%
15. **HEO:** Verify ICE powers down
16. **VCO:** Increase throttle (ICE) to 30%
17. **HEO:** Verify ICE powers up
18. **VCO:** Change EM set point to 40%
19. **HEO:** Verify EM powers up
20. **HEO:** Return to **ICE Only Mode**
21. **VCO/HEO/SP:** Proceed to **Card BT-07**

Notes: **Dur:** 30 min

draw)

Initial:

ICE: 19%;	EM: 30%;	3507 rpm
	1.9 A	

Adjust Dual Mode throttle:

ICE: 30%;	EM: 30%;	4500 rpm
	2.4 A	

Adjust EM Set point:

ICE: 40%;	EM: 50%;	4800 rpm
	5.2 A	

Notes/Observations: The EM was never able to overrun the ICE. ICE speed increased with EM throttle at all times. Also, above 50% EM throttle, the behavior of the ICE servo became erratic. Moving the ICE servo wire mitigated the behavior, but shielding should be included for the signal in the final aircraft, as the wire runs alongside the EM power and magneto.

6. BT-07: CONDOR HE Emergency Kill Bench Test Card

Completed: 1 February 2012, Attempt 1

Preconditions:
Aircraft secured in test stand, HE system passed functional check, and Autopilot installation and ground configuration procedures accomplished as described in Section 1 through Section 2.1 of the Procerus Installation and Configuration Guide Document Version 2.0, dated 10/27/08. Autopilot mode control add-in verified via HE functional check. Ensure adequate support and safety measures in place.

Note: Mission requires a Safety Observer (SO), HE System operator (HEO), and Virtual Cockpit operator (VCO). The entire test will be conducted in Manual Mode

CONDOR Configuration: No wings, N/A–lbs, 18x10 2-blade prop

Objective:
Verify HE ICE can be killed in emergency situation and that the EM still functions

BT-07: PROCEDURES	Notes: **Dur:** 30 min
<u>HE System Kill Verification</u> 1. **HEO:** Ensure system started & EM commutated 2. VCO: Verify system is in ICE mode 3. **VCO:** Ensure throttle (ICE) set to 30% 4. **HEO:** Activate ICE kill switch 5. **HEO:** Verify ICE stops (EM already off) 6. **VCO/HEO: Restart HE system in ICE Only Mode** 7. **VCO:** Set Dual Mode (EM Driver) to ICE constant value 40% 8. **VCO:** Set VC add-in to **Dual Mode (EM Driver)** 9. **HEO:** Verify EM operating at 30% & ICE operating at 40% 10. **HEO:** Activate ICE kill switch 11. **HEO:** Verify ICE stops 12. **VCO:** Increase throttle (EM) to 60%	**Notes/Observations:** Despite concerns about EM commutation loss during an ICE shutdown, EM functioned flawlessly with no loss of commutation.

BT-07: PROCEDURES	Notes: **Dur:** 30 min
13. **HEO:** Verify EM powers up & functions after ICE kill 14. **VCO:** Set throttle to 0% 15. **VCO:** Place VC in **Safe Mode** 16. **HEO:** Power down HE system 17. **VCO/HEO/SP:** Proceed to **Card BT-08**	

7. BT-08: CONDOR HE Emergency Kill Bench Test Card

Completed: 1 February 2012, Attempt 1

Preconditions:

Aircraft secured in test stand, HE system passed functional check, and Autopilot installation and ground configuration procedures accomplished as described in Section 1 through Section 2.1 of the Procerus Installation and Configuration Guide Document Version 2.0, dated 10/27/08. Autopilot mode control add-in verified via HE functional check. Ensure adequate support and safety measures in place.

Note: Mission requires a Safety Observer (SO), HE System operator (HEO), and Virtual Cockpit operator (VCO). The entire test will be conducted in Manual Mode

CONDOR Configuration: No wings, N/A–lbs, 18x10 2-blade prop

Objective:

Verify HE EM can be killed in emergency situation

BT-08: PROCEDURES | Notes: | **Dur:** 30 min

HE System EM Kill Verification

1. **SO:** Ensure fire safety and test stand safety measures in place
2. **HEO:** Verify RC Mode (control boxes grayed out) and in "Manual Mode"
3. **VCO:** Ensure VC and VC HE add-in loaded
4. **HEO:** Power-up and initiate HE system
5. **VCO:** Switch to RC Mode
6. **VCO:** Verify RC Mode (control boxes grayed out) and in "Manual Mode"
7. **VCO:** Set VC add-in ICE Only Mode
8. **VCO:** Set ICE throttle to 50% for start-up
9. **HEO:** Start HE system
10. **HEO:** Verify HE system operating correctly
11. **VCO:** Adjust throttle to ICE idle position
12. **VCO:** Set Dual Mode (EM Driver) with ICE constant value at 30 %

Response Verification:

(throttle settings, propeller speed)

ICE: 30%;	EM: 30%;	4500 rpm
ICE: 30%;	EM: Off;	4000 rpm

Notes/Observations: No issues with EM shutdown.

BT-08: PROCEDURES	Notes: **Dur:** 30 min
13. **VCO:** Set VC add-in to **Dual Mode (EM Boost)** 14. **HEO:** Verify EM throttle control & ICE operating at 30% 15. **HEO:** Set throttle (EM) at 30% 16. **HEO:** Activate EM kill switch 17. **HEO:** Verify EM stops 18. **HEO:** Verify ICE remains at 30% 19. **VCO/HEO/SP:** Proceed to **Card BT-09**	

8. BT-09: CONDOR HE ICE Crossover Bench Test Card

Completed: 3 February 2012, Attempt 3

Preconditions:
Aircraft secured in test stand, HE system passed functional check, and Autopilot installation and ground configuration procedures accomplished as described in Section 1 through Section 2.1 of the Procerus Installation and Configuration Guide Document Version 2.0, dated 10/27/08. Autopilot mode control add-in verified via HE functional check. Ensure adequate support and safety measures in place.

Note: Mission requires a Safety Observer (SO), HE System operator (HEO), and Virtual Cockpit operator (VCO). The entire test will be conducted in Manual Mode

CONDOR Configuration: No wings, N/A–lbs, 18x10 2-blade prop

Objective:
Verify HE ICE Crossover functions correctly

BT-09: PROCEDURES	Notes: **Dur:** 30 min
<u>**HE System ICE Crossover Verification**</u> 1. **VCO:** Set VC add-in to **ICE Mode** 2. **VCO:** Increase throttle (ICE) to 40% 3. **HEO:** Activate ICE Crossover switch 4. **VCO:** Switch from ICE mode to EM mode 5. **VCO:** Vary manual throttle 10-30% (Ice should respond to manual control in EM mode) 6. **HEO:** Verify ICE positive response 7. **VCO:** Verify HE (ICE control) mode control inactive & control through Kestral AP 8. **HEO:** Deactivate Crossover switch, verify ICE control 9. **VCO:** Switch from ICE mode to EM mode 10. **VCO:** Vary throttle 10-30% 11. **HEO:** Verify EM positive response 12. **VCO:** Verify HE mode control active & control through Kestral AP inactive 13. **VCO/HEO/SP:** Proceed to **Card BT-10**	**Notes/Observations:** No issues with EM shutdown. Attempt 1&2: When the crossover was activated, the engine speed increased rapidly and the belt came off of the EM pulley. There exists an offset between the manual and autopilot servo ranges, causing the rapid throttle variation. This servo range was correct before attempt 3.

9. BT-10: CONDOR HE Regen Test Card

Completed: 1 February 2012, Attempt 1

Preconditions:
Aircraft secured in test stand, HE system passed functional check, and Autopilot installation and ground configuration procedures accomplished as described in Section 1 through Section 2.1 of the Procerus Installation and Configuration Guide Document Version 2.0, dated 10/27/08. Autopilot mode control add-in verified via HE functional check. Ensure adequate support and safety measures in place.

Note: Mission requires a Safety Observer (SO), HE System operator (HEO), and Virtual Cockpit operator (VCO). The entire test will be conducted in Manual Mode

CONDOR Configuration: No wings, N/A–lbs, 18x10 2-blade prop

Objective:
Verify HE EM ReGen functions correctly

BT-10: PROCEDURES

<u>HE System ReGen Verification</u>

1. **HEO:** Record battery **starting battery voltage**, ensure at least 2V under max
2. **HEO:** Verify EM initially off
3. **VCO:** Set VC add-in to **Regen Mode,** Record **start time**
4. **VCO:** Increase throttle (ICE) to 30%
5. **HEO:** Monitor battery pack voltage, record time for voltage to increase 0.5V (do not start with fully charged battery packs)
6. **VCO:** Set VC add-in to **ICE Mode**
7. **VCO:** Decrease throttle to 20%
8. **HEO:** Verify ICE throttle response
9. **VCO:** Set VC add-in to **EM Mode**
10. **HEO:** Verify ICE goes to Idle
11. **VCO:** Increase throttle to 40%

Notes: **Dur:** 30 min

Starting Battery Voltage: 31.5 V
Start Time: 12:06:10

End Time:12:28:06
End Battery Voltage: 32.0 V
Total power (mAhr): 300

Regen Verification:
(throttle settings, propeller speed, pack current)
ICE: 30%; EM: Off; 4130 rpm
0 A
ICE: 30%; EM: Regen; 4050 rpm
1.15 A

Notes/Observations: Only two battery packs were used

BT-10: PROCEDURES	Notes: **Dur:** 30 min
12. **HEO:** Verify EM responds to throttle 13. **VCO:** Decrease throttle to 0% 14. **HEO:** Power down HE system 15. **VCO:** Power Down VC/Kestral AP 16. **VCO/HEO/SP:** End Test	during the Regeneration test for safety reasons.

10. GT-00: CONDOR HE Kill Mode Verification Test Card

Completed, Qualitatively, No Telemetry Data (interference issues), 15 February 2012

Preconditions:

Ground Control Station (GCS) set up and proper GCS operation verified. Ensure adequate support and safety measures in place.

Note: Mission requires a Safety Observer (SO), HE System operator (HEO), and Virtual Cockpit operator (VCO).

CONDOR Configuration: 12-ft, 35 lbs, 18x10 2-blade prop

Objective:

Verify HE system kill modes

GT-00: PROCEDURES	Notes: **Dur:** 30 min
Kill mode verification	
1. **SO:** Ensure fire safety and test safety measures in place	
2. **VCO:** Ensure VC in **Safe Mode** prior to HE RPA startup	
3. **VCO:** Perform Pre-engine start-up portion of *Launch Checklist*	
4. **VCO:** Verify RC Mode (control boxes grayed out) and in "**Manual Mode**"	
5. **SO:** Ensure RPA is restrained & personnel have PPE	
6. **HEO:** Conduct HE RPA startup checklist	
7. **VCO:** Set VC HE add-in to **ICE Only Mode**	**ICE Killed: Yes / No**
8. **HEO:** Activate ICE kill switch	
9. **HEO/VCO/SO:** Repeat steps 3-6	**EM Killed: Yes / No**
10. **VCO:** Set VC HE add-in to **EM Only Mode** (Ice idle)	
11. **HEO:** Activate EM kill switch	
12. **VCO:** Place VC in **Safe Mode**	
13. **SP/HEO/VCO:** Proceed to GT-01	

11. GT-01: CONDOR HE Takeoff and Dual Mode Ground Test Card

Completed, Qualitatively, No Telemetry Data (interference issues), 15 February 2012

Preconditions:
Ground Control Station (GCS) set up and proper GCS operation verified. Ensure adequate support and safety measures in place.

> Note: Mission requires a Safety Observer (SO), HE System operator (HEO), and Virtual Cockpit operator (VCO). The entire test will be conducted in Manual Mode

CONDOR Configuration: No Wings, 35 lbs, 18x10 2 blade prop

Objective:
Verify takeoff (simulated) & performance of integrated HE system in dual (ICE Boost) mode

GT-01: PROCEDURES	Notes: **Dur:** 30 min
Takeoff & Dual Mode (ICE boost)	
1. **SO:** Ensure fire safety and test safety measures in place	
2. **VCO:** Ensure CONDOR PID Values uploaded , & waypoints (WPAFB) loaded into VC	
3. **VCO:** Ensure VC in **Safe Mode** prior to HE RPA startup	
4. **HEO:** Record starting **fuel level** of RPA	**Starting Fuel Level:_______________**
5. **HEO:** Record starting **battery voltage** and **current draw**	**Starting Battery Voltage:___________** **Starting Current Draw:____________**
6. **VCO:** Perform Pre-engine start-up portion of *Launch Checklist*	
7. **VCO:** Verify RC Mode (control boxes grayed out) and in "**Manual Mode**"	
8. **VCO:** Place VC HE add-in to **ICE Only**	**ICE Start Time:___________________**
9. **HEO:** Conduct HE RPA startup checklist, record **ICE start time**	
10. **SP:** Adjust **ICE throttle** to **idle**	**Min EM Throttle Constant:_________**
11. **VCO:** Set VC HE add-in to **Dual Mode (ICE Boost),** set EM constant to 30%	
12. **VCO:** Adjust EM constant to lower value if needed to prevent taxi	**% Throttle:___, ___, ___, ___, ___**
13. **SP:** Increase ICE throttle until RPA begins to taxi	**Estimated Takeoff speed:___, ___, ___, ___, ___** **Propeller Speed:___, ___, ___, ___, ___** **Current Draw:___, ___, ___, ___, ___**

GT-01: PROCEDURES

14. **SP:** Accelerate RPA to simulate takeoff
15. **SP:** Record throttle position for estimated takeoff speed (if not 100%)
16. **VCO:** Record **<u>throttle</u>** position, **<u>estimated speed</u>, and <u>engine speed</u>**
17. **SP:** Reduce throttle, rotate RPA 180d eg and repeat in opposite direction
18. **SP:** Determine if EM throttle constant needs to be adjusted up or down
19. **VCO:** Adjust EM throttle constant as necessary for proceeding trial
20. **SP/VCO/HEO:** Repeat steps 10-15 until SP identifies preferred throttle combination
21. **VCO:** Place RPA in **IDLE Mode**
22. **VCO/HEO/SP:** Proceed to **Card GT-02**

Notes: **Dur:** 30 min

EM Throttle Constant:___, ___, ___, ___, ___

12. GT-02: CONDOR HE ICE Mode Test Card

Completed, Qualitatively, No Telemetry Data (interference issues), 15 February 2012

Preconditions:
Completion of Test Card GT-01, Ground Control Station (GCS) set up and proper GCS operation verified. Ensure adequate support and safety measures in place.

Note: Mission requires a Safety Observer (SO), HE System operator (HEO), and Virtual Cockpit operator (VCO). The entire test will be conducted in Manual Mode

CONDOR Configuration: 12-ft, 35 lbs, 18x10 2-blade prop

Objective:
Verify correct operation of HE RPA ICE mode & mode switching

GT-02: PROCEDURES	Notes: **Dur:** 30 min
<u>**ICE Only Mode Checkout**</u> 1. **VCO:** Set VC HE add-in to **ICE Only Mode** 2. **SP/HEO:** Verify EM off & ICE responds to manual throttle commands 3. **SP:** Increase throttle until RPA begins to taxi 4. **VCO:** Record min taxi throttle setting, min taxi speed, and engine speed 5. **SP:** Taxi RPA for 4 laps, operator choice of throttle 6. **VCO:** Place RPA in **Idle** 7. **VCO/HEO/SP:** Proceed to **Card GT-03**	**% Throttle for Taxi:**__________________ **Min Taxi Speed:**_____________________ **Min Propeller Speed:**_________________ **Taxi Throttle:**______________________ **Taxi Propeller Speed:**_________________

13. GT-03: CONDOR HE EM Mode Test Card

Completed, Qualitatively, No Telemetry Data (interference issues), 15 February 2012

Preconditions:
Completion of Test Card GT-02, Ground Control Station (GCS) set up and proper GCS operation verified. Ensure adequate support and safety measures in place.

Note: Mission requires a Safety Observer (SO), HE System operator (HEO), and Virtual Cockpit operator (VCO). The entire test will be conducted in Manual Mode

CONDOR Configuration: 12-ft, 35 lbs, 18x10 2-blade prop

Objective:
Verify correct operation of HE RPA EM mode & mode switching

GT-03: PROCEDURES	Notes: **Dur:** 30 min
<u>**EM Only Mode Checkout**</u>	
1. **VCO:** Set VC HE add-in to **EM Only Mode**	
2. **SP/HEO:** Verify EM responds to manual throttle commands & ICE goes to idle	
3. **SP:** Increase throttle until RPA begins to taxi	**% Throttle for Taxi:**________________
4. **VCO:** Record min taxi throttle setting, min taxi speed, and engine speed	**Min Taxi Speed:**____________________ **Min Propeller Speed:**________________
5. **SP:** Taxi RPA for 4 laps, operator choice of throttle	**Min Current Draw:**_________________
6. **VCO:** Place RPA in **Idle**	**Taxi Throttle:**______________________ **Taxi Propeller Speed:**_______________
7. **VCO/HEO/SP:** Proceed to **Card GT-04**	**Current Draw:**______________________

14. GT-04: CONDOR HE ICE Mode Test Card

Completed, Qualitatively, No Telemetry Data (interference issues), 15 February 2012

Preconditions:
Completion of Test Card GT-01, Ground Control Station (GCS) set up and proper GCS operation verified. Ensure adequate support and safety measures in place.

Note: Mission requires a Safety Observer (SO), HE System operator (HEO), and Virtual Cockpit operator (VCO). The entire test will be conducted in Manual Mode

CONDOR Configuration: 12-ft, 35 lbs, 18x10 2-blade prop

Objective:
Verify correct operation of HE RPA Dual mode & mode switching

GT-04: PROCEDURES	Notes: **Dur:** 30 min
<u>Dual Mode (EM Boost) Checkout</u>	
1. **VCO:** Set VC HE add-in throttle constant to 40% (ICE will be 40%)** Reduce if needed	**% Throttle (ICE) for Min Taxi:__________**
2. **VCO:** Set VC HE add-in to **Dual mode (EM boost)** mode	**Min Taxi Speed:______________________**
3. **SP/HEO:** Verify EM responds to manual throttle commands & ICE goes to 40%	**Min Propeller Speed:_________________**
4. **SP:** Increase throttle until RPA begins to taxi	**Current Draw:______________________**
5. **VCO:** Record min taxi throttle setting, min taxi speed, and engine speed	**% Throttle for Taxi:_________________**
6. **SP:** Adjust throttle until controllable taxi achieved	**Taxi Speed:_________________________**
7. **SP:** Taxi RPA for 4 laps	**Taxi Propeller Speed:_________________**
8. **VCO:** Place RPA in **Idle**	**Current Draw:_______________________**
<u>Dual Mode (ICE Boost) Checkout</u>	**% Throttle (EM) for Min Taxi:__________**
9. **VCO:** Set VC HE add-in throttle constant to 40% (EM will be 40%)** Reduce if needed	**Min Taxi Speed:______________________**
10. **VCO:** Set VC HE add-in to **Dual mode (ICE boost)** mode	**Min Propeller Speed:__________________**
	Current Draw:_______________________

GT-04: PROCEDURES	Notes: **Dur:** 30 min
11. **SP/HEO:** Verify ICE responds to manual throttle commands & EM goes to 40% 12. **SP:** Increase throttle until RPA begins to taxi 13. **VCO:** Record min taxi throttle setting, min taxi speed, and engine speed 14. **SP:** Adjust throttle until controllable taxi achieved 15. **SP:** Taxi RPA for 4 laps 16. **VCO:** Place RPA in **Idle** 17. **SP/HEO:** Kill RPA ICE 18. **HEO:** Record **<u>engine stop time</u>** and **<u>ending fuel state</u>** 19. **VCO/HEO/SP:** Proceed to **Card GT-05**	**% Throttle for Taxi:______________** **Taxi Speed:______________________** **Taxi Engine Speed:________________** **Current Draw:____________________** **Engine Stop Time:_________________** **Final Fuel State:__________________**

15. GT-05: CONDOR HE ICE Crossover & Cruise Test Card

Completed, Qualitatively, No Telemetry Data (interference issues), 15 February 2012

Preconditions:
Completion of GT-04

Note: Mission requires a Safety Observer (SO), HE System operator (HEO), and Virtual Cockpit operator (VCO). The entire test will be conducted in Manual Mode

CONDOR Configuration: 12-ft, 35 lbs, 18x10 2-blade prop

Objective:
Verify HE can transition manual control to autopilot and evaluate cruise performance

GT-05: PROCEDURES	Notes: **Dur:** 30 min
HE System ICE Crossover Verification	
1. **SO:** Ensure fire safety and test safety measures in place	
2. **VCO:** Ensure CONDOR PID Values uploaded , and waypoints loaded into VC (vary speeds for ground testing)	
3. **VCO:** Ensure VC in **Safe Mode** prior to HE RPA startup	**Starting Fuel Level:**______________
4. **HEO:** Record starting **fuel level** of RPA	
5. **VCO:** Perform Pre-engine start-up portion of *Launch Checklist*	
6. **VCO:** Verify RC Mode (control boxes grayed out) and in "**Manual Mode**"	**ICE Start Time:**________________
7. **VCO:** Place VC HE add-in to **ICE Only Mode**	
8. **HEO:** Conduct HE RPA startup checklist, record **ICE start time**	
9. **VCO:** Set VC HE add-in to **Dual Mode (ICE Boost),** EM throttle constant (~30%)	**Speed:** ________________________
10. **SP:** Accelerate RPA to approximated cruise speed (or appropriate for safe ground ops)	**% Throttle:**____________________ **Propeller Speed:**________________
11. **SP:** Begin test laps with RPA	
12. **VCO:** Reduce EM throttle constant if directed by SP	
13. **VCO:** Record **trim throttle** position, **trim airspeed, and engine speed**	

GT-05: PROCEDURES	Notes: **Dur:** 30 min
14. **HEO:** Activate Crossover switch 15. **SP/VCO:** Verify autopilot has control of aircraft (Ice should respond to manual control in EM mode) 16. **HEO:** Deactivate Crossover switch 17. **SP/VCO:** RPA in back in manual control (back to Dual Mode) 18. **VCO:** Switch to **ICE Only Mode** (now in manual ICE mode) 19. **HEO:** Verify EM off 20. **HEO:** Activate crossover switch 21. **SP/VCO:** Verify autopilot has control of aircraft 22. **HEO:** Deactivate Crossover switch (Back to manual ICE) 23. **SP/VCO:** Monitor RPA under manual control for 10+ min grnd test, set to cruise velocity 24. **SP:** Recover RPA 25. **VCO:** Place VC in **Safe Mode** 26. **HEO:** Record **engine stop time** and **ending fuel state** 27. **VCO/HEO/SP:** Proceed to **Card GT-06**	**Engine Stop Time:**_________________ **Final Fuel State:**__________________

16. GT-06: CONDOR HE ReGen Mode & Kill Switch Test Card

Kill Tests Completed, Qualitatively, No Telemetry Data (interference issues), 15 February 2012
Regen not attempted due to interference issues during testing,

Preconditions:
Completion of GT-06

Note: Mission requires a Safety Observer (SO), HE System operator (HEO), and Virtual Cockpit operator (VCO). The entire test will be conducted in Manual Mode

CONDOR Configuration: 12-ft, 35 lbs, 18x10 2-blade prop

Objective:
Verify HE EM ReGen and ICE Kill switch function correctly

GT-06: PROCEDURES	Notes: **Dur:** 30 min
<u>**HE System ReGen Verification**</u>	
1. **SO:** Ensure fire safety and test safety measures in place	
2. **VCO:** Ensure CONDOR PID Values uploaded , and waypoints loaded into VC	
3. **VCO:** Ensure VC in **Safe Mode** prior to HE RPA startup	
4. **HEO:** Record battery starting <u>**battery voltage**</u> & <u>**current**</u>, ensure at least 2V under max	**Starting Battery Voltage:**_________________
5. **HEO:** Record starting <u>**fuel level**</u> of RPA	**Starting Current:**_______________________ **Starting Fuel Level:**______________________
6. **VCO:** Perform Pre-engine start-up portion of *Launch Checklist*	
7. **VCO:** Verify RC Mode (control boxes grayed out) and in "**Manual Mode**"	
8. **VCO:** Place VC HE add-in to **ICE Only**	**Start Engine Start Time:**__________________
9. **HEO:** Conduct HE RPA startup checklist, record <u>**ICE start time**</u>	
10. **VCO:** Set VC HE add-in to **Dual Mode (ICE Boost),** EM throttle constant (~30%)	
11. **SP:** Accelerate RPA to approximated cruise speed (or appropriate for safe grnd ops)	
12. **SP:** Begin test laps with RPA	
13. **VCO:** Reduce EM throttle constant is directed by SP	

GT-06: PROCEDURES | Notes: | **Dur:** 30 min

14. **VCO:** Record **trim throttle** position, **trim airspeed, and engine speed**
15. **VCO:** Set VC add-in to **ICE Only Mode**
16. **HEO:** Verify EM off
17. **HEO:** Record Battery pack voltage & ReGen start time
18. **VCO:** Set VC add-in to **Regen Mode**
19. **HEO:** Maneuver RPA in lap pattern & monitor battery pack voltage, record time for voltage to increase 0.5V
20. **VCO:** Place VC HE add-in to **ICE Only**

Starting Battery Voltage:__________
Start ReGen Time:_______________

Pack Current:___________________

Ending Battery Voltage:__________
End ReGen Time:________________

****Simulated - HIGH RISK****

ICE Kill for Silent Operation

21. **VCO:** Set VC add-in to **EM Mode**
22. **HEO:** Verify EM powers up & ICE goes to idle
23. **SP:** Verify EM throttle response, prepare for simulated emergency landing
24. **HEO:** Activate **ICE Kill Switch**
25. **HEO:** Verify ICE killed & Record **engine stop time**
26. **SP:** Verify RPA performance under **EM Only Mode** (no ICE)

Engine stop time:_________________

EM Kill verification

27. **HEO:** Activate EM kill switch just prior to touchdown
28. **SP:** Recover ****Simulated Dead stick Landing””**
29. **VCO:** Place VC in **Safe Mode**
30. **HEO:** Record **final fuel state**
31. **VCO/HEO/SP:** End Testing

Final Fuel State:__________________

17. FT-00: CONDOR HE Kill Mode Verification Test Card

Preconditions:
Ground Control Station (GCS) set up and proper GCS operation verified. Ensure adequate support and safety measures in place.

Note: Mission requires a Safety Observer (SO), HE System operator (HEO), and Virtual Cockpit operator (VCO).

CONDOR Configuration: 12-ft, ____-lbs, 18x10 2-blade prop

Objective:
Verify HE system kill modes

FT-00: PROCEDURES	Notes: **Dur:** 30 min
<u>**Kill mode verification**</u>	
1. **SO:** Ensure fire safety and test safety measures in place	
2. **VCO:** Ensure VC in **Safe Mode** prior to HE RPA startup	
3. **VCO:** Perform Pre-engine start-up portion of *Launch Checklist*	
4. **VCO:** Verify RC Mode (control boxes grayed out) and in "**Manual Mode**"	
5. **SO:** Ensure RPA is restrained & personnel have PPE	
6. **HEO:** Conduct HE RPA startup checklist	
7. **VCO:** Set VC HE add-in to **ICE Only Mode**	**ICE Killed: Yes / No**
8. **HEO:** Activate ICE kill switch	
9. **HEO/VCO/SO:** Repeat steps 3-6	**EM Killed: Yes / No**
10. **VCO:** Set VC HE add-in to **EM Only Mode** (ICE idle)	
11. **HEO:** Activate EM kill switch	
12. **VCO:** Place VC in **Safe Mode**	
13. **SP/HEO/VCO:** Proceed to FT-01	

18. FT-01: CONDOR HE Dual Mode (ICE Boost) Flight Test Card

Preconditions:
Ground Control Station (GCS) set up and proper GCS operation verified. Ensure adequate support and safety measures in place.

Note: Mission requires a Safety Observer (SO), HE System operator (HEO), and Virtual Cockpit operator (VCO).

CONDOR Configuration: 12-ft, ____–lbs, 18x10 2-blade prop

Objective:
Verify takeoff & flight performance of integrated HE system in dual (ICE Boost) mode

FT-01: PROCEDURES	Notes: **Dur:** 30 min
Takeoff & Dual Mode (ICE boost)	
1. **SO:** Ensure fire safety and test safety measures in place	
2. **VCO:** Ensure CONDOR PID Values uploaded, and way/rally points loaded into VC	
3. **VCO:** Ensure VC in **Safe Mode** prior to HE RPA startup	**Starting Fuel Level:____________________**
4. **HEO:** Record starting **fuel level** of RPA	
5. **HEO:** Record starting **battery voltage** and **current draw**	**Starting Battery Voltage:_______________** **Starting Current Draw:________________**
6. **VCO:** Perform Pre-engine start-up portion of *Launch Checklist*	
7. **VCO:** Verify RC Mode (control boxes grayed out) and in "**Manual Mode**"	**ICE Start Time:______________________**
8. **HEO:** Conduct HE RPA startup checklist, record **ICE start time**	
9. **VCO:** Set VC HE add-in to **Dual Mode (ICE Boost)**	**Launch Airspeed:____________________**
10. **SP:** Launch aircraft, record throttle settings and speed if possible	**% Throttle Launch (EM):______________** **% Throttle Launch (ICE):______________**
11. **SP:** Trim the CONDOR for level flight at 700 ft	**Trim Propeller Speed:_________________**
12. **VCO:** Set VC HE add-in to **ICE Only Mode**	**Trim Airspeed:_______________________**
13. **VCO:** Record **trim throttle** position, **trim airspeed, and engine speed**	**% Throttle Trim:______________________** **Trim Propeller Speed:_________________**
14. **SP:** Fly minimum 4 laps around airfield	
15. **VCO/HEO/SP:** Proceed to **Card FT-02** (Do not land aircraft unless necessary)	

19. FT-02: CONDOR HE ICE Mode Flight Test Card

Preconditions:
Completion of FT-01, RPA in trimmed & stable flight, in Dual Mode (ICE Boost)

Note: Mission requires a Safety Observer (SO), HE System operator (HEO), and Virtual Cockpit operator (VCO). The entire test will be conducted in Manual Mode

CONDOR Configuration: 12-ft, ____–lbs, 18x10 2-blade prop

Objective:
Verify performance of integrated HE system in ICE only mode

FT-02: PROCEDURES	Notes: **Dur:** 30 min
<u>**ICE Mode Checkout (ICE Boost – ICE Only – EM Only)**</u>	
1. **SP/VCO:** Verify RPA trimmed at 700 ft	
2. **VCO:** Set VC HE add-in mode to **ICE Only Mode** (if not already)	**Trim Airspeed:**____________________
3. **SP:** Recover RPA to 700 ft and trimmed flight if needed	**% Throttle Trim:**__________________ **Trim Propeller Speed:**______________
4. **HEO:** Verify EM off	
5. **VCO:** Record <u>**trim throttle**</u> position, <u>**trim airspeed**</u>**, and** <u>**engine speed**</u>	
6. **SP:** Complete laps around airfield for 10 minutes, record number of laps	**Number of Laps:**____________________
7. **VCO:** Set VC HE add-in mode to **EM Only**	
8. **HEO:** Verify ICE goes to idle	
9. **SP:** Recover RPA to 700ft and trimmed flight if needed	
10. **VCO/HEO/SP:** Proceed to **Card FT-03** (Repeat this card on its own flight at a later point to quantify fuel burn)	

20. FT-03: CONDOR HE EM Mode Flight Test Card

Preconditions:
Completion of FT-02, RPA in trimmed & stable flight, in EM Mode

Note: Mission requires a Safety Observer (SO), HE System operator (HEO), and Virtual Cockpit operator (VCO). The entire test will be conducted in Manual Mode

CONDOR Configuration: 12-ft, ____–lbs, 18x12 2-blade prop

Objective:
Verify performance of integrated HE system in EM only mode

FT-03: PROCEDURES	Notes: **Dur:** 30 min
EM Mode Checkout (EM Only – ICE Only) 11. **SP/VCO:** Verify RPA trimmed at 700 ft and in EM Only mode, change if required 12. **SP:** Recover RPA to 700ft and trimmed flight if needed 13. **HEO:** Verify ICE at idle 14. **VCO:** Record **trim throttle** position, **trim airspeed**, and **engine speed** 15. **SP:** Complete laps for 3-5 minutes around airfield, record **starting pack voltage**, **starting mAhr**, **pack current draw**, **pack power draw**, **ending pack voltage**, and **ending mAhr**, use this time to stabilize the aircraft and to evaluate if aircraft can loiter in EM only 16. **VCO:** Set VC HE add-in mode to **ICE Only** 17. **SP:** Recover RPA to 700ft and trimmed flight if needed 18. **VCO/HEO/SP:** Proceed to **Card FT-04**	**Trim Airspeed:**____________________ **% Throttle Trim:**__________________ **Trim Propeller Speed:**______________ **Number of laps:**____________________ **Starting Pack Voltage:**_______________ **Starting mAhr:**______________________ **Pack Current Draw:**________________ **Pack Power Draw:**__________________ **Ending Pack Voltage:**_______________ **Ending mAhr:**______________________

21. FT-04: CONDOR HE Dual Mode Flight Test Card

Preconditions:
Completion of FT-03, RPA in trimmed & stable flight, in ICE Mode

Note: Mission requires a Safety Observer (SO), HE System operator (HEO), and Virtual Cockpit operator (VCO). The entire test will be conducted in Manual Mode

CONDOR Configuration: 12-ft, ____–lbs, 18x10 2-blade prop

Objective:
Verify performance of integrated HE system in Dual mode

FT-04: PROCEDURES	Notes: **Dur:** 30 min
Dual Mode Checkout (ICE – EM Boost)	
1. **SP/VCO:** Verify RPA trimmed at 700 ft and in ICE mode	
2. **VCO:** Set **Dual mode (EM Boost**) throttle constant to 10% above ICE idle (~ 40%)	
3. **VCO:** Set VC HE add-in mode to **Dual mode (EM Boost)**	
4. **SP:** Verify EM throttle control, Recover RPA to 700ft and trimmed flight if needed	
5. **HEO:** Verify ICE at constant setting (~40%) – step 2	**Trim Airspeed:**____________________
6. **VCO:** Record **trim throttle** position, **trim airspeed, and engine speed**, **pack current draw**, **pack voltage**, **and pack power**	**% Throttle Trim:**__________________ **Trim Propeller Speed:**______________
7. **SP:** Complete 4 laps around airfield, adjust ICE setpoint if required	**Pack Current Draw:**________________ **Pack Power Draw:**_________________
8. **VCO/HEO/SP:** Proceed to **Card FT-05**	**Pack Voltage:**_____________________

22. FT-05: CONDOR HE Endurance Test Card

Preconditions:
Completion of FT-05

Note: Mission requires a Safety Observer (SO), HE System operator (HEO), and Virtual Cockpit operator (VCO). The entire test will be conducted in Manual Mode

CONDOR Configuration: 12-ft, ____–lbs, 18x10 2-blade prop

Objective:
Verify HE can transition manual control to autopilot and evaluate endurance performance

FT-05: PROCEDURES	Notes: **Dur:** 30 min
1. **SO:** Ensure fire safety and test safety measures in place	
2. **VCO:** Ensure CONDOR PID Values uploaded , and way/rally points loaded into VC	
3. **VCO:** Ensure VC in **Safe Mode** prior to HE RPA startup	
4. **HEO:** Record starting **fuel level** of RPA	**Starting Fuel Level:___________________**
5. **HEO:** Record starting **battery voltage** and **pack power draw**	**Starting battery voltage:_______________** **Pack Power Draw:____________________**
6. **VCO:** Perform Pre-engine start-up portion of *Launch Checklist*	
7. **VCO:** Verify RC Mode (control boxes grayed out) and in "**Manual Mode**"	
8. **HEO:** Conduct HE RPA startup checklist, record **ICE start time**	**ICE/EM Start Time:___________________**
9. **VCO:** Set VC HE add-in to **Dual Mode (ICE Boost),** EM throttle constant (~40%)	
10. **SP:** Launch aircraft	
11. **SP:** Trim the CONDOR for level flight at 700 ft	
12. **VCO:** Reduce EM throttle constant is directed by SP	
13. **VCO:** Set VC HE add-in to **EM Only Mode**	
14. **SP:** Trim the CONDOR for level flight at 700 ft	
15. **HEO:** Verify ICE idle	

FT-05: PROCEDURES	Notes: **Dur:** 30 min
16. **VCO:** Record **trim throttle** position, **trim airspeed, and engine speed** 17. **SP/VCO: SP:** Complete laps for 10 minutes around airfield, record **starting pack voltage**, **starting mAhr**, **pack current draw**, **pack power draw**, **ending pack voltage**, and **ending mAhr** 18. **VCO:** Set VC HE add-in to mode choice of operator for landing, record **landing mode** 19. **SP:** Conduct landing approaches as required to determine necessary throttle settings 20. **VCO:** Adjust Dual mode throttle constant or aircraft mode if directed by SP 21. **SP:** Recover/Land RPA. Pilot should coordinate mode preference with VCO. 22. **VCO:** Place VC in **Safe Mode** 23. **HEO:** Record **engine stop time** and **ending fuel state and required battery charge** 24. **VCO/HEO/SP:** Proceed to **Card FT-07**	**Trim Airspeed:____________________** **% Throttle trim:___________________** **Trim Propeller Speed:______________** **Starting Pack Voltage:______________** **Starting mAhr:_____________________** **Pack Current Draw:________________** **Pack Power Draw:_________________** **Ending Pack Voltage:_______________** **Ending mAhr:______________________** **Landing Mode:____________________** **Engine stop time:__________________** **Final Fuel State:__________________** **Required Battery Charge:____________**

23. FT-06: CONDOR HE ICE Crossover & Cruise Test Card

Preconditions:
Completion of FT-04

Note: Mission requires a Safety Observer (SO), HE System operator (HEO), and Virtual Cockpit operator (VCO). The entire test will be conducted in Manual Mode

CONDOR Configuration: 12-ft, ____–lbs, 18x10 2-blade prop

Objective:
Verify HE can transition manual control to autopilot and evaluate cruise performance

FT-06: PROCEDURES	Notes: **Dur:** 30 min
<u>HE System ICE Crossover Verification</u>	
1. **SO:** Ensure fire safety and test safety measures in place	
2. **VCO:** Ensure CONDOR PID Values uploaded , and waypoints/rally points loaded into VC	
3. **VCO:** Ensure VC in **Safe Mode** prior to HE RPA startup	**Starting Fuel Level:________________**
4. **HEO:** Record starting **<u>fuel level</u>** of RPA	**Starting Battery Voltage:____________**
5. **HEO:** Record starting **<u>battery voltage</u>** and **<u>current draw</u>**	**Starting mAhr:____________________**
6. **VCO:** Perform Pre-engine start-up portion of *Launch Checklist*	
7. **VCO:** Verify RC Mode (control boxes grayed out) and in "**Manual Mode**"	**ICE Start Time:___________________**
8. **HEO:** Conduct HE RPA startup checklist, record **<u>ICE start time</u>**	
9. **VCO:** Set VC HE add-in to **Dual Mode (ICE Boost),** EM throttle constant (~40%)	
10. **SP:** Launch aircraft	
11. **SP:** Trim the CONDOR for level flight at 700 ft	**Trim Airspeed:____________________**
12. **VCO:** Set VC HE add-in to **ICE Only Mode**	**% Throttle Trim:__________________**
13. **SP:** Trim the CONDOR for level flight at 700 ft	**Trim Propeller Speed:______________**

FT-06: PROCEDURES	Notes: **Dur:** 30 min
14. **VCO:** Record **trim throttle** position, **trim airspeed, and engine speed** 15. **HEO:** Activate Crossover switch 16. **SP/VCO:** Verify autopilot has control of aircraft 17. **HEO:** Deactivate Crossover switch 18. **SP/VCO:** RPA in back in manual control (**ICE Only Mode**) 19. **SP/VCO:** Monitor RPA under autopilot control for 10+ min flight, set to cruise velocity 20. **SP:** Recover/Land RPA, pilots choice of landing mode. Pilot should coordinate mode with VCO. 21. **VCO:** Place VC in **Safe Mode** 22. **HEO:** Record **engine stop time** and **ending fuel state** 23. **VCO/HEO/SP:** Proceed to **Card FT-07**	**Landing Mode:**____________________ **Engine Stop Time:**__________________ **Final Fuel State:**___________________

24. FT-07: CONDOR HE ReGen Mode & Kill Switch Test Card

Preconditions:
Completion of GT-06

Note: Mission requires a Safety Observer (SO), HE System operator (HEO), and Virtual Cockpit operator (VCO). The entire test will be conducted in Manual Mode

CONDOR Configuration: 12-ft, ____–lbs, 18x10 2-blade prop

Objective:
Verify HE EM ReGen and ICE Kill switch function correctly

FT-07: PROCEDURES	Notes: **Dur:** 30 min
<u>**HE System ReGen Verification**</u>	
1. **If strating in air from FT-06, proceed to step**	
2. **SO:** Ensure fire safety and test safety measures in place	
3. **VCO:** Ensure CONDOR PID Values uploaded , and waypoints loaded into VC	
4. **VCO:** Ensure VC in **Safe Mode** prior to HE RPA startup	
5. **HEO:** Record battery starting <u>**battery voltage**</u> & <u>**current**</u>, ensure at least 2V under max	**Engine Start Time:**____________________
6. **HEO:** Record starting <u>**fuel level**</u> of RPA	**Starting Fule Level:**____________________
7. **VCO:** Perform Pre-engine start-up portion of *Launch Checklist*	
8. **VCO:** Verify RC Mode (control boxes grayed out) and in "**Manual Mode**"	
9. **VCO:** Place VC HE add-in to **ICE Only Mode**	
10. **HEO:** Conduct HE RPA startup checklist, record <u>**ICE start time**</u>	
11. **VCO:** Set VC HE add-in to **Dual Mode (ICE Boost),** EM throttle constant (~40%)	
12. **SP:** Launch aircraft	
13. **SP:** Trim the CONDOR for level flight at 700 ft	
14. **VCO:** Reduce EM throttle constant is directed by SP	

FT-07: PROCEDURES

15. **VCO:** Set VC HE add-in to **ICE Only Mode**
16. **SP:** Trim the CONDOR for level flight at 700 ft
17. **VCO:** Record **trim throttle** position, **trim airspeed, and engine speed**
18. **HEO:** Record **Battery pack voltage**, **ReGen start time**, **Starting Pack mAhr**, and **Pack Current Draw**
19. **VCO:** Set VC add-in to **Regen Mode**
20. **HEO:** Maneuver RPA in lap pattern & monitor battery pack voltage, record time for voltage to increase 0.3V
21. **HEO:** Record **Battery pack voltage**, **ReGen end time**, and **Ending Pack mAhr**
22. **VCO:** Place VC HE add-in to **ICE Only**
23. **Land RPA and complete any unfinished tests before proceeding to Step 24.**

****HIGH RISK****

ICE Kill for Silent Operation

24. **VCO:** Set VC add-in to **EM Mode**
25. **HEO:** Verify EM powers up & ICE goes to idle
26. **SP:** Verify EM throttle response, prepare for simulated emergency landing
27. **HEO:** Activate **ICE Kill Switch**
28. **HEO:** Verify ICE killed & Record **engine stop time**
29. **SP:** Verify RPA performance under **EM Only Mode** (no ICE)

Notes: **Dur:** 30 min

Trim Airspeed:____________________
% Throttle trim:____________________
Trim Propeller Speed:_______________

Starting Battery Voltage:_____________
Starting Pack mAhr:_________________
Start ReGen Time:___________________

Pack Current Draw:___________________

Ending Battery Voltage:_______________
Ending Pack mAhr:___________________
End ReGen Time:_____________________

Engine Stop Time:_________________
Final Fuel State:__________________

Works Cited

[1] (2011, December) "The Wright Brothers and the Invention of the Aerial Age." *Smithsonian: National Air and Space Museum*. [Online]. http://www.nasm.si.edu/wrightbrothers/ [Accessed: 8 December 2011]

[2] L. R. Newcome, *Unmanned Aviation: A Brief History of Unmanned Aerial Vehicles*. Reston, VA, United States of America: AIAA, 2004.

[3] (2011, March) General Atomics Website. [Online]. http://www.ga.com [Accessed: 8 December 2011]

[4] J. R. Wilson, "Roundup 2011," *Aerospace America*, pp. 22 -31, March 2011.

[5] Office of the Secretary of Defense, "Unmanned Systems Roadmap (2007-2032)," 2007.

[6] Headquarters United States Air Force, "USAF Unmanned Aircraft Systems Flight Plan (2009-2047)," United States Air Force, 2009.

[7] Office of the Secretary of Defense, "Unmanned Aircraft Systems Roadmap (2005-2030)," 2005.

[8] Robert Draper, "Rift in Paradise: Africa's Albertine Rift," *National Geographic Magazine*, pp. 82-117, November 2011.

[9] G. Warwick, "Hybrid-Electric UAVs Under Development," *Aviation Week & Space Technology*, p. 38, July 2009.

[10] Frederick G. Harmon, Andrew A. Frank, and Jean-Jacques Chattot, "Conceptual Design and Simulation of a Small Hybrid-Electric Unmanned Aerial Vehicle," *Journal of Aircraft*, vol. 43, no. 5, pp. 1490-1498, September-October 2006.

[11] Ryan M. Hiserote and Frederick G. Harmon, "Analysis of Hybrid Electric Propulsion System Designs for Small Unmanned Aircraft Systems," presented at the *46th AIAA/ASME/SAE/ASEE Joint Propulsion conference & Exhibit*, Nashville, TN, 2010.

[12] Ryan M. Hiserote, "Analysis of Hybrid-Electric Propulsion System Designs for Small Unmanned Aircraft Systems," Department of Aeronautical and Astronautical Engineering, Air Force Institute of Technology, Dayton, OH, M.S. Thesis ISBN/ISSN, 2010.

[13] Todd A. Rotramel, "Optimization of Hybrid Electric Propulsion Systems for Small Remotely Piloted Aircraft," Department of Aeronautical and Astronautical Engineering, Air Force Institute of Technology, Dayton, OH, M.S. Thesis 2010.

[14] Frederick G Harmon, "Neural Network Control of a Parallel Hybrid-Electric Propulsion System for a Small Unmanned Aerial Vehicle," Department of Mechanical and Aeronautical Engineering, University of California - Davis, Davis, CA, Ph.D. Dissertation 2005.

[15] Isseyas H. Mengistu, "Small Internal Combustion Engine Testing for Hybrid-Electric Remotely Piloted Aircraft Propulsion," Department of Aeronautical and Astronautical Engineering, Air Force Institute of Technology, Dayton, OH, Master's Thesis 2011.

[16] John Hagen, "PIC32 Lightning User's Manual," Department of Aeronautical and Astronautical Engineering, Air Force Institute of Technology, Dayton, OH, User Manual 2011.

[17] Collin M. Greiser, "Implementation of a Rule-Based Open-Loop Conrol Strategy for a Hybrid-Electric Propulsion System on a Small RPA," Department of Aeronautical and Astronautical Engineering, Air Force Institute of Technology, Dayton. OH, M.S. Thesis 2011.

[18] Christopher Giacomo, "Modeling, Simulation, and Flight Test for Automatic Flight Control of the Condor Hybrid-Electirc Remotely-Piloted Aircraft," Department of Aeronautical and Astronautical Engineering, Air Force Institute of Technology, Dayton, OH, M.S. Thesis 2012.

[19] Jacob English and Michael Molesworth, "Rapid Prototype Development of a Hybrid-Electric Remotely-Piloted Aircraft," Department of Systems and Logistics, Air Force Institute of Technology, Dayton, OH, M.S. Thesis 2012.

[20] Chevrolet Corporation. (2011, April) "Chevrolet Volt." *Chevrolet.com*. [Online]. http://www.chevrolet.com/volt/#technology [Accessed: 11 April 2011]

[21] Richard R. Glassock, Jane Y. Hung, Luis F. Gonzalez, and Rodney A. Walker, "Multimodal Hyrbid Powerplant for Unmanned Aerial Systems (UAS) Robotics," presented at the *Twenty-Fourth Bristol Internation Unmanned Air Vehicle Systems Conference*, Bristol, 2009.

[22] Richard Glassock, Jane Y. Yung, Louis Felipe Gonzalez, and Rodney Walker, "Design, Modeling and Measruement of Hybrid Powerplant for Unmanned Aerial Systems," presented at the *5th Austratilian Congress of Applied Mechanics, ACAM 2007*, Brisbane, 2007.

[23] Gael Putrich. (2010, November) "Global Observer Clears Wing Loading Test." *Flight Global*. [Online]. http://www.flightglobal.com/articles/2010/08/11/346040/global-observer-clears-wing-load-testing.html [Accessed: 28 April 2011]

[24] R. Wall, "New Engine Concepts Emerge for UAVs and UCAVs," *Aviation Week and Space Technology*, p. 24, March 2008.

[25] NASA. (2009) "Helios Prototype Solar-Powered Aircraft." *Dryden Flight Research Center*. [Online]. http://www.nasa.gov/centers/dryden/news/FactSheets/FS-068-DFRC.html [Accessed: 29 April 2011]

[26] NASA. (2009) "NASA Dryden Fact Sheet - Pathfinder Solar-Powered Aircraft." *Dryden Flight Research Center*. [Online]. http://www.nasa.gov/centers/dryden/news/FactSheets/FS-034-DFRC.html [Accessed: 30 April 2011]

[27] S. Gitlin and M. Boyer, "AeroVironment Puma Small UAS Achieves Record Flight of Over Nine Hours Using Fuel Cell Battery Hybrid System," *AeroVironment*, March 2008.

[28] AeroVironment. (2011, April) "UAS: Puma AE." *AeroVironment Inc*. [Online]. http://www.avinc.com/uas/small_uas/puma [Accessed: 1 May 2011]

[29] Michael Mecham. (2008, April) "Boeing Fuel Cell Points to UAVS." *AviationWeek.com*. [Online]. http://aviationweek.com [Accessed: 17 September 2009]

[30] Thomas H. Bradley, Blake A. Moffitt, Dimitri N. Mavris, Thomas F. Fuller, and David E. Parekh, "Hardware-in-the-Loop Testing of a Fuel Cell Aircraft Powerplant," *Journal of Propulsion and Power*, vol. 25, no. 6, pp. 1336-1344, November-December 2009.

[31] J. Paur, "Hybrid Power Comes to Aviation," *Wired.com*, July 2009. [Online]. http://www.wired.com/autopia/2009/07/hybrid-aviation

[32] Siemens, "World's First Serial Hybrid Electric Aircraft to FLy at Le Bourget," Munich, Germany, Press Release AXX201106.66 e, 2011.

[33] Peter Van den Bossche. (2006, Novemeber) "Structure of a Series Hybrid Vehicle." *Wikipedia*. [Online]. http://en.wikipedia.org/wiki/File:Hybridpeak.png [Accessed: 3 May 2011]

[34] Peter Van den Bossche. (2006, Novemeber) "Strucutre of a Parallel Hybrid Vehicle." *Wikipedia*. [Online]. http://en.wikipedia.org/wiki/File:Hybridpar.png [Accessed: 3 May 2011]

[35] Inc. Honda. "Insight Heritage." *Honda.com*. [Online]. http://automobiles.honda.com/insight-hybrid/heritage.aspx [Accessed: 2009 Septemeber 23]

[36] Peter Van den Bossche. (2006, Novemeber) "Structure of a Combined Hybrid Vehicle." *Wikipedia*. [Online]. http://en.wikipedia.org/wiki/File:Hybridcombined.png [Accessed: 3 May 2011]

[37] J. Garrett, "Toyota and Ford Reach Hybrid Milestones," *New York Times*, March 2009.

[38] G. Warwick, "Aurora Working on New Hybrid Engine for UAVs," *Aerospace Daily & Defense Report*, p. 4, April 2009.

[39] Jean Koster et al., "Hybrid Electric Integrated Optimized System (HELIOS): Design of a Hybrid Propulsion System for Aircraft," presented at the *49th AIAA Aerospace Sciences Meeting including the New Horizons Forum and Aerospace Exposition*, Orlando, FL, 2011.

[40] John B. Heywood, *Internal Combustion Engine Fundamentals*. New York, NY, United States of America: McGraw-Hill, 1988.

[41] John D. Anderson, *Aircraft Performance and Design*. Boston, MA, United States of America: McGraw-Hill, 1999.

[42] Shyam Menon and Christopher Cadou, "Experimental and Computational Investigations of Small Internal Combustion Engine Performance," presented at the *5th US Combustion Meeting*, College Park, MD, 2007.

[43] Michael, J. Moran and Howard N. Shapiro, "Fundamentals of Engineering Thermodynamics," in *Fundamentals of Engineering Thermodynamics*. Hoboken, NJ, United States of America: John Wiley and Sons, Inc, 2008, ch. 9.

[44] USD(AT&L), "DoD Management Policy for Energy Commodities and Related Services (DOD4140.25)," U.S. Department of Defense, 2004.

[45] Thomas J. Mueller, James C. Kellogg, Peter, G. Ifju, and Sergey V. Shkarayev, *Introduction to the Design of Fixed-Wing Micro Air Vehicles*. Reston, VA, United States of America: American Instutue of Aeronautics and Astronautics, 2007.

[46] D. Lundstrom, K. Amadori, and P. Krus, "Validation of Small Scale Electric Propulsion System Models," presented at the *46th AIAA Aerospace Sciences Meeting Including the New Horizons Forum and Aerospace Exposition*, Orlando, FL, 2010.

[47] M. Drela, "QPROP Documents: First-Order DC Electric Motor Model," Massachusetts Institute of Technology, Boston, MA, 2007.

[48] M. Drela, "QPROP Documents: DC Motor/Propeller Matching," Massachusetts Institute of Technology, Boston, MA, 2005.

[49] Monal P. Merchant and L. Scott Miller, "Propeller Performance Measurement for Low Reynolds Number UAV Applications," presented at the *44th AIAA Aerospace Sciences Meeting and Exhibit*, Reno, NV, 2006.

[50] Robert W. Deters and Michael S. Selig, "Static Testing og Micro Propellers," presented at the *26th AIAA Applied Aerodynamics Conference*, Honolulu, 2008.

[51] Daniel V. Uhlig and Michael S. Selig, "Post Stall Propeller Behavoir at Low Reynolds Numbers," presented at the *46th AIAA Aerospace Sciences Meeting and Exhibit*, Reno, 2008.

[52] Michael OL, Cale Zeune, and Mike Logan, "Analytical - Experimental Comparison for Small Electric Unmanned Air Vehicle Propellers," presented at the *26th AIAA Applied Aerodynamics Conference*, Honolulu, 2008.

[53] Ohad Gur and Aviv Rosen, "Optimization of Propeller Based Propulsion System," *Journal of Aircraft*, vol. 46, no. 1, pp. 95-106, January-February 2009.

[54] Martin Winter and Ralph J. Brodd, "What Are Batteries, Fuel Cells, and Supercapacitors," *Chemical Review*, vol. 104, no. 12, pp. 4245-4269, 2004.

[55] B Fultz, Types of Batteries, and Differences in Energy and Power, 2007, APh 150 Spring 2007 Lecture.

[56] I. Buchmann. (2006, November) "What's the best battery?" *BatteryUniversity.com*. [Online]. http://batteryuniversity.com/learn/article/whats_the_best_battery [Accessed: 2011 May 2011]

[57] Yuriy Mikhaylik, "Fundamental Chemistry of Sion Power Li/S Battery," presented at the *IBA-HBC 2006*, Waikoloa, HI, 2006.

[58] John B. Olson, Norman E. Smith, Chris R. Sheridan, and Philip C. Lyman, "Lithium-Ion Batteries for Electric and hybrid Electric Vehicles," presented at the *4th International Energy Conversion Engineering Conference*, San Diego, CA, 2006.

[59] Ui Deong Kim, Chee Burml Shin, and Chi-Su Kim, "Modeling for the Scale-up of a Lithium-Ion Polymer Battery," *Journal of Power Sciences*, pp. 841-846, 2009.

[60] Lijun Gao, Shengyi Liu, and Roger A. Dougal, "Dynamic Lithium-Ion Battery Model for System Simulation," *IEEE Transactions on Components and Packaging Technologies*, vol. 25, no. 3, pp. 495-505, September 2002.

[61] Frank Fleming, "Friction and Magnetism: The Basics of Electromagnetic Clutches and Brakes," Ogura Industrial Corporation, Somerset, NJ, 2009.

[62] Fletcher. (2008, May) "File:CentrifugalClutch.jpg." *Wikipedia*. [Online]. http://en.wikipedia.org/wiki/File:CentrifugalClutch.jpg [Accessed: 16 May 2011]

[63] Boca Bearing. (2011, May) *Boca Bearing*. [Online]. http://www.bocabearings.com/bearing-types/one-way-bearings [Accessed: 16 May 2011]

[64] Microchip. (2009, November) Microchip.com. [Online]. http://ww1.microchip.com/downloads/en/DeviceDoc/DS-39904j.pdf [Accessed: 16 May 2011]

[65] Procerus Technologies. (2011, May) Procerus Technologies. [Online]. http://procerusuav.com/productsKestrelAutopilot.php [Accessed: 16 May 2011]

[66] A. B. Fransisco, "Implementation of an Ideal Operating Line Control Strategy for Hybrid Electric Vehicles," University of California Davis, Davis, CA, Master's Thesis 2002.

[67] Robert W. Schurhoff, "The Development and Evaluation of an Optimal Powertrain Control Strategy for a Hybrid Electric Vehicle," University of California - Davis, Davis, CA, Master's Thesis, 2002.

[68] Scott. (2006, September) "State Machines in Windows Workflow." *OdeToCode.com*. [Online]. http://odetocode.com/code/460.aspx [Accessed: 2011 May 17]

[69] James M Payne, *Flight Test Handbook*. Edwards, CA: JP Aviation, 2002.

[70] Jon Neal Ostler, "Flight Testing Small, Electric Powered Unmanned Aerial Vehicles," Department of Mechanical Engineering, Brigham Young University, Master's Thesis 2006.

[71] Jon N. Ostler, Jerry W. Bowman, Deryl O. Snyder, and Timothy W. McLain, "Performance Flight Testing of Small, Electric Powered Unmanned Aerial Vehicles," *International Journal of Micro Air Vehicles*, vol. 1, no. 3, pp. 155-171, 2009.

[72] Eagle Tree Systems. (2011, May) "Seagull Wireless Telemetry." *Eagle Tree Systems*. [Online]. http://www.eagletreesystems.com/Plane/plane.html [Accessed: 26 May 2011]

[73] Honda Motor Corporation. (2011, December) "GX35." *Honda Engines*. [Online]. http://engines.honda.com/models/model-detail/gx35 [Accessed: 14 December 2011]

[74] Honda Motor Corporation. (2011, December) "GX25." *Honda Engines*. [Online]. http://engines.honda.com/models/model-detail/gx25 [Accessed: 14 December 2011]

[75] SynQor. (2009, January) "NiQor High Voltage DC/DC Converters." *SynQor.com*. [Online]. http://www.synqor.com/niqor/niqor-hivolt.html [Accessed: 20 December 2011]

[76] Maxon Motors. (2011, January) "Catalog: RE 50." *Maxon Motors USA*. [Online]. http://www.maxonmotor.com/maxon/view/catalog/ [Accessed: 20 December 2011]

[77] AXI Model Motor. (2006, January) "AXI 4130/20 Gold Line." *AXI Model Motors*. [Online]. http://www.modelmotors.cz [Accessed: 20 December 2011]

[78] (2011, Jan) *Tower Hobbies*. [Online]. http://www.towerhobbies.com [Accessed: 27 December 2011]

[79] Elmo Motion Control ltd., Solo Whistle Digital Servo Drive, March 2010.

[80] Elmo Motion Control. (2011, January) "SimplIQ Solo Whistle." *Elmo MC*. [Online]. http://www.elmomc.com/products/solo-elmo-integrated-servo.htm [Accessed: 20 December 2011]

[81] Dimension Engineering. (2011, January) "BattleSwitch Radio Controlled 10A Relay." *Dimension Engineering.com*. [Online]. http://www.dimensionengineering.com/battleswitch.htm [Accessed: 28 Decemeber 2011]

[82] (2011, Decemeber) *Hobby Lobby International*. [Online]. http://www.hobby-lobby.com [Accessed: 29 Decemeber 2011]

[83] (2011, December) *Small Engine Warehouse*. [Online]. http://www.smallenginewarehouse.com [Accessed: 29 December 2011]

[84] (2011, Decemeber) *ThunderPower RC*. [Online]. http://thunderpowerrc.com [Accessed: 29 December 2011]

[85] Jesse Rodgers, Quotation, May 2, 2011.

[86] Digikey Corporation. (2012, January) *Digikey.com*. [Online]. http://search.digikey.com [Accessed: 4 January 2012]

[87] Jesse Rodgers, Quotation, June 21, 2011.

[88] US Digital. (2011, December) "Quote." *US Digital*. [Online]. http://www.usdigital.com/products [Accessed: 29 December 2011]

[89] (2011 , December) *Belt Palace*. [Online]. http://www.beltpalace.com/ [Accessed: 29 December 2011]

[90] (2011, December) *Eagle Tree Systems*. [Online]. http://www.eagletreesystems.com [Accessed: 29 December 2011]

[91] (2011, December) *Blue Point Engineering*. [Online]. http://www.bpesolutions.com [Accessed: 29 December 2011]

[92] APC Propellers. (2012, January) *APCprops.com*. [Online]. http://www.apcprop.com [Accessed: 3 January 2011]

[93] Albert E. Von Doenhoff, *Theory of Wing Sections*. Mineola, NY, United States of America: McGraw-Hill, 1959.

[94] Western Museum of Flight. (2010, December) "Lockheed YO-3A." *Western Museum of Flight*. [Online]. http://www.wmof.com/yo-3a.htm [Accessed: 19 February 2012]

[95] NWUAV Propulsion Systems. (2011, Decemeber) *NWUAV Propulsion Systems*. [Online]. www.nwuav.com [Accessed: 19 February 2012]

Vita

Lieutenant Joseph K. Ausserer graduated as a salutatorian from Beavercreek High School, Beavercreek, OH in 2006. He earned Bachelor of Science degrees in Mechanical Engineering and Chemical Engineering from Rose-Hulman Institute of Technology, Terre Haute, IN in 2010, graduating first in his class. He also received his Air Force commission in 2010 from Air Force ROTC Detachment 218, Indiana State University, Terre Haute, IN.

Lieutenant Ausserer's first assignment after graduation was to attend the Air Force Institute of Technology. Upon completion of his Master's degree in Aeronautical Engineering in March 2012, Lieutenant Ausserer will be assigned to the Air Force Research Laboratory's Propulsion Directorate at Wright Patterson Air Force Base, OH.

REPORT DOCUMENTATION PAGE

Form Approved
OMB No. 0704–0188

1. REPORT DATE (DD–MM–YYYY)	2. REPORT TYPE	3. DATES COVERED (*From — To*)
22-03-2012	Master's Thesis	Sept 2010 - Mar 2012

4. TITLE AND SUBTITLE
Integration, Testing, and Validation, of a Small Hybrid-Electric Remotely-Piloted Aircraft

5a. CONTRACT NUMBER

5b. GRANT NUMBER

5c. PROGRAM ELEMENT NUMBER

6. AUTHOR(S)

Ausserer, Joseph K., Second Lieutenant, USAF

5d. PROJECT NUMBER

5e. TASK NUMBER

5f. WORK UNIT NUMBER

7. PERFORMING ORGANIZATION NAME(S) AND ADDRESS(ES)
Air Force Institute of Technology
Graduate School of Engineering and Management (AFIT/ENY)
2950 Hobson Way
WPAFB OH 45433-7765

8. PERFORMING ORGANIZATION REPORT NUMBER

AFIT/GAE/ENY/12-M02

9. SPONSORING / MONITORING AGENCY NAME(S) AND ADDRESS(ES)
Air Force Research Laboratory, Propulsion Directorate
Paul Litke (937-785-1673) Turbine Division (AFRL/RZT)
Benjamin Razidlo (937-785-6206) Power Division (AFRL/RZP)
1950 Fifth Street
WPAFB, OH 45433-7251

10. SPONSOR/MONITOR'S ACRONYM(S)
AFRL/RZTC, AFRL/RZPG

11. SPONSOR/MONITOR'S REPORT NUMBER(S)

12. DISTRIBUTION / AVAILABILITY STATEMENT
APPROVED FOR PUBLIC RELEASE; DISTRIBUTION UNLIMITED

13. SUPPLEMENTARY NOTES

14. ABSTRACT
Parallel hybrid-electric technology offers a wide variety of new mission capabilities including low-observable loiter operations and increased fuel efficiency for small remotely-piloted aircraft. This research focused on the integration, validation, and testing of a hybrid-electric propulsion system consisting of commercially available components to fabricate a small remotely-piloted aircraft capable of extended low-observable operation. Three novel aspects contributed to the success of the design: optimization of the propulsive components to the integrated system, torque control of the components for additive power, and a one-way bearing/ pulley mechanism (patent pending) mechanically linking the hybrid system components. To the knowledge of the author at the time of publication, this project represents the first functional parallel hybrid-electric propulsion system for a remotely-piloted aircraft. The integration phase entailed the selection, testing, and assembly of components chosen based on prior design simulations. The propulsion system was retrofitted onto a glider airframe with a 12 ft wingspan and a maximum takeoff weight of 35 lbs, also based on the initial design simulations. During the validation and testing phases, results from bench, ground, and flight testing were compared to the design simulations. The designed propulsion system was well matched to the power estimates of the design simulations. Bench and ground tests demonstrated that hybrid mode, electric only mode, combustion only mode, and regeneration mode are fully functional. Comparison of bench test results to an engine only variant of the airframe indicate the HE system is capable of flying the aircraft.

15. SUBJECT TERMS: Hybrid, electric, propulsion, remotely piloted aircraft, unmanned aerial vehicle, system integration, clutch

16. SECURITY CLASSIFICATION OF:			17. LIMITATION OF ABSTRACT	18. NUMBER OF PAGES	19a. NAME OF RESPONSIBLE PERSON Joseph K. Ausserer, Second Lieutenant, USAF
a. REPORT	b. ABSTRACT	c. THIS PAGE	UU	280	19b. TELEPHONE NUMBER (Include Area Code) (937)671-7365 Joseph.Ausserer@afit.edu
U	U	U			

Standard Form 298 (Rev. 8–98)
Prescribed by ANSI Std. Z39.18